# ISOPHOT Data Users Manual

**R.J. Laureijs[1], U. Klaas[2], P.J. Richards[3] and B. Schulz[1]**

[1] ISO Data Centre, Astrophysics Division,
Space Science Department of ESA,
Villafranca, P.O. Box 50727, E-28080 Madrid, Spain

[2] Max-Planck-Institut für Astronomie, ISOPHOT Data Centre,
Königstuhl 17, D-69117 Heidelberg, Germany

[3] CCLRC Rutherford Appleton Laboratory
Chilton, Didcot, Oxon OX110QX, United Kingdom

**SAI/95–220/Dc**

Version 4.1

October 1999

## Document Information

| | |
|---|---|
| Document Title: | ISOPHOT Data Users Manual |
| Reference Number: | SAI/95-220/Doc |
| Issue: | Version 4.1 |
| Issue Date: | 9 Oct 1999 |
| Authors: | R.J. Laureijs, U. Klaas, P.J. Richards, B. Schulz |

## Contributions to this Document

Many people have contributed to this document for. Main inputs have been provided by the following groups of persons:

**ISOPHOT Instrument Dedicated Team (PIDT):**

J. Acosta (IAC/MPIA)
M. Braun (MPIA)
H. Castaneda (IAC/MPIA)
L. Cornwall (RAL)
C. Gabriel (ESA)
I. Heinrichsen (MPIK)
S. Huth (MPIA)
U. Kinkel (MPIA)
G. Pelz (MPIA)

**ISO Data Centre in VILSPA:**

Y. Sato

**ISOPHOT Data Centre at MPIA Heidelberg:**

D. Lemke
P. Abraham
S. Bogun
U. Herbstmeier
H. Krüger
T. Müller
M. Radovich

**Infrared Processing and Analysis Center, Caltech, Pasadena:**

A.E. Wehrle

Document Change Record

| **Date** | **Revision** | **Comments** |
|---|---|---|
| 04/09/95 | Draft 1.0 | Initial Draft for comments |
| 17/11/95 | Version 1.0 | Pre-Launch Version |
| 08/05/96 | Version 2.0 | First public version for OLP 4.0 products<br>major update, no detailed change log |
| 01/09/97 | Version 3.0 | Updated version for OLP 6.0 products<br>Only for internal review, no detailed change log |
| 09/10/98 | Version 4.0 | Public version for OLP Version 7 products<br>major update, no detailed change log |
| 05/10/99 | Version 4.1 | Correction of errors and omissions in Version 4.0<br>minor update, no detailed change log |

# Contents


**1 Preface** **11**

**2 How to use this manual** **12**

**3 Instrument and AOT Overview** **14**

3.1 Overview . . . 14
3.2 Data Collection with ISOPHOT . . . 14
3.2.1 Signal Flow in ISOPHOT . . . 14
3.2.2 Cold readout Electronics (CRE) . . . 15
3.2.3 Detector Interface Electronics (DIE) . . . 17
3.2.4 readout timing control . . . 17
3.3 ISOPHOT measurement concept . . . 17
3.4 Detector Subsystems . . . 18
3.4.1 PHT-P . . . 18
3.4.2 PHT-C . . . 18
3.4.3 PHT-S . . . 19
3.5 Fine Calibration Sources (FCSs) . . . 19
3.6 Focal Plane Chopper (FPC) . . . 20
3.7 ISOPHOT Modes of Operation . . . 20
3.7.1 PHT-P: PHT03, PHT04, PHT05, PHT17/18/19 . . . 21
3.7.1.1 PHT03 . . . 21
3.7.1.2 PHT04 . . . 22
3.7.1.3 PHT05 . . . 23
3.7.1.4 PHT17/18/19 . . . 23
3.7.2 PHT-C: PHT22, PHT25, PHT32, PHT37/38/39 . . . 25
3.7.2.1 PHT22 . . . 25
3.7.2.2 PHT25 . . . 25
3.7.2.3 PHT32 . . . 26
3.7.2.4 PHT37/38/39 . . . 26
3.7.3 PHT-S: PHT40 . . . 27
3.7.4 Polarisation Observations: PHT50, PHT51 . . . 28
3.7.4.1 PHT50 . . . 28
3.7.4.2 PHT51 . . . 28

**4 Instrumental Characteristics** **29**
4.1 Overview . . . 29
4.2 Detector Properties . . . 29
4.2.1 Detector Responsivity/Linearity . . . 29
4.2.2 Transient behaviour after flux change . . . 30
4.2.3 Drift behaviour of responsivity . . . 33
4.2.4 Curing Procedures . . . 34
4.2.5 Dark Signal and Noise . . . 35
4.2.6 Detector flat-fields . . . 37
4.2.7 Detector Saturation . . . 37
4.3 Features due to electronics . . . 37
4.3.1 Anomalous first readouts on a ramp . . . 37
4.3.2 CRE (ramp) linearity . . . 37
4.3.3 Signal dependence on reset interval . . . 38
4.3.4 Detector bias: de-biasing effects . . . 38
4.3.5 Readout Saturation . . . 39
4.3.6 Disturbances by Chopper Commanding . . . 40
4.3.7 CRE latch-up . . . 40
4.4 Effects of Ionizing Radiation . . . 40
4.5 Optical Performance . . . 41
4.5.1 Instrumental Footprint on the Sky . . . 41
4.5.1.1 PHT-C footprints . . . 42
4.5.1.2 PHT-P footprints . . . 42
4.5.1.3 PHT-S footprints . . . 47
4.5.2 Point source intensity fractions . . . 48
4.5.3 Chopper vignetting/offset . . . 48
4.5.4 Inhomogeneous FCS illumination . . . 48
4.6 Spectral performance . . . 49
4.6.1 PHT-S instrumental line profile . . . 49
4.6.2 PHT-S wavelength calibration . . . 49
4.7 Straylight . . . 50
4.7.1 Straylight during FCS calibrations . . . 50
4.7.2 Instrumental Straylight . . . 50
4.7.2.1 Near-field straylight . . . 50
4.7.2.2 Straylight from Sun, Earth and Moon . . . 51
4.7.3 Spectral Straylight . . . 51
4.8 Instrumental Polarisation . . . 51
4.9 Backgrounds . . . 52
4.9.1 Confusion . . . 52
4.9.2 Zodiacal Light . . . 52
4.10 Global Instrument Data . . . 52

**5 Calibrations** **53**
5.1 Overview . . . 53
5.2 Calibration strategy . . . 53
5.2.1 Calibration strategy involving the FCS . . . 53

5.2.2 Absolute calibration of FCS . . . 54
5.2.3 Photometry with PHT-P and PHT-C . . . 55
5.2.4 Spectro-photometry with PHT-S . . . 56
5.3 Point sources versus extended sources . . . 57
5.4 Aperture calibration . . . 58
5.5 PHT-S wavelength calibration . . . 58
5.6 Photometric calibration in AOTs . . . 58
5.6.1 General signal derivation . . . 58
5.6.2 Multi-filter photometry: PHT03 and PHT22 . . . 59
5.6.3 Mapping: PHT03, PHT22, PHT32 . . . 59
5.6.4 Sparse maps: PHT17/18/19 and PHT37/38/39 . . . 59
5.6.5 Multi-aperture photometry: PHT04 . . . 59
5.6.6 Absolute photometry: PHT05 and PHT25 . . . 59
5.6.7 PHT-S: PHT40 . . . 59
5.7 Calibration files . . . 60
5.7.1 Calibration G files . . . 60
5.7.2 Calibration A files . . . 60

**6 Data Processing Level: Derive_ERD 61**

**7 Data Processing Level: Derive_SPD 63**
7.1 Overview . . . 63
7.2 Ramp Processing . . . 64
7.2.1 Discarding destructive read-outs . . . 64
7.2.2 Discarding disturbed non-destructive read-outs . . . 64
7.2.3 Discarding data with OTF or OPF "off" . . . 64
7.2.4 Sorting out the different data-types . . . 65
7.2.5 Conversion of digitized numbers to CRE output voltages . . . 65
7.2.6 Discarding saturated read-outs . . . 66
7.2.7 Correction for non-linearities of the integration ramps . . . 66
7.2.8 Ramp deglitching . . . 67
7.2.9 Extraction of the signals and their uncertainties . . . 67
7.3 Signal Processing . . . 68
7.3.1 Reset interval correction . . . 68
7.3.2 Dark signal subtraction . . . 68
7.3.3 Determine chopper position and step number . . . 69
7.3.4 Signal deglitching . . . 70
7.3.5 Transient correction . . . 70
7.3.6 Averaging signals of same instrument set-up . . . 71
7.3.7 Obtaining the median of all photo-currents . . . 72
7.3.8 Correction for chopper vignetting . . . 72
7.3.9 Correction for chopped signal losses . . . 73
7.3.10 Ramp statistics in PHT SPD and Cal-A headers . . . 73
7.4 In-band power calibration . . . 74
7.4.1 Determination in-band power from FCS . . . 74
7.4.2 Signal to in-band power conversion for P detectors . . . 74
7.4.3 Signal to-in band power conversion for C detectors . . . 75

7.4.4 In-band power for raster maps . . . 76
7.4.5 Default responsivities . . . 77
7.4.6 Dependencies on mission dates . . . 77
7.5 Quality flags for SPD records . . . 78

**8 Data Processing Level: Derive_AAR 79**
8.1 Overview . . . 79
8.2 PHT auto analysis processing per AOT . . . 79
8.2.1 PHT03 . . . 79
8.2.2 PHT04 . . . 80
8.2.3 PHT05 . . . 81
8.2.4 PHT17/18/19 . . . 81
8.2.5 PHT22 . . . 82
8.2.6 PHT25 . . . 83
8.2.7 PHT32 . . . 84
8.2.8 PHT37/38/39 . . . 84
8.2.9 PHT40 . . . 85
8.3 Common processing steps . . . 85
8.3.1 Read SPD header . . . 85
8.3.2 Read SPD record . . . 86
8.3.3 Determine celestial coordinates of each pixel in record . . . 87
8.3.3.1 Overview . . . 87
8.3.3.2 Extracting pointing data from IRPH . . . 87
8.3.3.3 Inclusion of chopper information . . . 88
8.3.4 Determination of the equatorial offsets of the detector centre . . . 89
8.4 Photometry . . . 89
8.4.1 Sorting out chopper plateaux . . . 89
8.4.2 Separation of source and background in-band power . . . 90
8.4.2.1 Rectangular mode . . . 91
8.4.2.2 Sawtooth mode . . . 91
8.4.2.3 Triangular mode . . . 92
8.4.3 Determine the in-band powers averaged over a measurement . . . 92
8.4.3.1 Rectangular mode . . . 92
8.4.3.2 Sawtooth and Triangular mode . . . 93
8.4.4 Staring mode . . . 93
8.4.5 Determine the mean off-source background . . . 93
8.4.6 Empirical correction for signal losses in chopped measurements . . . 93
8.4.7 Summation of the in-band powers of all detector pixels . . . 94
8.4.8 Fit two-dimensional Gaussian to point sources in the C-arrays . . . 94
8.4.8.1 Interpolate missing pixels . . . 95
8.4.8.2 Determination of Gaussian parameters . . . 95
8.4.9 Convert in-band power to point source flux density . . . 97
8.4.9.1 All AOTs except PHT40 . . . 97
8.4.9.2 PHT40 . . . 98
8.4.10 Convert in-band power to surface brightness . . . 98
8.4.10.1 All AOTs except PHT40 . . . 98

8.4.10.2 PHT40 . . . 99
8.4.11 Write PHT-P point source photometry product . . . 99
8.4.12 Write PHT-P extended source or raster photometry product . . . 99
8.4.13 Write PHT-C point source photometry product . . . 100
8.4.14 Write PHT-C extended source or raster photometry product . . . 100
8.5 Mapping . . . 100
8.5.1 Establish image pixel size . . . 100
8.5.2 Establish maximum image size . . . 101
8.5.3 Determination of the coverage by a sky sample in the image . . . 102
8.5.4 Binning sky samples onto image pixels . . . 103
8.5.5 Write image products . . . 104
8.6 Spectroscopy . . . 104
8.6.1 Write spectroscopy products . . . 104

**9 Caveats** **105**
9.1 Overview . . . 105
9.2 Caveats on this document . . . 105
9.3 Status of Scientific Validation of PHT AOTs . . . 106
9.3.1 Validated modes in OLP Version 7 . . . 106
9.3.2 Photometric Accuracies of Staring Modes . . . 106
9.4 OLP Version 7: Limitations and Caveats . . . 109
9.4.1 Error Calculation and Propagation . . . 109
9.4.2 Chopped Photometry . . . 110
9.4.3 Extended Source Photometry . . . 110
9.4.4 Spectroscopic Mode . . . 110
9.4.5 Validity Ranges of FCS Calibration Files . . . 111
9.4.6 Inhomogeneous FCS Illumination of PHT-P Apertures . . . 111
9.4.7 Non-geometric Aperture Beam Size Scaling . . . 111
9.4.8 Non-linearity of Detector Responsivity with Flux . . . 111
9.4.9 Detector Signal Transients . . . 111
9.4.10 Long Term Detector Drifts . . . 111
9.4.11 Missing Measurements and Chopper Correction . . . 112
9.4.12 Limitations in Use of PHT Color Correction Factors . . . 112
9.4.13 Empirical PPSF Correction Factors for Array Centered C200 Photometry . . . 112

**10 Getting Started** **113**
10.1 First look at the products . . . 113
10.2 Further processing . . . 113

**11 Guide to Data Products** **114**
11.1 Quick Reference: Synopsis of all ISOPHOT Products . . . 114
11.1.1 ERD Products . . . 114
11.1.2 SPD Products . . . 114
11.1.3 AAR Products . . . 115
11.1.4 Cal G Products: Derive_SPD . . . 116
11.1.5 Cal G Products: Derive_AAR . . . 116
11.1.6 Cal G Products: auxillary . . . 117
11.2 Product Types Sorted by AOT . . . 118

**12 Product Descriptions** **120**
12.1 Overview . . . 120
12.2 ERD product types . . . 120
12.2.1 Rationale behind product design . . . 120
12.2.2 Product PPER . . . 121
12.2.3 Product P1ER . . . 121
12.2.4 Product P2ER . . . 122
12.2.5 Product P2ES . . . 122
12.2.6 Product PSER . . . 122
12.2.7 Product PSTA . . . 123
12.3 SPD product types . . . 125
12.3.1 Rationale behind product design . . . 125
12.3.1.1 General SPD header items I . . . 125
12.3.1.2 Filter dependent SPD header items . . . 126
12.3.1.3 General PHT related SPD header items II . . . 127
12.3.1.4 Product specific SPD header items: PHT05 and PHT25 . . . 127
12.3.2 Product PPxS . . . 127
12.3.3 Product PC1S . . . 128
12.3.4 Product PC2S . . . 129
12.3.5 Product PSSS . . . 130
12.3.6 Product PSLS . . . 130
12.3.7 Product PPxA . . . 131
12.3.8 Product PCxA . . . 132
12.3.9 Product PPxD . . . 133
12.3.10 Product PC1D . . . 133
12.3.11 Product PC2D . . . 133
12.3.12 Pixel status flag . . . 134
12.4 AA product types . . . 135
12.4.1 Rationale behind product design . . . 135
12.4.2 Product PPAP . . . 135
12.4.3 Product PPAE . . . 136
12.4.4 Product PCAP . . . 137
12.4.5 Product PCAE . . . 138
12.4.6 Product PGAI . . . 139
12.4.7 Product PGAU . . . 140
12.4.8 Product PGAT . . . 140
12.4.9 Product PPAS . . . 141
12.4.10 Product PCAS . . . 142
12.4.11 Product PSAP . . . 142
12.4.12 Product PLAP . . . 143
12.4.13 Product PSAE . . . 143
12.4.14 Product PLAE . . . 144
12.4.15 Product PSAS . . . 144
12.4.16 Product PLAS . . . 144

**13 Calibration G Products** **146**
13.1 Overview . . . 146
13.2 Observation time dependent calibration . . . 146
13.2.1 Product PTIMEDEP: PHT calibration time dependency . . . 147
13.3 DIE power calibration tables . . . 147
13.3.1 Product PDIE1TRANS: PHT DIE1 power calibration table . . . 147
13.3.2 Product PDIE2TRANS: PHT DIE2 power calibration table . . . 148
13.4 Selection of read-outs . . . 148
13.4.1 Product PSELNDR: PHT non-destructive read-out selection . . . 148
13.5 CRE linearisation corrections . . . 149
13.5.1 Product PPCRELIN: Linearisations for P1, P2, and P3 . . . 149
13.5.2 Product PC1CRELIN: Linearisations for C100 . . . 149
13.5.3 Product PC2CRELIN: Linearisations for C200 . . . 149
13.6 Signal correction reset interval . . . 149
13.6.1 Product PP1RESETI: parameters for conversion to 1/4s reset interval for P1 . . . 150
13.6.2 Product PP2RESETI: parameters for conversion to 1/4s reset interval for P2 . . . 150
13.6.3 Product PP3RESETI: parameters for conversion to 1/4s reset interval for P3 . . . 150
13.6.4 Product PC1RESETI: parameters for conversion to 1/4s reset interval for C100 . 150
13.6.5 Product PC2RESETI: parameters for conversion to 1/4s reset interval for C200 . 150
13.7 Detector dark signals . . . 150
13.7.1 Product PSDARK: PHT-S dark signals . . . 151
13.7.2 Product PPDARK: dark signals for detectors P1, P2, and P3 . . . 151
13.7.3 Product PC1DARK: dark signals for detector C100 . . . 151
13.7.4 Product PC2DARK: dark signals for detector C200 . . . 151
13.8 Vignetting Corrections . . . 151
13.8.1 Product PP1VIGN: vignetting corrections for P1 . . . 152
13.8.2 Product PP2VIGN: vignetting corrections for P2 . . . 152
13.8.3 Product PP3VIGN: vignetting corrections for P3 . . . 152
13.8.4 Product PC1VIGN: vignetting corrections for C100 . . . 152
13.8.5 Product PC2VIGN: vignetting corrections for C200 . . . 152
13.9 Correction for signal losses in chopped mode . . . 152
13.9.1 Product PPCHOPCOR: chopper correction factors for PHT-P . . . 153
13.9.2 Product PC1CHOPCOR: chopper correction factors for C100 . . . 153
13.9.3 Product PC2CHOPCOR: chopper correction factors for C200 . . . 153
13.10FCS power calibration tables . . . 153
13.10.1Product PP1FCSPOW: PHT-P1 FCS power calibration table . . . 154
13.10.2Product PP2FCSPOW: PHT-P2 FCS power calibration table . . . 155
13.10.3Product PP3FCSPOW_01/02: PHT-P3 FCS power calibration table . . . 155
13.10.4Product PC1FCSPOW_01/02: PHT-C100 FCS power calibration table . . . 155
13.10.5Product PC2FCSPOW_01/02: PHT-C200 FCS power calibration table . . . 155
13.11PHT-P and PHT-C default responsivities . . . 156
13.11.1Product PRESP_01/02: PHT default responsivities for P1, P2 and P3 detectors . 157
13.11.2Product PC1RESP_01/02: PHT default responsivities for the C100 detector . . . 157
13.11.3Product PC2RESP_01/02: PHT default responsivities for the C200 detector . . . 157
13.12Array Illumination by FCS . . . 157
13.12.1Product PC1ILLUM_01/02: FCS illumination for C100 . . . 158

13.12.2 Product PC2ILLUM_01/02: FCS illumination for C200 . . . 158
13.13 Inhomogeneous FCS illumination of PHT-P . . . 158
13.13.1 Product PP1FCSAP: FCS aperture correction tables for P1 . . . 158
13.13.2 Product PP2FCSAP: FCS aperture correction tables for P2 . . . 159
13.13.3 Product PP3FCSAP: FCS aperture correction tables for P3 . . . 159
13.14 Wavelength dependent detector flat fields . . . 159
13.14.1 Product PC1FLAT: PHT C100 filter-to-filter flatfield correction . . . 159
13.14.2 Product PC2FLAT: PHT C200 filter-to-filter flatfield correction . . . 159
13.15 Point spread function corrections . . . 160
13.15.1 Product PPSF: point spread function corrections . . . 160
13.16 PHT-S Wavelength and Signal Calibration . . . 160
13.16.1 Product PSPECAL: PHT-S wavelength and signal calibration . . . 160
13.17 Conversion from power on detector to flux density . . . 161
13.17.1 Product PFLUXCONV: PHT-P/C power calibration . . . 161
13.18 Effective solid angles of apertures and pixels . . . 162
13.18.1 Product PPOMEGA: aperture dimensions and solid angles for P1, P2, and P3 . . . 162
13.18.2 Product PC1OMEGA: dimensions and solid angles for C100 pixels . . . 162
13.18.3 Product PC2OMEGA: dimensions and solid angles for C200 pixels . . . 163
13.19 Colour corrections . . . 163
13.19.1 Product PCCBB: black body $B_\nu(T)$ colour correction . . . 163
13.19.2 Product PCCMBBONE: modified black body $\nu^1 \cdot B_\nu(T)$ colour correction . . . 164
13.19.3 Product PCCMBBTWO: modified black body $\nu^2 \cdot B_\nu(T)$ colour correction . . . 164
13.19.4 Product PCCPOWER: Power law $\nu^\alpha$ colour correction . . . 164

**A Instrument Tables** **165**
A.1 Mean Filter/Aperture Specifications . . . 165
A.1.1 PHT-P Filters . . . 165
A.1.2 PHT-P Apertures . . . 165
A.1.3 PHT-C Filters . . . 165
A.1.4 Other Filterwheel Components . . . 165
A.2 Filter Transmission Data . . . 168

**B Conversion Algorithms for ERD** **169**
B.1 Temperature Sensors . . . 169
B.2 Selected FCS Power . . . 170
B.3 Focal Plane Chopper Deflection . . . 170
B.4 Description of the pixel status flag PIXF in ERD products . . . 172

**C Colour Corrections** **174**
C.1 Application of Tabulated Colour Correction Factors . . . 174
C.2 Computation of Colour Correction Factors . . . 174
C.2.1 Derivation of Flux Density Values from In-band Power Values . . . 174
C.2.2 Flux Density Conversion Factors for Different Spectral Energy Distributions . . . 176
C.2.3 Derivation of Colour Correction Factors from Flux Density Conversion Factors . . . 177

**D Acronyms** **178**

**E Glossary** **179**

# Chapter 1

# Preface

Version 4.0 of the ISOPHOT IDUM should provide all information necessary to understand the ISOPHOT data products as processed by off-line processing (OLP) version 7. Besides OLP software and product specific details, background information is provided about the ISOPHOT instrument itself, signal processing steps, and photometric calibration issues.

Although it has been tried to give as complete as possible ISOPHOT related information, it should be stressed that this manual is not intended for interactive data analysis. For specific algorithms to process and improve the results interactively we refer to the ISOPHOT Interactive Users Manual [9].

We have included cross references in the text wherever possible in view of the fact that a version of this document is also available in HTML.

Version 4.1 includes corrections of errors and omissions mainly spotted by Dr. Y. Sato who performed a thorough reading of the document.

The Authors

# Chapter 2

# How to use this manual

This manual serves as the reference for both the processing as well as the correct interpretation of ISOPHOT data as distributed by the ISO Data Centre. For immediate guidance we present a brief description of the purpose of the coming chapters:

**Chapter 3: Instrument and AOT Overview**

This chapter contains a technical description of the ISOPHOT instrument in the light of data collection. The detector - electronics chain is described in detail as this determines format of the raw data. Additional sections describe the features of optical/calibration systems like chopper, internal reference sources (FCSs), etc. The second part of this chapter provides an overview of the operational steps performed by the AOTs during observations.

**Chapter 4: Instrumental Characteristics**

This chapter describes the known instrumental features and how these can affect the (raw) data. It is recommended to consider this chapter to become aware of the possible instrumental effects before an in-depth astronomical interpretation of the data is carried out.

**Chapter 5: Calibration**

This chapter gives an overview of the photometric calibration of ISOPHOT.

The standard data-processing performed by the ISO observatory is referred to as off-line processing (OLP). The OLP data processing is sub-divided into three processing levels which will be described in detail in the next 3 chapters:

**Chapter 6: Data Processing Level: Derive_ERD**

The derivation of edited raw data (ERD) is described.

**Chapter 7: Data Processing Level: Derive_SPD**

The derivation of standard processed data (ERD) is described.

**Chapter 8: Data Processing Level: Derive_AAR**

The derivation of auto-analysis results (ERD) is described.

**Chapter 9: Caveats**

This is an important chapter since it describes the the applicability of the dataproducts and the limits of scientific interpretation. The observer must have read this chapter before drawing scientific conclusions from the ISOPHOT data.

**Chapter 10: Getting started**

Hints of how to become familiar with the data are described in this chapter.

**Chapter 11: Guide to data products**

This chapter gives an overview of the ISOPHOT data products listed per processing level or per AOT. For each product references to relevant sections in this manual are given.

**Chapter 12: Product descriptions**

The descriptions of the ISOPHOT data products directly related to an AOT can be found in this chapter.

**Chapter 13: Calibration G Products**

Detailed descriptions of the ISOPHOT general calibration files (or "Cal G" files) can be found in this chapter.

In the appendices the following is presented:

**Appendix A: Instrument tables**

Descriptions of the filters, apertures, and polarisers are given as well as their positions on the instrument filterwheels.

**Appendix B: Conversion Algorithms for ERD**

This appendix gives details on conversion algorithms necessary to convert telemetry information to parameters with standard physical units like temperature in K, chopper amplitudes in arcseconds, internal reference sources' heating powers in mW, etc.

**Appendix C: Colour correction**

Formulae are presented to derive colour corrections assuming different (modified) black-body and power-law spectral energy distributions. These relations are used to construct the colour correction (Cal G) products.

**Appendix ??: Acronyms**

This appendix gives a compulation of acronyms used in this document.

**Appendix E: Glossary**

This appendix gives a glossary of frequently used terms.

# Chapter 3

# Instrument and AOT Overview

## 3.1 Overview

The analysis and reduction of ISOPHOT data require a basic knowledge of the instrument itself and the instrument procedures performed during an observation. The way ISOPHOT data is taken is given in section 3.2. This section is of importance to understand the structure of ERD products (section 6). Details are given about the readout electronics and timing control in sections 3.2.2 and 3.2.4. The most important elements of the instrument are described such as the detector subsystems (section 3.4), the internal calibrations sources (section 3.5) and focal plane chopper (section 3.6). In section 3.7 the different steps necessary to perform an ISOPHOT observation are described.

## 3.2 Data Collection with ISOPHOT

### 3.2.1 Signal Flow in ISOPHOT

In this section we introduce the elements related to the ISOPHOT signal flow. For the understanding of the instrument output related to an astronomical observation, systems on both the cold and warm side of the cryostat are of importance, see also Fig. 3.1:

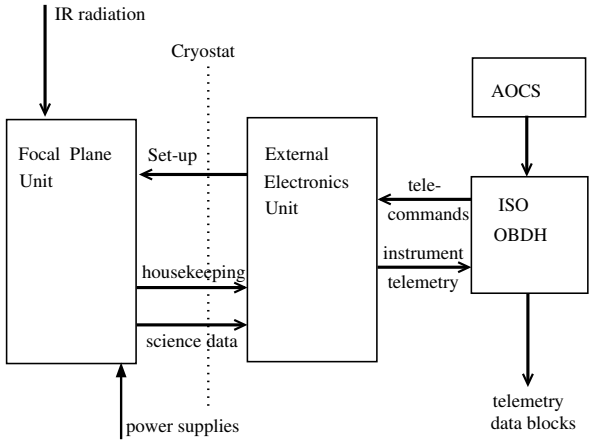


Figure 3.1: Main systems for data collection

- The cold focal plane unit (FPU) inside the cryostat containing the
  - detector subsystems with the cold readout electronics (CRE),

  - the change wheel (CHW) system,
  - the focal plane chopper (FPC), and
  - the internal reference sources (FCSs).

- The warm external electronics unit (EEU) containing
  - the central processing electronics,
  - the readout timing control and voltage supply units, and
  - the detector interface electronics (DIE) of the processing subsystem.

  Telecommands are processed by the central processing electronics. The electronics for the CHWs, temperature control, bias supplies, etc. are in the EEU.

- The ISO on-board data handling system (OBDH) which communicates with the instrument EEU. The instrument telemetry coming from the EEU is combined with the pointing data from the attitude and orbit control system (AOCS) and put in a telemetry block.

### 3.2.2 Cold readout Electronics (CRE)

The function of the Cold readout Electronics (CRE) unit is to pre-amplify and sample the photo-currents generated in the detector. To reach the maximum efficiency, the CRE is integrated on the chip containing the detector. In Fig 3.2, a diagram is presented of the cold electronics chain.

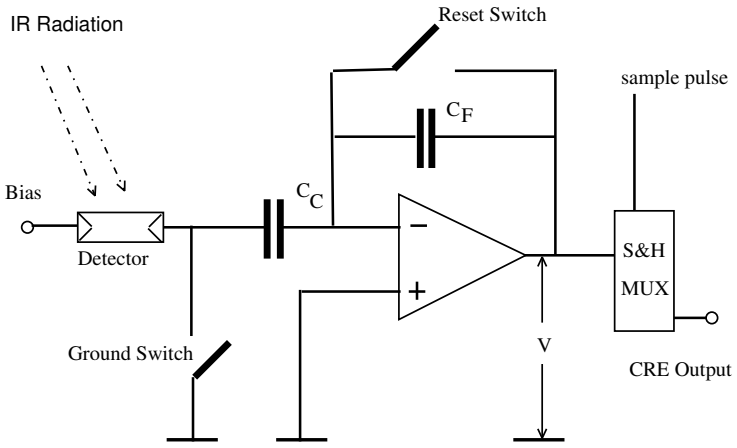


Figure 3.2: Schematic diagram showing the detector - CRE amplifier chain, the capacitance $C_F$ is also denoted by $C_{int}$ in this document.

The Detector/CRE chain in Fig 3.2 represents an integrating amplifier with capacitive feedback. Each detector pixel is connected to one input channel of a CRE. In case the detector is receiving IR photons from an astronomical or internal source, the voltage V at the output of the CRE will increase as a function of time. The voltage increase is proportional to the current through the detector which is in turn proportional to the number of photons falling on the detector. In the remainder of this manual this voltage increase or slope (in V/s) will be referred to as photo-current or *signal*. For the observer the signal is a fundamental concept: once signals from calibration standards have been measured, it is possible to relate the signal to a power from the source in the filterband.

After the amplifier stage there is a sample & hold (S&H) stage. By applying a sample pulse the voltage will be clamped and while the front-end continues to integrate, the clamped signal is read out through a multiplexer (MUX). In that way the readout does not disturb the integration.

Since the output voltage should stay within a limited range, the voltage is reset by short circuiting the capacitors using both the ground as well as reset switch. A reset pulse is applied in addition to a sample pulse after a number of desired voltages have been sampled. The readout associated with this reset is called the *destructive readout*, the other sampled voltages are called *non-destructive readouts* The time between two reset pulses (in seconds) is called the fundamental integration time or *reset interval* (RI). The duration of a reset interval is denoted by $t_{RI}$. All readouts collected during one reset interval are part of one integration ramp or *ramp*. In Fig 3.3, the readout data stream is shown schematically.

The voltage of the first readout after reset is not zero but starts at a arbitrary voltage level. This level is called the *reset level* since it has more or less the same value during a measurement. Variations are caused by instabilities in the amplifier electronics.

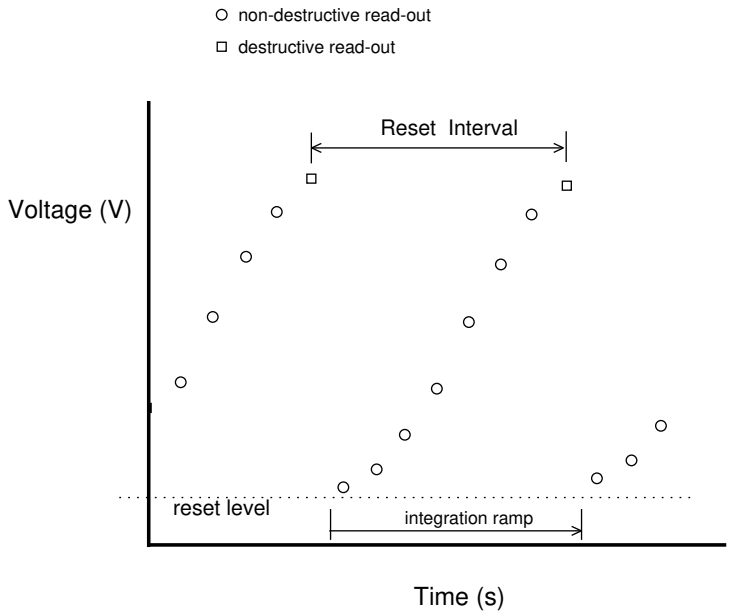


Figure 3.3: Schematic diagram showing CRE output for a ramp of 7 non-destructive readouts (NDR=3)

### 3.2.3 Detector Interface Electronics (DIE)

The detector interface electronics (DIE) acquires the output signals from the CREs and processes these for the telemetry transmission. It also serves as a multiplexer thus reducing the number of output lines. There are two DIEs in the EEU, each interfacing with the following groups of detectors:

- DIE1: C200, P1, P2, and SL
- DIE2: C100, P3, and SS

The DIE subtracts a commandable offset from the CRE output voltage and amplifies the difference with a commandable gain factor. Note that for PHT the gain is a constant unlike other instruments for which the gain is used to adjust the dynamical range.

The DIE also converts the analogue signal from the CRE to a digital signal. This DA conversion produces a 12 bits value per readout which means that each readout has a digitalisation resolution of $2^{12} = 4096$. The fact that there are several readouts per ramp increases the resolution in the signal.

### 3.2.4 readout timing control

To cover a dynamic range equivalent to the flux density range of astronomical sources (a few mJy to hundreds of Jy) within the available commanding bits in the telemetry, the design of the readout parameters has been based on an exponential scale with base 2. Only a power of 2 readouts per reset interval is commanded, and the duration of a reset interval (in seconds) has also be a power of 2. Since there are 4 bits available for commanding, the reset interval can have 16 values ranging from 1/256, 1/128, 1/64, . . . 128 s. Per ramp there are $2^n$ readouts. The last one, the destructive readout, is generally not reliable since it is disturbed by the reset. The number of non-destructive readouts is provided by the parameter *NDR*, it is equal to $2^{NDR} - 1$.

The parameter DR has been defined to set the chopper plateau time. DR is defined such that $2^{DR}$ is equal to the amount of destructive readouts (or number of ramps) per chopper plateau.

The *chopper dwell time* or duration of a chopper plateau $t_{chop}$ can be derived from:

$$t_{chop} = 2^{DR} \times t_{RI}. \tag{3.1}$$

The commanding of PHT imposes at least 4 ramps per chopper plateau, thus DR$\geq$2 for chopped observations. The maximum plateau time is 128 s. The first ramp of a chopper plateau is affected by the chopper transition and therefore unreliable.

For high readout rates the amount of data to be transferred can be too high. In order to avoid telemetry overflow, the parameter *data reduction* (DAT_RED) has been introduced. The value of DAT_RED is an integer indicating that only the first ramp of a sequence of DAT_RED ramps should be transmitted. For example, DAT_RED = 4 means that only the first of every 4 ramps is collected. DAT_RED = 1 indicates no reduction. Observations of bright sources will have a DAT_RED parameter larger than 1. The value of DAT_RED depends not only on NDR and RI, but also on the number of pixels per detector array.

## 3.3 ISOPHOT measurement concept

A PHT measurement comprises all detector readouts telemetered following a "start measurement" command with the instrument in a fixed configuration. A change of instrument configuration can be a change of detector, a change of aperture, a change of filter, a change of polarizer, or a switching-on or -off of the FCS. These changes can only occur *between* measurements and not *during* a measurement. The *measurement time* is the total time necessary to perform a measurement. This time is different from the *integration time* which is defined as the on target time and excludes the time when the background is measured by the chopper in case of a chopped measurement.

Data collected while the spacecraft is performing a raster map belong to the same measurement. The integration time per raster point, or the *raster point dwell time*, the time for the microslews between the

raster points as well as the time to slew back to the initial position after finalizing the raster are included in the measurement time.

Apart from the sky measurements, the observations provide a number of special measurements:

- FCS measurement. All AOTs except PHT40 include at least one FCS measurement, see also chapter 5 sections 5.2.2 and 5.7.2.
- Dark instrument configuration measurement. This measurement type is obtained with AOTs PHT05, PHT25, and PHT40 and is used to subtract dark signals (in case of PHT05 and PHT25) or to identify possible detector memory artifacts from a preceding measurement of a bright source (in case of PHT40).
- Cold FCS measurement. This measurement is used to assess the zero signal level of an accompanying FCS measurement by applying no heating power to the FCS. It is also referred to as "FCS straylight" measurement because parasitic light from the instrument can be measured. The absolute photometry AOTs PHT05 and PHT25 can contain such a measurement.

## 3.4 Detector Subsystems

### 3.4.1 PHT-P

Subsystem PHT-P is a multi-filter, multi-aperture photopolarimeter with 3 single element detectors with wide beam (up to 3 arcmin) capability for faint extended sources. The wavelength coverage is in the range ≈3–130 $\mu$m. The PHT-P detectors are each integrated in an integrating cavity and have a dimension of 1×1×1 mm$^3$. Detector P1 is of Si:Ga, P2 of Si:B and P3 of Ge:Ga.

### 3.4.2 PHT-C

PHT C100 is a 3×3 array of Ge:Ga with 0.7×0.7×1 mm$^3$ elements. Increased photon absorption is achieved by total reflection of a 30° wedged pixel surface and an integrating cavity. The telescope beam is fed into these cavities by 1.9×1.9 mm$^2$ anti reflection coated germanium fabry lenses mounted with spacing 100 $\mu$m which results in an optical fill factor of 93%. The effective size of the pixels on the sky is 43.5×43.5 arcsec$^2$, the distance between the pixel centers ('pitch') is 46.0 arcsec.

Throughout this manual the individual C100 pixels/detectors are labeled as in Table 3.1 where the +Z direction is upwards, and +Y is to the left. This corresponds to the projection of the array on the sky. The numbers (1...9) in Table 3.1 refer to the labeling and array counting in ERD, SPD and AAR products.

PHT C200 consists of 4 pixels arranged in a 2×2 matrix. The telescope beam is concentrated on the four detector pixels by anti-reflection coated germanium Fabry lenses of 3.9×3.9 mm$^2$. The detector crystals are mounted in an integrating cavity and have prismatic shape to increase photon absorption. The sizes of the detector pixels themselves are approximately 1 mm$^3$. The effective size of the pixels on the sky is 89.4×89.4 arcsec$^2$, the distance between the pixel centers is 92.0 arcsec.

The pixels are stressed by individual screws; the stress is maximized to give a cut-off wavelength of 240 $\mu$m. The labeling of the individual C200 pixels is given in Tables 3.2 and 3.3 for the ERD and SPD/AAR convention. The numbers (1...4) in the tables refer to the labeling and array counting in ERD, SPD and AAR products.

Table 3.1: C100 ERD, SPD and AAR pixel labels, +Z is up, +Y is left

| | | |
|---|---|---|
| 9 | 6 | 3 |
| 8 | 5 | 2 |
| 7 | 4 | 1 |

Table 3.2: C200 ERD pixel labels, +Z is up, +Y is left

| | |
|---|---|
| 4 | 3 |
| 1 | 2 |

Table 3.3: C200 SPD and AAR pixel labels, +Z is up, +Y is left

| | |
|---|---|
| 4 | 2 |
| 3 | 1 |

### 3.4.3 PHT-S

PHT-S consists of a dual grating spectrometer with resolving power of order 90 in two wavelength bands. Band SS covers the wavelength range 2.5–4.8 $\mu$m and band SL covers the range 5.8–11.8 $\mu$m. Each spectrometer uses a linear array of 64 element Si:Ga detectors with dimensions of $0.31\times0.37\times1.80$ mm$^3$ per element. PHT-S has one entrance aperture which is square with dimensions $24''\times24''$, this aperture is imaged onto each detector pixel. Two sides are parallel to the spacecraft Y axis, and the dispersion direction is in Z.

## 3.5 Fine Calibration Sources (FCSs)

The internal fine calibration sources act as stable reference sources and are used for photometric calibration of PHT-P or PHT-C observations, see Chapter 5. In terms of data collection, internal calibration measurements are similar to the celestial measurements except that they utilize one of the internal FCSs by imaging it via the chopper mirror, see also section 3.6. All ISOPHOT AOTs except for PHT40 contain one or more FCS measurements depending on the observing mode(s) requested.

There are two identical FCSs which can be operated independently. Each FCS consists of two Thermal Radiation Sources (TRSs): TRS1 is operated in reflecting mode via a mirror whereas TRS2 is operated in a transmitting mode via a beam splitter giving a factor of about 1000 lower flux level than for TRS1. The TRSs are heated diamond wafers, useable at temperatures up to 300 K. By controlling the source temperature between 5 K and 300 K with an accuracy of $\Delta T\approx0.1$ K, different flux levels in the range $5\times10^{-17}$ to $\geq10^{-12}$ W on the detector can be applied to all detectors except for PHT-SS (see section 5). The temperature is accomplished by tuning the heating power on the FCSs.

During the entire ISO mission FCS1 was calibrated against astronomical standards. In practice, FCS1 is used as the main reference source, its emission was directly compared with the flux of celestial standards. FCS2 has been cross calibrated against FCS1. This was accomplished by determining the heating power (in mW) that should be commanded on the FCS in order to mimic the power on the detector from a celestial calibration source (in W). Details of the calibration procedure can be found in Chapter 5.

One FCS measurement is obtained at the end of a sequence of measurements with a given detector subsystem for single pointing photometric observations. In case of multi-filter observations using more than one detector subsystem, several FCS measurements are collected, see section 3.7. For observations using raster mode where the execution of the AOT may be relatively long, the actual measurement is bracketed by two internal calibration measurements.

In AOT PHT40 (spectrophotometry with PHT-S) no FCS measurements are taken because the colour temperature of the FCS is too low to allow an homogeneous illumination of both PHT-SS and PHT-SL. In particular, in order to illuminate PHT-SS sufficiently, PHT-SL would have to be heavily saturated which could lead to long term drifts of the PHT-SL detector afterwards.

## 3.6 Focal Plane Chopper (FPC)

The Focal Plane Chopper (FPC) deflects the beam onto adjacent fields on the sky, or, in case of internal reference measurements, to the FCSs. The chopper can move the beam only along the spacecraft Y direction, positive chopper position commands yield throws in +Y direction. FCS1 is seen by the detectors when the chopper moves the beam beyond the (+) field at $+460''$, FCS2 is seen at $-460''$. The maximum scanning amplitude for the sky is $\pm 180''$. The chopper transition times are given in Table 3.4. The first column indicates the mode: either from the centre-field-of-view (CFOV) to one of the FCSs (FCS mode) or to a sky offset (FOV mode):

Table 3.4: Chopper transition times

| Mode | transition time in ITK units | transition time (s) |
|---|---|---|
| FCS | 832 | 0.051 |
| FOV | 224 | 0.014 |

note: 1 ITK (instrumental time key) unit = $2^{-14}$ sec.

The chopper can be commanded to operate in staring mode (i.e. one position for the whole measurement) or in chopped mode whereby two or more viewing directions may be chosen during a measurement. In the AOTs three distinct chopper modes can be selected:

- RECTANGULAR mode implies chopping between 1 reference position and the source position with an equal time spent on the reference and source positions. The reference offset is in –Y direction. The telescope pointing is not on target but located in the middle between the source and the reference position.
  ▷ A chopper cycle consists of 2 consecutive chopper plateaus:
  ref1⇒on-source.

- SAWTOOTH mode implies chopping between 2 reference positions and the source position with equal time spent on all 3 positions. The source position is coincident with the telescope pointing direction, and between the 2 reference positions.
  ▷ A chopper cycle consists of 3 consecutive chopper plateaus:
  ref1⇒on-source⇒ref2.

- TRIANGULAR mode implies chopping between 2 reference positions and the source position with a time equivalent to that spent on the source position split equally between the 2 reference positions. The source position is coincident with the telescope pointing direction, and between the 2 reference positions.
  ▷ A chopper cycle consists of 4 consecutive chopper plateaus:
  ref1⇒on-source⇒ref2⇒on-source.

The first chopper position in the above cases is an off-position in –Y direction. There are strong constraints for the chopper throw which are listed in [10] pages 23-25.

The chopper mode and amplitude is fixed per AOT and not per measurement. For AOT PHT32 the chopper is indirectly commanded depending on the detector (C100 or C200) one chooses. In the case of C100 the chopper is commanded to perform in sawtooth mode 13 chopper steps with 15" separation symmetrically with respect to the centre field if view. When C200 has been chosen, the chopper is commanded to perform in sawtooth mode with 7 chopper steps with 30" separation.

## 3.7 ISOPHOT Modes of Operation

In this section summaries of the logic behind the ISOPHOT AOTs are given. Only those operations that may be relevant for data processing are mentioned. Details on the parameters to be entered by

the observer are described in the ISOPHOT Observer's Manual [10]. For details on the the filter wheel settings see section A.1.

### 3.7.1 PHT-P: PHT03, PHT04, PHT05, PHT17/18/19

#### 3.7.1.1 PHT03

PHT03 includes the following operations:

1. Pointing procedure, pointing:

   - on source in case of single pointing observations except when rectangular chopped mode is requested;
   - in between the source position and the chopper position in case of rectangular chopper mode;
   - on the first raster point in case of raster maps (see below).

   Repeat points 2 - 5 for all detector assemblies selected:

2. In case of detectors P2 and P3, switch on heating and wait for heating stabilization. Activate detector.

   Repeat points 3 - 4 for each filter using the activated detector

3. Rotate the filter and aperture wheels to the commanded configuration, optimised to instrument requirements.

   To minimize memory effects of the detectors the measurements with the different filter/aperture combinations are performed according to increasing power on the detector. PGA should have warned the observer if the ratio between the highest and the lowest flux on one detector for the selected filter/aperture combinations is higher than 1000. Such a flux combination within one AOT could lead to poor calibration. In order to minimize heating and cooling stabilization times in multi-detector mode, the detectors are used in the order:

   ```
   P3 -> P1 ->P2
   ```

4. Integrate on the source for the specified or calculated exposure time. A measurement is performed in staring mode or one of the three following chopped modes:

   ```
   (i) RECTANGULAR
   (ii) SAWTOOTH
   (iii) TRIANGULAR
   ```

   In staring mode the observer has to provide an appropriate reference field measurement for background subtraction, which is not part of this AOT.

5. The internal calibration is performed with the last filter/aperture combination used with the current detector. This means that there will be one FCS calibration per detector used. If the observation is in staring mode a staring measurement on FCS1 is performed. If the sky is measured in any chopper mode, both FCS's are measured in rectangular chopped mode; FCS1 is tuned close to the [source+background] power, FCS2 close to the background power as given by the user.

   After calibration, the FCS's are switched off.

6. After the last integration, the electronics are set to standby and the instrument is reconfigured to the default state which is the C200 serendipity mode configuration.

PHT03 in raster mode:

For raster mode measurements, only one detector can be chosen per AOT. If more than 1 filter is selected the measurements are sorted according to increasing power on detector. While PHT is measuring, the spacecraft independently performs a raster map giving no feedback to PHT on the pointing progress in the raster. To synchronize the spacecraft rastering and the instrument data collection, the AOT logic already calculated the total time necessary to perform a complete raster including the microslews. After the elapse of that time the integration is stopped by a "pulse command" (a high priority interrupt to the PHT microprocessor) which also switches off all electronics including the detector heaters. After the pulse command a reinitialisation of the instrument is necessary, this is reflected in the AOT operations.

1. In case of a heated detector, switch on heating and wait for heating stabilization. Activate detector.

   Repeat points 2 - 6 for each filter:

2. Rotate the filter and aperture wheels to the commanded configuration.
3. An internal calibration on FCS1 is performed in staring mode. After the calibration FCS1 is switched off.
4. Set the instrument integration time such that it covers the time needed to perform a full raster map with the specified raster point integrations requested by the user. The spacecraft is commanded to perform a raster according to the requested parameters. PHT is collecting data during the raster slews. The raster point ID and the on-target flag are recorded to reconstruct where the spacecraft was pointing.
5. After the raster has been completed the integration is halted by a pulse command. This pulse command also stops the electronics. The detector is activated again and in case of a heated detector, a stabilisation heating time is included.
6. An internal calibration on FCS1 is performed in staring mode. After the calibration FCS1 is switched off.
7. After the last integration, the electronics are set to standby and the instrument is reconfigured to the default state which is the serendipity mode configuration.

#### 3.7.1.2 PHT04

PHT04 includes the following operations:

1. Pointing procedure, pointing:
   - on source in case of single pointing observations except when rectangular chopped mode is requested;
   - in between the source position and the chopper position in case of rectangular chopper mode;
2. In case of a heated detector, switch on heating and wait for heating stabilization. Activate detector.
3. Rotate filter wheel to the position of the required spectral bandpass

   Repeat points 4 - 5 for each aperture

4. Rotate the aperture wheel to the respective aperture configuration. Measurements will be ordered with increasing power on the detector, i.e. with increasing APERTURE size.
5. Integrate on the source for the specified (or calculated) integration time. Measurement is performed in staring mode or one of the three following chopped modes:

(i) RECTANGULAR
(ii) SAWTOOTH
(iii) TRIANGULAR

6. The internal calibration is performed with the last aperture used with the current detector. This means that there will be one FCS calibration per detector used. If the observation is in staring mode a staring measurement on FCS1 is performed. If the sky is measured in any chopper mode, both FCS's are measured in rectangular chopped mode; FCS1 is tuned close to the [source+background] power, FCS2 close to the background power as given by the user.

   After calibration, the FCS's are switched off.

7. After the last integration, the electronics are set to non-prime- state and the instrument is reconfigured to the default state.

#### 3.7.1.3 PHT05

For the absolute photometry AOT PHT05 only one filter and one aperture can be selected. Chopped and/or raster mode is not possible.

1. Pointing on target
2. In case of heated detector, switch on heating and wait for heating stabilization. Activate detector.
3. If a dark measurement is requested then
   - rotate the filter and aperture wheels to the dark instrument configuration for the requested subsystem (see Table 3.5)
   - perform a dark measurement of 256 s
4. Rotate the filter and aperture wheels to the commanded configuration
5. If a cold FCS measurement is requested then
   - perform an internal calibration measurement of 256 s in staring mode of FCS1 with zero electrical power applied
6. Perform the sky measurement
7. Perform the calibration measurement in staring mode on the heated FCS1 with an measurement time equal to the sky measurement. After the calibration the FCS1 is switched off.
8. The electronics are set to standby and the instrument is reconfigured to default mode.

Note that the dark instrument configuration is different for the different P detectors in order to ensure that no (stray-)light can reach the detector, see Table 3.5 for the selected filterwheel settings. The mnemonics given in the table are explained in section A.1.

#### 3.7.1.4 PHT17/18/19

PHT17 initiates the following operations:

1. Pointing on requested position

   Repeat points 2 - 3 for each filter using the selected detector

2. Rotate the filter and aperture wheels to the commanded configuration, optimised according to instrument requirements. To minimize memory effects of the detectors the measurements are sorted according to increasing power on the detector. The measurements with the different filters are performed in the same order. The selected filters must belong to the same detector.

Table 3.5: Filterwheel settings for dark measurements in AOTs

| Detector | Wheel I mnemonic | Wheel II mnemonic | Wheel III mnemonic |
|---|---|---|---|
| P1 | PHT_S | 5_SEC | P3_100_UM |
| P2 | PHT_S | 5_SEC | P1_3P29_UM |
| P3 | PHT_C_NO_POL | 5_SEC | P1_11P5_UM |
| C100 | PHT_S | C200_200_UM | P3_100_UM |
| C200 | PHT_S | C100_50_UM | P3_100_UM |
| SS/SL | PHT_P_NO_POL | 180_SEC | P1_7P3_UM |

3. Integrate on the source for the specified (or calculated) integration time. Measurement is performed in staring mode.

4. The internal calibration is performed in staring mode on FCS1 with the last filter of the selected detector. After the calibration, FCS1 is switched off.

PHT18 initiates the following operations:

1. Pointing on requested position

   Repeat points 2–3 for each filter using the activated detector

2. Rotate the filter (and aperture) wheel(s) to the commanded configuration, optimised according to instrument requirements. The measurements are sorted according to increasing power on the detector.

3. Integrate on the source for the specified (or calculated) integration time.

PHT19 initiates the following operations:

1. Pointing on requested position

   Repeat points 2–3 for each filter using the activated detector

2. Rotate the filter (and aperture) wheel(s) to the commanded configuration, optimised according to instrument requirements.

3. Integrate on the source for the specified (or calculated) integration time.

4. At the end of the filter sequence a calibration measurement is performed in the last filter in staring mode on FCS1.

5. The electronics are switched to standby and the instrument is reset to the default configuration

All measurements are performed in staring mode, thus the observer has to provide an appropriate reference field measurement for background subtraction, which may be one or more measurements in the sequence.

Prior to PHT18, a PHT17 must have been performed. After the last PHT18 has been done, a PHT19 is performed. Prior to a PHT19, a PHT17 must have been performed. During the whole sequence the detector remains activated, but the measurements are only performed on the target positions.

### 3.7.2 PHT-C: PHT22, PHT25, PHT32, PHT37/38/39

#### 3.7.2.1 PHT22

PHT22 initiates the following operations:

1. Pointing procedure, pointing:

   - on source in case of single pointing observations except when rectangular chopped mode is requested;
   - in between the source position and the chopper position in case of rectangular chopper mode;

   Repeat points 2 - 5 for all detector assemblies selected:

2. Switch on heating and wait for heating stabilization in case C100 is used. Activate detector.

   Repeat points 3 - 4 for each filter using the activated detector

3. Rotate the filter and aperture wheels to the commanded configuration, optimised according to instrument requirements. If filters of both C100 and C200 are requested, detectors will be operated in the following order:

   ```
   C200 -> C100
   ```

   To minimize memory effects of the detectors the measurements per detector are performed according to increasing power on the detector.

4. Integrate on the source for the specified (or calculated) integration time. The measurement is performed in staring mode or chopped mode. If only filters of the C100 filter set are selected one of the three following chopped modes is possible:

   ```
   (i) RECTANGULAR
   (ii) SAWTOOTH
   (iii) TRIANGULAR
   ```

   If at least one filter of the C200 filter set is selected, the chopper mode is automatically restricted to RECTANGULAR chopping with 180″ throw. In staring mode the observer has to provide an appropriate reference field measurement for background subtraction which is not part of this AOT.

5. The internal calibration is performed with the last filter used with the current detector. This means that there is one FCS calibration per detector used. If the observation is in staring mode a staring measurement on FCS1 is performed. If the sky is measured in any chopper mode, both FCS's are measured in rectangular chopped mode; FCS1 is tuned close to the [source+background] power, FCS2 close to the background power as given by the user.

   After calibration, the FCS's are switched off.

6. After the last integration, the electronics are set to non-prime state and the instrument is reconfigured to the default state.

PHT22 in raster mode (restricted to filter sets belonging to either C100 or C200):

Procedure is identical to the raster logic presented for PHT03.

#### 3.7.2.2 PHT25

See description of PHT05. The available detectors are C100 and C200 for which C100 needs heating. The cold measurement time in the case of C200 is 128 s instead of 256 s.

#### 3.7.2.3 PHT32

PHT32 initiates the following operations:

1. Pointing on the first raster point
2. Activate either PHT C100 or C200 depending on selection of filters and wait for stabilization of the detector in case C100 has been selected.

   Repeat steps 3-7 for all filters:

3. Rotate the filter wheel to the commanded filter position.
4. An FCS1 calibration measurement is performed in staring mode.
5. Set the instrument integration time such that it covers the time needed to perform a full raster map with the specified raster point integrations requested by the user. The spacecraft is commanded to perform a raster according to the requested parameters. On each raster position a number of chopper sweeps are performed. PHT is collecting data during the raster slews.
6. After the raster has been completed the integration is halted by a pulse command (see PHT03 raster description). This pulse command also stops the electronics. The detector is activated again and in case of a heated detector, a stabilisation heating time is included.
7. The map is concluded by a repetition of an FCS1 calibration measurement in the last commanded filter at the last raster position.
8. After the last filter, the electronics are set to standby and the instrument is reconfigured to the default state.

#### 3.7.2.4 PHT37/38/39

The PHT37 AOT is the first AOT in the cocatenated sequence PHT37, [PHT38], PHT39 which form the sparse map. It initiates the following operations:

1. Pointing on requested position
2. For C100 switch on heating and wait for heating stabilization. Activate detector.

   Repeat points 3 - 4 for each filter using the activated detector. To minimize memory effects of the detectors the measurements are sorted to increasing power on the detector.

3. Rotate the filter wheel to the commanded configuration, optimised according to instrument requirements.
4. Integrate on source for the specified (or calculated) integration time.
5. Perform calibration in staring mode on FCS1.

PHT38 will initiate the following operations:

1. Pointing on requested position

   Repeat points 2–3 for each filter using the activated detector To minimize memory effects of the detectors the measurements are sorted to increasing power on the detector.

2. Rotate the filter wheel to the commanded configuration, optimised according to instrument requirements.
3. Integrate on the source for the specified (or calculated) integration time.

PHT39 is the last AOT in the concatenated sequence PHT37, [PHT38], PHT39 which form the sparse map. It will initiate the following operations:

1. Pointing on requested position

   Repeat points 2–3 for each filter using the activated detector To minimize memory effects of the detectors the measurements are sorted to increasing power on the detector.

2. Rotate the filter wheel to the commanded configuration, optimised according to instrument requirements.

3. Integrate on source for the specified (or calculated) integration time. Measurement is performed in the staring mode, thus the observer has to provide an appropriate reference field measurement for background subtraction, which may be one or more positions in the sequence.

4. Perform calibration measurement in staring mode on FCS1.

5. Switch electronics to standby and reset instrument to default configuration.

The minimum number of sparse maps is two: one PHT37 followed by one PHT39.

### 3.7.3 PHT-S: PHT40

PHT40 will initiate the following operations:

1. Pointing procedure, pointing:

   - on source in case of single pointing observations except when rectangular chopped mode is requested;
   - in between the source position and the chopper position in case of rectangular chopper mode;
   - on the first raster point in case of raster mapping.

2. Activate detectors

3. Rotate wheels to configure DARK configuration for PHT-S (see Table 3.5).

4. Integrate in dark position for the specified dark current measurement time of 32 s. Measurement is performed in staring mode.

5. Rotate wheels to configure beam path to PHT-S.

6. Integrate on the source for the specified (or calculated) integration time. Measurement is performed in staring mode or one of the three following chopped modes:

   ```
   (i) RECTANGULAR
   (ii) SAWTOOTH
   (iii) TRIANGULAR
   ```

7. After the integration the electronics are set to standby and the instrument is reconfigured to the default state.

PHT40 in raster mode:

Start with points 2– 6 at first raster position. Set the integration time such that it is longer than the time to perform the requested raster map. Perform point 6 in staring mode. After the raster has been completed the integration is halted by a pulse command (see PHT03 raster description). The instrument is measuring during micro-slews. Proceed with point 7.

### 3.7.4 Polarisation Observations: PHT50, PHT51

#### 3.7.4.1 PHT50

For PHT50 only the 25 $\mu$m filter can be used with the 79″ aperture. The logic rounds the requested integration time per polariser to the nearest higher multiple of 128 s with a minimum of 256 s. A description of CHW1 (change wheel I) is given in section A.1.4. PHT50 initiates the following operations:

1. Pointing on target
2. Switch on heating, wait for heating stabilisation, and activate P2
3. Rotate the filter to P_25 and aperture wheel to 79″

   repeat steps 4–6 to accumulate the requested integration time per polariser
4. Rotate CHW1 to PHT-P polariser 1 (0°) and perform measurement of 128 s
5. Rotate CHW1 to PHT-P polariser 2 (120°) and perform measurement of 128 s
6. Rotate CHW1 to PHT-P polariser 3 (240°) and perform measurement of 128 s
7. Rotate CHW1 to PHT-P polariser 1 (0°) and perform measurement of 128 s
8. Rotate CHW1 to PHT-P 'no polariser' position and perform a sky measurement of 128 s
9. Perform the calibration measurement in staring mode on the heated FCS1 with an measurement time of 128 s. After the calibration the FCS1 is switched off.
10. The electronics are set to standby and the instrument is reconfigured to default mode.

The additional measurement in the 0° polariser at the end of the polariser cycle is introduced to correct for long term drifts of the P2 detector.

#### 3.7.4.2 PHT51

For PHT51 only the C200 detector array with the 170 $\mu$m filter can be used. The logic rounds the requested integration time per polariser to the nearest higher multiple of 128 s with a minimum of 256 s. A description of the first filterwheel (CHWI) is given in section A.1.4. PHT51 initiates the following operations:

1. Pointing on target
2. Activate the C200 detector
3. Rotate the filterwheel 2 to C_160
   repeat steps 4–6 to accumulate the requested integration time per polariser
4. Rotate CHW1 to PHT-C polariser 1 (0°) and perform measurement of 128 s
5. Rotate CHW1 to PHT-C polariser 2 (120°) and perform measurement of 128 s
6. Rotate CHW1 to PHT-C polariser 3 (240°) and perform measurement of 128 s
7. Rotate CHW1 to PHT-C 'no polariser' position. and perform a sky measurement of 128 s
8. Perform the calibration measurement in staring mode on the heated FCS1 with an measurement time of 128 s. After the calibration the FCS1 is switched off.
9. The electronics are set to standby and the instrument is reconfigured to default mode.

In many cases the full sequence is repeated in a 2×2 raster map with 1 pixel displacement and the source centred on each pixel. This yields a 4-fold redundancy for the central position of the resulting 3×3 raster map. This method gives the highest source to background contrast and provides a consistency check from the results of the 4 individual pixels.

# Chapter 4

# Instrumental Characteristics

## 4.1 Overview

The ISOPHOT data processing contains several corrections due to the proporties of the detector, due to instrumental effects by the electronics and optics, and due to external effects such as cosmics. In this chapter are described the effects that could lead to a better understanding of the data and of the photometric calibration. Most of the effects have been studied by the instrument dedicated team. Since the investigations are ongoing updates on several issues are expected. The descriptions start with the detector and its properties in section 4.2, the features generated by the instrument electronics in section 4.3, and ionizing radiation effects in section 4.4 which have a dramatic impact on the detectors. Subsequently the optical (section 4.5), spectral (section 4.6), and straylight performance (section 4.7) are discussed. Finally, we mention the instrumental polarisation (4.8) and the influence of the background on the photometric data (section 4.9).

## 4.2 Detector Properties

### 4.2.1 Detector Responsivity/Linearity

All ISOPHOT detectors are photoconductors. Therefore the crucial calibration measure is the photocurrent generated by the incident infrared photons. A detector is characterised by the *detector responsivity* $R_{det}$ which is the ratio between the photocurrent $I$ and in-band power $P_{src}$:

$$R_{det} = \frac{I}{P_{src}} \qquad (A/W). \tag{4.1}$$

In the first stage of data collection the output voltage from an integrating amplifier is measured. From these data the *signal* or voltage increase per unit time is obtained, see Chapter 3. The in-band power can be derived from signal and responsivity if the capacitance of the integration capacitor, $C_{int}$, is known:

$$P_{src} = \frac{C_{int} s_{src}}{R_{det}} \qquad (W), \tag{4.2}$$

where $s_{src}$ is the source signal in V/s. The value for $C_{int}$ depends on the detector used and is assumed to be constant throughout the mission. $R_{det}$, however, is not a constant and can depend on external parameters such as the strength of the ionizing radiation and flux history.

In principle, FCS measurements scheduled in all PHT-P and PHT-C AOTs should ensure that $P_{src}$ can directly be obtained from the comparison between the sky and the FCS signal without knowledge of the exact value of $R_{det}$.

FCS measurements are obtained in all ISOPHOT AOTs except P40. However, for some observations the FCS measurements can be of insufficient quality, or, in the case of P40, completely absent. In such cases a default responsivity should be adopted.

The default detector responsivities were derived during the in-orbit calibration. The values of the default responsivities are provided in Cal G files, see section 13.11. The relationships between FCS heating power and the corresponding in-band power measured by the different detectors are also given in the Cal G files.

A detector is linear if Eqn. 4.1 is independent in-band power on the detector. Deviations from linearity introduce a bias when deriving the responsivity from the FCS measurement or when using a single (default) value for $R_{det}$. To avoid this bias the FCS signal is tuned close to the source signal by the AOT logic. This strategy may fail in the following cases:

- multi-aperture photometry,
- multi-filter photometry with the same detector on sources with a strong spectral gradient or a mixture of narrow and wide bands,
- maps and scans for which the source-background contrast is high.

In these cases the dynamic range of the signals is high whereas the calibration is performed by one or more FCS measurements using a single heating power.

In case of a PHT-S observation with AOT PHT40 no FCS measurement is performed (cf. section 3.5). The PHT-S signals are directly converted to fluxdensities assuming constant responsivities for each pixel. The Cal G file containing the conversion factors for each PHT-S pixel is described in section 13.16. The conversion factors for each pixel are derived by frequent observations of a number of calibration stars. Due to this procedure detector non-linearities can influence the PHT-S results. Currently, these effects are under investigation.

The above description of the detector responsivity is still idealised and is only valid for responsivity values averaged over timescales longer than the measurement time. On shorter timescales the responsivity can still vary. The stability of the responsivity depends on the radiation history including the history of ionisation radiation. Detailed descriptions of the most important phenomena are presented in the next section.

### 4.2.2 Transient behaviour after flux change

After an illumination change, the output signal of a PHT detector shows a systematic drift in time. Such a drift effect is also referred to as a detector *transient*. A common feature to all transient curves is the asymptotic approximation to a stable level. This typical slow response is due to the presence of low ohmic contact material necessary to connect the detector substrate with the metallic wires.

Typical drift curves are presented in Fig. 4.1. In case of a flux drop a signal decay and in case of increasing flux steps a signal rise (Fig. 4.1) is observed. The doped silicon detectors (SS, SL, P1, and P2) exhibit a *hook response* during the first 40 seconds after large positive flux steps (Fig. 4.1b). The signal shows a behaviour similar to a strongly damped oscillation around the asymptotic level. For even higher flux steps the signal behaviour can be restricted to an overshoot followed by a slow decay.

The characteristic stabilisation time scales depend on (1) the detector material, (2) the flux change, (3) the illumination level, and (4) the temperature of the detector. They vary from a few seconds up to several minutes.

Typical timescales for stabilisation after a given flux step for the PHT-SS/SL detectors are presented in Table 4.1. These timescales can be taken as approximate values for detector P2 and lower limits for P1. The stabilisation time is defined as the time after flux step to reach 90 % of the signal at $t = \infty$ ($S_\infty$).

Note that a signal of 0.5 mV/s is very close to the dark signal and - in practice - cannot be determined accurately. The relative stabilisation time is faster for positive flux steps - cf. table values below the diagonal versus those above the diagonal. Flux steps at low flux levels will take more time to stabilise. However in such cases the S/N and the detector stability (see next section) might be more important.

The doped germanium detectors P3 and C100 tend to stabilise faster than the doped silicon detectors. C200 shows the shortest transient time scales. Typical time scales are 100 sec for P3 and C100 and 40 sec for C200.

Table 4.1: Stabilisation times for a given flux step in seconds. The first row lists the initial signal, the first column the final signal in V/s

| | 5.e-4 | 0.001 | 0.01 | 0.1 | 1 | 10 |
|---|---|---|---|---|---|---|
| 5.e-4 | ... | 6800 | 11500 | 11880 | 11900 | 11900 |
| 0.001 | 4070 | ... | 5570 | 5900 | 5960 | 5960 |
| 0.01 | 1500 | 1220 | ... | 560 | 592 | 595 |
| 0.1 | 240 | 210 | 122 | ... | 55 | 59 |
| 1 | 32 | 30 | 21 | 12 | ... | 5 |
| 10 | 4 | 4 | 3 | 2 | 1 | ... |

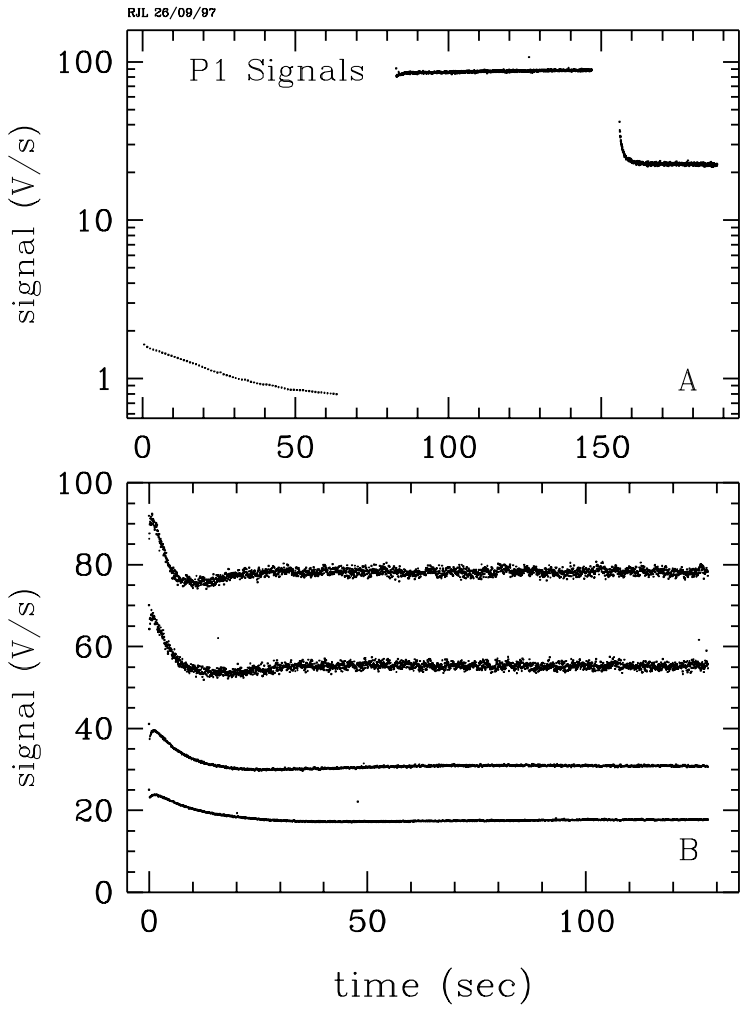


Figure 4.1: Examples of P1 detector transients. Upper panel (A): multi-filter observation of the star HR6705, filter sequence P_16 (64 sec integration), P_3.6 (64 sec) followed by the P_3.6 (32 sec) FCS measurement. Both the P_16 as well as the P_3.6 FCS measurement show a downward drift, with a longer stabilization time for the fainter P_16 signal. Lower panel (B): 4 transient curves after a flux step overplotted in the same graph for comparison, the highest curve corresponds to the largest positive flux step. In all cases the signal prior to each step was the same and had a strength of about 35 V/s. For these flux steps a signal overshoot is detected followed by a strongly damped oscillation.

For chopped measurements the same drift behaviour description applies. Due to the chopper modulation, the signal evolution on each chopper plateau can be regarded as a drift curve after a flux step. Consequently, the difference signal between the on- and off-target chopper plateaux is not only a function of flux step but also a function of chopper frequency. Without applying drift corrections use of the difference signal seriously underestimates the actual flux of the target. It has been observed that the signal differences between neighbouring chopper plateaux remain stable, even in case of a measurement containing a general drift (see section 4.2.3), provided that the flux difference between the chopper plateaux is less than 50% of the total signal. An example of a chopped measurement with P2 is presented in Fig. 4.2.

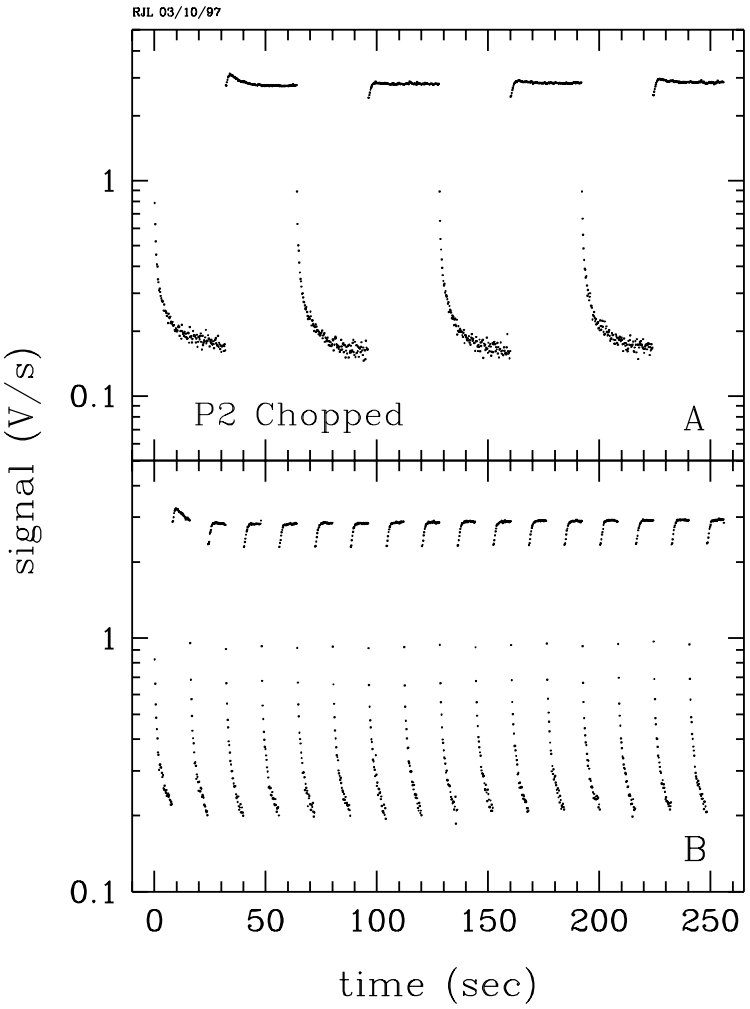


Figure 4.2: Examples of P2 detector transients induced by the chopper modulation on a very high source-background contrast. Upper panel (A): slow (32 sec per chopper plateau) chopped measurement on a high source-background contrast. Lower panel (B) same source-background contrast as under (A) but with a a higher chopper frequency (8 sec per plateau). Note the strong overshoot in the first higher plateau; a straight signal average per chopper plateau would underestimate the background subtracted source signal in both cases

PHT32 uses the chopper in the sawtooth mode to obtain oversampled maps. Detector transients of bright sources can introduce ghost images in neighbouring areas. This can happen when a bright source is observed at the end of a sawtooth sweep. When the chopper is directed back to the starting point the transient causes an increased signal which is measured at the beginning of the next chopper sweep. The signal decays with the relevant time scale thereby mimicing a point source detection. Consequently, the ghost is always displaced from the bright source by $180''$ (=amplitude of the chopper sweep) in Y-direction.

The study of transients have led to the development of an PHT AOT logic which should minimise disturbing effects by detector transients:

1. in multi-filter observations the measurements for a given detector are sorted according to increasing power on the detector (see section 3.7).
2. in multi-aperture photometry P04 the measurements are arranged according to increasing aperture size.
3. the absolute photometry AOTs P05 and P25 comprise of relatively long (64 to 128 sec) staring measurements in order to ensure a stable signal at the end of each measurement.
4. each PHT-S observation (P40) starts with a dark signal measurement to assess the presence of possible transients still present from a previous observation of a bright target.
5. telescope nodding has been made available to achieve repeated quasi-staring observations between target and one or more background positions. Nodding is suitable for photometry of relatively bright targets for which the high frequency of the chopper can cause serious transient effects. The nodding mode is in essence PHT03/PHT22/PHT40 raster mode for which the step in spacecraft Z-direction is set to $0''$.

Not every measurement will last long enough to provide a stabilised signal. Laboratory and in-flight measurements showed that the transient curves are reproducible under the same flux conditions. Methods to correct for these transient drifts based on physical models as well as on empirical results are currently under development by the PHT instrument dedicated team.

For the present OLP software (Version 7) no sophisticated treatment of transients is applied. Instead, an algorithm is used which determines per chopper plateau whether a significant signal drift is present. In case such a drift is found, the last stable part of a chopper plateau is used (see also section 7.3.5).

A description of detector transients tested against the doped silicon detectors (PHT-S and PHT-P) can be found in Schubert et al. 1995 [27]) and Acosta-Pulido et al. 1999 [1]. C200 detector transients have been studied by Wilke [36]). A study of in-orbit transients and descriptions of correction methods and practical recipes are presented in Acosta-Pulido et al. 1999 [1].

### 4.2.3 Drift behaviour of responsivity

Besides the transient behaviour, the responsivity of a detector can vary or *drift* on timescales ranging from less than an hour up to the entire science window of 16 hours (see ISO Satellite and Data Manual [17]). Responsivity drifts are mainly observed for the doped germanium detectors (P3, C100 and C200) and are a result of both the illumination history of the detector as well as the rate of ionising radiation falling on the detector, see also section 4.4.

Ionising radiation causes the detector responsivity to *increase* in time. This increase can be as high as 80%, 100% and 30% for P3, C100, and C200, respectively. The responsivity drift for these detectors is steeper at the end of the science window where the amount of ionizing radiation rapidly increases. Long integrations with the same detector can be affected by this effect. Examples are multi-filter photometry with PHT22 and multi-aperture photometry with P3 in PHT04. For large (raster) maps available in AOTs P03, P22, P32, and in the sparse map modes P17/18/19 and P37/38/39, the responsivity drift can be assessed from the two FCS measurements collected at the beginning and end of each map. For polarisation observations the polarisers are cycled with a cycle time of at most 128 sec per polariser to assess the long term stability of the detector during the observation.

On the other hand, very high flux levels in excess of 5 V/s for P3 and C100, and 10 V/s for C200 can cause the detector to cure during the measurement (see also section 4.2.4). The resulting effect is a *decrease* of the detector responsivity during the measurement. This decrease can amount to several percent up to a factor 1.5 of the initial responsivity. Such drifts are very difficult to correct for.

The observed responsivity drifts for the doped silicon detectors P1, P2 and PHT-SS/SL are less than 20% over the entire science window.

### 4.2.4 Curing Procedures

Due to the high ionizing radiation during perigee passage of ISO the responsivities and noise levels of the ISOPHOT detectors are strongly increased before the beginning of the new science window. Therefore different *curing procedures* have been designed for different detectors to restore the nominal responsivities. The procedures are applied after switch-on before the beginning of the science window.

For the doped germanium detectors (P3, C100 and C200) a combination of bias boost (absolute increase of the bias voltage) and two to three infrared flashes using one of the FCSs are applied. For the doped silicon detectors (SS, SL, P1, and P2) curing is achieved by exposing the detector to a higher temperature at a reduced bias voltage for a defined period of time. In addition, P1 undergoes a flash curing.

The doped germanium detectors are much more susceptible to drifts caused by accumulating effects of the high energy radiation impacts (section 4.4). In order to keep their responsivities within the nominal range a second curing procedure is applied around apogee passage in the hand-over window when the satellite control is switched from VILSPA (Madrid) to Goldstone (California) (see [17]). More about the effects of ionizing radiation inside the science window is described in section 4.4.

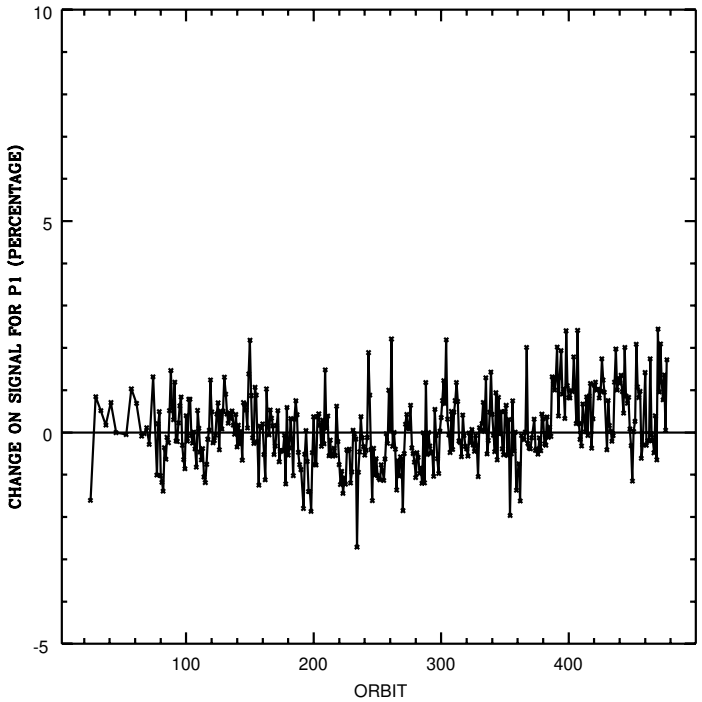


Figure 4.3: The relative variation of the responsivity of the P1 detector with respect to the mean value as a function of revolution number for the first 500 ISO revolutions. Each revolution lasts to good approximation 23 hours and 56 min.

Trend analysis of responsivity measurements performed immediately after the curing procedures indicates that the nominal responsivities are reestablished with ±2% accuracy for all detectors if the space environment conditions are stable.

The doped silicon detectors are not very sensitive to geomagnetic storms. Typical responsivity variations for detector P1 are shown in Fig 4.3. It shows that the responsivity can be restored to better than 2% off the mean value. A long term variation can be noticed which is possibly correlated with the position of the Earth with respect to the Sun.

The doped germanium detectors are more sensitive to the space environment with variations in the responsivity between 20-50% during geomagnetic storms. A striking example is given in Fig 4.4 where the C200 responsivity variations are shown. C200 responsivity peaks can last for several revolutions. They are correlated in time with the geomagnetic storm activity induced by solar flares.

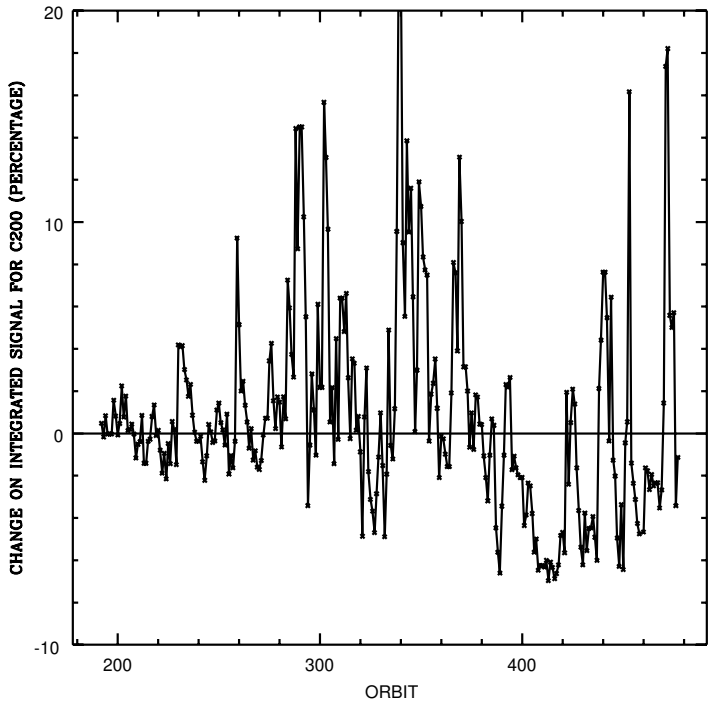


Figure 4.4: The relative variation of the C200 detector responsivity with respect to the mean value as a function of revolution. The responsivities of the 4 detector pixels have been averaged

### 4.2.5 Dark Signal and Noise

Dark current in the detector assembly adds a spurious *dark signal* to the source signal. Dark signals for the different detectors have been measured by means of dedicated observations in dark instrument configuration. These observations have been collected frequently throughout the mission. The in-orbit dark signals were found to be several factors higher than expected from pre-flight data. For all detectors except P3, the dark signals increased by a factor 2-3. For P3 the dark signal is up by a factor $\leq$50. The increase is attributed to the effects of ionizing radiation on the detectors.

The typical equivalent fluxes to dark signals for a number of detector/filter combinations are listed in Table 4.2. A flat power spectrum is assumed in the derivation of the dark flux values. In case one would like to know the typical dark flux for a different filter of the same detector one should multiply the values in the table with the factor C1(table_filter)/C1(new_filter) where C1 is the transmission parameter described in section 5.2.3. The values in Table 4.2 were derived by assuming default responsivities for

Table 4.2: Dark signal equivalent fluxes

| Detector ID | Filter ID | Dark Flux (mJy) |
|---|---|---|
| P1 | P_11p5 | 41 |
| P2 | P_25 | 410 |
| P3 | P_60 | 48 |
| C100(1) | C_100 | 55 |
| C100(2) | C_100 | 116 |
| C100(3) | C_100 | 81 |
| C100(4) | C_100 | 50 |
| C100(5) | C_100 | 100 |
| C100(6) | C_100 | 395 |
| C100(7) | C_100 | 48 |
| C100(8) | C_100 | 56 |
| C100(9) | C_100 | 95 |
| C200(1) | C_160 | 34 |
| C200(2) | C_160 | 36 |
| C200(3) | C_160 | 27 |
| C200(4) | C_160 | 35 |

the detectors (given in section 13.11). Note that pixel 6 of the C100 array shows a factor 3-7 higher dark signal than the other pixels in the C100 array.

The pixels of the PHT-S arrays have dark signals that show systematic variations with wavelength. Improper dark signal subtraction could cause the presence of spurious features in the spectrum. The dark signals for a number of PHT-SS detectors can be negative, this is not due to a negative dark current but due to a CRE effect. The equivalent flux to the dark signal in PHT-SL is typically 50 mJy for pixel 65 up to 250 mJy for pixel 128.

Trend analysis of dark calibration observations shows for all detectors a systematic variation as a function of orbital position. The dark signal gradually rises by a few percent per hour, accumulating nearly factor 2 towards the end of the revolution. Around 18 hours after perigee, in the last few hours of the science window, the dark signal steeply increases. This effect is caused by the rapidly increasing amount of ionizing radiation at the end of the science window. The germanium doped detectors (P3, C100 and C200) exhibit the largest increase of up to a factor 2–3. Dark signal corrections depending on orbital position has been included in OLP Version 7.

The dark signals can be higher for all detectors during a geomagnetic storm. If there are suspicions that observations may be affected by *space weather* activity it is advised to check the planetary "K-index". This parameter is strongly correlated with the space weather conditions. If within the 48 hours previous to a given measurement or on the same day the K-index is larger or equal than 4, it is possible that the measurement has been affected by the space weather. Tables of the K-index during the ISO mission will be made available in the future.

For differential observations the dark signal cancels out if the observations were taken close in time ($< 1$ hour). Possible uncertainties in the target signal caused by the dark signal are in such cases automatically removed. For absolute photometry measurements in which the total sky flux must be determined the dark signal contribution can be important. For these observing modes (PHT05 and PHT25) PHT has offered the possibility to include a dedicated dark signal measurement.

All standard observations with PHT-S (AOT PHT40) is preceeded by a measurement in dark instrument configuration of 32 sec. This "pseudo dark" measurement cannot be used to subtract PHT-S dark signals, but offers the possibility to assess remaining detector transients from an earlier PHT-S observation, see section 5.6.7.

Average dark signal values obtained from many calibration observations are stored in a Cal G file (see section 13.7). These values are used to remove the dark signal from each measurement during SPD level processing.

### 4.2.6 Detector flat-fields

The pixels of the C100 and C200 arrays can be regarded as a number of individual detectors with their own responsivities. The detector *flat-field* gives the relative variation of the responsivites among the pixels with respect to the average responsivity over the array. The flat-fields measured in-orbit were found to be wavelength dependent. Therefore for each C-detector/filter combination a separate flat-field is necessary.

For those observations where the associated FCS measurement is done with the same filter, the flat-field correction is included in the responsivity values derived from the FCS measurements after correction for illumination variations (see section 4.5.4). However, observations with different filters compared to the FCS measurement need additional correction for the wavelength dependence of the flat field. See also section 7.4.3.

### 4.2.7 Detector Saturation

In rare cases, for very bright targets the power on the detector can be too high causing the detector to go into break-through condition. This means that the detector goes into a low ohmic stage and a high current is flowing onto the amplifier. In case such an event occurs all readouts will be saturated, and the observation should have been aborted by the instrument controllers. Illumination levels higher than $5\times10^{-10}$ W can be potentially harmful to the detector/CRE chain of the PHT-P1 and PHT-S detectors. Safety resistors have been built into the circuits in order to limit the amount of the current. To avoid any risk only a few astronomical targets are forbidden to be observed with P1: IRC+10216, 07 Car, VY CMa. Jupiter observations cannot be scheduled for P1 and PHT-S.

## 4.3 Features due to electronics

### 4.3.1 Anomalous first readouts on a ramp

The CRE output voltage of the first few readouts on a ramp does not follow a linear increase in time but can remain constant or even show a decrease in voltage. The effect becomes more pronounced in case only a small fraction of the CRE dynamic range is used. This can happen in observations where the source + background flux is severely overestimated by the observer or in the low brightness regions of maps with high dynamic range.

To exclude this non-linear part of a ramp, the first fraction of the total number of non-destructive readouts is discarded in the SPD processing. The value of the fraction is stored in a dedicated calibration file (see section 13.4)

### 4.3.2 CRE (ramp) linearity

Integration ramps are not exactly linear but exhibit higher order variations or in some cases "knees" which are caused by the CRE. The deviations from linearity only depend on the absolute value of the CRE output voltage and not on e.g. the slope of the ramp (see [28]). Non-linearities can cause systematic errors up to 50% when comparing signals from the same source using ramps with different dynamic range in CRE voltage. This effect introduces an error in the flux calibration in case the FCS readouts span a different dynamic range than the source readouts. Improper correction for ramp non-linearities can also cause serious systematic brightness errors in maps with high dynamic range between background level and target. In addition, ramp non-linearities introduce a larger formal uncertainty in the signal when deriving a signal value by fitting a straight line through the ramps.

The deviations from linearity for all detectors except for PHT-SS and SL have been determined with respect to a standard linear ramp which was constructed from a stack of several thousand individual ramps. An example of the resulting deviations is presented in Fig. 4.5.

In the SPD processing the CRE output voltage for each readout is corrected before deriving the signals. Calibration tables for the P, C100, and C200 detectors have been created containing CRE output voltages and the corresponding voltage corrections. These calibration tables are stored in Cal G files (see section 13.5).

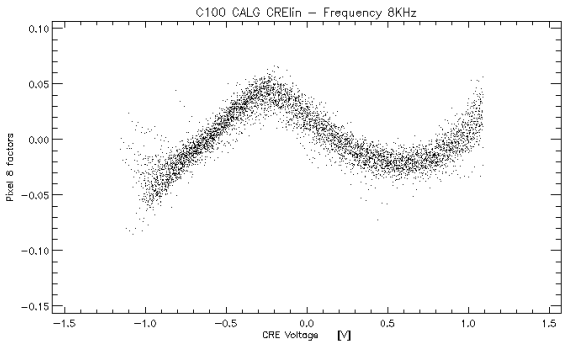


Figure 4.5: Example of non-linear CRE output voltages for detector C100 pixel 8. Plotted are the deviations from a standard linear ramp as a function of CRE output voltage for a large number of in-orbit measured ramps that span a large CRE range. The mean relationship has been used in the corresponding Cal G table

Non-linearities in the CRE output of PHT-SS/SL data are presently not corrected for. It is expected that calibration tables for PHT-S will become available in a future OLP version.

### 4.3.3 Signal dependence on reset interval

Measurements of a given target obtained with the same detector/filter/aperture combination but with different readout timing (ROT) parameters have indicated that the signal can depend on the commanded reset interval. For a constant detector illumination the signal level is found to vary systematically from one reset interval to the other.

For C100 and C200 these variations are of the order of 10–20% between measurements which differ in reset interval by a factor of 2. For reset intervals a factor of 8 apart the signal difference can be as large as 40%. P1, P2 and P3 show much less variations. For the PHT-S detectors the situation is still not completely clarified.

As long as the FCS calibration measurement is obtained with the same reset interval as the target measurement no corrections are necessary. However, in case of multi-filter photometry, the reset interval used in each filter measurement is generally different from the one in the FCS measurement. Also for multi-aperture observations where the signal range is large, different reset intervals are used for different aperture measurements.

The effect can be removed by correcting all signals with respect to a single reference reset interval. Correction tables are included in OLP Version 7 (cf 7.3.1).

### 4.3.4 Detector bias: de-biasing effects

Detectors PHT-SS, PHT-SL, and PHT-P1 are high bias, PHT-P2 medium and the PHT-P3, -C100, -C200 low bias detectors (see Table 4.3). For the low bias detectors *de-biasing* can occur when the full integrator voltage is used. Infrared photons induce charge carriers in the detector which are accumulated on the feedback capacitor of the readout electronics ($C_{int}$, cf. Fig. 3.2) during the integration. An electrical field is built up which reduces the actual bias. The stronger the illumination, the stronger the field and herewith the bias reduction. For the C200 detector the effect is strongest: the bias can drop by factor about 2 from 80 down to 40 mV for very high dynamic range. This effect causes the ramps to become non-linear with a downward curvature.

In contrast to the CRE ramp non-linearity (section 4.3.2), the non-linearities caused by de-biasing depend on *i* the CRE reset level (cf. section 3.2) which can float and *ii* the strength of the photo-current. This complicates possible solutions for correction. Presently no distinction is made between de-biasing and CRE non-linearity when correcting the ramps. For a given detector, there is one correction table taking

Table 4.3: Detector bias voltages

| Detector ID | Default Bias (V) |
|---|---|
| SS | −37 |
| SL | −37 |
| P1 | −90 |
| P2 | −10 |
| P3 | −0.25 |
| C100 | −0.2 |
| C200 | −0.08 |

care of both effects. Section 7.2.7 describes the correction that has been applied by the SPD processing software.

Consequently, signals are more underestimated the stronger the signals are. Signals derived from partially saturated ramps (section 4.3.5) suffer most noticably from this effect. Observers who collected maps with high dynamic range in bright regions using P3, C100, or especially C200 should be aware of this effect before interpreting their results.

In addition, for high signals on low bias detectors charges on the feed-back capacitor can cause an increased glitch rate (section 4.4) of the detector.

### 4.3.5 Readout Saturation

If the astronomical source is brighter than anticipated it may happen that parts of the integration ramps are *saturated*, i.e. the maximum CRE voltage level is reached before the next destructive readout. For most detectors the subsequent readouts after saturation remain at the maximum CRE voltage level until the next destructive readout. However, for some detectors the voltage of the saturated readouts can drop back below the threshold voltage.

The same can occur in case the actual detector responsivity exceeds the nominal responsivity by a large factor. A nominal responsivity was used to a-priori set the ROT parameters before execution of the observations.

The readouts taken during CRE saturation cannot be used and should be discarded. During SPD processing, all readouts in a ramp that are subsequent to a saturated readout are removed (section 7.2.6). The threshold CRE voltages for saturation are presented in Table 4.4.

Table 4.4: CRE saturation thresholds

| Detector | Threshold (V) |
|---|---|
| P1 | 1.091 |
| P2 | 1.091 |
| P3 | 1.097 |
| C100(1,2,3) | 1.063, 1.088, 1.095 |
| C100(4,5,6) | 1.097, 1.098, 1.099 |
| C100(7,8,9) | 1.098, 1.098, 1.097 |
| C200(1,2) | 1.091, 1.090 |
| C200(3,4) | 1.091, 1.088 |
| PHT-SS(1..64) | 1.040, 1.093, 62×1.095 |
| PHT-SL(1..64) | 1.007, 1.099, 62×1.102 |

The signal can still be determined from the remaining readouts that are below the CRE threshold voltage.

### 4.3.6 Disturbances by Chopper Commanding

The first ramp of each chopper plateau is always disturbed due to the electronics commanding the chopper movement. Even in case of a staring measurement the chopper is still commanded to perform a zero deflection after integrating for 128 sec. This *virtual chopper step* can be noticed in the datastream of a long staring measurement where one disturbed ramp occurs every 128 sec.

For the disturbed ramps the CRE reset level (cf. section 3.2.2) is high and also the ramp signal is higher than the average signal derived for the corresponding chopper plateau.

As part of the SPD processing, the first ramp on each chopper plateau is discarded and therefore not taken into account when computing the average signal per chopper plateau.

### 4.3.7 CRE latch-up

The CRE for the ISOPHOT detectors were fabricated in CMOS technology. A known phenomenon of CMOS devices is the occurence of high supply currents after switch-on, which is called *latch-up*. The effect is due to the presence of a parasitic transistor in the CRE. A small amount of charges left in the basis region of this transistor can cause it to conduct thereby creating the high supply current.

During the instrument activation sequence at the beginning of each revolution a latch-up recovery is performed which resets the CREs into their nominal status. The recovery procedure consists of a pseudo measurement which selects and subsequently deselects a given CRE.

Besides the switch-on effect some CREs tend to show latch-up effects during the science window. As a result, the integration ramps become very noisy. The latch-up is accompanied by an increase of the CRE supply voltage above a certain critical limit. The CRE supply voltages for each detector-CRE combination are monitored by the instrument controllers.

When a latch-up event occurs the measurement is aborted in real time by the instrument controllers. Subsequently they must initiate a latch-up recovery procedure. Due to the duration of this procedure also the following AOT could be skipped. All affected AOTs are flagged as failed and the observations enter the queue for rescheduling.

During the first 270 revolutions it was found that the P2 detector suffered from latch-up events when switching the device on. This problem was solved by introducing a proper command timing and introducing for safety a pseudo measurement in the AOT. The inclusion of this measurement required a change in AOT logic which adds an extra overhead of 10 sec to the AOT on-target time. The pseudo measurement was inserted when one or more P2 measurements were selected in PHT03, PHT04, PHT05, or PHT17. From revolution 690 onwards the AOT logic was changed such that no pseudo measurements were taken anymore. The timing overhead remained the same.

The pseudo measurement is present in the telemetry data (of revolutions 270–690) but is removed in Derive_ERD and should be transparent to the observer who starts processing from ERD.

## 4.4 Effects of Ionizing Radiation

Ionizing radiation has a strong disturbing effect on the performance of the detectors. The high flux of protons and electrons trapped in the earth's radiation belts makes operation impossible. At about $2^h30^m$ after perigee passage the temporary radiation damages of the detectors are cured by a combination of heating, illuminating and bias increase (see section 4.2.4). Outside the radiation belts, during the 16 hours science window, the ionizing radiation remains a limiting factor to detector performance. Not only direct hits on the detector, but also secondary electrons released by satellite materials after a hit cause disturbances.

Ionizing radiation consists of high energy protons and heavier nuclei. It causes several effects in the photoconducting detectors:

- spiking, according to the hit rate,
- increase of the responsivity, caused by a lower recombination rate in sensors suffering from too many carriers produced by charged particles,

- increase in detector noise, faster than the responsivity gain, combined with an increased dark current.

A *glitch* can be recognised by a step on the integration ramp between two readouts. The influence of low level glitches to low signal data is illustrated in Fig. 4.6.

Note that the energy of the particle passing the detector is not directly correlated with the (measured) glitch energy. The glitch energy depends on the amount of electrons freed by the high energy particle along its path through the detector. Higher energy glitches can cause ramps to saturate or can even cause a transient for several seconds. Low level glitches become more apparent in measurements with low in-band power. Examples are faint sources on a low background, PHT-S spectra of faint targets, observations with small apertures using detectors P1 or P2.

The glitch rate is a function of the detector size and the energy deposited. Calibration measurements have been carried out to determine the particle hit rate as well as the signature of the glitches as a function of orbital position of the satellite with respect to perigee passage. On average, a clear glitch is detected every 10 sec for standard science observations.

Analyses of glitches have shown that they have a continuous energy distribution (Fig. 4.7). Detectors P3 and C100 are more vulnerable to cosmics. These detectors exhibit a temporary responsivity variation for several seconds. Although special algorithms have been developed to remove these disturbances they can determine the sensitivity limit of these channels.

The slow responsivity increase caused by cosmic rays in the 16 hours science window is about 20% for the silicon doped detectors P1, P2 and PHT-S. It can reach a factor 2 for the P3 and C200 detector. These variations are calibrated out by FCS reference measurements which are equally affected as the celestial targets in the same observation sequence. Moreover, to minimize the disturbance, an extra curing procedure has been introduced for the detectors P3, C100 and C200 to be carried out near apogee when the satellite is handed over between the two ground stations.

The radiation effects described here become worse during periods of higher solar activity. Also measurements carried out near the end of the science window when ISO is approaching the radiation belts, suffer from increased radiation effects.

The tuning of the parameters controlling the OLP deglitching algorithms has been performed empirically after evaluation of many datasets. Descriptions of the algorithms are presented in section 7.3.4.

## 4.5 Optical Performance

### 4.5.1 Instrumental Footprint on the Sky

The image of a perfect point source obtained with a given detector or the *footprint* of a detector should be known in case one would like to perform:

- accurate flux determination of extended sources,
- accurate flux determination of point sources in the case of sources not centred in the aperture,
- image reconstruction, or
- determining relatively faint extensions around bright sources e.g. with multi-aperture measurements.
- a refined colour correction by including the wavelength dependence of the beam profiles.

As part of the PHT calibration programme, extensive mapping of astronomical point sources have been carried out in order to determine the footprints of the PHT-SS/SL, C100 and C200 detectors and the PHT-P apertures.

#### 4.5.1.1 PHT-C footprints

The footprints of the C100 detector array pixels were observed at 60 and 105 $\mu$m (filterbands C_60 and C_105) and of the C200 array at 120 and 200 $\mu$m. Footprint maps of the four C200 pixels at 120 $\mu$m are presented in Fig. 4.8.

The measurements were compared with a theoretical model based on the telescope point spread function measured with ISOCAM. The model assumes a two mirror f/15 telescope with radii for the primary and secondary mirror of 30 and 10 cm, respectively. It includes the stray cones of the secondary's support tripod. The model footprint is calculated from the convolution of the point spread function with the pixel surface. Comparison between the predicted and the measured footprint shows good agreement. The inferred effective solid angles of the pixels are all larger by 20 - 60% than the values given in the Observers Manual (Table 9 in [10]). This can be understood by the widening of the point source profile due to infrared light scattered by the support legs.

The effective solid angle enters the extended source calibration in the conversion from Jy/pixel to MJy/sr, see section 5.3.

#### 4.5.1.2 PHT-P footprints

From the large number of different footprints of the PHT-P group the results for the following combinations have been analyzed:

- P2 detector, P_25 filter and 79″ aperture;
- P3 detector, P_60 filter, 52″, 99″, 120″, 127″×127″ and 180″ apertures;
- P3 detector, P_60 filter, high resolution one dimensional raster scan with 23″ aperture;
- P3 detector, P_100 filter, 79″ and 180″ apertures

The P2 profiles show that the central plateau of the footprint is asymmetric along the spacecraft Z-axis. It also does not peak at the central position. Cuts through the profile are plotted in Fig. 4.9.

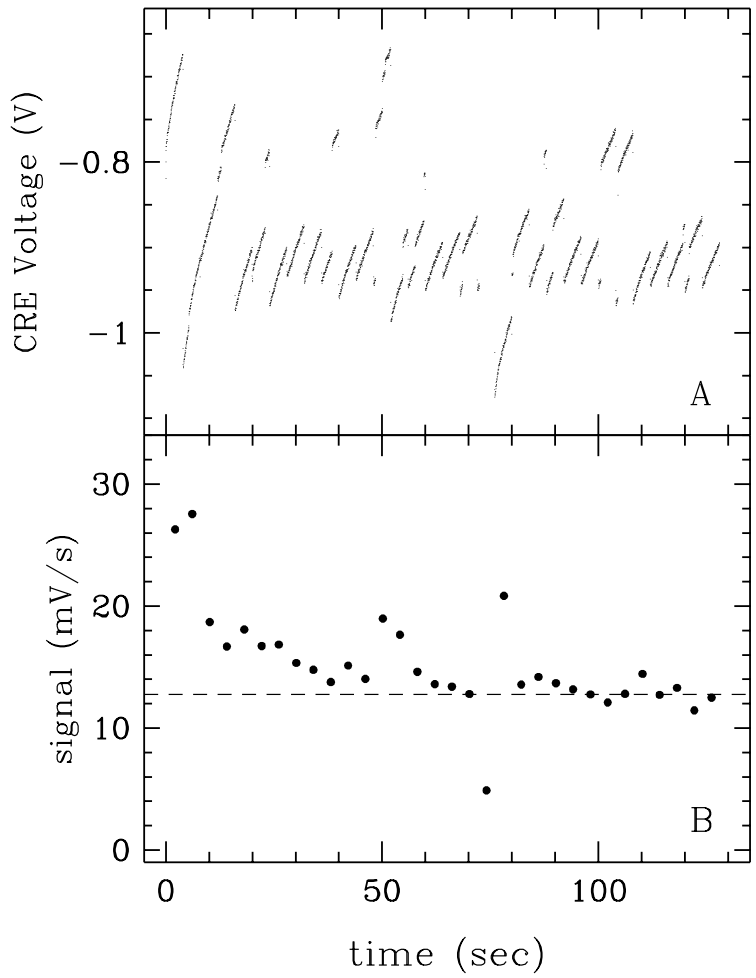


Figure 4.6: Example of the effects of glitches during a measurement. The measurement is at a very low flux level (about 5 times the dark signal) so that even "weak" glitches can clearly be distinguished. Upper panel (A): the "raw" CRE voltage level as a function of time, each dot is a non-destructive readout. The measurement consists of 32 integration ramps of 4 sec reset interval, each ramp contains 128 readouts. Most of the ramps show one or more significant voltage jumps between consecutive readouts caused by ionizing radiation. Based on the average increase in voltage between the readouts in a ramp these glitches can be removed. Lower panel (B): the resulting signals after deglitching at CRE voltage level. Despite this deglitching the signals still show disturbances. The glitch which occured around t=50 sec caused a variation in detector responsivity lasting about 10–20 sec. The dashed line is the final mean signal level after removing signal outliers and after applying a drift recognition algorithm. The corrections presented here are also used in Derive_SPD

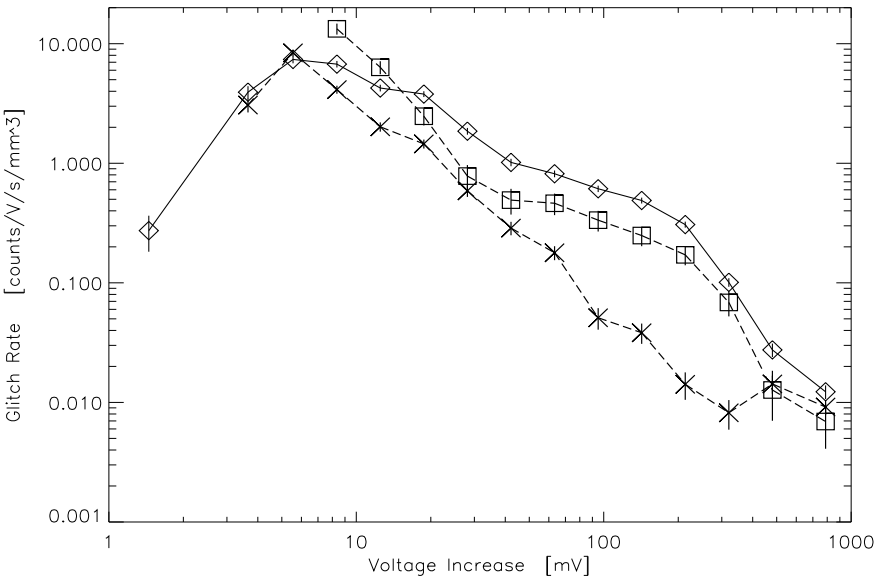


Figure 4.7: The in-orbit glitch energy deposition spectra of detectors P3 (squares), C100 (diamonds), C200 (crosses). The spectra were obtained on the basis of dark signal calibration measurements collected throughout the mission, see [4].

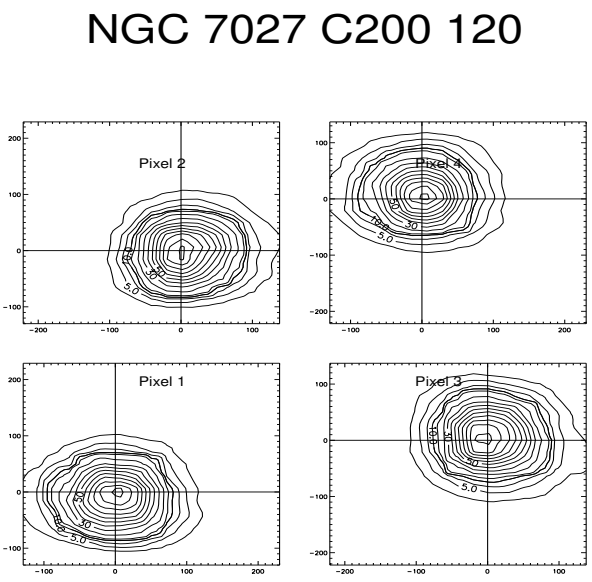


Figure 4.8: The measured pixel images in the C_120 filter of the planetary nebula NGC7027 which is assumed to be a point source for ISO. The footprints have been normalized to 1 at peak position. Contour levels are 2.5, 5, 10, 12.5%, 20 to 90 with step of 10%, and 98% of peak.

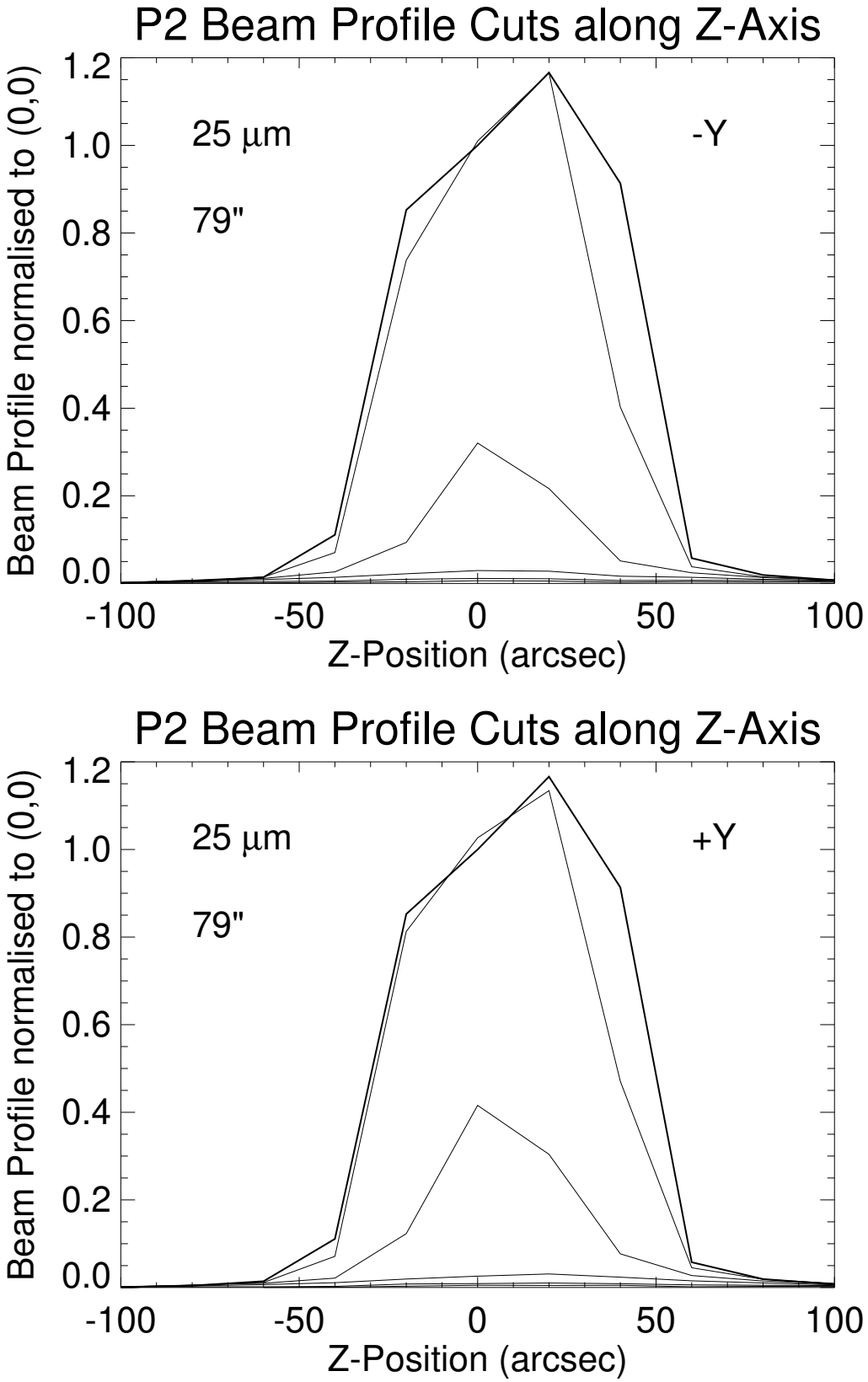


Figure 4.9: Slices along the Z-axis through the footprint of P2 at 25 $\mu$m using the 79$''$ aperture. The bold curves give the central slice, the step size between neighbouring slices is 20". The profiles are asymmetric suggesting that the point spread function is not fully centred on the aperture.

The P3 profiles show less pronounced asymmetries in the central plateau. All profiles are currently compared to the theoretical model described in the previous section. First results indicate an effective solid angle to deviate ±5–20% from the values given in the Observers Manual ([10]). In Fig. 4.10 we present a high resolution one dimensional scan over the star HR6705 ($\gamma$Dra). Assuming that HR6705 is a true point source and applying the same observing mode to a given astronomical target, the scan can be used to decide whether the target is pointlike or extended. The observation comprise a forward and backward going raster scan; this is achieved by setting the number of raster steps to 2 with stepsize 0″ for the cross-scan parameters.

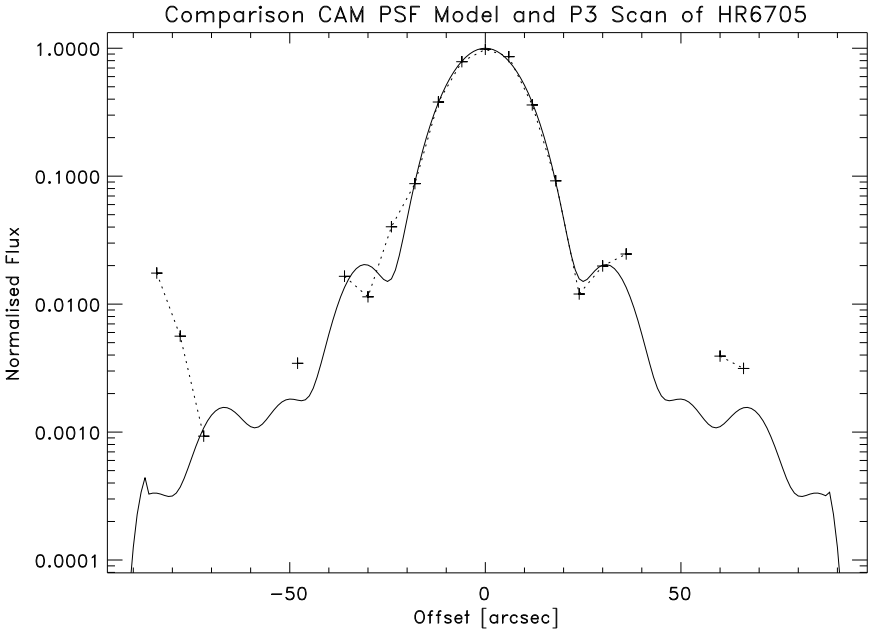


Figure 4.10: High resolution scan of the star HR6705 at 60 $\mu$m (P3, P_60) using the 23″ aperture and 6″ step. The observations are marked by crosses, negative values are not shown. The solid line gives the expected profile using an ISO PSF model convolved with the 23″ aperture.

#### 4.5.1.3 PHT-S footprints

The size of the PHT-S aperture (24″×24″) has been designed to mask the part of the sky which is directly mapped onto the PHT-S pixel at a given wavelength. In-orbit observations have shown that the PHT-S response is very sensitive to pointing variations perpendicular to the dispersion direction which is the spacecraft Y-direction.

By scanning a point source over the PHT-S aperture in Y and Z-direction, and assuming axisymmetry, PHT-S footprints have been determined for each pixel in both the SS and SL arrays. The resulting profiles show that the general shape of the PHT-S footprints are sharply peaked in non-dispersion direction (spacecraft Y-direction). The profile in dispersion direction (spacecraft Z-direction) is flatter over the aperture. These in-orbit calibrations confirm the results of ground based measurements of the beam profiles. An example of a footprint is given in Fig. 4.11.

Another feature of the PHT-S footprints is that not all peak at the centre of the aperture. For some pixels the centre of the array is on a steep flank of a footprint. As a result, the shape of the spectrum strongly depends on the exact pointing in Y-direction. For example, in case of pixel 60 (Fig. 4.11) a pointing error of ±3 arcsec in Y directon can cause a change in response of the order of 20%.

The PHT-S spectral response function used in the current OLP version is only valid for the centre position of the PHT-S aperture. Corrections for pointing offsets can be applied using the footprints of the individual pixels. In a later version of this manual the pixel profiles in Z and Y direction will be made available.

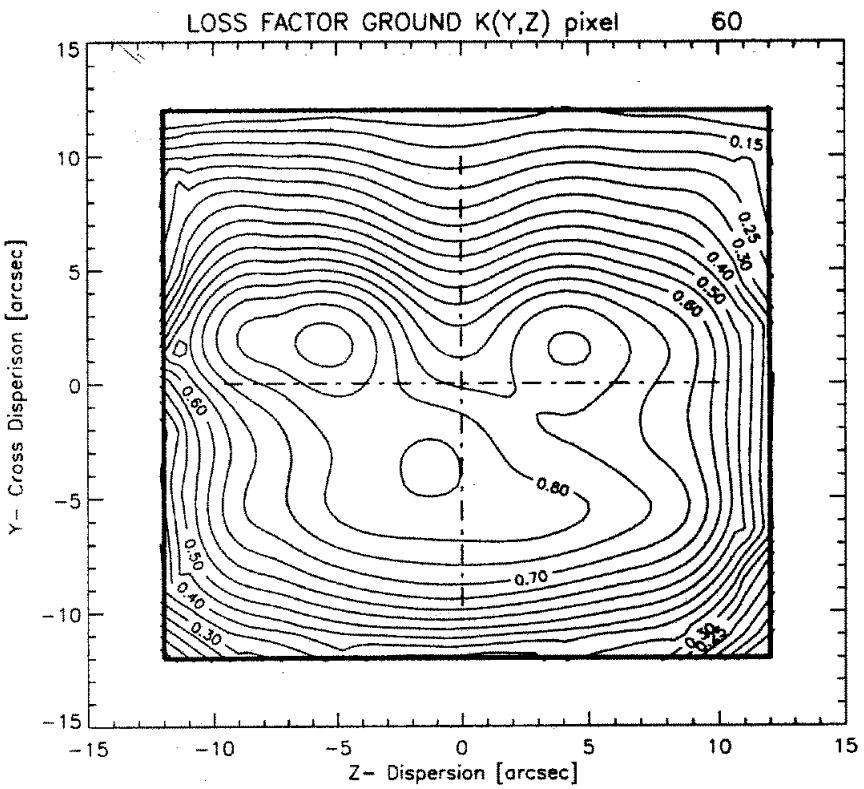


Figure 4.11: Two dimensional beam profile of PHT-S pixel 60 as measured in the ISOPHOT ground calibration facility. This is an example where the intensity maxima are multiple and are off the major axes. In-orbit cross-scans along the major axes were performed which show qualitatively the same behaviour: a relatively flat and symmetrical shape in the dispersion direction and a slightly off-centre and steeply falling off profile in cross-dispersion direction.

Based on the footprints of all PHT-S pixels the correction factors for the transformation from point source flux to extended source surface brightness have been derived. A homogeneous illumination of the PHT-S aperture is assumed.

### 4.5.2 Point source intensity fractions

The intensity fractions, or $f_{psf}$, of a point source passing through a given filter/aperture combination for PHT-P or filter/pixel combination for PHT-C has been calculated using a simplified model of the point spread function. This model assumes a uniformly illuminated round mirror of 30 cm radius with a f15 focal length and a central obscuration of 10 cm radius. The sizes of the apertures and detectors as determined on ground together with the central wavelength of the filters have been used to determine $f_{psf}$.

For C200 the fraction of light falling on the whole array is significantly different from the fraction calculated for the model described above in which the physical dimension of the detector arrays have been included. This is probably due to losses and diffraction at the inter-pixel gaps of order 100 $\mu$m when the point spread function is centred on the C200 array and not on one of the pixels. Empirical correction factors obtained from calibration observations have been determined to correct for this effect.

The resulting values for $f_{psf}$ are stored in a Cal-G file, see section 13.15.1.

### 4.5.3 Chopper vignetting/offset

Although the guaranteed unvignetted field of view for the ISO instruments is 3 arcmin, PHT can have chop throws up to $\pm 90''$ for the largest aperture of $180''$ and $\pm 165''$ for the smallest aperture w.r.t. the CFOV. It is therefore expected that for larger chopper throws corrections should be made for possible *vignetting* of the chopper beams. As the chopped beam has a different ray path through the telescope-instrument system additional *chopper offsets* can occur which have been observed, too.

The combined effect of chopper vignetting and chopper offset can cause a relative signal difference between the on- and off- chopper beams for an otherwise flat sky. As a consequence, chopped observations of faint sources which are only a few percent brighter than the sky background can only be analyzed after corrections for these effects.

Calibration observations indicate that chopper offsets for the PHT-P detectors are small: less than 1% flux difference between the chopper positions for a flat sky. For the PHT-C detectors, the offsets depend on the chopper throw and can become substantial for the largest amplitudes (as high as 6%). Note that maps obtained with PHT32 need to be corrected for this effect.

See section 13.8 for a description of the corresponding Cal G file.

### 4.5.4 Inhomogeneous FCS illumination

The detectors are not homogeneously illuminated by the FCS. For the PHT-P detectors the measured flux does not scale proportionally with the aperture area, while for the PHT-C detectors the different pixels are not receiving the same in-band power. *Illumination matrices* or factors for correcting the inhomogeneous illumination over the 180 arcsec field of view have been determined for each filter/detector/aperture by in-flight measurements.

For the PHT-C arrays the illumination matrices include the relative differences in responsivity among the pixels, i.e. the flat-field averaged over many observations (see also section 4.2.6). This means that an observation of a flat region of the sky should yield a flat image after calibration with the FCS measurement in the same filter.

The FCS illumination matrix is filter dependent. As a consequence, when using an FCS measurement made e.g. in the C_90 band to calibrate a measurement made in the C_60 band, the filter dependent flat-fields have to be accounted for, see section 4.2.6.

For the PHT-P detectors strong deviations from a linear scale have been measured when changing the FCS aperture while maintaining the same FCS heating power. The calibration of the FCS against astronomical standards (section 5.2) has been performed only with a few selected apertures:

- $23''$ aperture for P1 filters with a central wavelength less or equal than 7.7 $\mu m$,
- $52''$ aperture for P1 filters with wavelengths longer than 10 $\mu m$,
- $79''$ aperture for P2 filters, and
- $180''$ aperture for the P3 filters.

Studies with a limited set of calibration data have indicated that the deviations from a linear scale can be as high as 20% for detectors P2 and P3. For P1 the effect can even be stronger, upto a factor 2. This means that a systematic error in the photometric calibration is made when using apertures for the FCS measurements that are different from the standard ones listed above.

The corrections using illumination matrices for C100 and C200 are included in the SPD processing, see section 13.12 for a description of the related Cal G file. It is planned for a future version of the software to include aperture corrections.

## 4.6 Spectral performance

### 4.6.1 PHT-S instrumental line profile

The PHT-S instrumental line profiles have been measured in laboratory. The profiles exhibit a Gaussian shape to good approximation. For the PHT-SS pixels the FWHM is 43±5 nm, for SL 100±10 nm. The physical distance between adjacent pixels is 350 $\mu$m which corresponds to 38.3 nm and 91.8 nm in wavelength for SS and SL respectively, assuming a linear scale. The physical size of a pixel in dispersion direction is 310 $\mu$m which corresponds to a width in wavelength of 33.9 and 81.3 nm for SS and SL. In Table 4.5 we have summarized the laboratory data. Also listed are the fraction of the incident power measured by the detector pixel in the case the line is centered on a pixel and in case the line falls exactly in between two pixels of the PHT-S arrays. For these values it is assumed that the detectors have an ideal flat-topped responsivity profile in dispersion direction. Since this is not the case (see section 4.5.1.3) the ratio between the centre and adjacent pixel in case the line is centred on the pixel is somewhat higher. For the values in Table 4.5 an accurate approximation for the wavelength scale is used. For the exact scale see section 4.6.2. Under the given assumptions, a 10% variation in the FWHM changes the fraction in the centre pixel by less than 7%.

Table 4.5: Instrumental line profile parameters

| parameter | SS | SL | unit | description |
|---|---|---|---|---|
| $\Delta$x | 350 | 350 | $\mu$m | physical distance between pixels |
| $\Delta\lambda$ | 38.3 | 91.8 | nm | wavelength difference corresponding to pixel distance |
| $\Delta$l | 310 | 310 | $\mu$m | physical size pixel in Z-direction |
| $\Delta\lambda_{pix}$ | 33.9 | 81.3 | nm | pixel width in wavelength |
| FWHM | 43 | 100 | nm | mean full width at half power of profile |
| $P_C/P_{total}$ | 0.73 | 0.74 | – | power fraction measured on pixel if line is centred |
| $P_C^1/P_{total}$ | 0.09 | 0.08 | – | power fraction measured on adjacent pixel if line is centred |
| $P_M/P_{total}$ | 0.43 | 0.43 | – | power fraction on pixel if line is centred between two pixels |

### 4.6.2 PHT-S wavelength calibration

The PHT-S wavelength scale, i.e. the relation between pixel number and wavelength, is approximately linear. In orbit calibration confirms the presence of a small second order term. The wavelength scale has been calibrated to an accuracy of less than 1/10 of a pixel (see also Table 4.5) from the analysis of

Table 4.6: Coefficients for the conversion of PHT-S pixel to wavelength

| Coefficient | SS | SL |
|---|---|---|
| $a_1$ | 2.4687 | 5.8396 |
| $a_2$ | $4.0765\ 10^{-2}$ | $9.4263\ 10^{-2}$ |
| $a_3$ | $4.1563\ 10^{-5}$ | $3.9702\ 10^{-4}$ |

several targets with well defined emission lines. A polynomial fit to the wavelength scale for PHT-SS and PHT-SL gives:

$$\lambda(pix) = a_1 + a_2 * pix + a_3 * pix^2 \qquad (\mu m) \tag{4.3}$$

where $pix$ is the integer pixel number in the SS or SL array, counting from 1 to 64 for both SS and SL. The coefficients $a_1, a_2$, and $a_3$ are presented in Table 4.6.

## 4.7 Straylight

### 4.7.1 Straylight during FCS calibrations

The FCS signal is obtained by deflecting the focal plane chopper outside the sky field-of-view to one of the FCS positions (see section 3.5). In-orbit tests have shown that FCS measurements do not only contain signals from the FCS proper and dark signal of the detectors but also a straylight component from the sky entering the instrument. This is due to the absence of a mechanical shutter to block the external beam. Both the dark signal as well as this straylight signal should be removed from the total FCS signal before calibrating the target signal.

In the derivation of the FCS calibration tables, the straylight contribution in the signal has been eliminated by subtracting the sky straylight signal obtained while pointing at the calibration target (see section 5.2.2). For C200 the straylight contribution to the FCS signal can be as high as 10% of the background signal in case of observations near the galactic plane. The other detectors show a lower straylight contribution.

It is possible to separate the straylight and dark signal components in the absolute photometry AOTs P05 and P25 to increase the observational accuracy. The observer has the option including an FCS measurement with no FCS heating power applied to it as well as a measurement when a special configuration of the filter wheel blocks the sky light.

The PHT instrument team is currently investigating how the FCS straylight can be corrected for the other AOTs.

### 4.7.2 Instrumental Straylight

Dedicated in-orbit calibration measurements were performed to determine the *straylight* from sources outside the ISOPHOT field of view. The off-axis straylight rejection requirement is that the parasitic light level in the focal plane should not exceed 10% of the diffuse astronomical background at any wavelength. The thermal self-emission from the optical system should also be less than 10% of the diffuse astronomical background. Main straylight sources are the Sun, Earth, Moon, and Jupiter. The observer is recommended to check the position of the brightest celestial sources with respect to the target position, particularly for absolute photometric observations.

#### 4.7.2.1 Near-field straylight

The *near-field straylight* is the off-axis rejection within about 1 degree radius from the field of view of ISOPHOT. This was measured by performing cross-scans on Saturn using C200 in band C_160, $o$ Ceti (Mira) with P2 in P_25, and $\gamma$ Dra (HR 6705) with PHT-S. The target fluxes in the given filter bands are 32 kJy, 1.8 kJy, and between 3 kJy (at 3 $\mu$m) and 140 Jy (at 10 $\mu$m) for C200, P2 and PHT-S, respectively.

Table 4.7: Near-field off-axis rejection at 160–200 $\mu$m predicted by an APART study of Breault Research, Tucson

| Angle (arcmin) | Level |
|---|---|
| 0 | 1 |
| 3 | $3.6\ 10^{-3}$ |
| 10 | $2.9\ 10^{-4}$ |
| 30 | $6.2\ 10^{-6}$ |
| 60 | $1.0\ 10^{-6}$ |
| 120 | $1.6\ 10^{-7}$ |
| 300 | $1.3\ 10^{-8}$ |

Comparison between the measured profiles and the beam profiles shows small or negligible straylight contributions, even from very bright sources, out to off axis angles where the natural sky brightness dominates. An in-depth study for C_160 carried out before the mission has predicted straylight levels now being confirmed by the in-orbit measurements of Saturn. This proves that the design assumptions were correct.

The computed straylight levels in the 160–200 $\mu$m range for a point source are listed in Table 4.7. Major straylight contributors are:

- the diffraction from the struts contributing near the edge of the field of view,
- the edge of the secondary mirror contributing between 3 arcmin and 1 degree, and
- the secondary mirror contributing further away.

Because the 3 channels selected for the in-orbit verification of the straylight rejection are representative for the major subsystems of the instrument, it is concluded that straylight corrections can be made for all channels. Further near-field measurements are not required.

#### 4.7.2.2 Straylight from Sun, Earth and Moon

Straylight measurements of Sun and Moon were performed in Autumn 1997 during eclipses of ISO. The results will be described in a later version of this manual. A description of the results can be found in Klaas et al. 1998 [13].

### 4.7.3 Spectral Straylight

At the time of writing of this document, there is no indication of any spectral impurity as well as the presence of ghosts in the PHT-S spectra.

## 4.8 Instrumental Polarisation

The instrumental polarisation for ISOPHOT without the contribution of the ISO optical elements (primary, secondary and pyramidal mirrors) has been modelled in laboratory, see [26] These measurements have shown that the polarisation of the P detectors is less than 10%. The polarisation of the arrays varies from pixel to pixel, some pixels have measured polarisations as high as 10%.

For PHT-S the instrumental polarisation degree is measured to be considerably higher: starting at 10% at 2.5 $\mu$m rising approximately linearly to 45% at 5 $\mu$m with a polarisation angle of -6$\pm$3 degrees, and for PHT-SL starting at 12% at 6 $\mu$m rising approximately linearly to 40% at 12 $\mu$m with a polarisation angle of -2$\pm$2 degrees. The main source of PHT-S instrumental polarisation is the grating.

## 4.9 Backgrounds

During performance verification phase and routine phase the PHT Instrument team together with the PHT Consortium have undertaken programmes to investigate the astronomical backgrounds.

A study of the infrared background structure due to infrared cirrus and extragalactic emission based on ISOPHOT data can be found in Herbstmeier et al. 1998 [8].

### 4.9.1 Confusion

See ISOPHOT observers manual [10] Chapter 4 and [8].

### 4.9.2 Zodiacal Light

For many types of ISOPHOT observations knowledge of the emission contribution from the zodiacal dust cloud is necessary. Data from COBE can be used but have to be adapted to the higher angular resolution observations of ISOPHOT. Absolute photometric observations in a number of ISOPHOT bands at several ecliptic longitudes/latitudes were obtained to establish the zodiacal emission distribution as seen by ISO. These observations will be applied for the adaptation of the COBE data for ISOPHOT purposes.

COBE did not cover wavelengths between 5 and 12 $\mu$m, in the range where the brightness of the zodiacal light rises very steeply. The first results obtained with PHT-S, PHT-P and ISOCAM suggest that the zodiacal emission spectrum can be well approximated by a blackbody of 260 K. In addition, ISOCAM CVF and ISOPHOT-S measurements demonstrated that the spectrum is featureless between 5 and 16 $\mu$m.

## 4.10 Global Instrument Data

See appendix A for the following tables:

1. global filter specifications (sections A.1.1, A.1.3),
2. aperture specifications (section A.1.2),
3. other filterwheel components (section A.1.4), and
4. filter/detector transmission curves (section A.2).

# Chapter 5

# Calibrations

## 5.1 Overview

The photometric calibration of ISOPHOT observations is described in this chapter. The calibration strategy for PHT-P and PHT-C using the FCS and the strategy for PHT-S are given in section 5.2. In the subsequent sections the extended source photometry, aperture calibration, and the PHT-S wavelength calibration are described. Section 5.6 summarizes the specific calibration procedures per AOT. Finally, a general description of the kind of calibration files used in OLP is given in section 5.7. Note that the uncertainties in the calibration are not addressed in this chapter, we refer to the related documents 'ISOPHOT Error Budgets' [15] and 'ISOPHOT calibration accuracies' [11] for full discussions. A number of observation modes are not scientifically validated, see chapter 9.

## 5.2 Calibration strategy

### 5.2.1 Calibration strategy involving the FCS

An observation with PHT-P or PHT-C always includes a photometric reference measurement using one or both internal fine calibration sources (FCSs, see also section 3.5) which are assumed to be stable troughout the mission. The emission from an FCS can be changed by adjusting the FCS heating power. The FCS reference measurement assesses the actual detector responsivity at the time of the measurement.

The crucial photometric calibration as contained in the Cal G files is the relationship between heating power applied to the FCS as commanded by the AOT logic, and the resulting in-band power illuminated on the detector. This is the basis of the derivation of the detector responsivity which characterises the detector at a given time. The detector responsivity enables *transfer of calibration* between filters of the same detector and/or between apertures.

Transfer of calibration is in practice necessary in case of multi-filter photometry (PHT03, PHT22) or multi-aperture photometry (PHT04) where one FCS measurement is taken for combinations of several filters and apertures.

The FCS calibration itself is obtained empirically by comparing the signal of a designated celestial calibration target and signals of several FCS measurements. Based on the known flux of the calibration target, its signal, and the known instrument transmissions, the in-band power is derived for each FCS measurement. These in-band powers are then related to the FCS heating powers.

Three types of astronomical targets - all being point sources - have been used as prime calibrators for the FCSs:

- stars
  Stellar calibrators are most suitable for the 2.5 to 35 $\mu$m wavelength range. A dedicated ground based preparatory programme for ISO calibration standards was carried out to provide the ISO mission with the most consistent and most accurate set of calibration stars, see Jourdain de Muizon and Habing 1992 [23], van der Bliek et al. 1992 [34], and Hammersley et al. 1998 [7]. Another set

of calibrated stellar spectral energy distributions was provided by M. Cohen from an independent calibration programme (Cohen et al. 1995 [3]). The confidence in the absolute calibration of the calibration stars is about 3% in the 2.5 to 35 $\mu$m wavelength range and better than 10% at longer wavelengths up to 300 $\mu$m. The model spectral energy distribution (SED) for Vega ($\alpha$ Lyr) has been used to define the zero point for both programmes.

- asteroids
  Asteroids are used to cover the 35 to 200 $\mu$m wavelength range. An extensive ground and airborne based calibration programme was carried out to quantify the fluxes and to monitor the light curves of the prime asteroids 1 Ceres, 2 Pallas, 4 Vesta, and 10 Hygiea, and other asteroids that have been observed with ISO. For the current calibration the absolute fluxes of the asteroids were derived using a thermophysical model (Müller and Lagerros 1998 [22]). The accuracy of the predicted asteroid fluxes is in general $\pm$10% in the wavelength range from 24 to 500 $\mu$m.

- planets
  Outer planets Neptune and Uranus were used for calibration at the longer wavelengths in the high flux density range up to 1000 Jy. The model SED's for a given time in the mission were provided by M. Abbas. Comparison with independent model predictions for Uranus showed a consistency of better than 20% in the wavelength range between 30 and 240 $\mu$m. At shorter wavelengths the models become less certain.

The stability of both FCSs was monitored against the bright secondary standard NGC6543 as well as against a set of fainter stars. A full description of the ISOPHOT calibration involving the FCS can be found in Schulz et al. 1998 [30].

### 5.2.2 Absolute calibration of FCS

The FCS calibration against celestial standards has been determined for 25 filter bands over the full range of possible astronomical flux densities.

The ISOPHOT instrument dedicated team has measured fluxes of prime calibrators in each available filterband spanning 3–5 decades of flux range per filterband. For a given calibration target, the following measurements were obtained in a given filter:

- measurement of the FCS for which zero heating power is applied (also referred to as 'cold FCS measurement' or 'FCS straylight measurement'),
- measurement of the calibration target,
- measurement of one or more background positions, and
- measurement of one to several FCS illumination levels.

The cold FCS measurement provided the zero FCS signal level. All measurements of the celestial calibrators included an uncalibrated amount of background emission which had to be subtracted. The background level was determined by performing one or more separate background pointings in the same aperture. In the case of multiple FCS measurements, the FCS illumination levels were tuned such that their in-band powers span a range of about one decade around the power expected from the calibration target plus background emission. It is assumed that the responsivity is linear in the measured power range.

Using the total optical transmission of the instrument and detector chain, the in-band power from the calibration source on the detector was computed using Eqn 5.6 below. By relating the in-band power of the calibration target to its corresponding signal, the FCS signals were converted to in-band powers. These together with the commanded FCS heating powers were used to derive the FCS power calibration tables. Assuming a measurement for a given aperture in case of PHT-P or pixel in case of PHT-C:

$$P^f_{fcs}(h) = P_{cal} \cdot \frac{(S^f_{fcs} - S_{str})}{S_{cal}} \qquad (W), \tag{5.1}$$

where

- $P^f_{fcs}(h)$: the in-band power in W for filter $f$ and FCS heating power $h$ in mW;
- $P_{cal}$: in-band power in W of the celestial calibrator;
- $S_{cal}$: measured signal in V/s of the prime calibrator after subtraction of the background signal;
- $S^f_{fcs}$: measured FCS signal in V/s;
- $S_{str}$: measured dark FCS signal (straylight) in V/s.

It is assumed that the difference signal between calibration source and background scales linearly with the signals from FCS measurements. Consequently, the accuracy of the absolute calibration of the background level depends on the linearity of the detector from zero to the background level and on the suppression of parasitic flux, such as straylight. Uncertainties become higher for flux levels close to the astronomical background because of the absence of reliable celestial calibrators that are faint.

Eqn. 5.1 is a simplification of the relation used to determine the actual FCS power tables. For PHT-P the tables are normalized to the aperture area, and for PHT-C the tables refer to a pixel, after correction for inhomogeneous FCS illumination (cf. section 5.2.3).

The FCS calibration makes the observation independent of long term responsivity drifts. However, on measurement time scales of order of 32-2048 s, detector transients (sect. 4.2.2) due to flux changes occur and have to be corrected for. For the determination of the overall FCS calibration drift corrections have been applied to estimate the signal level of the asymptotic limit.

### 5.2.3 Photometry with PHT-P and PHT-C

The FCS measurement together with the FCS power calibration tables (cf. section 13.10) are used to determine the detector responsivity. In the following derivations a separation will be made between single detector, multi-aperture, and multi-filter subsystems PHT-P and the multi-filter detector arrays PHT-C.

For a given PHT-P FCS measurement taken with detector $det$, filter $f'$, and aperture $a'$, the responsivity $R_{det}$ is derived from:

$$R_{det} = \frac{S_{fcs}(a) C^{det}_{int}}{P^{f'}_{fcs}(h) A(a) \alpha^{f'}(a)} \quad (A/W) \tag{5.2}$$

For a given PHT-C FCS measurement taken with detector $det$ and filter $f'$, and for pixel $i$, the responsivity $R_{det}$ is derived from:

$$R_{det}(i) = \frac{S_{fcs}(i) C^{det}_{int}}{P^{f'}_{fcs}(h) \Gamma^{f'}(i) \chi^{f'}(i)} \quad (A/W) \tag{5.3}$$

where the prime ($'$) indicates the FCS measurement configuration and

- $S_{fcs}$: the signal in V/s from the FCS measurement after subtraction of dark signal or FCS straylight (only possible with PHT05 and PHT25);
- $C^{det}_{int}$: the integration capacity in A/(V/s) (=farad) associated with detector $det$ (see Fig. 3.2 and Table 13.5);
- $P^{f'}_{fcs}(h)$: the in-band power in W for filter $f'$ and FCS heating power $h$ in mW as obtained from the FCS power table, for PHT-P the power is per mm$^2$, for PHT-C per pixel;
- $A(a)$: the area of aperture $a$ in mm$^2$;
- $\alpha^{f'}(a)$: dimensionless correction for inhomogeneous illumination of PHT-P aperture $a$ by the FCS in filterband $f$;
- $\Gamma^{f'}(i)$: dimensionless correction for PHT-C pixel $i$ due to inhomogeneous illumination of the array by the FCS;

- $\chi^{f'}(i)$: dimensionless correction for pixel $i$ for non-uniform filter-to-filter responsivity of the PHT-C pixels.

Once the detector responsivity is known, measurements of a celestial source with filters of the same detector in a multi-filter photometry observation can be calibrated. For a given PHT-P measurement, the in-band power $P^f_{src}(a)$ for filter $f$ and aperture $a$ is:

$$P^f_{src}(a) = \frac{[S_{src}(a) - S^{det}_{dark}]C^{det}_{int}}{R_{det}} \qquad (W) \tag{5.4}$$

For a given PHT-C measurement, the in-band power $P^f_{src}(i)$ for filter $f$ and for pixel $i$ is:

$$P^f_{src}(i) = \frac{[S_{src}(i) - S^{det}_{dark}]C^{det}_{int}}{R_{det}\chi^f(i)} \qquad (W) \tag{5.5}$$

where $S_{src} - S^{det}_{dark}$ is the source signal in V/s after dark signal subtraction. Note that the correction $\chi^f(i)$ cancels out for a PHT-C source measurement taken in the same filter band as for the FCS measurement. To convert from in band power to point source flux density on the sky, the following relation is used for PHT-P:

$$\frac{F^f_\nu}{k_f} = \frac{P^f_{src}(a)}{C1^f f^f_{PSF}(a)} \qquad (Jy), \tag{5.6}$$

and for PHT-C:

$$\frac{F^f_\nu}{k_f} = \frac{\sum_{pixi} P^f_{src}(i)}{C1^f f^f_{PSF}} \qquad (Jy), \tag{5.7}$$

where:

- $F^f_\nu$: the source flux density in Jy for an assumed spectral energy distribution $\nu f_\nu$ = constant;
- $k_f$: the colour correction;
- $C1^f$: constant in m$^2$Hz describing[1] the transmission of the whole optical path for a given filter. The effective size of the primary mirror, reflections, filter transmission, spectral response of the detector, etc. are included;
- $f^f_{PSF}$: (dimensionless) fraction of the ISO point spread function entering the field aperture in case of PHT-P or falling onto the entire array in case of PHT-C for filter $f$.

$F^f_\nu$ is also referred to as the flux density at the reference wavelength of the filter band and is the value of the flux density computed by OLP. It is required that the constant $C1^f$ is identical to the one used in the determination of the FCS power tables.

### 5.2.4 Spectro-photometry with PHT-S

In the short wavelength range below 10 $\mu$m very high FCS heating powers are required to get a reasonable in-band power. Due to the wavelength coverage of PHT-S no single FCS power can illuminate both SS and SL arrays without causing saturation in the SL array. Therefore, the PHT-S measurements (PHT40) are not accompanied by any FCS measurement. It is assumed that the PHT-S responsivity is sufficiently stable throughout the ISO mission.

The flux calibration for point sources is carried out by direct comparison between the signals (in V/s) of the PHT-S pixels and the flux (in Jy) of the calibration target. Only stars have been used for the determination of the PHT-S spectral response function. The responsivity was monitored on a weekly basis using calibration stars. The flux density $F_\lambda(i)$ of pixel $i$ is derived as follows:

[1] C1 is the same parameter as the $C1$ factor given on page 58 of the ISOPHOT Observers Manual [10]. Beware that the values of C1 have changed.

$$F_\lambda(i) = 10^{-20}\frac{[S_{src}(i) - S_{dark}(i)]}{C_{s,pnt}(i)} \cdot \frac{c}{\lambda^2(i)} \qquad (Wm^{-2}\mu m^{-1}), \tag{5.8}$$

where

- $S_{src}(i) - S_{dark}(i)$: the source signal in V/s of a PHT-S pixel after dark signal subtraction;
- $C_{s,pnt}(i)$: the conversion in (V/s)/Jy from signal to point source flux density in Jy;
- $c$: is the speed of light in m/s;
- $\lambda(i)$ is the central wavelength of the PHT-S pixel.

similarly, for extended sources:

$$I_\lambda(i) = 10^{-26}\frac{[S_{src}(i) - S_{dark}(i)]}{C_{s,ext}(i)} \cdot \frac{c}{\lambda^2(i)} \qquad (Wm^{-2}\mu m^{-1}sr^{-1}), \tag{5.9}$$

where $C_{s,ext}(i)$ is the conversion in (V/s)/(MJy/sr) from signal to point source flux density in MJy/sr.

Monitoring of the PHT-S responsivity at the beginning and end of each revolution has shown that the daily responsivity variation is at most 10% depending on the space weather conditions. Relative variations along a revolution and from revolution to revolution can be inferred by comparison with the PHT-S responsivity checks performed in the activation and de-activation windows at the begin and end of a revolution. Shorter time scale responsivity variations are mainly due to detector transients which can be corrected using a transient model.

## 5.3 Point sources versus extended sources

All targets used for flux calibration are point sources in the ISOPHOT wavelength range. For an extended source which is much larger than the aperture or pixel, the surface brightness is derived by involving the effective solid angle of the aperture or pixel.

For the P subsystems, the effective solid angle for each aperture corresponds to the area of the aperture in the focal plane projected on the sky. The areas were determined from the measured physical dimensions of the apertures.

The conversion form point source flux $F_\nu^f$ in Jy to a surface brightness can be written for PHT-P as follows:

$$I_\nu^f = \frac{F_\nu^f f_{PSF}^f}{(1-\epsilon^2)\Omega_{eff}^f} \qquad (MJy/sr) \tag{5.10}$$

where $\epsilon$ is the obscuration factor for the ISO secondary mirror, $\Omega_{eff}^f$ in sr is the effective solid angleof the aperture or pixel, for a given filter $f$. In OLP Version 7 the PHT-C surface brightness is derived from the in-band powers of each pixel. The computation for PHT-C is as follows (with the same notations):

$$I_\nu^f = \frac{k^f P^f(i)}{C1^f(1-\epsilon^2)\Omega_{eff}^f} \qquad (MJy/sr) \tag{5.11}$$

A model of detector *footprints* (or beamprofile) is used to determine the effective solid angles of the C100 and C200 detector pixels $\Omega_{eff}$ for each filter band. The model takes into account the ISO primary mirror, secondary mirror, tripod, and the linear sizes of the detectors as measured pre-flight.

For PHT-S the values of $\Omega_{eff}$ for each pixel were determined from in-flight calibration observations of the detector footprints. These values are included in the conversion from signal to extended source flux density, see Eqn. 5.9.

## 5.4 Aperture calibration

For a given filter of the PHT-P subsystems, the FCS calibration has been determined from observations always taken with the same standard aperture (section 4.5.4). In OLP Version 7, the applicability of the calibration to any given aperture is based on the following assumptions:

1. the apertures are perfectly circular or rectangular,
2. the solid angle of an aperture is proportional to its area,
3. the solid angle of an aperture is independent of filter,
4. the FCS in-band power is proportional to the area of an aperture.

The physical dimensions of the apertures were measured on ground and are given in section A.1.2. From available calibration measurements deviations from these simple assumptions are clearly indicated:

- Aperture sequences on the FCS indicated that assumption 4 is not valid. Deviations up to 100%, 15%, and 40% were measured for P1, P2, and P3 respectively; the deviations also show a dependency on FCS heating power.
- Observations of flat sky areas have indicated a disproportional increase of signal for the largest apertures (size$> 120''$) arguing against assumption 2.
- Scans of point sources for a given aperture give profiles that show large deviations from the expected profiles based on assumption 1, probably due to spatial inhomogeneities of the system transmission.

The assessment is ongoing. In OLP Version 7 no corrections are made for these deviations. Corrections are foreseen in a future version of the software.

## 5.5 PHT-S wavelength calibration

The in-orbit PHT-S wavelength calibration was performed by measuring emission line objects with PHT-S; see section 4.6.2. The accuracy in the central wavelength for each pixel is somewhat smaller than one tenth of a pixel except for a small part of SL where the uncertainty is marginally larger. The accuracy of the wavelength calibration is discussed in [11]

## 5.6 Photometric calibration in AOTs

### 5.6.1 General signal derivation

All raw PHT measurements undergo the same processing steps to obtain the mean signal per chopper plateau or mean signal per raster point. These steps are described in detail in Chapter 7. Here we only list the relevant correction steps:

- correction for non-linearities of the integration ramps,
- ramp deglitching,
- reset interval correction,
- dark signal subtraction,
- signal deglitching,
- transient correction,
- chopper vignetting,
- correction for chopped signal losses.

### 5.6.2 Multi-filter photometry: PHT03 and PHT22

Single pointing photometry AOTs include one FCS measurement for each detector used. The FCS measurement is taken after completion of the filter sequence for a given detector (see section 3.7).

Assuming that the derived responsivity applies to all filters of the same detector, the signal from each filter is converted to a in-band power. Depending on the filter and aperture selected, the powers are converted to an a flux density in Jy or MJy/sr using equations in section 5.2.3.

### 5.6.3 Mapping: PHT03, PHT22, PHT32

For AOTs in mapping mode each raster measurement is bracketed by two FCS measurements with identical FCS heating power. For the calibration it is assumed that the responsivity varies proportionally with time between the two FCS measurements. A linear interpolation in time between the responsivities of the two FCS measurements is performed to determine the responsivity at the time of the integration on a raster point. Since the map plus FCS measurements are obtained for one filter at a time, no uncertainties due to $\chi^f(i)$ are involved.

### 5.6.4 Sparse maps: PHT17/18/19 and PHT37/38/39

During a sparse map concatenated chain (P17/18/19 for PHT-P or P37/38/39 for PHT-C) two FCS measurements are obtained, the first measurement after the sky measurement(s) in PHT17/PHT37 and the second after the sky measurement(s) in PHT19/PHT39. The FCS in-band powers are adapted to the flux levels as specified in the start and end AOTs and can therefore be different FCS heating power settings.

For the sparse map AOTs P17/18/19 and P37/38/39, the multi-filter option can be used. In such case a linear interpolation in time between the responsivities of the two FCS measurements is performed as well as a transfer of the calibration to the filters for which no FCS calibration are obtained.

### 5.6.5 Multi-aperture photometry: PHT04

In this mode one FCS measurement is collected for the last (largest) aperture in the sequence. An important source of photometric uncertainty is the accuracy in the aperture scaling (see 5.4). Uncertainties in the beamprofile can be minimized by comparison with a similar observation on a point source.

### 5.6.6 Absolute photometry: PHT05 and PHT25

For P05 and P25 only one filter band can be selected and the FCS measurement has the same integration time as the source measurement. The observer can therefore minimize statistical and transient uncertainties. Uncertainties due to dark signal and FCS straylight can be minimized by including dedicated dark and cold FCS measurements in the observation. Since the absolute photometry AOTs are single filter observations, the photometric accuracy only depends on the uncertainties in the FCS power calibration tables and either in the illumination matrix for PHT-C or the aperture scaling for PHT-P (both for FCS and sky).

### 5.6.7 PHT-S: PHT40

The instrument set-up of a P40 observation is always the same. After dark signal subtraction, the signal of each pixel is directly converted to a flux density in units of $\mathrm{Wm}^{-2}\mu\mathrm{m}^{-2}$. The PHT-S spectral response function was determined from observations of calibration stars (section 5.2.4). In-orbit beam profile measurements were used to determine the conversion from a point source flux to an extended source flux.

Each target measurement with PHT40 is preceded by a "pseudo" measurement of 32 seconds in dark instrument configuration. This measurement offers a qualitative assessment whether the responsivity of the PHT-S detectors is affected by a transient introduced by a preceding PHT40 observation.

For example, in case the preceding PHT40 observation involved a source with bright spectral features, the pixels that detected the features can still be in a transient while the pseudo dark is being taken. It

Table 5.1: Cal G files related to the parameters described in this chapter

| parameter | Description | full description |
|---|---|---|
| $P^f_{fcs}(h)$ | FCS power calibration tables | section 13.10 |
| $R_{det}$ | Default detector responsivities | section 13.11 |
| $f^f_{PSF}$ | Point Spread Function factors | section 13.15 |
| $\alpha^f(a)$ | Inhomogeneous FCS illumination of PHT-P | section 13.13 |
| $\Gamma^f(i)$ | Array Illumination by FCS | section 13.12 |
| $\chi^f(i)$ | Wavelength dependent detector flat fields | section 13.14 |
| $C1^f$ | Conversion from in-band power to flux density | section 13.17 |
| $S^{det}_{dark}$ | Default dark signals | section 13.7 |
| $\Omega^f_{eff}$ | Effective solid angles of apertures and pixels | section 13.18 |
| $C_{s,pnt}(i)$, $C_{s,ext}(i)$, $\lambda(i)$ | PHT-S wavelength and signal calibration | section 13.16 |
| $k_f$ | Colour corrections | section 13.19 |

is also found that different pixels in the PHT-S array show different transient behaviour. This can cause artifacts in the spectrum, especially after observing a strong continuum source.

Possible features in the dark spectrum at a certain wavelength should caution the observer that features in the same pixels of the actual source spectrum could have an instrumental cause. The dark measurement in PHT40 is *not* intended for subtraction from the source spectrum.

## 5.7 Calibration files

### 5.7.1 Calibration G files

The instrument characteristics required for the processing of the raw ISOPHOT data into calibrated products are stored in calibration files which are referred to as "Calibration G" or "Cal G" files. All Cal G files are in FITS format. The Cal G files are updated depending on the outcome of the dedicated calibration observations.

In the Table 5.1 the types of Cal G information mentioned in this chapter are listed together with references to the full descriptions elsewhere in this manual. A complete description of all Cal G files can be found in chapter 13.

### 5.7.2 Calibration A files

Cal G files should not be confused with the ISOPHOT dataproducts related to the FCS measurements which are part of all PHT AOTs except P40. These products are called "Calibration A" or "Cal A" files. Cal A files are generated at the SPD processing level. Among other data items the Cal A products contain the signal per chopper plateau. The FCS heating power as well as the expected in-band power is provided so that the responsivity of the detector close to the time of the target measurement can be obtained. The derived responsivity together with its uncertainty for each detector pixel has been included in the FITS header of the related SPD product.

See also sections 12.3.7 and 12.3.8.

# Chapter 6

# Data Processing Level: Derive_ERD

The *telemetry distribution files* (TDFs) from an entire revolution have been scanned in order to obtain a number of histories which are used to control the succeeding processing phases. These histories are: (*i*) the continuous compact status history (CCSH) and (*ii*) the executed observation history (EOH). The CCSH and EOH contain all necessary information to extract the telemetry data covering a target dedicated time (TDT, see glossary section E). This first global step is called TDF_FIRST_SCAN.

The telemetry is accessed again to generate the first level of data products, called *edited raw data* (ERD), being the format in which raw ISO telemetry will be distributed to observers. ERD is basically reformatted TDF data from which invalid sections are removed. No scientific or instrument-specific processing is performed. ERD products are in the form of binary FITS tables.

ERD generation is performed in units of an observation. The start and end times which are recorded in the EOH determine the interval of telemetry for a given observation[1]

The ERD processing also cuts the CCSH into compact status history (CSH) products. A CSH product contains all compact status information belonging to a given TDT for a given instrument.

As the telemetry data are in "raw" engineering units, conversion algorithms should be applied to convert these engineering units to "physical" units. In appendix B descriptions of the main conversions are provided.

In order to facilitate the processing steps in the succeeding Derive_SPD level, the orbital phase of the spacecraft for 3 reference times (start, middle, and end) of a TDT are included in the ERD data. The corresponding ERD header keywords are TREFCORn and TREFPHAn (with n=1, 2, 3) for the UTC of reference time and corresponding orbital phase, respectively. The information is necessary for the application of calibration data which depend on the position of the spacecraft in the orbit. The orbital phase data are derived from the orbit file. Since this is processed with the APH (aperture pointing history) data, the orbital phase information is already available on ERD processing level.

[1] These times correspond to the Start_TDT and End_TDT times in the pointed observation file (POF)

The ISOPHOT ERD products have been defined on the basis of the data format of the different subsystems. There are 5 types of ERD:

1. with prefix PPER for single detector subsystems PHT-P1, P2, and P3 (see section 12.2.2),
2. with prefix P1ER for PHT-C100 (see section 12.2.3),
3. with prefix P2ER for PHT-C200 (see section 12.2.4),
4. with prefix PSER for PHT-S (both PHT-SS and SL together in one file, see section 12.2.6), and
5. with prefix P2ES for PHT-C200 Serendipity Mode scans (see section 12.2.5).

The CSH data format is the same for all detector subsystems.

# Chapter 7

# Data Processing Level: Derive_SPD

## 7.1 Overview

Conceptually, for a given AOT the derivation of *standard processed data* (SPD) can be divided into three main stages:

- *ramp processing*: Integration ramps in V are reduced to signals in V/s.
- *signal processing*: Signals are corrected for instrumental effects and averaged over a given period in time.
- *in-band power calibration*: One or more FCS measurements that were collected according to the AOT logic are processed to determine calibration factors. These factors are used to convert the signals from the sky measurements to an in-band power (in W) on the detector for the selected filter band. In case FCS measurements cannot be applied, the conversion is based on a default detector responsivity.

SPD processing derives a record for each consecutive period in the sky measurement for which the power on the detector is expected to be constant:

- a staring measurement yields one SPD record;
- a chopped measurement yields 2 or 3 times the number of chopper cycles as SPD records depending on the chopper mode (2 for rectangular, 3 for sawtooth and triangular);
- a raster yields one SPD record per raster position;
- a PHT32 sky measurement contains one SPD record for each chopper plateau.

Apart from the mean in-band power, each record contains additional information such as the power uncertainty, median value, etc (see section 12.3).

The above description of SPD records applies to all AOTs except AOT P40 (PHT-S spectro-photometry). SPD for P40 contains signals (in V/s) instead of in-band powers (in W). In the processing level following SPD (see chapter 8) the PHT-S signal is directly converted to an astronomical flux (in Jy). This is a consequence of the absence of FCS measurements, filters, and apertures in the PHT-S subsystem.

Besides the SPD products that yield the processed data for the sky measurements a number of other products are derived based on non-sky internal measurements. The products refer to the following type of measurements (see section 3.3):

- FCS measurement. The resulting product is also referred to as a *Calibration A* ("Cal A") file.
- Dark instrument configuration measurement. This measurement type is obtained with AOTs PHT05, PHT25, and PHT40 and is used to subtract dark signals (in case of PHT05 and PHT25) or to identify possible detector memory artifacts from a preceding measurement of a bright source (in case of PHT40)

- Cold FCS measurement. This type of measurement occurs in the absolute photometry AOTs PHT05 and PHT25 to correct for FCS straylight.

## 7.2 Ramp Processing

### 7.2.1 Discarding destructive read-outs

**Detailed description:** section 3.2.2

The destructive read-out is the last read-out of a ramp prior to the reset of the read-out electronics and is in general disturbed by the pulse pattern of the electronics. Destructive read-outs usually do not follow the highly linear relationship between time and read-out voltage as is the case for the non-destructive read-outs.

In Derive_SPD the destructive read-out is assumed unreliable and is discarded.

**Ancillary data required:**

None

### 7.2.2 Discarding disturbed non-destructive read-outs

**Detailed description:** section 4.3.1

At the beginning of an integration ramp immediately after a reset, the first non-destructive read-out is unreliable. In case of a large number of non-destructive read-outs per ramp, more than one read-out can be disturbed.

In Derive_SPD the first fraction $x$ of an integration ramp is discarded, where $x$ depends on the number of non-destructive read-outs.

**Ancillary data required:**

The value of $x$ as a function of number of non-destructive read-outs. The table is stored in Cal G file PSELNDR, see section 13.4.

### 7.2.3 Discarding data with OTF or OPF "off"

**Detailed description:** none

During a sky measurement the source can drift out of its nominal pointing due to telescope pointing instabilities. When this happens the *on-target flag* (OTF) is automatically set to "off".

Similarly, if the chopper is not correctly positioned, a chopper *on-position flag* (OPF) is also set to "off".

Initially, until revolution 524, the OTF is set to off when the actual pointing drifts out of a cone with radius of $10''$ around the intended pointing. Due to the good pointing performance of ISO the OTF cone has been reduced to $2''$ for ISOPHOT as of revolution 524.

The OTF and OPF flags are contained in the read-out records of the ERD products. If either of these flags is set to off then the current integration ramp is abandoned and excluded from further processing. A record is kept per pixel per measurement of the number of integration ramps that are rejected for this reason.

For raster scans, it is assumed that the spacecraft moves off target to the next raster point when one of the two raster point identifiers changes. To avoid the inclusion of off-target data while the spacecraft is slewing and repositioning all data are rejected for a fixed (1 sec) period after the change in the raster point identifier. After this period the OTF is checked: if the OTF is off then data are rejected until the OTF is on again.

**Ancillary data required:**

None

### 7.2.4 Sorting out the different data-types

**Detailed description:** none

The different measurements that were performed as part of an AOT (like sky, FCS, and dark measurements) need to be identified and separated before they can be processed. For a given TDT all output data records of the same detector and measurement type will be stored inside the same SPD product.

Different measurements are sorted out by performing a cross-correlation between the ERD record and the corresponding CSH record with the same time key. The following flags are then inserted at the beginning of each data record in Derive_SPD to identify the type of measurement:

- Raster point ID
- Aperture ID
- Chopper position
- Filter ID
- Polarizer ID

Note that the filter ID also determines the detector.

**Ancillary data required:**

None

### 7.2.5 Conversion of digitized numbers to CRE output voltages

**Detailed description:** section 3.2.3

The detector interface electronics (DIE) in the PHT external electronics unit subtracts a commandable offset from the CRE voltage and amplifies the difference with a commandable gain factor before the analogue to digital conversion. The CRE output voltage must be reconstructed from the *digitized numbers* (DN).

There are two DIE chains. Each detector subsystem has a default connection to one of them (see 3.2.3). A change in default connection is indicated by the "cross status" flag in the CSH (actually never used during the mission). The CSH also contains the value of the selected gain of the differential amplifier in the DIE electronics. The CRE output voltage and DNs are related by the following formula for a given DIE electronics chain and selected gain:

$$\mathrm{CRE[V]} = (\mathrm{D_o} - \mathrm{DN} - \mathrm{GAIN_2} \times (\mathrm{DI} - 2048)) \times \frac{20.0[\mathrm{V}]}{4096 \times \mathrm{GAIN_1}} + \mathrm{U_{off}[V]} \tag{7.1}$$

where,

$\mathrm{D_o}$ = fixed offset

$\mathrm{GAIN_2}$ = offset gain

DI = selected OFFSET data word (0...4095)

$\mathrm{GAIN_1}$ = signal gain

$\mathrm{U_{off}}$ = $\mathrm{GAIN_1}$ dependent offset

**Ancillary data required:**

1. The selected OFFSET from the measurement record in the CSH.
2. The DIE transfer function table which is a Cal G files PDIE1TRANS and PDIE2TRANS, see 13.3.

### 7.2.6 Discarding saturated read-outs

**Detailed description:** section 4.3.5

If the source is significantly brighter than anticipated, integration ramps can saturate, i.e. the CRE output voltage has reached its maximum value prior to reset. The read-outs taken during times of detector saturation are useless and must be discarded. Saturation also occurs in case the responsivity of the detector exceeds the nominal value by a large factor. In practice this frequently happened towards the end of the science window where both FCS and sky measurement got saturated due to high responsivity. For detectors P3, C100 and C200 many FCS measurements taken during revolutions 94–191 were saturated due to over-illumination by changed FCS behaviour.

Threshold voltages for each detector are listed in section 4.3.5. As soon as the threshold voltage has been crossed, all following read-outs up to the end of the ramp are discarded.

**Ancillary data required:**

In the current OLP version it is assumed for all detectors that saturation is reached for CRE output voltages greater than 1.0 V.

### 7.2.7 Correction for non-linearities of the integration ramps

**Detailed description:** sections 4.3.2 and 4.3.4

Integration ramps are not perfectly straight but show deviations from linearity. The non-linearity is caused by two independent effects:

- non-linearities due to the CRE (section 4.3.2)
- downward curving due to de-biasing. Only low-bias germanium detectors P3, C100 and in particular C200 show this effect (section 4.3.4).

The integration ramps are corrected for non-linearities before signals are derived.

In Derive_SPD it is assumed that the corrections are only a function of the absolute value of the CRE output voltage. In addition it is assumed that non-linearities due to both CRE and debiasing (as is the case for the germanium detectors P3, C100 and C200) can be corrected using one function which only depends on the CRE output voltage.

The ramps are linearized using tables which contain for a given CRE output voltage the correction voltage to be subtracted. In the tables the sampling of the CRE voltages is sufficiently fine to allow searching for the table value closest to the measured CRE voltage and using its corresponding correction.

**Ancillary data required:**

The CRE Transfer Function Table per detector pixel and clock frequency are stored in Cal G files PC1CRELIN, PC2CRELIN, and PPCRELIN (section 13.5). There is no ramp linearisation for PHT-S measurements.

### 7.2.8 Ramp deglitching

**Detailed description:** section 4.4

A radiation hit or glitch shows up as a voltage increase between read-outs which is larger than the increase expected from the source photo-current. In case the hit is very energetic, the voltage increase can be so high that it saturates a ramp or even causes a responsivity transient. In SPD two different deglitching algorithms are applied: the first algorithm is described in this section and is based on an analysis of the read-outs per ramp; the second one checks for any outliers in the signals of a given chopper plateau and is described in section 7.3.4.

For ramp deglitching, an iterative algorithm has been implemented which identifies and removes excessive increases in CRE output voltage. The algorithm has the following settings:

| | | | |
|---|---|---|---|
| $N_{it}$ | = | 4 | number of iterations |
| $N_\sigma$ | = | 4.5 | minimum number of standard deviations for glitch detection |
| $N_{min}$ | = | 25 | minimum number of read-outs/ramp for application of algorithm |

For integration ramps with less than $N_{min}$ read-outs no ramp deglitching is applied and the deglitching can only take place at signal level (section 7.3.4). For an integration ramp consisting of $N > N_{min}$ read-outs with voltages V(1), V(2),...V(N), taken at times t(1), t(2),...t(N), the slope between each consecutive read-out is calculated:

$$S(i) = \frac{V(i+1) - V(i)}{t(i+1) - t(i)} \qquad V/s. \tag{7.2}$$

In addition, the mean, $S$, and standard deviation, $\sigma$(S), of these slopes are determined. In case,

$$S(j) > S + N_\sigma * \sigma(S) \qquad V/s, \tag{7.3}$$

then the voltages j+1 to N are corrected conform to the mean slope,

$$V_{corrected}(i+1) = (V(i+1) - V(i)) - (V(j+1) - V(j)) + \Delta V \quad V, \quad i = j, ..., N-1 \tag{7.4}$$

where $\Delta V$ is the mean voltage difference for all read-outs. This procedure is repeated $N_{it}$ times to remove successively smaller glitches.

**Ancillary data required:**

None

### 7.2.9 Extraction of the signals and their uncertainties

**Detailed description:** section 3.2.2

The slope of each ramp $s_{ph}$ (or *signal* in V/s) is proportional to the photo-current which is a measure for the number of photons falling on the detector per unit time. In the SPD processing all valid read-outs between two reset intervals are used to fit a first order polynomial. The uncertainty $\Delta s_{ph}$ is the rms of the fit residuals.

**Ancillary data required:**

None

## 7.3 Signal Processing

### 7.3.1 Reset interval correction

**Detailed description:** section 4.3.3

The detector CRE's give systematically different signals for different reset intervals under constant illumination conditions. Analysis of a photometric measurement requires signal information of other measurements such as internal calibration, background, external calibration, target, etc. If these measurements have not the same read-out set-up systematic errors are introduced into the photometric calibration.

It is found that a signal $s(RI,\ DAT_RED)$ obtained with a given reset interval RI and data reduction DR can be converted to a signal $s(RI_x,\ DAT_RED_x)$ of a different CRE settings according to:

$$\begin{aligned} s(RI_x,\ DAT_RED_x) \ = \ & A_0^x(RI_x, DAT_RED_x, RI, DAT_RED) \\ & + A_1^x(RI_x, DAT_RED_x, RI, DAT_RED) \cdot s(RI,\ DAT_RED) \qquad V/s, \end{aligned} \tag{7.5}$$

where $A_0^x$ is the offset value and $A_1^x$ is the slope in the relationship. Both parameters differ for different detectors. In OLP the reset interval dependence is corrected by transforming all signal values $s(RI)$ to the corresponding values for a *reference reset interval* $s(RI = \frac{1}{4}\,s, DAT_RED = 1)$:

$$\begin{aligned} s(RI = \frac{1}{4}\,s,\ DAT_RED = 1) \ = \ & A_0(RI,\ DAT_RED) \\ & + A_1(RI,\ DAT_RED) \cdot s(RI,\ DAT_RED) \qquad V/s, \end{aligned} \tag{7.6}$$

where the superscript $^x$ has been dropped to indicate that the constants $A_0$ and $A_1$ refer to the reference reset interval.

**Ancillary data required:**

For each detector the correction factors $A_0$ and $A_1$ are stored in Cal G files PP1RESETI, PP2RESETI, and PP3RESETI for the P detectors and PC1RESETI and PC2RESETI for the C detectors (section 13.6). There is no reset interval correction for PHT-S measurements.

### 7.3.2 Dark signal subtraction

**Detailed description:** section 4.2.5

Dark signals need only to be subtracted for staring mode measurements. Therefore, if the chopper mode is used (see eg. Table 12.2) in AOTs PHT03, PHT22, or PHT40, then the dark signal is not subtracted. In all other cases the dark signal is subtracted from the signal:

$$s'(\phi(t)) \ = \ s(\phi(t)) - s_{dark}(\phi(t)) \tag{7.7}$$

$$s' \ = \ s \qquad\qquad if\ chopper\ mode\ used \tag{7.8}$$

Where $s'(\phi(t))$, $s(\phi(t))$, and $s_{dark}(\phi(t))$, are the corrected, initial, and dark signal, respectively. The orbital phase $\phi(t)$ ranges between 0 and 1 where 0 is the moment of perigee passage and 1 is a full revolution later. The ERD contains the keyword TREFPHA2, which is the orbital phase the start of the measurement. The value for $\phi(t)$ in Eqn. 7.8 corresponds to the time mid-point of a chopper plateau.

**Ancillary data required:**

Dark signal tables for each detector-pixel combination have been derived from dedicated in flight observations. The tables contain a value for the dark signal plus uncertainty (in V/s) for each detector pixel as a function of orbital phase. The data are stored in Cal G files PPDARK (for detectors P1, P2, P3), PC1DARK (contains 9 pixels of C100), PC2DARK (4 pixels of C200), PSDARK (128 pixels of PHT-S), see section 13.7.

### 7.3.3 Determine chopper position and step number

**Detailed description:** sections 3.2.4, 3.6 and appendix B.3

The telemetry contains the actual chopper position which is recorded every 2 s. The data are provided as voltages and must be converted to a deflection angle. The conversion algorithm can be found in appendix B.3.

The chopper dwell time is directly related to the instrument read-out timing parameters (see section 3.2.4) and is therefore a reliable parameter in the instrument commanding. Using the chopper dwell time corrected for the chopper movement (section 3.6), the moment is determined in ITK units when the chopper should have changed its position.

From the inferred chopper transitions and the ITK of the read-outs the chopper step number is obtained. In principle the same can be done from direct analysis of the chopper position in the telemetry data. The reasons why time is used rather than the chopper position are:

- the chopper position associated with the first integration ramp after a chopper transition is unreliable (on-board software feature), and
- the algorithm allows recovery of the correct position in the chopper cycle if there is a gap in the data due to telemetry dropouts.

To remove possible contamination by unreliable chopper positions in the data products, a median filter is applied to the positions associated with each integration for a fixed chopper position.

Before the chopper position can be calculated it is necessary to determine the *step number* $I_{step}$ within a cycle. The amount of steps in a cycle depends on the chopper mode as follows:

| | |
|---|---|
| Staring | 1 |
| Rectangular | 2 |
| Sawtooth | $2 \times steps + 1$ |
| Triangular | $4 \times steps$ |

Where *steps* indicate the number of chopper offset positions at one side of the central field of view (CFOV). The ITK is used to calculate the position in the cycle. In general, for rectangular, sawtooth and triangular chopping, the first chopper position is an "off-source" position, the second position is an "on-source" position (section 3.6). This is then digitised to the step number $I_{step}$ as follows:

**Staring:** $I_{step} = 1$, unless pointing at the FCS, in which case it is defined to be -1.

**Rectangular:** $I_{step}$ = -1 on-source, 1 for background.

**Sawtooth:** $I_{step}$ varies from $-steps$ at maximum negative angle to $+steps$ at maximum positive angle. Step number 0 represents the CFOV.

**Triangular:** As for sawtooth.

**Ancillary data required:**

None

Table 7.1: Parameters for signal deglitching

| Parameter | Value | Description |
|---|---|---|
| min_deglitch | 5 | minimum points to apply |
| max_error | 1 V/s | maximum error allowed if number of points is less than min_deglitch |
| n_iter | 2 | number of iterations of deglitch filter |
| n_local | 20 | number of points in local distribution |
| n_step | 1 | the number of points to move the 'box' for the local distribution each time |
| n_sigma | 3 | Rejection factor: number of standard deviations from local median. |
| n_bad | 2 | number of times point has to be flagged as 'bad' before it is rejected. |

### 7.3.4 Signal deglitching

**Detailed description:** section 4.4

The charges released by a cosmic particle hit cause an effective increase in signal level. Low energetic hits affect only one signal, but high energetic hits can cause several consecutive signals to be higher. A high hit rate can cause the mean signal level in a measurement to increase.

Assuming that the signal distribution is normal on a local scale, a *local distribution* method is used to filter out signal outliers. The method consists of a 'box' sliding along the time axis and local distributions are calculated as it goes. Signals are flagged that are outside a given number of standard deviations from the median for a given local distribution. A signal is eventually discarded in case it is flagged a pre-set number of times. This process is iterated several times.

If the number of available signals is insufficient then a signal is discarded whenever its uncertainty $\Delta s_{ph}$ (section 7.2.9) is greater than a given threshold. The controlling parameters of the algorithm are given in Table 7.1.

The accuracy of this method depends on the glitch frequency and the values of the tuning parameters (ref. *Deglitching of ISOPHOT Data* by S.Guest [5]). The number of signals affected by glitches is stored in the header of the SPD product (keyword RAMPDEGL, see section 12.3.1.3)

**Ancillary data required:**

None

### 7.3.5 Transient correction

**Detailed description:** section 4.2.2

A routine has been implemented which detects the presence of a significant signal transient on a chopper plateau. When a transient is detected, a range of unreliable signals will be flagged. The algorithm is iterative and is applied until either

- no significant systematic variation can be detected in the remaining signals or,
- a minimum amount of signals is left.

It is assumed that a detector transient shows up as a trend which causes either a systematic increase or decrease of the signal level. The signal level will eventually become stable in time when the signal reaches its asymptotic limit. The presence of such a trend is detected by applying the non-parametric Mann statistical test to the signals (e.g. [38]). This involves computing a statistic C:

$$C = \sum_{i=1}^{N-1} \sum_{j=i+1}^{N} Q \tag{7.9}$$

where,

$$\begin{aligned} \mathrm{Q} = \mathrm{sign(S(j) - S(i))} &= +1 \quad \text{if S(j)} > \text{S(i)} \\ &= 0 \quad \text{if S(j)} = \text{S(i)} \\ &= -1 \quad \text{if S(j)} < \text{S(i)} \end{aligned}$$

for all signals S(i), where i = 1,...,N and N is the number of signals on the chopper plateau. The presence of a transient can be detected by comparing C against the corresponding Kendall k-statistic for a given confidence level.

Alternatively, as the number of signals is generally large, it is more convenient to compute the statistic C(*) which can be compared with the quantile of a normal distribution:

$$C(*) = \frac{C}{\sqrt{N(N-1)(2N+5)/18}} \ . \tag{7.10}$$

The algorithm requires the following parameters:

- N(min) = 7 - the minimum number of signals for application of the Mann test,
- $\alpha = 0.05$ - the probability that the null hypothesis (=no drift) is rejected.

The result, $C(*)$, is tested against the null hypothesis which assumes absence of drift. This corresponds to a critical value of $C(*) < 1.645$ for $\alpha = 0.05$. A test is made on whether the drift is up ($C(*) < 1.645$) or down ($C(*) > -1.645$).

The algorithm initially performs the test on all available signals on a chopper plateau. If the null hypothesis is rejected then the test is performed on the second half of the data and the first half is rejected. If the null hypothesis is again rejected then the second half of the second half is tested etc. The iteration stops either when the null hypothesis is accepted or when there are too few signals (N≤N(min)) to apply the test. Information on the outcome of the procedure is stored per chopper plateau by setting the pixel status flags 2 ("drift fit applied successfully") or 4 ("drift fit may not be accurate") in the SPD records (see Section 12.3.12).

**Ancillary data required:**

None

### 7.3.6 Averaging signals of same instrument set-up

**Detailed description:** section 4.2.5

To increase the signal-to-noise ratio, all valid signals on a single chopper plateau are averaged. The following formula is applied:

$$\langle s \rangle = \frac{\sum_1^N w_i \times s_i'}{\sum_1^N w_i} \qquad V/s, \tag{7.11}$$

where $N$ is the total number of valid signals on the plateau and $w_i = \Delta^{-2} s_{ph}$ is the statistical weight of each signal obtained from its associated statistical uncertainty propagated from the previous signal processing steps. The value for $N$ is stored in an SPD record PxxSNSIG.

The plateau average is either (1) the average of the signals which are not flagged as drifting according to the test described in section 7.3.5 or (2) the average of the last 7 signals of the plateau in case the test fails.

If it is not possible to calculate a weight for *any* of the signals on a plateau then all signals will have a weight $w_i = 1$ assigned. This can happen when the ramps consist of only 2 useful read-outs. If no weight can be calculated for a subset of the signals on the plateau then these will be weighted out by setting $w_i = 0$.

The uncertainty on the average signal is derived from the rms of the individual signals:

$$\Delta\langle s\rangle = \sqrt{\frac{\sum_1^N w_i \times (s_i' - \langle s\rangle)^2}{(N-1)\sum_1^N w_i}} \quad V/s. \tag{7.12}$$

**Ancillary data required:**

None

### 7.3.7 Obtaining the median of all photo-currents

**Detailed description:** none

The signal distribution can be non-gaussian due to signal transients or due the presence of many positive signal outliers caused by glitches which have not been filtered out completely. In such case, the median signal is a better estimate for the signal per chopper plateau than the average. The median and the quartiles in conjunction with the weighted average should retain information on non-gaussion signal distribution. For a gaussian distribution the median is close to the average, and the quartiles fall within the uncertainty interval.

Therefore the median ($\langle s_{ph}\rangle^M$) and first and third quartile of all available signals are calculated. Different from the computation of the weighted average, the determination of the median, first, and third quartile values does not exclude signals that are flagged as unreliable by the signal deglitching or transient correction.

**Ancillary data required:**

None

### 7.3.8 Correction for chopper vignetting

**Detailed description:** section 4.5.3

The throughput of the ISO and ISOPHOT optics depends on the chopper deflection. The level of variation is of order of a few percent for the maximum chopper deflection in case of the C100 and C200 subsystems. Especially for weak sources on a strong background this phenomenon can cause spurious detections or negative signals for some pixels on the arrays.

For each average and median signal $\langle s\rangle$ the correction $t_{chop}$ is applied:

$$\langle s_c\rangle = t_{chop}(filter, pixel, chopper\ deflection) \times \langle s\rangle \qquad V/s. \tag{7.13}$$

In case of an absence of chopper vignetting $t_{chop} = 1$.

**Ancillary data required:**

The correction for C100 and C200 are stored in the Cal G files PC1VIGN and PC2VIGN, see section 13.8. Since for the P detectors no measureable ($> 2\%$) effect could be found, the correction factors in the designated Cal G files PPxVIGN (x= 1, 2, 3) have been set to 1.

The structure of the related Cal G files is described in section 13.8.

### 7.3.9 Correction for chopped signal losses

**Detailed description:** none

For chopped observations the signal is modulated by the chopper between source and background. Due to the long response time of the detectors relative to the duration of a chopper plateau, the signal on a chopper plateau cannot stabilize. The resulting signal difference is less than the signal difference between two stabilized source and background measurements in staring mode.

Analysis of in-orbit calibration observations have shown that

- the losses are only significant ($> 10\%$) for measurements with detectors P3 and C100, the other detectors are less affected.
- the difference signal ratio obtained from chopped and staring mode observations $(s_{chop,on} - s_{chop,off})/(s_{staring,on} - s_{staring,off})$ depends to first order only on the chopper plateau time $t_{chop}$ given by $t_{chop} = DR \times RI$, where DR is the number of destructive readouts per chopper plateau and RI is the reset interval (see section 3.2.4).
- the detector responsivity that can be derived from the FCS observation (also taken in chopped mode between FCS1 and FCS2) cannot be used for flux calibration. Instead a default responsivity will be used, see section 7.4.

The computation of the difference flux between the on and off chopper plateaux is beyond Derive_SPD (cf. section 7.1) and reserved for Derive_AAR. As a consequence, in this processing step only the correction factors are obtained by reading the relevant Cal G files based on the value of $t_{chop}$. The correction factor is subsequently transferred to Derive_AAR processing via the SPD product in the header of the FITS file. The keyword is "CHCjRi" (Chopper correction factor) where i=[1, no. of pixels] and j=[1, no. of measurements].

As will be described in section 7.4 the individual chopper plateaux are calibrated using the default responsivity without any correction for losses.

**Ancillary data required:**

The correction factors are stored in Cal G files PPCHOPCOR, PC1CHOPCOR, and PC2CHOPCOR for the P, C100 and C200 detectors respectively. The structure of the Cal G files are described in section 13.9.

### 7.3.10 Ramp statistics in PHT SPD and Cal-A headers

**Detailed description:** none

Useful statistics about readout and signal discarding collected along the signal processing chain is made available to the observer. The statistical information is stored in the SPD product headers.

- **RAMPINVD:** number of times that the OTF indicated that the spacecraft was off-target during an observation, which can happen during raster observing modes
- **PLATNORP:** number of times during an observation that all ramps of a plateau have been rejected. In most cases this is due to the spacecraft being off target
- **RAMPSAT:** number of times that only one readout in an integration ramp is available for processing. This can happen at the end of a chopper cycle or due to partial saturation of ramps.
- **READSUSP:** number of ERD records that have been flagged as 'suspicious' due to the presence of a corrupted science floating block in the telemetry.
- **RAMPZSG:** number of signal values less than or equal to zero and occurs frequently when processing PHT-S data.

- **RAMPFROP:** number of first ramps on plateaux that have been ignored in the processing during an observation. The keyword is written to the SPD, Cal A and dark current product headers.
- **PdxcNSIG:** where d=P,C,S for PHT-P, PHT-C, or PHT-S subsystems, x=1,2,3,S,L for detector IDs, c=S,A,D for SPD, Cal A or dark signal files. This *record* provides the number of signals per chopper plateau that was used to compute the weighted mean per chopper plateau.

**Ancillary data required:**

None

## 7.4 In-band power calibration

**Detailed description:** section 5, 4.5.4

The steps described in this section are applied to all astronomical measurements except those collected with PHT-S. The PHT-S SPD processing finishes without this last step.

The detector responsivity varies along a revolution, in particular the long wavelength detectors P3, C100, and C200 show significant variations. To guard against such drifts, all PHT AOTs except P40 contain at least one FCS measurement per detector that has been used during an AOT. The FCS measurement determines the responsivity of the detector at approximately the same time as the sky is observed.

The derivation of the target's in-band power using the FCS calibration requires important instrumental corrections to ensure the best photometric calibration. The related processing steps are described in the following sections.

### 7.4.1 Determination in-band power from FCS

**Detailed description:** section 5

The electrical heating power $p$ applied to the FCS directly corresponds to an FCS power on the detector $P_{FCS}$. The conversion is obtained from dedicated in-orbit FCS calibration observations where the signal of a calibration source is directly compared with the signal of the FCS for a given heating power $p$. However, the calibration observations could only cover a limited range in $p$ due to limited availability of suitable calibration targets. FCS measurements with values for $p$ outside the calibratable range will get unreliable $P_{FCS}$ based on extrapolations.

In Derive_SPD the value for $p$ is checked. In case the value is outside the valid range an extrapolated value for $P_{FCS}$ will be retrieved, and a warning will be issued in the SPD file header.

**Ancillary data required:**

The valid heating power ranges are included in the FCS power calibration Cal G files PPxFCSPOW (x=1,2,3) for the P detectors, and PCxFCSPOW (x=1,2) for the C100 and C200 detectors, see section 13.10.

### 7.4.2 Signal to in-band power conversion for P detectors

**Detailed description:**5.2.3

From the electrical power (in mW) applied to the FCS, an in-band power on the detector $P_{FCS}$ normalized to the aperture area (in W/mm$^2$) is obtained using FCS calibration tables, see Chapter 5. The FCS measurement provides the detector responsivity $R$:

$$R = \frac{\langle s_{FCS} \rangle \cdot C_{det}}{P_{FCS} \cdot A_{FCS}} \qquad A/W, \tag{7.14}$$

where

- $\langle s_{FCS} \rangle$ is the weighted mean signal of the FCS measurement (in V/s),
- $C_{det}$ is the detector capacitance (in F),
- $P_{FCS}$ is the in-band power on the detector from the FCS (in W/mm),
- $A_{FCS}$ is the aperture area of the FCS measurement in mm$^2$.

The in-band power $P_{target}$ is obtained by:

$$P_{target} = \frac{\langle s_{target} \rangle C_{int}^{det}}{R} \qquad W, \tag{7.15}$$

and

$$\Delta P_{target} = \frac{\Delta \langle s_{target} \rangle}{\langle s_{target} \rangle} P_{target} \qquad W, \tag{7.16}$$

where $P_{target}$ and $\langle s_{target} \rangle$ can refer to any filter in a multi-filter sequence taken with detector P1, P2, or P3. $C_{int}^{det}$ is the capacitance of the detector.

**Caveat:** In principle, inhomogeneous illumination by the FCS (see section 7.4.3) affects the calibration involving apertures. The FCS power on the detector is not proportional with aperture area for a given electical power applied to the FCS. Although the correction method has been implemented in OLP Version 7, the present version of the Cal G files provide no correction. The investigations are ongoing, and non-unity correction factors are expected in a future version of the calibration files.

**Ancillary data required:**

- The PHT-P FCS calibration tables in units of W/mm$^2$ are stored in Cal G files PP1FCSPOW, PP2FCSPOW, and PP3FCSPOW for the three P detectors, see section 13.10.
- The values of the FCS aperture area in mm$^2$ from the aperture ID are hardcoded in the software. The values used are listed in section A.1.2. These areas were obtained from on-ground measurements of the instrumentation.
- The correction method for inhomogeneous FCS illumination of the apertures assume the following Cal G files (see section 13.13): PP1FCSAP, PP2FCSAP, and PP3FCSAP.

### 7.4.3 Signal to-in band power conversion for C detectors

**Detailed description:** section 5.2.3

The detector flat-field or pixel-to-pixel variation in the PHT-C responsivity is found to be filter dependent. Correction for the pixel-to-pixel variation is in principle taken care of by the FCS measurement which determines the responsivity for each individual pixel. However, for a multi-filter observation the FCS measurement is done in only one filter. Therefore a correction is necessary that relate the flat field obtained from the FCS measurement with those in the other filter bands.

Firstly, the FCS measurement is used to determine the responsivity of each pixel $R(i)$ for the filter in which the FCS measurement is taken:

$$R(i) = \frac{\langle s_{FCS}(i,f) \rangle \cdot C_{int}^{det}}{P_{FCS}(p,f) \cdot \Gamma(i,f) \cdot \chi(i,f)} \quad A/W, \tag{7.17}$$

where

- $f$ indicates the filter, $i$ the pixel number,

- $\langle s_{FCS}(i,f)\rangle$ is the FCS signal per chopper plateau,
- $C_{int}^{det}$ is the detector capacitance,
- $P_{FCS}(p,f)$ is the in-band power (in W) for a given FCS heating power $p$,
- $\Gamma(i,f)$ is the *illumination matrix*, and
- $\chi(i,f)$ the *detector flat field correction* characterizing the filter-to-filter response.

The illumination matrix $\Gamma(i,f)$ is needed to correct for the fact that the FCS illumination is not flat but varies from pixel to pixel in the C100 and C200 arrays. This correction is applied to each pixel in the array with respect to a reference pixel for which the FCS calibration tables apply (section 4.5.4).

Secondly, the power on each pixel for any filter $f'$ can be derived from the mean signal per chopper plateau $\langle s_{target}(i,f')\rangle$:

$$P_{target}(i,f') = \frac{\langle s_{target}(i,f')\rangle \cdot C_{int}^{det}}{R(i)\cdot\chi(i,f')} \qquad W, \tag{7.18}$$

and

$$\Delta P_{target}(i,f') = \frac{\Delta\langle s_{target}(i,f')\rangle}{\langle s_{target}(i,f')\rangle} P_{target}(i,f') \qquad W. \tag{7.19}$$

**Ancillary data required:**

- The PHT-C FCS calibration tables in units of W/pixel are stored in Cal G files PC1FCSPOW and PC2FCSPOW. The tables give the mean in-band power from the FCS averaged over all pixels, see section 13.10.
- The illumination matrices which give the FCS illumination for each pixel normalized to the mean pixel illumination are stored in Cal G files PC1ILLUM and PC2ILLUM, see section 13.12.
- The filter-to-filter flatfield correction for C100 and C200 are stored in Cal G files PC1FLAT and PC2FLAT, see section 13.14. For each pixel the correction is normalized to the mean correction of all filters in the C100 or C200 detector.

### 7.4.4 In-band power for raster maps

**Detailed description:** None

In case of a raster map, two FCS measurements are collected: one at the beginning and one at the end of the map. It is assumed that differences between the derived responsivities of the two FCS measurements can be attributed to a detector responsivity drift which is linear in time. In order to compute the detector responsivity at the mean time of the plateau signal a linear interpolation in time between the two FCS signals is performed for the P detectors, and a linear interpolation in time between the two responsivities $R(i)$ is performed for the C detectors (cf. eqn. 7.18).

**Ancillary data required:**

None

### 7.4.5 Default responsivities

**Detailed description:** None

It can happen that one or more FCS measurements are of insufficient quality for the derivation of a reliable detector responsivities. Such an event occurs e.g. in case all ramps/signals during the FCS measurement were rejected due to saturation or glitches.

For all chopped observations using the PHT03, PHT04 and PHT22 AOTs, the detector responsivity that can be derived from the chopped FCS measurement is assumed to be too unreliable for further use. In the current version of PHT-OLP the default responsivity is used for the in-band power calibration.

The default responsivity is time dependent and depends on the orbital phase of an measurement. For each measurement the orbital phase is read from ERD keyword TREFCOR2 which gives the orbital phase corresponding to the mid point of an AOT, and the default responsivity is determined by linear interpolation in the Cal G file which gives the default responsivity versus orbital position for a given detector.

Derive_SPD will also compute the FCS1 responsivity from the FCS measurement and the results are stored in the designated Cal A file. To give the observer some information on the discrepancies, the ratio:

$$r(i) = \frac{R_{FCS}(i)}{R_{default}(i)}, \tag{7.20}$$

is stored for each pixel $i$ in the SPD header with keyword RESPRi.

**Ancillary data required:**

Default detector responsivities are stored in Cal G files PPRESP, PC1RESP, and PC2RESP for the P, C100 and C200 subsystems, respectively, see section 13.11.

### 7.4.6 Dependencies on mission dates

**Detailed description:** None

During the mission two main events took place which seriously impacted on the ISOPHOT calibration:

- the change in FCS1-TRS2) emission properties (cf section 3.5 in revolution 94. This event caused the FCS emission for the long wavelength detectors (P3, C100 and C200) to become about a factor 2 higher than before for the same electrical power. Consequently, new uplink and FCS power tables had to be constructed after extensive in-orbit measurements of the FCS/TRS2 properties.
- an extra curing procedure was introduced approximately halfway in the ISO science window for detectors P3, C100 and C200 as of revolution 150 onwards. The extra curing was performed during the handover period between the VILSPA and Goldstone ground stations. The procedure restored the nominal detector performance whereas, without the procedure, both detector noise and responsivity continue increasing.

As a consequence, the following calibration files have different entries depending on the revolution date:

- FCS power Cal G files (PP3FCSPOW, PCxFCSPOW see section 7.4.1) are different before and after revolution 94.
- orbit dependent default responsivities Cal G files (PPRESP, PCxRESP see section 7.4.5) are different before and after revolution 150.

**Ancillary data required:**

Information on the time dependence of ISOPHOT Cal G files is stored in Cal G file PTIMEDEP, a detailed description is given in section 13.2.

## 7.5 Quality flags for SPD records

The quality of the processed data in each SPD record is given in the SPD quality flag field **PxxSFLAG** where **xx** identifies the detectors as follows C1, C2, P1, P2, P3 SS, and SL. Table 7.2 gives the coding of each bit in the (8 bit) flag.

Table 7.2: Quality flags for SPD records

| **Bit** | **Description** |
|---|---|
| 0 | nominal |
| 1 | calibration measurement saturated |
| 2 | part of plateau data affected by drift |
| 3 | all ramps on plateau rejected |
| 4 | plateau data affected by residual drift |
| 5 | zero standard deviation |
| 6 | empty |
| 7 | zero signal for plateau |

# Chapter 8

# Data Processing Level: Derive_AAR

## 8.1 Overview

In *derive auto-analysis results (Derive_AAR)*, the calibrated data from Derive_SPD are further processed to more advanced astronomical products such as point source flux per filter, flux sequences in multi-aperture mode, spectra, or maps. PHT SPD products provide in essence the average power on the detector in Watts per record and are independent of the observing mode. Each SPD record corresponds to a chopper plateau or raster position. Differences among PHT SPD products emerge mainly from the detector subsystem (PHT-P, -C or -S) used.

In contrast to SPD, the auto-analysis results (AAR) products are defined by the observing mode selected. As a consequence, the processing sequence and resulting AAR product are to large extent determined by the observing template (AOT) applied and the specific instrument settings used in the AOT.

Nevertheless, different ISOPHOT AOT's may require identical Derive_AAR processing steps. To avoid repetition in the descriptions, we first describe the common routines. The following generic observing modes can be identified, for which a more global description can be given:

- Photometry (section 8.4)
- Mapping (section 8.5)
- Spectroscopy (section 8.6)

In the remainder of this section we first give an overview of the processing steps for each AOT (section 8.2). In the subsequent sections the processing steps shared by all PHT AOTs (section 8.3) and the processing details related to the different observation modes are described.

## 8.2 PHT auto analysis processing per AOT

No description is given of the polarisation AOTs PHT50 and PHT51 because these AOTs are not included in the pipeline SPD and AAR levels.

### 8.2.1 PHT03

This AOT performs photometry in user-selected wavebands using the PHT-P subinstrument, with either the staring or chopping mode. If the staring mode is selected a raster scan may be performed.

The description of the processing required for rasters is incorporated, since the same steps are required to process measurements at each raster position.

**Processing steps:**

1. Read SPD Header
   Common step 8.3.1.

2. Read SPD record
   Common step 8.3.2.

3. If single pointing:

   (a) Average source power and off-source background(s) power

   **Staring mode** No action required.

   **Chopped mode** Photometry step 8.4.2.
   Obtain mean powers averaged over all valid chopper cycles.
   Apply empirical signal difference correction 8.4.6.

   (b) If point source observed:

      i. Convert power to flux density
      Photometry step 8.4.9.

      ii. Write point source photometry product
      Photometry step 8.4.11.

   (c) If extended source observed:

      i. Convert power to flux density
      Photometry step 8.4.9.

      ii. Convert flux density to surface brightness
      Photometry step 8.4.10;

      iii. Write extended source or raster photometry product
      Photometry step 8.4.12.

4. If raster mapping performed:

   (a) Determine celestial coordinates of detector origin and centre; loop over all measurements in AOT
   Common step 8.3.3;

   (b) For each record, convert power to surface brightness
   Photometry step 8.4.10;

   (c) Produce photometric image
   All mapping steps 8.5;

   (d) Write raster map products 8.5.5.

### 8.2.2 PHT04

This AOT performs multi-aperture photometry with a single user-selected filter at one sky position using the PHT-P subinstrument. The focal plane chopper may be operated in either staring or chopping mode. Raster scans may *not* be selected.

**Processing steps:**

1. Read SPD Header
   Common step 8.3.1.

2. Read SPD record
   Common step 8.3.2.

3. Average source power and off-source background(s) power

   **Staring mode** No action required.

   **Chopped mode** Photometry step 8.4.2.
   Obtain mean powers averaged over all valid chopper cycles.
   Apply empirical signal difference correction 8.4.6.

4. If point source observed:

   (a) Convert power to flux density
   Photometry step 8.4.9.

   (b) Write point source photometry product
   Photometry step 8.4.11.

5. If extended source observed:

   (a) Convert power to flux density
   Photometry step 8.4.9;

   (b) Convert flux density to surface brightness
   Photometry step 8.4.10;

   (c) Write extended source or raster photometry product
   Photometry step 8.4.12.

### 8.2.3 PHT05

This AOT performs absolute photometry of the sky brightness with a single filter/aperture combination at one sky position using the PHT-P subinstrument. Raster scans cannot be selected.

**Processing steps:**

1. Read SPD Header
   Common step 8.3.1.

2. Read SPD record
   Common step 8.3.2.

3. If point source observed:

   (a) Convert power to flux density
   Photometry step 8.4.9.

   (b) Write point source photometry product
   Photometry step 8.4.11.

4. If extended source observed:

   (a) Convert power to flux density
   Photometry step 8.4.9.

   (b) Convert flux density to surface brightness
   Photometry step 8.4.10;

   (c) Write extended source or raster photometry product
   Photometry step 8.4.12.

### 8.2.4 PHT17/18/19

These AOTs perform photometry in user-selected wavebands with a single user-selected aperture as part of a sparse map using the PHT-P subinstrument. Only staring mode can be used. The following processing steps are performed:

**Processing steps:**

1. Loop over all PHT17, PHT18. . ., PHT19 of the same TDT

   (a) Read SPD Header
   Common step 8.3.1.

(b) Read SPD record
Common step 8.3.2.

2. If last product was found then loop over all measurements read:

(a) If point source observed:

i. Convert power to flux density
Photometry step 8.4.9.

ii. Write point source photometry product
Photometry step 8.4.11.

(b) If extended source observed:

i. Convert power to surface brightness
Photometry step 8.4.10;

ii. Write extended source or raster photometry product
Photometry step 8.4.12.

### 8.2.5 PHT22

This AOT performs photometry in user-selected wavebands using the PHT-C subinstrument, with either the staring or chopping mode. If the staring mode is selected a raster scan may be performed.

1. Read SPD Header
Common step 8.3.1.

2. Read SPD record
Common step 8.3.2.

3. If single pointing:

(a) Average source power and off-source background(s) power
This step is applied to *each* pixel.

**Staring mode** No action required.

**Chopped mode** Photometry step 8.4.2.
Obtain mean powers per pixel averaged over all valid chopper cycles.
Apply empirical signal difference correction 8.4.6.

(b) Determine mean off-source background power over all pixels
Photometry step 8.4.5.

(c) Summation of powers in array, step 8.4.7

(d) If point source observed:

i. Determine Gaussian parameters

**Interpolation:** Interpolate missing pixels
Photometry step 8.4.8.1;

**Fitting:** Determine source peak and position
Photometry step 8.4.8.2;

ii. Convert power to flux density
Photometry step 8.4.9;

iii. Write point source photometry product
Photometry step 8.4.13.

(e) If extended source observed:

i. Convert power to flux density
Photometry step 8.4.9;

ii. Convert flux density to surface brightness
Photometry step 8.4.10;

iii. Write extended source or raster photometry product
Photometry step 8.4.14.

4. If raster mapping performed:

   (a) Determine celestial coordinates of each detector pixel for each record; loop over all measurements
   Common step 8.3.3;

   (b) For each record and pixel, convert power to flux density
   Photometry step 8.4.9;

   (c) For each record and pixel, convert flux density to surface brightness
   Photometry step 8.4.10;

   (d) Produce photometric image
   All mapping steps 8.5;

   (e) Write raster map products 8.5.5.

### 8.2.6 PHT25

This AOT performs absolute photometry of the sky brightness with a single filter on one sky position using the PHT-C subinstrument. Raster scans cannot be selected, only staring mode is available.

**Processing steps:**

1. Read SPD Header
   Common step 8.3.1.

2. Read SPD record
   Common step 8.3.2.

3. If point source observed:

   (a) Summation of powers in array, step 8.4.7

   (b) Determine Gaussian parameters

   **Interpolation:** Interpolate missing pixels
   Photometry step 8.4.8.1;

   **Fitting:** Determine source peak and position
   Photometry step 8.4.8.2;

   (c) Convert power to flux density
   Photometry step 8.4.9.

   (d) Write point source photometry product
   Photometry step 8.4.13.

4. If extended source observed:

   (a) Convert power to flux density
   Photometry step 8.4.9.

   (b) Convert flux density to surface brightness
   Photometry step 8.4.10;

   (c) Write extended source photometry product
   Photometry step 8.4.14.

### 8.2.7 PHT32

This AOT performs multi-filter mapping using either the C100 or C200 arrays. The map may take the form of a linear scan. A raster scan is performed; the focal plane chopper being used to sample at intermediate positions from the raster pointings in sawtooth mode.

1. Read SPD Header
   Common step 8.3.1.
2. Read SPD record
   Common step 8.3.2.
3. Determine celestial coordinates of each detector pixel for each record; loop over all measurements
   Common step 8.3.3;
4. For each record and pixel, convert power to flux density
   Photometry step 8.4.9;
5. For each record and pixel, convert flux density to surface brightness
   Photometry step 8.4.10;
6. Produce photometric image
   All mapping steps 8.5;
7. Write raster map products 8.5.5.

### 8.2.8 PHT37/38/39

These AOTs perform photometry in user-selected wavebands as part of a sparse map using the PHT-C subinstrument. Only staring mode observations are performed.

1. Loop over all PHT37, PHT38. . ., PHT39 of the same TDT
   (a) Read SPD Header
   Common step 8.3.1.
   (b) Read SPD record
   Common step 8.3.2.
2. If last product was found then loop over all measurements read:
   (a) If point source observed:
      i. Convert power to flux density
      Photometry step 8.4.9.
      ii. Write point source photometry product
      Photometry step 8.4.13.
   (b) If extended source observed:
      i. Convert power to flux density
      Photometry step 8.4.9.
      ii. Convert flux density to surface brightness
      Photometry step 8.4.10;
      iii. Write extended source or raster photometry product
      Photometry step 8.4.14.

### 8.2.9 PHT40

Spectrophotometry with the PHT-S subsystem. Staringg, chopped, and mapping modes are available. Point or extended sources can be observed. The short (SS) and the long (SL) wavelength detectors are processed separately.

**Processing steps:**

1. Read SPD Header
   Common step 8.3.1.
2. Read SPD record
   Common step 8.3.2.
3. If single pointing:
   (a) Average source power and off-source background(s) power
   This step is applied to *each* pixel.
   **Staring mode** No action required.
   **Chopped mode** Photometry step 8.4.2.
   Obtain mean powers averaged over all valid chopper cycles.
   (b) If point source observed:
   i. Convert power to flux density
   Photometry step 8.4.9.
   ii. Write point source photometry product
   Photometry step 8.6.1.
   (c) If extended source observed:
   i. Convert power to surface brightness
   Photometry step 8.4.10;
   ii. Write extended source or raster photometry product
   Photometry step 8.6.1.
4. If raster mapping performed:
   (a) Determine celestial coordinates of each raster point; loop over all measurements in AOT
   Common step 8.3.3;
   (b) For each record, convert power to flux density
   Photometry step 8.4.10;
   (c) For each record, convert flux density to surface brightness
   Photometry step 8.4.10;
   (d) Write raster map products.

For raster observations no images are produced. For each raster pointing a photometry record plus associated coordinates are obtained.

## 8.3 Common processing steps

### 8.3.1 Read SPD header

**Operation:** Extract all relevant data from the SPD header.

The keywords from the SPD FITS header are read and stored internally for processing. The information is eventually passed to the AAR product headers. The following items are extracted from the SPD, the symbols in parenthesis will be used in the remainder of this chapter:

- **General SPD header keywords:**

  DETECTOR, detector used
  NMEAS, number of measurements
  PTOREXT, point or extended source expected
  FPCMODE, chopper mode used

- **Spacecraft attitude data:**

  INSTRA, reference instrument J2000 right ascension in degrees ($\alpha_c$)
  INSTDEC, reference instrument J2000 declination in degrees ($\delta_c$)
  INSTROLL, reference instrument J2000 roll angle in degrees ($\phi$)
  in case a raster mode was executed:
  ATTRNPTS, number of raster points (M)
  ATTRNLNS, number of raster lines (N)
  ATTRDPTS, increment between points (dM)
  ATTRDLNS, increment between lines (dN)
  ATTRROTA, raster rotation angle $\phi_{raster}$

- **Chopper mode information if FPCMODE is not staring:**

  FPCNSTEP, number of chopper steps
  FPCINCR, increment between steps

- **Spectrophotometric mode information if PHT40 used; for each pixel:**

  LAMBDA, LUNC, the central wavelengths and uncertainty
  if point source: RESPP, RPUNC, point source responsivity and uncertainty ($C_{phts,pixel}$, $\Delta C_{phts,pixel}$)
  if extended source: RESPE, REUNC, extended source responsivity and uncertainty ($C^E_{phts,pixel}$, $\Delta C^E_{phts,pixel}$)

- **Information for remaining AOTs; for each filter:**

  FILTER, filter identification
  EXFLUX, expected fluxdensity
  UNCFLX, uncertainty in expected fluxdensity
  MXBACK, maximum expected background

- **Corrections for signal losses in chopped mode:**

  CHC$n$P$i$, chopper correction for measurement $n$ and pixel $i$
  CHU$n$P$i$, chopper correction uncertainty for measurement $n$ and pixel $i$

- **Check whether default responsivity was used in SPD:**

  RESPDEF, (logical) *true* if default responsivity was used.

**Ancillary data required:**

SPD product

### 8.3.2 Read SPD record

**Operation:** Extract necessary information from an SPD record.

The following data are taken from each SPD record:

Instrument time key (ITK)
Raster point identifiers
Filter identifier

Aperture identifier
Polarizer identifier
Number of destructive readouts
Chopper plateau length (chopper dwell time)
Measurement time (secs)
Chopper position (arcsecs)
Chopper step number
Measured powers averaged over a plateau plus uncertainty
Plateau lengths (sec)
Data quality flags

For PHT-C and PHT-S, power, uncertainty, plateau length, and quality flags refer to each pixel separately.

**Ancillary data required:**

SPD product

### 8.3.3 Determine celestial coordinates of each pixel in record

**Operation:** For all SPD records, derive:
(1) the sky position (in RA and Dec) of the detector origin, and
(2) the RA and Dec offsets (in arcsec) for each detector pixel with respect to the raster centre
.

#### 8.3.3.1 Overview

For a given SPD record, the position of a pixel on the sky is determined by:

- the pixel's position in the detector array;
- a deflection of the focal plane chopper, by design the deflection is only in spacecraft Y direction;
- application of the raster mode, the raster mode can be defined either in spacecraft reference coordinates (i.e. raster increments only in Y and Z directions) or equatorial coordinates (raster increments in RA and Dec directions).

All three instances can occur during the same measurement in case of AOT PHT32 where the chopper is performing a saw-tooth scan using one of the C-arrays while the spacecraft is rastering in spacecraft reference coordinates.

For single pointing photometry the pointing keywords in the SPD product header (Section 8.3.1) are used.

For raster maps the PHT OLP software will determine for each SPD record the equatorial coordinates of the PHT centre field of view thereby considering the raster position as well as a possible chopper deflection. Subsequently, the RA and Dec offsets in arcseconds with respect to the centre of the map or *image coordinates* are computed. The map centre has been provided by the observer. Finally, the image coordinates for each pixel are derived taking into account the individual pixel offsets and the spacecraft roll angle.

#### 8.3.3.2 Extracting pointing data from IRPH

The instrument reference pointing history (IRPH) contains pointing information expressed in quaternions (see Appendix A of the ISO Satellite and Data Manual [17]). The quaternion $Q_{raster}$ that defines the position of the PHT central field of view for a given raster point in the J2000 inertial frame can be computed from:

$$Q_{raster} = Q_{str} \cdot Q_{r} \cdot Q_{str/qss} \cdot Q_{qss/pht} \cdot Q_{cor}, \tag{8.1}$$

where quaternions

- $Q_{str}$ defines the J2000 pointing of the ISO star tracker,
- $Q_r$ defines the raster point relative to the raster centre of the scan,
- $Q_{str/qss}$ describes the misalignment between the star tracker and the quadrant star sensor (QSS),
- $Q_{qss/pht}$ describes the QSS to instrument aperture alignment, there is one value for $Q_{qss/pht}$ per PHT subsystem and is listed in the focal plane geometry Cal G file IFPG.FITS (see [17]),
- $Q_{cor}$ gives a fine pointing correction to the star tracker calibration, since this correction depends on the position of the guide star in the star tracker field of view, a different correction is given for each raster position.

The following records are read from the IRPH:

ATTMISQ(1:4), =Q(str/qss), startracker to QSS misalignment quaternion
ATTINSQ(1:4), =Q(qss/pht), QSS to instrument aperture misalignment quaternion

A more detailed description on the contents of the IRPH is given in the ISO Data Satellite and Data Manual [17]. Note: due to different conventions adopted for the misalignment, Q(str/qss) as given in the IRPH should be converted to the PHT OLP convention:
$Q^{PHT}_{str/qss}(2) = -Q^{IRPH}_{str/qss}(2)$
$Q^{PHT}_{str/qss}(3) = -Q^{IRPH}_{str/qss}(3)$

For each raster record in the IRPH, the following parameters are extracted:

- raster point ID (RPID)
- $Q_r$, raster point quaternion (RPQ)
- $Q_{str}$, star tracker quaternion (STRQ)
- $Q_{cor}$, raster point correction quaternion (CORQ)

With this information the quaternion $Q_{raster}$ in eqn. 8.1 can be derived.

#### 8.3.3.3 Inclusion of chopper information

We define the *detector origin* to be the centre of the aperture in case of a P detector, the centre of the central pixel 5 in case of C100, and the centre of the array in case of C200.
Assuming a perfect alignment between chopper and spacecraft Y-axis, the quaternions representing the rotations of the detector origin with respect to a given raster point are:

$$\begin{aligned} Q_1 = &\quad (0, 0, \sin(y_{det}/2), \cos(y_{det}/2)) \\ Q_2 = &\quad (0, \sin(-z_{det}/2), 0, \cos(-z_{det}/2)), \end{aligned}$$

where $y_{det}$ is the chopper deflection and $z_{det} = 0$ is the spacecraft z-offset.
The quaternion of the detector origin for a given chopper position in a raster can now be computed via:

$$Q_{chop} = Q_{raster} \cdot (Q_1 \cdot Q_2), \tag{8.2}$$

where $Q_{raster}$ is the raster point quaternion as derived in eqn. 8.1. $Q_{chop}$ can be converted to RA ($\alpha$), Dec ($\delta$), and Roll-angle ($\phi$) according to standard quaternion transformation:

$$\begin{aligned} \sin(\delta) &= 2Q(1)Q(3) - Q(2)Q(4) \\ \sin(\alpha)\cos(\delta) &= 2Q(1)Q(2) - Q(3)Q(4) \\ \sin(\phi)\cos(\delta) &= 2Q(1)Q(4) - Q(2)Q(3). \end{aligned}$$

### 8.3.4 Determination of the equatorial offsets of the detector centre

We define the *detector centre* to be the centre of the aperture in case of PHT-P or the centre of a detector pixel in case of PHT-C. Note that for PHT-P the detector origin and centre are identical.

Based on the position of the *detector origin* the detector centre is obtained. For a given record the sky position in RA and Dec of the detector origin is converted into offsets ($\Delta\alpha$ and $\Delta\delta$) with respect to the centre of the raster ($\alpha_c$, $\delta_c$). The offsets are aligned with the RA and Dec axes in the equatorial coordinate system.

For each pixel the RA and Dec offsets with respect to the detector origin are computed from the detector roll angle and the relative pixel positions. In the current OLP version (Version 7) it is assumed that the pixels are positioned in an idealized configuration:

- the pixels in the C100 array are arranged in a regular 3×3 grid with 46″ spacings in spacecraft Y and Z direction and with the centre of pixel 5 in the origin at (0″, 0″);
- the pixels in the C200 array are arranged in a regular 2×2 grid with 92″ spacings in Y and Z direction. The origin is at the centre of the array;
- in case of PHT-P the detector centre is the detector origin.

Adding the offsets of the detector origin this will give the map offsets in arcsec for any raster position, detector pixel, and chopper plateau combination.

**Ancillary data required:**

1. SPD product
2. IRPH product

## 8.4 Photometry

A large fraction of this section is dedicated to the processing of chopped measurements. Although the chopped observing mode is not scientifically validated for OLP Version 7, it is not expected that the algorithms for determining the background subtracted signal will change. A preliminary correction for signal losses in chopped mode with respect to staring mode has been implemented in this version of the software. This correction is not scientifically validated and is likely to change in a future version.

In this section the extraction of (point-)source emission from source+background emission in chopped and staring measurements (whenever possible) is described in detail. Subsequently the conversion from power on the detector in units of W to flux density in Jy or surface brightness in MJy/sr is presented. Finally, the writing of the resulting data to product files is briefly described.

### 8.4.1 Sorting out chopper plateaux

**Operation:** Sorts out the source and background records for each chopper cycle; possible data gaps from telemetry drops are handled.

In case the observation consists of one or more measurements, each valid chopper cycle should be determined in order to be able to perform the background subtraction.

The size of a chopper cycle depends on the chopper mode used:

1. staring mode:
   cycle = 1 record
2. rectangular chopping mode:
   cycle = 2 consecutive records
   record 1 gives the background and record 2 gives [source+background] power.

3. sawtooth chopping mode:
   cycle = 2×NSTEP + 1 consecutive records
   NSTEP is the number of chopper steps; for NSTEP=1 record 1 and 3 give the respective first and second background powers, record 2 gives the [source+background] power.

4. triangular chopping mode:
   cycle = 4×NSTEP consecutive records
   NSTEP is the number of chopper steps; for NSTEP=1 record 1 and 3 give the respective first and second background powers, record 2 and 4 give the [source+background] power.

In case of a chopped measurement, the first chopper step is always on the background and in negative spacecraft Y-direction (cf. section 3.6). For all available AOTs except PHT32, NSTEP is set to 1 in case sawtooth or triangular chopping mode was selected. The PHT-S dark measurement is always treated as a staring measurement.

The presence of possible data gaps due to telemetry drop-outs is determined by checking whether the time difference between the current and the next record is according to the chopper dwell time. If this is not the case, the current and following records are skipped until the beginning of a new cycle is found. The start of a new cycle is inferred from the chopper step number. As each chopper cycle starts with the maximum negative offset, the step number should have the value:

1. –1 for rectangular chopping mode
2. –NSTEP for sawtooth or triangular chopping mode

As soon as a full valid cycle has been encountered, the data are passed to perform the background subtraction. In case of staring mode, this step is skipped and a flux calculation is performed.

### 8.4.2 Separation of source and background in-band power

**Operation:** Perform the background subtraction for a given chopper cycle and chopper mode.

**Caveat:** OLP Version 7 include weighting factors (cf. sections 8.4.2.3 and 8.4.2.2) which have not been scaled by the factor 2 in the average. This does not invalidate the weighting, but in the calculation of the $\sigma$ of the mean in section 8.4.3 the value of $\sigma$ will be too low by a factor 2. The observer should multiply the final uncertainty by 2 to obtain the correct values. In a future version of the software this omission will be corrected.

For a given chopper cycle the background in-band power is subtracted from the [source+background] in-band power to obtain the source in-band power. This operation is repeated until the end of a measurement is encountered. Weighting factors are derived from the uncertainties which are used for the averaging of all chopper cycles at the end of a measurement.

In the following sub-sections we describe the background subtraction method for the different chopper modes. Note that each cycle in triangular chopping mode consists of 4 plateaux referring to 2 [source+background] and 2 different background positions. In sawtooth mode there are 3 plateaux: 1 [source+background] and two different background positions. The following symbols are used:

- $P_i(s+b)_1$, $w_i(s+b)_1$: power and weight for first [source+background] plateau for chopper cycle i;
- $P_i(s+b)_2$, $w_i(s+b)_2$: power and weight for second [source+background] plateau (triangular mode only);
- $P_i(b1)$, $w_i(b1)$: power and weight for the background at the first reference positiont;
- $P_i(b2)$, $w_i(b2)$: power and weight for the background at the second reference position;
- $P_i(s+b)$, $w_i(s+b)$: average power and weight from source plus background plateaux;
- $P_i(s)$, $w_i(s)$: source power and weight;
- $P_i(b)$, $w_i(b)$: background power and weight.

All in-band powers are given in Watts, the weights are dimensionless.

#### 8.4.2.1 Rectangular mode

Each cycle contains only 1 [source+background] plateau and 1 reference background position. For chopper cycle i:

$$\begin{aligned} \mathrm{P_i(b)} &= \mathrm{P_i(b1)} \\ \mathrm{P_i(s)} &= \mathrm{P_i(s+b)_1 - P_i(b1)} \end{aligned}$$

The weighting factor is determined from the in-band power uncertainties:

$$w_i(s+b) = \frac{1}{\sigma_i^2(s+b)}$$

$$w_i(b) = \frac{1}{\sigma_i^2(b)}$$

$$w_i(s) = \frac{1}{[\sigma_i^2(s+b) + \sigma_i^2(b)]}$$

where $\sigma_i(s+b)$ is the uncertainty in power for the measurement on [source+background], etc.

#### 8.4.2.2 Sawtooth mode

Each chopper cycle contains 1 [source+background] chopper plateau and 2 reference positions. For chopper cycle i:

$$P_i(b) = \frac{P_i(b1) + P_i(b2)}{2}$$

$$P_i(s) = P_i(s+b) - P_i(b).$$

With weighting factors:

$$w_i(s+b) = \frac{1}{\sigma_i^2(s+b)}$$

$$w_i(b1) = \frac{1}{\sigma_i^2(b1)}$$

$$w_i(b2) = \frac{1}{\sigma_i^2(b2)}$$

$$w_i(b) = \frac{\gamma}{[\sigma_i^2(b1) + \sigma_i^2(b2)]}$$

$$w_i(s) = \frac{1}{[\sigma_i^2(s+b) + (\sigma_i^2(b1) + \sigma_i^2(b2))/\gamma]}$$

where $\gamma = 1$ in OLP7, but the correct value should be 4; $\sigma_i(s+b)$ is the uncertainty in power for the measurement on [source+background], etc.

#### 8.4.2.3 Triangular mode

Each chopper cycle contains 2 [source+background] chopper plateaux and 2 reference positions. For chopper cycle i:
For chopper cycle i:

$$P_i(s+b) = \frac{P_i(s+b)_1 + P_i(s+b)_2}{2}$$

$$P_i(b) = \frac{P_i(b1) + P_i(b2)}{2}$$

$$P_i(s) = P_i(s+b) - P_i(b)$$

A weighting factor is also determined from the power uncertainties:

$$w_i(s+b)_1 = \frac{1}{\sigma_i^2(s+b)_1}$$

$$w_i(s+b)_2 = \frac{1}{\sigma_i^2(s+b)_2}$$

$$w_i(b1) = \frac{1}{\sigma_i^2(b1)}$$

$$w_i(b2) = \frac{1}{\sigma_i^2(b2)}$$

$$w_i(s+b) = \frac{\gamma}{[\sigma_i^2(s+b)_1 + \sigma_i^2(s+b)_2]}$$

$$w_i(b) = \frac{\gamma}{[\sigma_i^2(b1) + \sigma_i^2(b2)]}$$

$$w_i(s) = \frac{\gamma}{[\sigma_i^2(s+b)_1 + \sigma_i^2(s+b)_2 + \sigma_i^2(b1) + \sigma_i^2(b2)]}.$$

$\gamma$ has the same meaning as in the previous subsection.

### 8.4.3 Determine the in-band powers averaged over a measurement

**Operation:** determine the average source and background powers of all chopper cycles in a measurement.
For all chopper cycles in a measurement, the weighted average is computed from the parameters per chopper cycle. For a given set of powers $\mathrm{P_i(X)}$ with weights $\mathrm{w_i}$ obtained over a measurement, the weighted mean is derived from:

$$\mathrm{P(X)} = \frac{\sum_{\mathrm{i=1}}^{\mathrm{N}} \mathrm{w_i(X)P_i(X)}}{\sum_{\mathrm{i=1}}^{\mathrm{N}} \mathrm{w_i(X)}}. \tag{8.3}$$

P(X) can be either the power of the source or background. The corresponding uncertainty is calculated from the weights:

$$\sigma(\mathrm{P(X)}) = \sqrt{\frac{1}{\sum_{\mathrm{i=1}}^{\mathrm{N}} \mathrm{w_i(X)}}}. \tag{8.4}$$

#### 8.4.3.1 Rectangular mode

In rectangular mode the following mean powers are derived for each pixel:

- $\mathrm{P(s)} \pm \sigma(\mathrm{P(s)})$
- $\mathrm{P(b)} \pm \sigma(\mathrm{P(b)})$
- $\mathrm{P(s+b)} \pm \sigma(\mathrm{P(s+b)})$

#### 8.4.3.2 Sawtooth and Triangular mode

In sawtooth and triangular mode the following mean powers are derived for each pixel:

- P(s) $\pm \sigma$(P(s))
- P(b) $\pm \sigma$(P(b))
- P(s + b) $\pm \sigma$(P(s + b))
- P(b1) $\pm \sigma$(P(b1))
- P(b2) $\pm \sigma$(P(b2))

### 8.4.4 Staring mode

**Operation:** Derive the average target powers in staring mode.

This is a null operation as there is only one record per measurement.

### 8.4.5 Determine the mean off-source background

**Operation:** Compute the background averaged over all pixels in the array for a chopper reference position.

A weighted mean of all the pixels is found – if there are $n$ of these where

$$w_j = \frac{1}{\sigma^2(P_j(b))}$$

then

$$P_{back} = \frac{\sum_{j=1}^{n} w_j P_j(b)}{\sum_{j=1}^{n} w_j} \tag{8.5}$$

$$\sigma(P_{back}) = \sqrt{\frac{1}{\sum_{j=1}^{n} w_j}}, \tag{8.6}$$

where j refers to the pixels in an array. For sawtooth and triangular chopped modes, this is done at both background positions.

### 8.4.6 Empirical correction for signal losses in chopped measurements

**Operation:** Correct the background subtracted source in-band power for possible signal losses due to the application of chopped mode.

In Derive_SPD, see section 7.3.9, the empirical correction factors per detector pixel were determined for signal losses in chopped mode. The correction factors are transferred to Derive_AAR processing via the SPD product header (section 8.3.1). The correction can only be applied as soon as the difference signal between [source+background] and background is known which is only computed in Derive_AAR. Since the in-band power is proportional to signal the correction can be carried out at the present processing stage.

In case of the C100 array, it has been observed that the chopped signal of pixel 6 responds completely differently compared to the other pixels in the array. It is therefore decided for OLP Version 7 to remove the observed background subtracted in-band power and to replace this by the average of the in-band powers of the equivalent pixels - in terms of illumination - on the array (cf Table 3.1):

$$P(s, pixel\ 6) = (P(s, pixel\ 2) + P(s, pixel\ 4) + P(s, pixel\ 8))/3, \tag{8.7}$$

where $s$ refer to the source flux after background subtraction. Subsequently, to correct for signal losses, for a given pixel j:

$$P^c(s,\ j) = \quad P(s, pixel\ j)/C_{chop}(j) \tag{8.8}$$
$$\sigma(P^c(s,\ j)) = \quad \sigma(P(s, pixel\ j))/C_{chop}(j) \tag{8.9}$$

where $P^c$ refer to the corrected in-band power and $C_{chop}(j)$ is the signal loss correction for pixel $j$.

### 8.4.7 Summation of the in-band powers of all detector pixels

**Operation:** Derive the sum of the in-band powers of all pixels for a given PHT-C array.

In case the observer requested the measurement of a point source flux with the PHT-C detector arrays, the total [source+background] power as well as the background power on the array is determined by summing the respective powers over all pixels.

$$\mathrm{P(s)} = \sum_{\text{all pixels}} \mathrm{P_{pixel}(s)}, \tag{8.10}$$

and for the [source+background] and background power:

$$P(s+b) = \quad \textstyle\sum_{all\ pixels} P_{pixel}(s+b), \tag{8.11}$$
$$P(b) = \quad \textstyle\sum_{all\ pixels} P_{pixel}(b). \tag{8.12}$$

The uncertainties are computed according to:

$$\sigma(\mathrm{P(s)}) = \sqrt{\sum_{\text{all pixels}} \sigma^2(\mathrm{P_{pixel}(s)})}. \tag{8.13}$$

The relations for $\sigma(\mathrm{P(s+b)})$ and $\sigma(\mathrm{P(b)})$ are similar.

### 8.4.8 Fit two-dimensional Gaussian to point sources in the C-arrays

**Operation:** In case the observer has requested a point source measurement, a 2 dimensional Gaussian function is fitted to the intensity pattern on the array. This processing is done in addition to the sum of all pixel in-band powers (section 8.4.7).

**Caveat:** This method of providing point source photometry is not scientifically validated. In particular in the case of faint sources and noisy data, the derived fluxes and uncertainties are not reliable.

To secure a converging fit, an interpolation is performed whenever there are undefined in-band powers for some pixels. The fitting of the 2 dimensional Gaussian itself is performed using standard iterative fitting routines provided by the NAG mathematical routines library (routines E04FDF and E04YCF).

The following parameters are obtained:

- $\mathrm{P_{gauss}(s)}, \sigma(\mathrm{P_{gauss}(s)})$: peak power value plus associated error (indicated with $d$ in section 8.4.8.2);
- $\mathrm{P_{gauss}(b)}, \sigma(\mathrm{P_{gauss}(b)})$: background power value plus error (indicated with $c$ in section 8.4.8.2);
- $\alpha, \sigma(\alpha)$: x offset of peak in arcsec plus error;
- $\beta, \sigma(\beta)$: y offset of peak in arcsec plus error;

- $g_{fit}$: goodness of fit
- fit status, if status=0, fit is successful.

Details of the procedure are given in the next subsections (sections 8.4.8.1 and 8.4.8.2).

#### 8.4.8.1 Interpolate missing pixels

The fitting routine described in section 8.4.8.2 requires only valid pixel intensities on the detector array. Interpolation is necessary in case there are 'bad' data pixels. The observed in-band power on a pixel is flagged 'bad' if there is no valid chopper plateau cycle during a given measurement.

A check is performed to determine whether there is a sufficient number of good pixels for interpolation. For C200 one pixel is allowed to be missing. For C100 the criteria are (1) the presence of the centre pixel (pixel 5) where the source is expected to be and (2) there must be at least 2 good pixels on any side of the array. Criterion (2) is imposed to avoid interpolation using an already interpolated value.

The rules for interpolation are

```
C200:  a b    :   a = b + c - d
       c d

C100:  a b c  :   b = (a + c)/2
       d e f
       g h i      a = b + d - (c + g)/2
```

Note that there is a rotational symmetry about each side; only one orientation is given. The accuracy of the method depends on

- the location of the source in the array,
- the presence of any extended features, and
- the uniformity of the pixel response.

#### 8.4.8.2 Determination of Gaussian parameters

The height of the source peak, its position, and the background level is obtained by fitting a Gaussion function to the data. The accuracy of this method depends on the correctness of the assumption of a Gaussian on top of a constant background. The in-band power dstribution is considered as a 2 dimensional array:

$$g(x, y) = c + de^{\frac{-z^2}{2}}$$

where

$$z^2 = (x - \alpha)^2 + (y - \beta)^2$$

and

- $\alpha$ is the x-axis offset of the peak from the centre of the array.
- $\beta$ is the y-axis offset of the peak from the centre of the array.
- $c$ is a constant background.
- $d$ is the (background subtracted) height of the source peak.

The x and y axes are the first (along spacecraft Z-axis) and second (along spacecraft Y-axis) dimension of the pixel array, respectively, with origin at the centre of the array. A chi-squared "goodness of fit" function is defined as

$$\chi^2 = \sum_{x,y} (P_{x,y}(s+b) - g(x,y))^2$$

The best fit can be found by determining the minimum of $\chi^2$.

For C100, estimates of the uncertainties on the parameters can be derived from the Jacobian of the function at the solution. Detailed discussion of the method is beyond the scope of this document; the NAG algorithm E04YCF is used. The nominal uncertainty of the fit is

$$s = \sqrt{\frac{\chi^2}{\delta}},$$

where $\delta$ is the number of degrees of freedom which is determined by the number of pixels $n$, the number of parameters (4), and the number of interpolations $\iota$ performed on C100 (section 8.4.8.1):

$$\delta = n - 4 - \iota$$

Since the position of the peak $(\alpha, \beta)$ is irrelevant of the size of it and the background it is located, $(\alpha, \beta)$ and $(c, d)$ are largely independent of each other. Thus adding 2 to the degrees of freedom is justified. This argument implies that the uncertainties for C100 may be overestimated. For C200 it is assumed that:

$$\delta = 2$$

The variances are calculated from:

$$\sigma_\alpha^2 = \frac{\chi^2}{(\delta+2) \cdot m_{pix}^2}$$

$$\sigma_\beta^2 = \frac{\chi^2}{(\delta+2) \cdot m_{pix}^2}$$

$$\sigma_c^2 = \frac{\chi^2}{(\delta+2)}$$

$$\sigma_d^2 = \frac{\chi^2}{(\delta+2)}$$

where $m_{pix}$ is the mean pixel value used to scale into the correct units:

$$m_{pix} = \frac{\sum_{pixels} P_{pix}}{N_{pix} \cdot (P^{max} - P^{min})}$$

The uncertainty of the fit is estimated as

$$s' = \sqrt{\frac{\chi^2}{\delta+2}}$$

**Ancillary data needed**

Estimates of reasonable boundariess for $\alpha, \beta, c, d$, these are obtained by considering the residuals of the fit during the iteration.

### 8.4.9 Convert in-band power to point source flux density

**Operation:** Convert the mean in-band power on a detector to a monochromatic flux density (Jy) assuming a $\nu^{-1}$ or - equivalently - constant $\nu F_\nu$ spectral energy distribution.

**Caveat:** The uncertainty in the PHT-S flux densities contains a systematic term coming from the uncertainty in the spectral response function (see eqn. 8.17 and 8.21), this term should have been removed.

The PHT-S subsystem is not calibrated by performing an FCS measurement within the AOT. Therefore the PHT-S signals are directly converted to flux density assuming a fixed responsivity for each PHT-S pixel and a fixed spectral response function. This requires a flux density computation with is different from all other AOTs. The distinction is made in the following subsections.

**Ancillary data needed**

- power calibration factors C1 for all filters read from Cal G file PFLUXCONV, see sections 5.2.3 and 13.17.1
- central wavelengths $\lambda_{pixel}$ for all PHT-P and C bands also stored in PFLUXCONV, see section 13.17.1
- point spread function factors which are stored in Cal G file PPSF, see section 13.15, note: for the C arrays the fraction of the psf on the entire array;
- PHT-S spectral response function i.e. signal calibration factors $C_{phts,pixel}$ plu uncertainties for all PHT-S pixels. The values are read from the SPD product header, for description of contents see section 13.16.1;
- PHT-S central wavelengths $\lambda_{pixel}$ for all PHT-S pixels, these are also read from the SPD product header, see also section 13.16.1.

#### 8.4.9.1 All AOTs except PHT40

The monochromatic flux density $F_\nu$ in Jy is derived as follows (cf eqn. 5.6):

$$F_\nu(\lambda_c) = 10^{26}\frac{P}{C1 \cdot f_{psf}(\lambda_c, \text{aperture})} \qquad \text{(Jy)} \tag{8.14}$$

with uncertainty

$$\Delta F_\nu(\lambda_c) = 10^{26}\frac{\sigma(P)}{C1 \cdot f_{psf}(\lambda_c, \text{aperture})} \qquad \text{(Jy)} \tag{8.15}$$

where,

- $F_\nu(\lambda_c)$ in Jy is the flux density at the centre wavelength of the filter, and
- $\Delta F_\nu(\lambda_c)$ the corresponding uncertainty;
- P in W is the in-band power on the detector in the selected filter band, and
- $\sigma$(P) the corresponding uncertainty;
- C1 in $m^2Hz$ is a constant related to each filter band and describes the total transmission of the bandpass along the optical path onto the detector; this includes the size of the mirror, reflections, filter transmission, spectral response of the detector, etc.;
- $f_{psf}(\lambda_c, \text{aperture})$ (unity) is the fraction of the telescope point-spread function falling into given aperture for PHT-P or onto the full array for PHT-C. at a given wavelength.

#### 8.4.9.2 PHT40

In the case of PHT-S (AOT P40) the signal $s_{pixel}$ with uncertainty $\sigma(\mathrm{s_{pixel}})$ (in V/s) for each pixel is converted to a flux density through:

$$\mathrm{F_\lambda(\lambda_{pixel}) = 10^{-20} \frac{s_{pixel}}{C_{phts,pixel}} \cdot \frac{c}{\lambda^2_{pixel}}} \qquad (\mathrm{W\,m^{-2}\mu m^{-1}}) \tag{8.16}$$

with uncertainty

$$\mathrm{\Delta F_\lambda(\lambda_{pixel}) = |F_\lambda(\lambda_{pixel})| \cdot \sqrt{(\frac{\Delta C_{phts,pixel}}{C_{phts,pixel}})^2 + (\frac{\sigma s_{pixel}}{s_{pixel}})^2}} \qquad (\mathrm{W\,m^{-2}\mu m^{-1}}) \tag{8.17}$$

where,

- $\mathrm{F_\lambda(\lambda_{pixel})}$ in $\mathrm{W\,m^{-2}\mu m^{-1}}$ is the flux density in wavelength units, and
- $\mathrm{\Delta F_\lambda(\lambda_{pixel})}$ the corresponding uncertainty;
- $\mathrm{C_{phts,pixel}}$ in (V/s)/Jy is the spectral response function which gives the conversion from signal in V/s to Jy for a given pixel, and
- $\mathrm{\Delta C_{phts,pixel}}$ the corresponding uncertainty;
- $\mathrm{\lambda_{pixel}}$ in $\mu$m is the centre wavelength of a pixel;
- c = 299792500 m/s is the speed of light used in OLP.

### 8.4.10 Convert in-band power to surface brightness

**Operation:** Convert flux density $\mathrm{F_\nu}$ in Jy to surface brightness $\mathrm{I_\nu}$ in MJy/ster.

The surface brightness calculation assumes that the point source flux density has been derived. Based on the point source flux density the surface brightness is determined.

**Ancillary data needed**

- Effective solid angles $\Omega_\lambda$ for each filter/aperture and filter/pixel combination. The values are read from Cal G files PPOMEGA in case of PHT-P, PC1OMEGA in case of PHT-C100 and PC2OMEGA in case of PHT-C200. See also appendix A.1.2, and section 13.18.
- PHT-S spectral response function for extended emission i.e. signal calibration factors $C^s_{phts,pixel}$ plus uncertainties for all PHT-S pixels. The values are read from the SPD product header, for a description of contents see section 13.16.1.
- PHT-S central wavelengths $\lambda_{pixel}$ for all PHT-S pixels, these are also read from the SPD product header, see also section 13.16.1.

#### 8.4.10.1 All AOTs except PHT40

The surface brightness is obtained by applying the relationship:

$$\mathrm{I_\nu(\lambda_c) = \frac{F_\nu(\lambda_c) \cdot f_{psf}}{(1-\epsilon^2) \cdot \Omega_\lambda}} \qquad (\mathrm{MJy/ster}) \tag{8.18}$$

with the uncertainty computed according to

$$\mathrm{\Delta I_\nu(\lambda_c) = \frac{\Delta F_\nu(\lambda_c) \cdot f_{psf}}{(1-\epsilon^2) \cdot \Omega_\lambda}} \qquad (\mathrm{MJy/ster}) \tag{8.19}$$

where with the same definitions as in the previous sections,

- $I_\nu(\lambda_c)$ in MJy/ster is the surface brightness at the centre wavelength of the filter, and
- $\Delta I_\nu(\lambda_c)$ the corresponding uncertainty;
- $\Omega$ in ster is the effective solid angle on the sky of the detector pixel or selected aperture;
- $(1\text{-}\epsilon^2)$=0.91 ($\epsilon$=0.30) is the correction for the obscuration by the secondary mirror.

The values of $\Omega_\lambda$ were computed by using a model which takes into account the ISO telescope mirrors as well as the physical sizes of the apertures in case of PHT-P or detectors in case of PHT-C. The model provided the 2-dimensional beam profile (or "footprint") of each possible aperture/filter (PHT-P) or pixel/filter (PHT-C) combination. The value of $\Omega_\lambda$ was eventually obtained from the integral of the footprint.

#### 8.4.10.2 PHT40

In the case of PHT-S (AOT P40) the signal $s_{pixel}$ (in V/s) with uncertainty $\sigma s_{pixel}$ is directly converted to surface brightness:

$$I_\lambda(\lambda_{\rm pixel}) = 10^{-26}\frac{s_{\rm pixel}}{C^{\rm E}_{\rm phts,pixel}}\cdot\frac{c}{\lambda^2_{\rm pixel}} \qquad ({\rm W\,m^{-2}\mu m^{-1}sr^{-1}}) \tag{8.20}$$

with uncertainty

$$\Delta I_\lambda(\lambda_{\rm pixel}) = |I_\lambda(\lambda_{\rm pixel})|\cdot\sqrt{(\frac{\Delta C^{\rm E}_{\rm phts,pixel}}{C^{\rm E}_{\rm phts,pixel}})^2+(\frac{\sigma s_{\rm pixel}}{s_{\rm pixel}})^2} \qquad ({\rm W\,m^{-2}\mu m^{-1}sr^{-1}}), \tag{8.21}$$

where

- $I_\lambda(\lambda_{\rm pixel})$ in ${\rm W\,m^{-2}\mu m^{-1}sr^{-1}}$ is the surface brightness for a given pixel, and
- $\Delta I_\lambda(\lambda_{\rm pixel})$ is the corresponding uncertainty;
- $\lambda_{pixel}$ in m is the central wavelength of a PHT-S detector pixel;
- $C^{\rm E}_{\rm phts,pixel}$ in (V/s)/(MJy/sr) is the spectral response function for the conversion from signal (in V/s) to surface brightness (in MJy/sr);
- $\Delta C^{\rm E}_{\rm phts,pixel}$ is the corresponding uncertainty;
- c = 299792500 m/s is the speed of light.

### 8.4.11 Write PHT-P point source photometry product

**Operation:** Write a complete PHT-P point source photometry product.

Write the product FITS header followed by the processed data in a binary table with each record containing the data for a single filter or aperture.
Detailed product descriptions can be found in section 12.4, subsection 12.4.2 (product PPAP).

### 8.4.12 Write PHT-P extended source or raster photometry product

**Operation:** Write a complete PHT-P extended source or raster photometry product.

Write the product FITS header followed by the processed data in a binary table with each record containing the data for a single filter, aperture or raster point.
Detailed product descriptions can be found in section 12.4, subsections 12.4.3 (PPAE) and 12.4.9 (PPAS) for single pointing and raster products, respectively.

### 8.4.13 Write PHT-C point source photometry product

**Operation:** Write a complete PHT-C point source photometry product.

Write the product FITS header followed by the processed data in a binary table with each record containing the data for a single filter.
Detailed product descriptions can be found in section 12.4, subsection 12.4.4 (PCAP).

### 8.4.14 Write PHT-C extended source or raster photometry product

**Operation:** Write a complete PHT-C extended source or raster photometry product.

Write the product FITS header followed by the processed data in a binary table with each record containing the data for a single filter or raster point.
Detailed product descriptions can be found in section 12.4, subsections 12.4.5 (PCAE) and 12.4.10 (PCAS) for single pointing and raster products, respectively.

## 8.5 Mapping

Two dimensional raster and spatially oversampled mapping observations are processed to images in the equatorial (RA and Dec) coordinate system. For the construction of the images it is assumed that a detector footprint (or beamprofile) can be represented by a simple "top-hat" function: the emission is 1 inside the detector area and zero outside. In addition, the circular apertures have perfectly circular footprints and the square PHT-P apertures and PHT-C detector pixels are considered to be perfectly square. The positions of each detector pixel per raster point have already been determined in the processing steps described in section 8.3.3. This section describes the co-addition steps to obtain an image.
Note that in the remainder of this section a clear distinction should be made between *detector pixel* and *image pixel*, the former being one of the 9 (for C100) or 4 (for C200) elements in the detector array and the latter being a picture element of an image.
The mapping software yields three products:

- surface brightness map in units of MJy/sr, this is the average surface brightness of all detector pixel exposures for each image pixel;
- uncertainty map in units of MJy/sr, mean brightness uncertainty per image pixel;
- exposure map in s, giving for each image pixel the total time that it has been covered by any detector pixel.

### 8.5.1 Establish image pixel size

**Operation:** Define the size of the image pixel

The angular dimensions of an image pixel depend only on the detector subsystem used and is independent on the filter/aperture combination. The values used in the current version of the OLP are given in Table 8.1.
Based on the image pixel size, the *fine-grid* is defined. The fine-grid is used to compute the fractional pixel coverage. The optimum fine-grid size in terms of realistic processing efforts has been decided to be:

$$S_{\text{fine grid}} = S_{\text{pixel}}/5 \qquad \text{(arcsec)} \tag{8.22}$$

**Ancillary data needed**

- None, parameters are hardcoded

Table 8.1: image pixel sizes

| Detector used | Shortest wavelength ($\mu$m) | Airy disc diameter (arcsec) | Pixel size (arcsec) |
|---|---|---|---|
| P1 | 3.2 | 2.8 | 8.0 |
| P2 | 20 | 17.7 | 8.0 |
| P3 | 60 | 50.3 | 8.0 |
| C100 | 70 (C_50) | 41.9 | 15.0 |
| C200 | 120 | 101.0 | 15.0 |

### 8.5.2 Establish maximum image size

**Operation:** Calculate the angular dimensions of the image required to contain the full raster scan in equatorial coordinates.

The maximum size of the image is calculated using the following parameters:

- M: the number of raster steps along a raster leg;
- N: the number of raster legs;
- dM: step size in arcsec along raster leg;
- dN: step size in arcsec in between raster legs;
- $\alpha_c$, $\delta_c$: the J2000 RA and Dec position in decimal degrees of the raster centre;
- $\alpha_{m,n}$, $\delta_{m,n}$: the J2000 RA and Dec position in decimal degrees of raster point (m,n), with m= 1...M, and n= 1...N;
- $D_A$: the diameter in arcsec of the aperture used, in case of a C-array: the sidelength of the array in arcsec;
- $\theta_{chop}$: the maximum chopper deflection while mapping (only for PHT32 maps).

The centre of the raster scan is defined as the image centre. The dimensions of the frame in equatorial coordinates are derived as follows. For all raster points (m,n) determine:

$$\begin{aligned} \alpha_{max} &= max(\Delta\alpha(m,n)) \\ \alpha_{min} &= min(\Delta\alpha(m,n)) \\ \delta_{max} &= max(\Delta\delta(m,n)) \\ \delta_{min} &= min(\Delta\delta(m,n)) \end{aligned}$$

where:

- $\Delta\alpha(m,n)$: RA component of the difference vector between $(\alpha_{m,n}, \delta_{m,n})$ and $(\alpha_c, \delta_c)$
- $\Delta\delta(m,n)$: Dec component of the difference vector between $(\alpha_{m,n}, \delta_{m,n})$ and $(\alpha_c, \delta_c)$

The components $\Delta\alpha(m,n)$ and $\Delta\delta(m,n)$ are computed using spherical trigonometry. The margins around the raster grid is determined by $D_A$ and the maximum chopper deflection $\theta_{chop,max}$, in raster orientation:

$$\begin{aligned} x_m &= D_A/2 + \theta_{chop,max} \\ x_n &= D_A/2 \end{aligned}$$

Then the map dimensions $L_\alpha$ and $L_\delta$ are computed from:

$$\begin{aligned} L_\alpha = &\quad \alpha^*_{max} - \alpha^*_{min} \\ L_\delta = &\quad \delta^*_{max} - \delta^*_{min} \end{aligned}$$

with

$$\begin{aligned} \alpha^*_{max} = &\quad \alpha_{max} + (|x_m cos(\phi)| + |x_n sin(\phi)|) \\ \alpha^*_{min} = &\quad \alpha_{min} - (|x_m cos(\phi)| + |x_n sin(\phi)|) \\ \delta^*_{max} = &\quad \alpha_{max} + (|x_m sin(\phi)| + |x_n cos(\phi)|) \\ \delta^*_{min} = &\quad \delta_{min} - (|x_m sin(\phi)| + |x_n cos(\phi)|) \end{aligned}$$

where $\phi$ is the spacecraft roll angle.

The rectangular image frame is therefore chosen so large that the entire area covered by the detectors in the raster fits inside. Depending on the rotation angle of the raster as well as the sampling step sizes with respect to the size and rotation of the detector, undefined frame areas may be present.

The minimum number of image pixels required to map the whole of the raster area is calculated from the dimensions of the raster and the image pixel size $s_{pixel}$, as follows :

$$\begin{aligned} n_\alpha &= 2(\|\frac{L_\alpha}{2s_{pixel}}\| + 1) + 1 \\ n_\delta &= 2(\|\frac{L_\delta}{2s_{pixel}}\| + 1) + 1, \end{aligned}$$

in which $\|$ denotes "the integer value of" - i.e. the initial value is rounded down to the nearest integer.

Also calculated at this stage are the angular coordinates of the image pixel origin which is defined as the bottom left hand corner (blhc) of image pixel $(1, 1)$.

$$\begin{aligned} x_0 &= -\frac{n_\alpha s_{pixel}}{2} \\ y_0 &= -\frac{n_\delta s_{pixel}}{2} \end{aligned}$$

These are used subsequently to translate between the coordinate origin at the centre of the image and the origin of the pixel coordinates.

The blhc of an image pixel $(i, j)$ is thus given by :

$$\begin{aligned} x_o(i,j) &= (i - 1 - \frac{n_\alpha}{2}) s_{pixel} \\ &= (i-1)s_{pixel} + x_0 \\ y_o(i,j) &= (j - 1 - \frac{n_\delta}{2}) s_{pixel} \\ &= (j-1)s_{pixel} + y_0 \end{aligned}$$

### 8.5.3 Determination of the coverage by a sky sample in the image

**Operation:** Map data from a given detector pixel, raster position, and chopper offset combination onto the image.

We define a *sky sample* to be a sky observation for a given detector pixel, at raster position (m,n), and chopper deflection $\theta_{chop}$. A sky sample has a raster dwell time or chopper dwell time (in case of PHT32 maps).

The fine grid (section 8.5.1) is used to determine the fractional coverage of the image pixel by the detector footprint. The fine-grid size is chosen such that it is a simple factor of the image pixel size: there is an integral number of grid points per image pixel.

Therefore for each sky sample the following steps are performed:

- determine the image pixel range $([x_{min}, x_{max}], [y_{min}, y_{max}]$ in which the detector pixel footprint can completely be contained;
- for each image pixel contained in this range determine the number of fine-grid positions $N_{fg}$ which fall within the detector footprint.
- for each image pixel in the range determine the coverage factor $F = N_{fg}/N_{total}$, where $N_{total}$ is the total number of fine-grid positions on a pixel.

### 8.5.4 Binning sky samples onto image pixels

**Operation:** Accumulate the sky samples and derive the average surface brightness, uncertainty and exposure.

The contribution from the $n^{th}$ sky sample to the mean brightness, brightness uncertainty, and exposure time at image pixel $i, j$ are denoted $b_n(i,j)$, $u_n(i,j)$ and $e_n(i,j)$ respectively. The accumulated sums of the contributions from the first $n$ pointings are denoted by $B_n(i,j)$, $U_n(i,j)$ and $E_n(i,j)$.

The effective exposure time of sky sample $n$ at image pixel $i, j$ is the fraction of the image pixel covered by the aperture for a given sample multiplied by the dwell time $t_n$:

$$e_n(i,j) = F(i,j) \cdot t_n \tag{8.23}$$

To calculate the total exposure on the image pixel, the contributions from all sky samples are summed. The surface brightness values and the corresponding uncertainties are summed thereby using the exposure times as weights.

$$\begin{aligned} E_{n+1}(i,j) = &\quad E_n(i,j) + e_{n+1}(i,j) \\ B_{n+1}(i,j) = &\quad B_n(i,j) + e_{n+1}(i,j) b_{n+1}(i,j) \\ U_{n+1}(i,j) = &\quad U_n(i,j) + e_{n+1}(i,j) u^2_{n+1}(i,j). \end{aligned}$$

The accumulated sums for all sky samples are used to derive images of total exposure time $E_{total}$, mean brightness $\overline{B}$ and brightness uncertainty $U_{rms}$.

$$\begin{aligned} E_{total}(i,j) &= E_N(i,j) \\ &= \sum_{n=1}^{N} e_n(i,j) \end{aligned}$$

$$\begin{aligned} \overline{B}(i,j) &= B_N(i,j)/E_N(i,j) \\ &= \frac{1}{E_N} \sum_{n=1}^{N} e_n(i,j) b_n \end{aligned}$$

$$
\begin{aligned}
U_{rms}(i,j) &= \left(\frac{1}{E_N} U_N(i,j)\right)^{\frac{1}{2}} \\
&= \left(\frac{1}{E_N} \sum_{n=1}^{N} e_n(i,j)\, u_n^2(i,j)\right)^{\frac{1}{2}}
\end{aligned}
$$

### 8.5.5 Write image products

**Operation:** Write a set of complete photometric image products.

First write the product FITS header followed by the processed data in a primary array. The derived surface brightness (in MJy/sr), brightness uncertainty (in MJy/sr) and exposure time (in s) images are stored in separate products.

Detailed product descriptions can be found in section 12.4, subsections 12.4.6 (product PGAI), 12.4.7 (product PGAU), and 12.4.8 (product PGAT) for the brightness, uncertainty and exposure time images.

## 8.6 Spectroscopy

The processing of PHT-S data is similar to that of the photometry data. Detectors PHT-SS and PHT-SL are processed separately in line with the separate treatment in SPD. The differences in processing between PHT-S and the other detectors have been described in sections 8.4.9 and 8.4.10. Due to the relatively few PHT-S raster maps collected during the mission, no raster images with PHT-S are produced.

### 8.6.1 Write spectroscopy products

**Operation:** Write spectroscopy products.

To maintain the separation between the short wavelength and long wavelength PHT-S detector arrays SS and SL, the different array data are stored in separate products.

Detailed product descriptions can be found in section 12.4, subsections 12.4.11 (product PSAP), 12.4.12 (product PLAP), 12.4.13 (product PSAE), 12.4.14 (product PLAE), 12.4.15 (product PSAS), 12.4.16 (product PLAS), for the PHT-SS and SL point source, extended source and raster products, respectively.

# Chapter 9

# Caveats

## 9.1 Overview

The quality and reliability of data products and documentation depend on several aspects. In this chapter we summarize the pending issues related to documentation, to product reliability, and, closely connected to the products, to the OLP software.

In section 9.2 the shortcomings of the present version of the documentation are given.

In section 9.3 we give the present status of the scientific validity of products of the ISOPHOT AOTs. The scientific validity of an observing mode is decided after thorough evaluation of the corresponding Auto Analysis (AAR) products (see chapter 8) of observations of known test targets. Only when the results are according to the expectations a mode is declared "scientifically valid".

The reliability of the OLP products is best described by the photometric accuracies that can be achieved per observing mode. The photometric accuracies for those modes that are scientifically validated are presented in 'ISOPHOT calibration accuracies' [11]. A full discussion of the error budgets and resulting uncertainties is given in 'ISOPHOT error budgets' [15]. The sections on scientific validation have been taken from the OLP Version 7 validation report by Klaas and Radovich [12]. This document is available for those who would like to compare their data with the results from test cases.

In section 9.4 of this chapter the present (known) limitations and caveats on the ISOPHOT data and software are given. Issues concerning incomplete instrumental calibrations and pending software implementation are discussed in detail.

## 9.2 Caveats on this document

The ISOPHOT Data Users Manual is a living document and sections have to be revised as soon as the calibration is improved and the software is upgraded. Due to the ongoing calibration research, sections in chapter 4 can become outdated or incomplete. In particular:

- the derivation of orbit dependent parameters is not discussed in detail. These parameters are implemented in OLP Version 7 and calibration files are available (cf. chapter 13).
- a description of the OLP Version 7 correction for signal losses in chopped mode is not provided. Despite the corrections the ISOPHOT team has not validated chopped mode observations. Investigations for a better correction method are ongoing.

In chapters 7 and 8 we have embedded a number of caveats on the software. These caveats were found in the process of writing this document - see caveats in chapter 7: section 7.4.2, and chapter 8: sections 8.4.2, 8.4.8, and 8.4.9. Due to incorrect software we also give a caveat on some data products, see section 12.4.6.

The descriptions of the header fields of the AOT products given in chapter 12 can still contain omissions and inconsistencies. Although it has been tried to be as complete as possible, not all combinations in

observing mode, measurement sequences, and detector subsystem could be checked especially for the AAR products. A review of the header items is planned for a later version of the software. This could lead to changes in the structure of the FITS headers.

## 9.3 Status of Scientific Validation of PHT AOTs

### 9.3.1 Validated modes in OLP Version 7

The OLP Version 7 validation status per AOT submode is given in Table 9.1. The table also provides an overview of the next steps to further upgrade both validated and non-validated modes and for which OLP version improvements can be expected.

It should be noted that in the case of AOT PHT22 raster maps are only partly scientifically validated. It has been demonstrated that mini-maps give reliable results for faint source photometry. Most of the photometric accuracy numbers presented for faint source measurements of C100 and C200 are based on mini-map photometry. However, in order to validate PHT22 raster maps in general, the following items must be verified before:

- valid results for all different combinations of raster parameters
- conservation of flux regardless of raster parameters and re-gridding algorithm.

These checks are less related to calibration upgrades but more to the establishment of a sufficiently large test data set and inspection of the observations case by case.

In Table 9.2 we list the validated modes per detector sub-system. For completeness we have added the polarisation modes which can only be evaluated interactively using PIA and special FORTRAN routines.

### 9.3.2 Photometric Accuracies of Staring Modes

Global calibration accuracies were estimated from the investigation of test cases and the comparison with published reference photometry, for details see [11]. They can be applied, if not one of the caveats on photometry applies, cf. section 9.4.

The terms **absolute accuracy**, **relative accuracy** and **reproducibility** have been defined in the following context:

- **absolute accuracy** is the accuracy achieved w.r.t. the reference Photometry, if the filter measurement had a corresponding FCS transfer measurement in the same filter. Hence, the quality of the FCS calibration against celestial standards is directly verified. Note that no calibration accuracy of the reference photometry (models, IRAS) has been taken into account, as this is beyond the scope of this report. A typical order of the absolute accuracy of the reference photometry is 2 – 10%.
- **relative (filter-to-filter) accuracy** is the accuracy achieved with respect to the reference photometry, if the filter measurement was not performed in the filter in which the FCS calibration was done. Currently, assumptions about the constancy of the responsivity over the full flux range and for all filters, and, related to that relative filter-to-filter correction factors, apply. It has been proven that this is in general not correct, and it is considered that in future OLP versions corrections for non-linearities of the responsivity with the in-band power will be applied. Hence, the relative uncertainty can be much larger than the absolute one in multi-filter measurements with certain source SEDs. The number of suitable test cases performed in multi-filter mode is much smaller than the number of test cases in any of the absolute measurement modes (i.e. with an FCS measurement in the respective filter). The relative filter-to-filter accuracy could only be established for a minor subset with no test case for C200.
- absolute and relative accuracy are assumed to add to the total Photometric uncertainty. In multi-filter measurements with one FCS measurement the absolute measurement uncertainty is subtracted from all measurements in non-FCS filters in order to derive the relative measurement accuracy.

Table 9.1: Scientific Validation of OLP AOT Processing, July 98

| **AOT** | **submode** | **scientifically valid since** | **next upgrades** | **foreseen in OLP Vx.y** |
|---|---|---|---|---|
| PHT03 | staring point source | V6 | non-lin R & FCS aper | 8.2 |
| | staring extended source | no | beam | 8.2 |
| | nodding | V6 | non-lin R & FCS aper | 8.2 |
| | chopped point source | no | chop | 8.2 |
| | raster map | no | map cal & drift | 8.2/9.2 |
| PHT04 | staring point source | no | beam & FCS aper | 8.2 |
| | staring extended source | no | beam | 8.2 |
| | chopped point source | no | chop & beam | 8.2 |
| PHT05 | staring point source | V6 | FCS aper | 8.2 |
| | staring extended source | no | beam | 8.2 |
| PHT17 | staring point source | V6 | non-lin R & FCS aper | 8.2 |
| 18,19 | staring extended source | no | beam | 8.2 |
| PHT22 | staring point source | V7 | non-lin R | 8.2 |
| | staring extended source | V7 | non-lin R | 8.2 |
| | nodding | V7 | non-lin R | 8.2 |
| | chopped point source | no | chop | 8.2 |
| | raster map | no | map cal & flat-field | 9.2 |
| PHT25 | staring point source | V7 | | |
| | staring extended source | V7 | | |
| PHT32 | chopped mapping | no | chop & map cal | 9.2 |
| PHT37 | staring point source | V7 | non-lin R | 8.2 |
| 38,39 | staring extended source | V7 | non-lin R | 8.2 |
| PHT40 | staring point source | V5 | | |
| | staring extended source | V6 | beam | 8.2 |
| | chopped point source | V6 | | |

Table 9.2: Scientifically Validated Observing Modes per Detector, July 98

| **det.** | **scientifically validated mode** | **AOT** |
|---|---|---|
| P1 | absolute photometry point sources | PHT05 |
| | staring multi-filter photometry point sources | PHT03 |
| | faint source multi-filter nodding | PHT03 |
| | multi-filter sparse map point sources | PHT17/18/19 |
| P2 | absolute photometry point sources | PHT05 |
| | staring multi-filter photometry point sources | PHT03 |
| | faint source multi-filter nodding | PHT03 |
| | multi-filter sparse map point sources | PHT17/18/19 |
| | polarimetry (PIA) | PHT50 |
| P3 | absolute photometry point sources | PHT05 |
| | staring multi-filter photometry point sources | PHT03 |
| | faint source multi-filter nodding | PHT03 |
| | multi-filter sparse map point sources | PHT17/18/19 |
| C100 | absolute photometry point sources | PHT25 |
| | absolute photometry extended sources | PHT25 |
| | staring multi-filter photometry point sources | PHT22 |
| | staring multi-filter extended sources | PHT22 |
| | faint source multi-filter nodding | PHT22 |
| | multi-filter sparse map | PHT37/38/39 |
| C200 | absolute photometry point sources | PHT25 |
| | absolute photometry extended sources | PHT25 |
| | staring multi-filter photometry point sources | PHT22 |
| | staring multi-filter extended sources | PHT22 |
| | faint source multi-filter nodding | PHT22 |
| | multi-filter sparse map | PHT37/38/39 |
| | polarimetry (PIA) | PHT51 |
| SS/SL | staring point source spectroscopy | PHT40 |
| | extended source spectroscopy | PHT40 |
| | chopped point source spectroscopy | PHT40 |

- **reproducibility** is the relative consistency of measurements repeated several times with the same measurement set-up. It is a measure of the internal stability of the instrument and describes also the current limitations in signal processing.

In summary, the following calibration accuracies have been achieved per detector:

**P1: 10% absolute accuracy and 20% relative accuracy for bright sources (> 50 Jy). For fainter sources the absolute accuracy is within 30%.**
**The relative reproducibility accuracy is 5% for bright sources and 10% for faint sources.**

**P2: Better than 15% absolute accuracy and 10% relative accuracy.**
**The relative reproducibility accuracy is 2% for bright sources and 12% for faint sources.**

**P3: 15% absolute accuracy and 20% relative accuarcy down to ~ 0.5 Jy. For fainter sources the absolute accuracy is around 30%.**
**The relative reproducibility accuracy is 7% for bright sources and 7% for faint sources. Under extreme Space Weather conditions and for the very end of the science window the achieved accuracy for faint sources is poorer.**

**C100: 15% absolute accuracy and 10% relative accuracy down to ~ 0.5 Jy. For fainter fluxes the absolute accuracy in mini-map mode is ~ 30%.**
**The relative reproducibility accuracy is 3% for bright sources and 20% for faint sources.**

**C200: ~ 20% absolute accuracy for brighter sources. Note that in array centered mode accuracies are poorer for the 180 and 200 $\mu$m filters due to an inadequate PSF correction factor. Photometry in these filters has to be corrected in general by 20–30% towards higher flux values. For fainter sources (< 1 Jy) the accuracy achieved in mini-map mode is ~ 30%. There was no suitable test case allowing to judge the relative filter-to-filter accuracy. The investigated test cases of standard stars ($\alpha$ Boo, $\gamma$ Dra and Sirius) did not give conclusive results due to their faintness in the C200 range and application of less optimal observing modes.**
**The relative reproducibility accuracy is around 10% both for bright and faint sources.**

## 9.4 OLP Version 7: Limitations and Caveats

This section addresses the limitations and caveats of the PHT calibration file Version 4.0 and the OLP Version 7 which have been identified during the scientific pipeline validation process.

### 9.4.1 Error Calculation and Propagation

Whenever possible uncertainties had been included in the Cal-G files. It turned out, however, that the simple propagation of relative uncertainties as originally specified did not yield reasonable results, as the uncertainties are of different types: statistical and systematic uncertainties and photometric bias. The relative contribution of these different types of uncertainty depends on the details of the measurement mode.

OLP Version 7 is restricted to the pure statistical uncertainty from signal evaluation. This can be seen as a minimal error. For an estimate of the total uncertainty associated with a specific measurement the observer is referred to [15] and [11].

**Caveat:** The PHT OLP software does only provide an uncertainty from the statistical signal evaluation. It does not give any estimates of the systematic uncertainties of all performed calibration steps. Therefore, OLP 7.0 uncertainties are **minimal** errors. It is essential to refer to special documentation which provide an overview of the uncertainties introduced step by step. These depend on the exact observing conditions and evaluation steps which may even not be completed inside OLP (e.g. background subtraction in maps or from independent staring measurements).

### 9.4.2 Chopped Photometry

On the basis of the investigated test cases the chopped photometry of AOTs PHT03 and PHT22 cannot be declared scientifically valid.

The most reliable results have been found for chopped P2 photometry for which in many cases an absolute calibration accuracy of around 20% could be achieved.

This rejection is based on the following findings:

- In particular for P3 and C100 a general over-correction of the chopped Photometric fluxes w.r.t. reference photometry from the literature or ISOPHOT staring mode photometry is observed.
- In multi-filter modes the scatter of the photometric data points, including non-detection of the source, or discontinuitites in the resulting SEDs larger than 30% are found which do not allow a sound scientific analysis.

Reasons for this behaviour of the chopped modes which need follow-up investigations are supposed to be:

- Limitations in the usage of an average default responsivity (the orbit dependence alone appears to be too weak to account for the variation of the responsivity values).
- A not yet sufficient signal evaluation for chopped measurements. In particular for C100 the restriction to use the central pixel only in the case of chopped point source photometry seems to be mandatory taking the test results into account.
- Not yet final signal correction factors. Here, more calibration data have been acquired.

### 9.4.3 Extended Source Photometry

Wavelength dependent solid angles for the PHT-C arrays derived from refined beam calculations have been successfully tested and make the surface brightness values for all investigated test cases comparable to COBE annual map results.
The PHT22 AOT extended source photometry can therefore be declared scientifically validated with an absolute accuracy of 30% and a relative filter-to-filter accuracy of 20%.
The PHT03 AOT extended source photometry needs still further refinement of the solid angles and a detailed check-out of the dependence on the aperture size.

Note that the accuracy of COBE annual maps for 140 and 240 $\mu$m is typically 20%. For weekly maps it can be even worse. For wavelengths less equal than 100 $\mu$m the quoted accuracy is in general $\leq$ 1%.

### 9.4.4 Spectroscopic Mode

Under the following conditions significant deviations in flux from earlier (validated) OLP Version 6 results can occur:

- The newly introduced orbit dependent dark signal subtraction shows noticeable differences in the resulting fluxes for continuum levels below 6 $10^{-14}$ W m$^2$ $\mu$m$^{-1}$ for SS and 4 $10^{-14}$ W m$^2$ $\mu$m$^{-1}$ for SL, respectively (for staring mode observations).
- For faint continuum sources changes in the continuum level of about 50% can occur w.r.t. OLP V6 results. For the investigated test case (NGC 6543) no final conclusion could be drawn by comparison with reference spectroscopy (IRAS LRS and CAM-CVF) and further refined cross calibration is necessary. The line fluxes are in general not affected, if the peak intensity is above the levels where dark current subtraction becomes crucial (see above).

### 9.4.5 Validity Ranges of FCS Calibration Files

**Caveat:** A poorer calibration accuracy can be expected for observations for which the headers of the PHT data products indicate that the FCS power settings were outside the validity range given in the header of the P*FCSPOW*.FITS CAL-G files (see section 13.10). The deviation is larger for extrapolations further away from the validity range.

**Caveat:** The FCS calibration for P3, C100 and C200 before revolution 94 is less well sampled with standard calibration observations, than after revolution 94. Therefore, the quality of the FCS calibration of observations before revolution 94 can be poorer as compared to observations taken later in the mission. This also applies to the FCS flat-field calibration for the C100 and C200 detectors.

### 9.4.6 Inhomogeneous FCS Illumination of PHT-P Apertures

**Caveat:** In case the FCS calibration of an observation is performed in a non-standard aperture of this filter strong deviations (factor $\simeq 2$) of the correct responsivity and thus the derived fluxes can occur. The deviations are strongest for the usage of the largest apertures in combination with P1 filters.

### 9.4.7 Non-geometric Aperture Beam Size Scaling

**Caveat:** If observations are performed in apertures, which are different in diameter from the ones used in standard calibration, deviations from the correct flux calibration can occur. This implies especially for extended source or background observations using the largest apertures with P1 and P2.

### 9.4.8 Non-linearity of Detector Responsivity with Flux

There are meanwhile strong indications from the huge data base of standard star measurements that ISOPHOT detectors do not behave linear in their response with incident flux. By design of the AOTs the PHT uplink logic matches the FCS flux to the expected source flux and consequently the non-linearity should be minimal in many cases. However, in multi-filter AOTs it is possible, that the flux in one filter deviates quite strongly from the flux in the filter in which the FCS calibration is performed (especially for P1). In these cases the filter that deviates most from the inband power used for the FCS calibration (usually the first measurements of an AOT sequence) can show calibration problems due to this effect. Similar problems can occur for maps and for multi-aperture observations, which show a wide dynamic range in flux.

**Caveat:** Measurements with inband powers far away ($\geq$ factor 10) from the ones used for the related FCS measurement(s) have poorer calibration accuracy.

### 9.4.9 Detector Signal Transients

**Caveat:** The transient correction only works satisfactory for measurements longer than the detector transient time constant at a given illumination. The transients are very often the limiting factor for the achieved accuracy. Measurements flagged by the OLP software as "plateau data affected by residual drift" can show strong deviations (residual drift is greater than 5%) from the correct result.

### 9.4.10 Long Term Detector Drifts

For single pointing measurements with one FCS measurement per detector no attempt is made by PHT OLP 7.0 software to correct for long term detector responsivity drifts, i.e. stability of the detector responsivity during the execution time of an AOT is assumed. For raster pointing observations and sparse maps OLP does a linear interpolation with time of the responsivity values derived from the two bracketing FCS measurements. Detailed investigation of PHT-C maps has shown that the detector long term drift is not linear, but very often shows an exponential behaviour due to switch-on effects. Therefore, models of the detector behaviour or baseline fits would be required for optimum results.

**Caveat:** PHT OLP does not correct (in case of single pointings) or correct only with a linear interpolation (in case of maps) for long term detector drifts within an AOT.

### 9.4.11 Missing Measurements and Chopper Correction

The current version of OLP does not perform a consistency check whether the number of measurements which were actually performed does match the number of measurements expected from the EOHA (see Chapter ??, except for an initial check during DERIVE_SPD. In case there are measurements missing in an AOT it is possible that there is a mismacth between the keywords written into the SPD header concerning the chopper correction parameters, w.r.t. the measurement number and the filter number that was actually used in a measurement.

**Caveat:** In case there are measurements missing from an AOT there may be a mismatch between the chopper correction keywords and the related filter number.

### 9.4.12 Limitations in Use of PHT Color Correction Factors

**Caveat:** For the establishment of the color correction factors provided by CAL-G Version 4.0 not yet final PHT filter bandpass data including a wide wavelength range outside the nominal bandpass have been used. For some filters and in the case of extremely rising or falling SEDs this can mean an underestimate by out-of-band contributions. Color correction factors above 2 should be considered as less accurate and factors above 4 only as an indication of the order of the correction, as they clearly depend on the integration and interpolation method used. This applies in particular to SEDs of cold sources in combination with the P1 filters which fall onto the steep Wien branch of these SEDs. In these cases it is recommended to contact the ISO Data Centres for the most recent bandpass transmission and establish the color correction factor yourself.

### 9.4.13 Empirical PPSF Correction Factors for Array Centered C200 Photometry

During OLP V6 Scientific Validation it had been realised that the theoretically calculated point spread function correction factors (PPSF) for photometry with the source centered on the C200 array were not the correct ones. Hence, empirical correction factors were established by comparing the relative intensities in the pixels for targets which had been measured both in array centered and pixel raster mode. These empirical correction factors compare with the theoretical ones as shown in Table 9.3:

Table 9.3: PPSF Factors for Array Centered C200 Photometry

| **C200 Filter** | **theoretical PPSF** | **empirical PPSF** |
|---|---|---|
| C_120 | 0.900 | 0.574 |
| C_135 | 0.864 | 0.668 |
| C_160 | 0.810 | 0.708 |
| C_180 | 0.782 | 0.972 |
| C_200 | 0.736 | 1.054 |

A plausible explanation for the reverse behaviour (increasing PPSF with wavelength instead of decreasing PPSF) is diffraction at the edges of the field lenses which are mounted with an inter-pixel gap of about 100 $\mu$m, so that the effect is expected to be strongest for the short wavelength C200 filters.

Detailed investigation of several test cases during OLP V7 Scientific Validation clearly points out that the photometry in the C_180 and C_200 filters always gives too low fluxes. Comparison with reference photometry suggests that the PPSF factors for the two filters must be some 20 to 30% smaller, hence close to the theoretical value. This issue will be followed up in a detailed calibration program to establish refined PPSF correction factors for array centered C200 photometry.

Therefore, the following caveat has to be put onto the CAL-G V4.0 empirical PPSF correction factors for array centered C200 photometry:

**Caveat:** The correction factors for the filters C_180 and C_200 appear to be too large by 20 to 30%. Photometric fluxes derived for both filters in array centered mode should be corrected towards larger values by this percentage (as the uncorrected flux value is divided by the PPSF factor).

# Chapter 10

# Getting Started

## 10.1 First look at the products

The ISOPHOT auto-analysis products consist of binary FITS tables in case of single pointing photometry or FITS images in case raster maps or PHT32 observations were requested. All products contain a header in which general information can be found about an observation and the contents of the tables or images. As the headers of all products are in given ascii, the header information of the FITS files can be browsed with a "type" (in VMS) or "more" (in unix) command. Detailed descriptions of the headers as well as the FITS records of the products are given in chapters 12 and 13.

For a quick look of the binary FITS table data, utilities are required to convert the binary contents of a FITS file into an ascii file. For the single pointing photometry data, the tables are usually not very big, so that the ascii file can immediately be downloaded in a general utility such as e.g. a spreadsheet.

A utility which can be used for such a purpose is the "ldump" routine in FTOOLS. For more information on FTOOLS see

`http://heasarc.gsfc.nasa.gov/docs/software/ftools/ftools_menu.html`

Any image processing or displaying system should be able to display the AA FITS image files (PGAI, PGAU, PGAT). A frequently used tool for such purposes is SAOimage, see

`http://cfa165.harvard.edu/software/saoimage.html`

The Infrared Processing and Analysis Center has developed "ISO First Look Tools" to look and display ISO products. These products are available to the general astronomical community. For detailed information see

`http://www.ipac.caltech.edu/iso/ipacsoft.html`

## 10.2 Further processing

The ESA Astrophysics Division and the ISOPHOT consortium led by the Max Planck Institut für Astronomie in Heidelberg (MPIA) have developed in a joint effort the ISOPHOT Interactive Analysis Package (PIA). Although this package was initially developed for the processing of the calibration data, the package is available for the general astronomical community. PIA runs under IDL 5.0 and many routines are available for the processing and scientific analysis of ISOPHOT products. For more information we refer to:

`http://isowww.estec.esa.nl/manuals/PHT/pia/`

# Chapter 11

# Guide to Data Products

This chapter may serve as a starting point for ISOPHOT data product queries.

## 11.1 Quick Reference: Synopsis of all ISOPHOT Products

In the next subsections the data products generated at the different processing levels are tabulated. For each product, 4 columns are given. The first defines the product. The next names the type of product. The third column indicates for which AOT's the product is generated. The final column refers to which section of this manual contains a full description of the product.

### 11.1.1 ERD Products

| Product | Description | AOTs | Section |
|---|---|---|---|
| PSTA | Compact Status | All | 12.2.7 |
| PPER | P ERD | P03, 04, 05, 17/18/19, 50 | 12.2.2 |
| P1ER | C100 ERD | P22, 25, 32, 37/38/39 | 12.2.3 |
| P2ER | C200 ERD | P22, 25, 32, 37/38/39, 51 | 12.2.4 |
| PSER | S ERD | P40 | 12.2.6 |
| P2ES | Serendipity Mode | – | 12.2.5 |

### 11.1.2 SPD Products

| Product | Description | AOTs | Section |
|---|---|---|---|
| PP1S | P1 SPD | P03, 04, 05, 17/18/19 | 12.3.2 |
| PP2S | P2 SPD | P03, 04, 05, 17/18/19 | 12.3.2 |
| PP3S | P3 SPD | P03, 04, 05, 17/18/19 | 12.3.2 |
| PC1S | C100 SPD | P22, 25, 32, 37/38/39 | 12.3.3 |
| PC2S | C200 SPD | P22, 25, 32, 37/38/39 | 12.3.4 |
| PSSS | SS SPD | P40 | 12.3.5 |
| PSLS | SL SPD | P40 | 12.3.6 |

### Calibration A files generated

see section 5.7.2

| Product | Description | AOTs | Section |
|---|---|---|---|
| PP1A | P1 Cal A | P03, 04, 05, 17/18/19 | 12.3.7 |
| PP2A | P2 Cal A | P03, 04, 05, 17/18/19 | 12.3.7 |
| PP3A | P3 Cal A | P03, 04, 05, 17/18/19 | 12.3.7 |
| PC1A | C100 Cal A | P22, 25, 32, 37/38/39 | 12.3.8 |
| PC2A | C200 Cal A | P22, 25, 32, 37/38/39 | 12.3.8 |

### Dark signal files generated by the absolute photometry AOTs

see sections 12.3.9, 12.3.10, and 12.3.11. Note that the cold FCS measurements of P05 and P25 are processed to Cal A files.

| Product | Description | AOTs | Section |
|---|---|---|---|
| PP1D | P1 Dark | P05 | 12.3.9 |
| PP2D | P2 Dark | P05 | 12.3.9 |
| PP3D | P3 Dark | P05 | 12.3.9 |
| PC1D | C100 Dark | P25 | 12.3.10 |
| PC2D | C200 Dark | P25 | 12.3.11 |

## 11.1.3 AAR Products

| Product | Description | AOTs | Section |
|---|---|---|---|
| PPAP | P point source photom. | P03, 04, 05, 17/18/19 | 12.4.2 |
| PPAE | P extended source photom. | P03, 04, 05, 17/18/19 | 12.4.3 |
| PPAS | P raster map photom. | P03 | 12.4.9 |
| PCAP | C point source photom. | P22, 25, 32, 37/38/39 | 12.4.4 |
| PCAE | C extended source photom. | P22, 25, 37/38/39 | 12.4.5 |
| PCAS | C raster map photom. | P22, 32 | 12.4.10 |
| PGAI | surface brightness image | P03, 22, 32 | 12.4.6 |
| PGAU | uncertainty image | P03, 22, 32 | 12.4.7 |
| PGAT | exposure time image | P03, 22, 32 | 12.4.8 |
| PSAP | SS point source spectros. | P40 | 12.4.11 |
| PSAE | SS ext. source spectros. | P40 | 12.4.13 |
| PSAS | SS scan spectros. | P40 | 12.4.15 |
| PLAP | SL point source spectros. | P40 | 12.4.12 |
| PLAE | SL ext. source spectros. | P40 | 12.4.14 |
| PLAS | SL raster map spectros. | P40 | 12.4.16 |

### 11.1.4 Cal G Products: Derive_SPD

| Product | Description | Section |
|---|---|---|
| PTIMEDEP | calibration file time dependency | 13.2.1 |
| PDIE1TRANS | DIE1 power calibration table | 13.3.1 |
| PDIE2TRANS | DIE2 power calibration table | 13.3.2 |
| PSELNDR | NDR (de-)selection | 13.4.1 |
| PPCRELIN | P CRE Linearisation | 13.5.1 |
| PC1CRELIN | C100 CRE Linearisation | 13.5.2 |
| PC2CRELIN | C200 CRE Linearisation | 13.5.3 |
| PP1RESETI | P1 reset interval correction | 13.6.1 |
| PP2RESETI | P2 reset interval correction | 13.6.2 |
| PP3RESETI | P3 reset interval correction | 13.6.3 |
| PC1RESETI | C100 reset interval correction | 13.6.4 |
| PC2RESETI | C200 reset interval correction | 13.6.5 |
| PSDARK | S Dark Current correction | 13.7.1 |
| PPDARK | P Dark Current correction | 13.7.2 |
| PC1DARK | C100 Dark Current correction | 13.7.3 |
| PC2DARK | C200 Dark Current correction | 13.7.4 |
| PP1VIGN | P1 vignetting correction | 13.8.1 |
| PP2VIGN | P2 vignetting correction | 13.8.2 |
| PP3VIGN | P3 vignetting correction | 13.8.3 |
| PC1VIGN | C100 vignetting correction | 13.8.4 |
| PC2VIGN | C200 vignetting correction | 13.8.5 |
| PPCHOPCOR | P chopper correction factors | 13.9.1 |
| PC1CHOPCOR | C100 chopper correction factors | 13.9.2 |
| PC2CHOPCOR | C200 chopper correction factors | 13.9.3 |
| PP1FCSPOW | P1 FCS power calibration table | 13.10.1 |
| PP2FCSPOW | P2 FCS power calibration table | 13.10.2 |
| PP3FCSPOW | P3 FCS power calibration table | 13.10.3 |
| PC1FCSPOW | C100 FCS power calibration table | 13.10.4 |
| PC2FCSPOW | C200 FCS power calibration table | 13.10.5 |
| PRESP | P default responsivities | 13.11.1 |
| PC1RESP | C100 default responsivities | 13.11.2 |
| PC2RESP | C200 default responsivities | 13.11.3 |
| PP1FCSAP | P1 FCS aperture correction | 13.13.1 |
| PP2FCSAP | P2 FCS aperture correction | 13.13.1 |
| PP3FCSAP | P3 FCS aperture correction | 13.13.1 |
| PC1ILLUM | C100 illumination correction | 13.12.1 |
| PC2ILLUM | C200 illumination correction | 13.12.2 |
| PC1FLAT | C100 filter-to-filter correction | 13.14.1 |
| PC2FLAT | C200 filter-to-filter correction | 13.14.2 |

### 11.1.5 Cal G Products: Derive_AAR

| Product | Description | Section |
|---|---|---|
| PPSF | point spread function | 13.15.1 |
| PSPECAL | S wavelength calib. and spectral response | 13.16.1 |
| PFLUXCONV | P/C power to flux density calib. | 13.17.1 |
| PPOMEGA | P apertures and $\Omega$'s | 13.18.1 |
| PC1OMEGA | C100 dimensions and $\Omega$'s | 13.18.2 |
| PC2OMEGA | C200 dimensions and $\Omega$'s | 13.18.3 |

### 11.1.6 Cal G Products: auxillary

| Product | Description | Section |
|---|---|---|
| PCCBB | colour correction: blackbody | 13.19.1 |
| PCCMBBONE | colour correction: $\nu^1 \cdot B_\nu(T)$ | 13.19.2 |
| PCCMBBTWO | colour correction: $\nu^2 \cdot B_\nu(T)$ | 13.19.3 |
| PCCPOWER | colour correction: $\nu^\alpha$ | 13.19.4 |

## 11.2 Product Types Sorted by AOT

Per AOT the observer receives a set of dataproducts. Depending on the details of the AOT, different data sets are distributed. In this section all possible combinations of sets of ISOPHOT data products have been listed. Each horizontal line in the following table represents a possible set.

| AOT | ERD | SPD | AAR | Comment |
|---|---|---|---|---|
| **P03** | PSTA,PPER | PP1S,PP1A | PPAP | P1, sp, ps |
| | PSTA,PPER | PP1S,PP1A | PPAE | P1, sp, es |
| | PSTA,PPER | PP1S,PP1A | PPAS,PGAI,PGAU,PGAT | P1, raster |
| | PSTA,PPER | PP2S,PP2A | PPAP | P2, sp, ps |
| | PSTA,PPER | PP2S,PP2A | PPAE | P2, sp, es |
| | PSTA,PPER | PP2S,PP2A | PPAS,PGAI,PGAU,PGAT | P2, raster |
| | PSTA,PPER | PP3S,PP3A | PPAP | P3, sp, ps |
| | PSTA,PPER | PP3S,PP3A | PPAE | P3, sp, es |
| | PSTA,PPER | PP3S,PP3A | PPAS,PGAI,PGAU,PGAT | P3, raster |
| **P04** | PSTA,PPER | PP1S,PP1A | PPAP | P1, sp, ps |
| | PSTA,PPER | PP1S, PP1A | PPAE | P1, sp, es |
| | PSTA,PPER | PP2S, PP2A | PPAP | P2, sp, ps |
| | PSTA,PPER | PP2S, PP2A | PPAE | P2, sp, es |
| | PSTA,PPER | PP3S, PP3A | PPAP | P3, sp, ps |
| | PSTA,PPER | PP3S, PP3A | PPAE | P3, sp, es |
| **P05** | PSTA,PPER | PP1S,PP1A,PP1D | PPAP | P1, sp, ps |
| | PSTA,PPER | PP1S,PP1A,PP1D | PPAE | P1, sp, es |
| | PSTA,PPER | PP2S,PP2A,PP2D | PPAP | P2, sp, ps |
| | PSTA,PPER | PP2S,PP2A,PP2D | PPAE | P2, sp, es |
| | PSTA,PPER | PP3S,PP3A,PP2D | PPAP | P3, sp, ps |
| | PSTA,PPER | PP3S,PP3A,PP2D | PPAE | P3, sp, es |
| **P17** | PSTA,PPER | PP1S,PP1A | PPAP | P1, sp, ps |
| | PSTA,PPER | PP1S,PP1A | PPAE | P1, sp, es |
| | PSTA,PPER | PP2S,PP2A | PPAP | P2, sp, ps |
| | PSTA,PPER | PP2S,PP2A | PPAE | P2, sp, es |
| | PSTA,PPER | PP3S,PP3A | PPAP | P3, sp, ps |
| | PSTA,PPER | PP3S,PP3A | PPAE | P3, sp, es |
| **P18** | PSTA,PPER | PP1S | PPAP | P1, sp, ps |
| | PSTA,PPER | PP1S | PPAE | P1, sp, es |
| | PSTA,PPER | PP2S | PPAP | P2, sp, ps |
| | PSTA,PPER | PP2S | PPAE | P2, sp, es |
| | PSTA,PPER | PP3S | PPAP | P3, sp, ps |
| | PSTA,PPER | PP3S | PPAE | P3, sp, es |
| **P19** | PSTA,PPER | PP1S,PP1A | PPAP | P1, sp, ps |
| | PSTA,PPER | PP1S,PP1A | PPAE | P1, sp, es |
| | PSTA,PPER | PP2S,PP2A | PPAP | P2, sp, ps |
| | PSTA,PPER | PP2S,PP2A | PPAE | P2, sp, es |
| | PSTA,PPER | PP3S,PP3A | PPAP | P3, sp, ps |
| | PSTA,PPER | PP3S,PP3A | PPAE | P3, sp, es |

| AOT | ERD | SPD | AAR | Comment |
|---|---|---|---|---|
| **P22** | PSTA,P1ER | PC1S,PC1A | PCAP | C100, sp, ps |
| | PSTA,P1ER | PC1S,PC1A | PCAE | C100, sp, es |
| | PSTA,P1ER | PC1S,PC1A | PCAS,PGAI,PGAU,PGAT | C100, raster |
| | PSTA,P2ER | PC2S,PC1A | PCAP | C200, sp, ps |
| | PSTA,P2ER | PC2S,PC1A | PCAE | C200, sp, es |
| | PSTA,P2ER | PC2S,PC1A | PCAS,PGAI,PGAU,PGAT | C200, raster |
| **P25** | PSTA,P1ER | PC1S,PC1A,PC1D | PCAP | C100, sp, ps |
| | PSTA,P1ER | PC1S,PC1A,PC1D | PCAE | C100, sp, es |
| | PSTA,P2ER | PC2S,PC2A,PC2D | PCAP | C200, sp, ps |
| | PSTA,P2ER | PC2S,PC2A,PC2D | PCAE | C200, sp, es |
| **P32** | PSTA,P1ER | PC1S,PC1A | PCAS,PGAI,PGAU,PGAT | C100 |
| | PSTA,P2ER | PC2S,PC1A | PCAS,PGAI,PGAU,PGAT | C200 |
| **P37** | PSTA,P1ER | PC1S,PC1A | PCAP | C100, sp, ps |
| | PSTA,P1ER | PC1S,PC1A | PCAE | C100, sp, es |
| | PSTA,P2ER | PC2S,PC1A | PCAP | C200, sp, ps |
| | PSTA,P2ER | PC2S,PC1A | PCAE | C200, sp, es |
| **P38** | PSTA,P1ER | PC1S | PCAP | C100, sp, ps |
| | PSTA,P1ER | PC1S | PCAE | C100, sp, es |
| | PSTA,P2ER | PC2S | PCAP | C200, sp, ps |
| | PSTA,P2ER | PC2S | PCAE | C200, sp, es |
| **P39** | PSTA,P1ER | PC1S,PC1A | PCAP | C100, sp, ps |
| | PSTA,P1ER | PC1S,PC1A | PCAE | C100, sp, es |
| | PSTA,P2ER | PC2S,PC1A | PCAP | C200, sp, ps |
| | PSTA,P2ER | PC2S,PC1A | PCAE | C200, sp, es |
| **P40** | PSTA,PSER | PSSS,PSLS | PSAP,PLAP | sp |
| | PSTA,PSER | PSSS,PSLS | PSAE,PLAE | es |
| | PSTA,PSER | PSSS,PSLS | PSAS,PLAS | raster |
| **P50** | PSTA,PPER | none | none | P2 pola |
| **P51** | PSTA,P2ER | none | none | C200 pola |

**Notes**

| | |
|---|---|
| sp: | single pointing |
| ps: | point source |
| es: | extended source |
| staring: | staring mode |
| pola: | polarisation |
| raster: | raster mode |

# Chapter 12

# Product Descriptions

## 12.1 Overview

This chapter contains detailed descriptions of all ISOPHOT OLP products except for the Cal G files (see chapter 13). The contents and structure of the FITS headers and records are presented. References to additional information given in this manual are provided. It must be noted that
*in case of any discrepancies with the IDPD [25], the IDPD takes precedence.*

The PHT instrument incorporates several subsystems including single detector photometers, detector arrays and a low-resolution grating spectrometer. Those can be operated with several filters, polarizers and apertures in single pointing and raster pointing mode, the latter one with different sampling steps by the chopper. This means that a wide variety of products are produced for the various detectors and operating modes.

All products have header information which can be divided into the following categories.

- General FITS information which is part of the FITS standard. For more about the FITS standard see the ISO Satellite and Data Manual [17].
- ISO (spacecraft) related information. This includes descriptions of ISO related fields - see also the ISO Satellite and Data Manual for complete lists.
- General ISOPHOT header information which is used for several PHT products.
- Product specific header fields.

Table 12.1 gives a summary of ISO common fields in headers. More information is available in the ISO Satellite Data Manual [17].

For the binary FITS records, the following abbreviations are used in the tables given in this chapter:

**Off** offset in bytes of field in record
**N** number of values
**T** type of field (I=integer, R=real, C=character, L=logical)

## 12.2 ERD product types

### 12.2.1 Rationale behind product design

As the ERD is reformatted telemetry data, the different ERD products reflect the data structures related to the different PHT sub-systems: single pixel data (P1, P2, and P3), 9 pixel data (PHT-C100), 4 pixel data (PHT-C200) and 128 pixel data (PHT-S). Each ERD product is accompanied by one compact status product with product name prefix "PSTA". A compact status record defines the instrument configuration for one measurement. The structure of the compact status product is the same for all PHT subinstruments.

Table 12.1: List of ISO common fields in the product header

| Field | Description |
|---|---|
| OLPVERS | Version of OLP used to generate this file |
| CALGVERS | Version of the calibration files used to generate this file |
| EOHA... | Executed Observation History per AOT |
| ATT... | Attitude information |
| TREF... | Information on Spacecraft motion |
| GPSC... | General prefix for main science ERD/SPD |
| GEPR... | General prefix for ERD files |
| ISR... | Information on events logged during the execution of the observation from the 'instrument station report' which was generated on-line by the real-time and quick-look analysis (RTA/QLA) software. |
| VERS.. | Versions of files from previous steps used in OLP |

### 12.2.2 Product PPER

PHT-P Edited Raw Data
Record length: 28 bytes

| FIELD | Off | N | T | Description | Comment |
|---|---|---|---|---|---|
| GPSCTKEY | 0 | 1 | I*4 | Instrument time key | see IDPD, unit= $2^{-14}$ s |
| GPSCRPID | 4 | 2 | I*1 | Raster point ID | points and lines |
| GPSCFILL | 6 | 1 | I*2 | Filler | empty |
| PPERPIXF | 8 | 1 | I*2 | Bit flags accompanying pixels | appendix B.4 |
| PPERPCS1 | 10 | 1 | I*2 | Power of calibration source 1 | appendix B.2 |
| PPERPCS2 | 12 | 1 | I*2 | Power of calibration source 2 | appendix B.2 |
| PPERFIL1 | 14 | 1 | I*2 | Spare | |
| PPERTEMP | 16 | 1 | I*2 | Measured temperature P1, P2, or P3 | appendix B.1 |
| PPERFIL2 | 18 | 2 | I*2 | Spare | |
| PPERCPOS | 22 | 1 | I*2 | Measured chopper position | appendix B.3 |
| PPERMBV | 24 | 1 | I*2 | Measured bias voltage P1, P2, or P3 | |
| PPERPIX | 26 | 1 | I*2 | IR data (1 pixel) | 12 bits used<br>see appendix B.2 |

### 12.2.3 Product P1ER

PHT C100 Edited Raw Data
Record length: 48 bytes

| FIELD | Off | N | T | Description | Comment |
|---|---|---|---|---|---|
| GPSCTKEY | 0 | 1 | I*4 | Instrument time key | see IDPD, unit= $2^{-14}$ s |
| GPSCRPID | 4 | 2 | I*1 | Raster point ID | points and lines |
| GPSCFILL | 6 | 1 | I*2 | Filler | |
| P1ERPIXF | 8 | 1 | I*2 | Bit flags accompanying pixels | appendix B.4 |
| P1ERPCS1 | 10 | 1 | I*2 | Power of calibration source 1 | appendix B.2 |
| P1ERPCS2 | 12 | 1 | I*2 | Power of calibration source 2 | appendix B.2 |
| P1ERCREV | 14 | 1 | I*2 | Measured CRE checkout voltage | see note below |
| P1ERTEMP | 16 | 1 | I*2 | Measured temperature C100 | appendix B.1 |
| P1ERFILL | 18 | 2 | I*2 | Spare | |
| P1ERCPOS | 22 | 1 | I*2 | Measured chopper position | appendix B.3 |
| P1ERMBV | 24 | 1 | I*2 | Measured bias voltage C100 | |
| P1ERPIXR | 26 | 1 | I*2 | IR data (resistor) | see note below |

| | | | | | |
|---|---|---|---|---|---|
| P1ERPIXO | 28 | 1 | I*2 | IR data (open) | |
| P1ERPIX | 30 | 9 | I*2 | IR data: 9 pixels | for ordering see 3.4.2<br>12 bits used<br>see appendix B.2 |

**Note :** The CRE checkout voltage is of no importance for the analysis of the IR data. It was a diagnosis DC voltage which was applied to the CRE resistor pixel for PHT-C and PHT-S and produced a kind of load curve at the output of the resistor pixel. This worked like a connection to a normal CRE channel of a detector pixel, however the resistance of this special channel was much smaller than the one of a high-ohmic detector pixel.

### 12.2.4 Product P2ER

PHT C200 Edited Raw Data
Record length: 44 bytes

| FIELD | Off | N | T | Description | Comment |
|---|---|---|---|---|---|
| GPSCTKEY | 0 | 1 | I*4 | Instrument time key | see IDPD, unit= $2^{-14}$ s |
| GPSCRPID | 4 | 2 | I*1 | Raster point ID | points and lines |
| GPSCFILL | 6 | 1 | I*2 | Filler | |
| P2ERPIXF | 8 | 1 | I*2 | Bit flags accompanying pixels | appendix B.4 |
| P2ERPCS1 | 10 | 1 | I*2 | Power of FCS 1 | appendix B.2 |
| P2ERPCS2 | 12 | 1 | I*2 | Power of FCS 2 | appendix B.2 |
| P2ERCREV | 14 | 1 | I*2 | Measured CRE checkout voltage | cf. note 12.2.3 |
| P2ERTEMP | 16 | 1 | I*2 | Measured temperature C200 | appendix B.1 |
| P2ERFILL | 18 | 2 | I*2 | Spare | |
| P2ERCPOS | 22 | 1 | I*2 | Measured chopper position | appendix B.3 |
| P2ERMBV1 | 24 | 1 | I*2 | Measured bias voltage pixel 1 | see section 3.4.2– |
| P2ERMBV2 | 26 | 1 | I*2 | Measured bias voltage pixel 2 | –for pixel position on– |
| P2ERMBV3 | 28 | 1 | I*2 | Measured bias voltage pixel 3 | –sky |
| P2ERMBV4 | 30 | 1 | I*2 | Measured bias voltage pixel 4 | |
| P2ERPIX1 | 32 | 1 | I*2 | IR data (pixel 1) | see section 3.4.2 – |
| P2ERPIX2 | 34 | 1 | I*2 | IR data (pixel 2) | –for pixel position on– |
| P2ERPIX3 | 36 | 1 | I*2 | IR data (not used) | –sky |
| P2ERPIX4 | 38 | 1 | I*2 | IR data (pixel 3) | – see – |
| P2ERPIX5 | 40 | 1 | I*2 | IR data (pixel 4) | – appendix B.2– |
| P2ERPIX6 | 42 | 1 | I*2 | IR data (resistor) | – for bit usage – |

### 12.2.5 Product P2ES

PHT C200 Edited Raw Data for PHT serendipity mode
Record length: 44 bytes
Identical record structure as for product P2ER (section 12.2.4), the prefix P2ER should be replaced by P2ES.

### 12.2.6 Product PSER

PHT-S Edited Raw Data
Record length: 292 bytes

| FIELD | Off | N | T | Description | Comment |
|---|---|---|---|---|---|
| GPSCTKEY | 0 | 1 | I*4 | Instrument time key | see IDPD, unit= $2^{-14}$ s |
| GPSCRPID | 4 | 2 | I*1 | Raster point ID | points and lines |
| GPSCFILL | 6 | 1 | I*2 | Filler | |

| | | | | | |
|---|---|---|---|---|---|
| PSERPIXF | 8 | 1 | I*2 | Bit flags accompanying pixels | appendix B.4 |
| PSERPCS1 | 10 | 1 | I*2 | Power of calibration source 1 –always off in AOT | no meaning, FCS – |
| PSERPCS2 | 12 | 1 | I*2 | Power of calibration source 2 –always off in AOT | no meaning, FCS – |
| PSERCREV | 14 | 1 | I*2 | Measured CRE checkout voltage | cf. note 12.2.3 |
| PSERTEM1 | 16 | 1 | I*2 | Measured temperature S1(SL) | appendix B.1 |
| PSERTEM2 | 18 | 1 | I*2 | Measured temperature S2(SS) | appendix B.1 |
| PSERFILL | 20 | 1 | I*2 | Spare | |
| PSERCPOS | 22 | 1 | I*2 | Measured chopper position | appendix B.3 |
| PSERMBV1 | 24 | 1 | I*2 | Measured bias voltage S1(=SL) | |
| PSERMBV2 | 26 | 1 | I*2 | Measured bias voltage S2(=SS) | |
| PSERPIX1 | 28 | 66 | I*2 | IR data for SL branch | includes 2 resistor pixels values 65 and 66 12 bits used – – appendix B.2 |
| PSERPIX2 | 160 | 66 | I*2 | IR data for SS branch | includes 2 resistor pixels values 65 and 66 12 bits used – – appendix B.2 |

### 12.2.7 Product PSTA

PHT-ERD Compact Status
Record length 128 bytes

| FIELD | Off | N | T | Description | Comment |
|---|---|---|---|---|---|
| CSGPUKST | 0 | 1 | I*4 | UTK start time | Universal Time Keys– |
| CSGPUKEN | 4 | 1 | I*4 | UTK end time | – see ISDM [17] |
| CSGPIKST | 8 | 1 | I*4 | ITK start time | |
| CSGPIKEN | 12 | 1 | I*4 | ITK end time | |
| CSGPUTST | 16 | 2 | I*4 | UTC start time | Universal Time– |
| CSGPUTEN | 24 | 2 | I*4 | UTC end time | – Coordinated |
| CSGPOSN | 32 | 1 | I*1 | Observation Sequence Number | also ION, as in PGA |
| CSGPFILL | 33 | 15 | I*1 | Spare | |
| PSTASPAR | 48 | 1 | I*4 | Spare | |
| PSTASUBS | 52 | 1 | I*2 | Subsystem | |
| PSTAOPFO | 54 | 1 | I*2 | Chopper OPF Override | |
| PSTAF1TS | 56 | 1 | I*2 | TRS(FCS1) | value: 1 or 2 see 3.5 |
| PSTAF2TS | 58 | 1 | I*2 | TRS(FCS2) | value: 1 or 2 |
| PSTAF1PS | 60 | 1 | I*2 | FCS1 power sel. | in mW |
| PSTAF2PS | 62 | 1 | I*2 | FCS2 power sel. | in mW |
| PSTAC1PS | 64 | 1 | I*2 | CHW1 position (selected) | value: 1 - 14, see A.1 |
| PSTAC2PS | 66 | 1 | I*2 | CHW2 position (selected) | idem |
| PSTAC3PS | 68 | 1 | I*2 | CHW3 position (selected) | idem |
| PSTACMOD | 70 | 1 | I*2 | Chopper mode | see Table 12.2 |
| PSTACAMP | 72 | 1 | I*2 | Chopper amplitude | as commanded in arcsec |
| PSTACSTE | 74 | 1 | I*2 | Chopper step | as commanded in arcsec |
| PSTACINC | 76 | 1 | I*2 | Chopper increment | as commanded in arcsec |
| PSTACRES | 78 | 1 | I*2 | CRE switch | |
| PSTADETA | 80 | 1 | I*2 | Detector assy | detector assembly |
| PSTADRS | 82 | 1 | I*2 | Data reduction size | integer, see 3.2.4 |
| PSTAMUX1 | 84 | 1 | I*2 | MUX1 line | multiplexer line |
| PSTAMUX2 | 86 | 1 | I*2 | MUX2 line | multiplexer line |
| PSTAXSTA | 88 | 1 | I*2 | Cross status | of multiplexer line |
| PSTAD1OF | 90 | 1 | I*2 | DIE1 offset | see 7.2.5 |

| | | | | | |
|---|---|---|---|---|---|
| PSTAD1GA | 92 | 1 | I*2 | DIE1 gain | idem |
| PSTAD2OF | 94 | 1 | I*2 | DIE2 offset | idem |
| PSTAD2GA | 96 | 1 | I*2 | DIE2 gain | idem |
| PSTAFREQ | 98 | 1 | I*2 | clock speed of CRE | value 1, 4, or 8 (kHz) |
| PSTANNDR | 100 | 1 | I*2 | No. NDRs per ramp | $2^n - 1$ † |
| PSTANDR | 102 | 1 | I*2 | No. DRs per chopper plateau | $2^n$ † |
| PSTAINTT | 104 | 1 | I*2 | Integration time | $2^{7-n}$ sec † |
| PSTAMEAT | 106 | 1 | I*2 | Measurement time | $2^n$ sec † |
| PSTAMPC1 | 108 | 1 | I*2 | Measurement position CHW1 | value: 1 - 14, see A.1 |
| PSTAMPC2 | 110 | 1 | I*2 | Measurement position CHW2 | idem |
| PSTAMPC3 | 112 | 1 | I*2 | Measurement position CHW3 | idem |
| PSTAMET | 114 | 1 | I*2 | Measured EEU temperature | see appendix B.1 |
| PSTASER | 116 | 1 | I*2 | PHT serendipity mode flag | 1= serendipity<br>0= normal prime instrument |
| PSTAFILL | 118 | 10 | I*1 | Filler | |

Table 12.2: Coding of chopper mode

| **Mode** | **Description** |
|---|---|
| 0,1 | sawtooth chopping |
| 2, 3 | triangular chopping |
| 4, 5, 6, 7 | rectangular chop |
| 8 | chop between FCS1 and FCS2 |
| 13 | staring CFOV |
| 14 | staring FCS1 |
| 9, 10, 11, 12, 15 | not used in AOTs |

† The value given in the product is $n$. The formula in the last column above gives the actual value.

## 12.3 SPD product types

### 12.3.1 Rationale behind product design

PHT generates per detector an SPD record for each signal per chopper plateau or for each raster point. There are 7 separate SPD products:

1. - C100 SPD data
2. - C200 SPD data
3. - P1 SPD data
4. - P2 SPD data
5. - P3 SPD data
6. - PHT-SS SPD data
7. - PHT-SL SPD data

In order to retain the information on the actual observing conditions, each SPD record contains additional information to identify the operating conditions under which the data were collected. Within an SPD file, the type of record is determined by:

- spacecraft viewing direction (e.g. in case of raster maps)
- chopper viewing direction (CFOV, offset position, or FCS)
- aperture
- filter

Within one AOT, data of different types can be archived inside the same SPD file. Examples:

- For chopped measurements, each on-source and background plateau is stored as a separate record in the same SPD file
- Data from each raster position within a raster map are stored in separate records in chronological order in the same SPD file.
- Multi-filter AOT's produce one SPD file per detector. Data from different filters for a given detector are stored as a series of records ordered chronologically inside the same SPD file.
- In case of multi-aperture photometry with PHT04, one SPD file is created. The aperture measurements are stored as series of records ordered chronologically inside the same SPD file.
- In case of oversampled maps with PHT32, each map position can yield several records corresponding to the number of chopper plateaux collected on that position.

#### 12.3.1.1 General SPD header items I

The following header keywords are included in all PHT SPD products.

| FIELD | T | Description | Comment |
|---|---|---|---|
| DETECTOR | C | Detector subsystem | |
| NMEAS | I | Number of measurements | |
| CALSEQU | I | Calibration sequence | |
| PTOREXT | C | Point(P) or Extended(E) | |
| FPCMODE | C | Focal plane chopper mode | see Table 12.2 |
| FPCAMP | I | Chopper amplitude(arcsec) | |

| | | | |
|---|---|---|---|
| FPCNSTEP | I | Number of chopper steps | only if chop mode |
| FPCINCR | I | Increment between steps (arcsec) | only if chop mode |
| DARKPn | R | dark current | for pixel n, both keywords – |
| DARKUPn | R | dark current uncertainty | –repeated for each pixel |

Notes:

- the dark currents (DARK..) are given in signal units of V/s.
- FPC modes: 'ST' = staring, 'RE' = rectangular, 'SW' = sawtooth, 'TR' = triangular,'CB' = chop between FCS1 and FCS2.

#### 12.3.1.2 Filter dependent SPD header items

The following header keywords are repeatedly given for each filter $m$:

| **FIELD** | **T** | **Description** | **Comment** |
|---|---|---|---|
| FILTERm | C | Filter | filter name |
| EXFLUXm | R | Expected source flux (Jy or MJy/sr) | Jy if PTOREXT=P |
| UNCFLXm | R | Uncertainty (Jy or MJy/sr) | Jy if PTOREXT=P |
| MXBACKm | R | Maximum background ($^{10}$log MJy/sr) | |
| CALP1Fm | C | Cal used in SPD calculations | see notes below |
| CALDATE | C | Date default calibration file | in 'dd/mm/yy' |
| CHC1Pm | R | Chopper correction | only if chopped mode |
| CHU1Pm | R | Chopper correction uncertainty | only if chopped mode |
| A0RIm | R | Reset interval corr. offset, A0 (V/s) | |
| A0RIUm | R | Uncertainty in A0 (V/s) | |
| A1RIm | R | Reset interval corr. slope, A1 | |
| A1RIUm | R | Uncertainty in A1 | |
| CALPnFm | C | Calibration used in SPD | present if $npix > 1$ |
| CALDATE | C | Date default calibration file | in dd/mm/yy |
| CHCnPm | R | Chopper corrections | only if chopped mode |
| CHUnPm | R | Chopper correction uncertainty | only if chopped mode |
| TRS1Sm | I | Selected TRS for FCS1 | |
| POW1Sm | R | Selected power for FCS1 | |
| POW1Mm | R | Measured power for FCS1 | |
| CALPOW1 | R | In-band power on detector for cal (Watts) | |
| RESPDEF | L | TRUE if default responsivity is used. | |
| CALPOLm | I | CHWI position | see section A.1 |
| CALTYPm | I | Type of processing for cal measurement | number of cal. measurements |
| RS1PnFm | R | Responsivity (A/W) for first cal. | for pixel n |
| RU1PnFm | R | Uncertainty (A/W) | for pixel n |
| RS2PnFm | R | Responsivity (A/W) for second cal. | for pixel n |
| RU2PnFm | R | Uncertainty | for pixel n |

Notes:

- CALP1F can have the following values: *single, first, second, both,* and *default*, depending on the calibration method in the AOT and the quality of the FCS measurements.
- EXFLUX, UNCFLX, and MXBACK were the initial estimates from the observer entered in PGA.
- for AOT PHT32 there is no one-to-one match between the keyword description and the AOT parameter as given by the observer in the ISO proposal generation aids (PGA): EXFLUX= maximum unsaturated surface brightness, UNCFLX= minimum surface brightness flux.

#### 12.3.1.3 General PHT related SPD header items II

The following header keywords are appended after all filters have been listed:

| FIELD | T | Description | Comment |
|---|---|---|---|
| SATLIMn | R | Saturation limit | in Volts for pixel n |
| FITDRn | L | Drift fit flag | always T (no fitting implemented) |
| MINDEG | I | Min points for deglitcher | see section 7.3.4– |
| MAXERR | R | Max error if points < MINDEG | –for signal deglitching |
| NITERATE | I | No. of iterations of deglitcher | |
| NLOCAL | I | No. of local points used by deglitcher | |
| NSTEP | I | Deglitcher step size | |
| NSIGMA | R | Deglitcher: rms from local median | |
| NBAD | I | Deglitcher: badness count limit | |
| CALFCS | I | FCS used for cal calculations | FCS 1 or 2 |
| RDITER | I | Ramp deglitch: no. iterations | see section 7.2.8– |
| RDFSIG | R | Ramp deglitch: sigma for detection | –for ramp deglitching |
| RDMINP | I | Ramp deglitch: min. readouts in ramp | |
| DRALPHA | R | Drift removal: significance level | see section 7.3.5 – |
| DRMINPTS | I | Drift removal: min. points | –for drift recognition |
| READAUTO | I | Readouts with automatic data reduction | |
| READSUSP | I | Readouts flagged as suspicious | |
| READOFFT | I | Readouts off-target | |
| READCOP | I | Readouts with chopper off position | |
| RAMPSAT | I | Ramps saturated | |
| RAMPDEGL | I | Ramps deglitched | |
| RAMPPCT | I | % ramps accepted | |
| RAMPUSET | I | % time for accepted ramps | |
| RAMPINVD | I | Bad cycles | |
| RAMPFROP | I | First ramps ignored | |
| RAMPZSG | I | Zero signals on plateau | plateaux with no accepted signals |
| PLATNORP | I | Plateaux with no good ramps | |
| PLATDROP | I | Plateaux dropouts due to gaps | |
| USEDRS | L | Use destructive readouts? | always 'F' for OLP7 |
| DISCNDRS | I | Discard 1st NDRs of ramps | number of read-outs removed<br>see section 7.2.2 |

#### 12.3.1.4 Product specific SPD header items: PHT05 and PHT25

The following keywords are only present in SPD products from absolute photometry observations PHT05 and PHT25.

| FIELD | T | Description | Comment |
|---|---|---|---|
| MEASPW1 | R | FCS1 heating power (mW) | |
| POWFCS1 | R | Power from FCS1 (W) | |
| RESPRn | R | ratio Actual/Default responsivity | for pixel n |
| CALPn | R | FCS measurement signal in V/s | for pixel n |
| CALUPn | R | uncertainty in V/s | for pixel n |
| CALQPn | R | FCS quality | for pixel n |
| COLDPn | R | Cold FCS measurement signal in V/s | for pixel n |
| COLDUPn | R | Uncertainty in V/s | for pixel n |

### 12.3.2 Product PPxS

PHT-P1/2/3 Standard Processed Data where x = 1,2, or 3

**HEADER**
Product specific header entries:

CALAPER I Aperture used for FCS calibration (CHW position)

**RECORD**
record length: 68 bytes

| FIELD | N | T | Description | Comment |
|---|---|---|---|---|
| GPSCTKEY | 1 | I*4 | Instrument time key | |
| GPSCRPID | 2 | I*1 | Raster point ID | points and lines |
| GPSCFILL | 1 | I*2 | Filler | |
| PPxSKYID | 1 | I*2 | Keyword identifier | |
| PPxSMNUM | 1 | I*2 | Measurement number | |
| PPxSSPAR | 1 | I*2 | Spare | |
| PPxSFILT | 1 | I*2 | CHW3 position | value: 1 - 14, see A.1 |
| PPxSAPER | 1 | I*2 | CHW2 position | idem |
| PPxSPOLZ | 1 | I*2 | CHW1 position | idem |
| PPxSNDRS | 1 | I*2 | Number of destructive readouts | per chopper plateau |
| PPxSCSTP | 1 | I*2 | Chopper step number | see 7.3.3 |
| PPxSDWEL | 1 | I*4 | Chopper dwell time in $2^{-7}$ s | commanded time |
| PPxSMEAS | 1 | I*4 | Measurement time (secs) | |
| PPxSCPOS | 1 | I*4 | Chopper position (arcsec) | |
| PPxSMNPW | 1 | R*4 | Mean or fitted power | in W |
| PPxSMNPU | 1 | R*4 | Uncertainty | in W |
| PPxSMDPW | 1 | R*4 | Median power | in W |
| PPxSQ1PW | 1 | R*4 | 1st quartile of power | in W |
| PPxSQ3PW | 1 | R*4 | 3rd quartile of power | in W |
| PPxSPLEN | 1 | I*4 | Chopper plateau length in $2^{-7}$ s | effective time– –after discarding signals |
| PPxSNSIG | 1 | I*4 | No. of valid signals on the plateau | |
| PPxSFLAG | 1 | I*1 | Status flag | see section 12.3.12 |
| PPxSFILL | 3 | I*1 | Filler | |

### 12.3.3 Product PC1S

PHT-C100 Standard Processed Data

**HEADER**
Product specific header entries:

STATPIX I Pixel used in statistics

**RECORD**
Record length: 300 bytes

| FIELD | N | T | Description | Comment |
|---|---|---|---|---|
| GPSCTKEY | 1 | I*4 | Instrument time key | |
| GPSCRPID | 2 | I*1 | Raster point ID | points and lines |
| GPSCFILL | 1 | I*2 | Filler | |
| PC1SKYID | 1 | I*2 | Keyword identifier | |
| PC1SMNUM | 1 | I*2 | Measurement number | |
| PC1SSPAR | 1 | I*2 | Spare | |
| PC1SFILT | 1 | I*2 | CHW3 position | value: 1 - 14, see A.1 |

| | | | | |
|---|---|---|---|---|
| PC1SAPER | 1 | I*2 | CHW2 position | idem |
| PC1SPOLZ | 1 | I*2 | CHW1 position | idem |
| PC1SNDRS | 1 | I*2 | Number of destructive readouts | |
| PC1SCSTP | 1 | I*2 | Chopper step number | see 7.3.3 |
| PC1SDWEL | 1 | I*4 | Chopper dwell time in $2^{-7}$ s | commanded time |
| PC1SMEAS | 1 | I*4 | Measurement time (secs) | |
| PC1SCPOS | 1 | I*4 | Chopper position (arcsec) | |
| PC1SMNPW | 9 | R*4 | Mean or fitted power | in W |
| PC1SMNPU | 9 | R*4 | Uncertainty | in W |
| PC1SMDPW | 9 | R*4 | Median power | in W |
| PC1SQ1PW | 9 | R*4 | 1st quartile of power | in W |
| PC1SQ3PW | 9 | R*4 | 3rd quartile of power | in W |
| PC1SPLEN | 9 | I*4 | Chopper plateau length in $2^{-7}$ s | effective time– –after discarding signals |
| PC1SNSIG | 9 | I*4 | No. of valid signals on the plateau | |
| PC1SFLAG | 9 | I*1 | Status flag | see section 12.3.12 |
| PC1SFILL | 3 | I*1 | Filler | |

### 12.3.4 Product PC2S

PHT-C200 Standard Processed Data

**HEADER**
Product specific header entries:

STATPIX I Pixel used in statistics

**RECORD**
Record length: 152 bytes

| **FIELD** | **N** | **T** | **Description** | **Comment** |
|---|---|---|---|---|
| GPSCTKEY | 1 | I*4 | Instrument time key | |
| GPSCRPID | 2 | I*1 | Raster point ID | points and lines |
| GPSCFILL | 1 | I*2 | Filler | |
| PC2SKYID | 1 | I*2 | Keyword identifier | |
| PC2SMNUM | 1 | I*2 | Measurement number | |
| PC2SSPAR | 1 | I*2 | Spare | |
| PC2SFILT | 1 | I*2 | CHW3 position | value: 1 - 14, see A.1 |
| PC2SAPER | 1 | I*2 | CHW2 position | idem |
| PC2SPOLZ | 1 | I*2 | CHW1 position | idem |
| PC2SNDRS | 1 | I*2 | Number of destructive readouts | |
| PC2SCSTP | 1 | I*2 | Chopper step number | |
| PC2SDWEL | 1 | I*4 | Chopper dwell time in $2^{-7}$ s | |
| PC2SMEAS | 1 | I*4 | Measurement time (secs) | |
| PC2SCPOS | 1 | I*4 | Chopper position (arcsec) | |
| PC2SMNPW | 4 | R*4 | Mean or fitted power | in W |
| PC2SMNPU | 4 | R*4 | Uncertainty | in W |
| PC2SMDPW | 4 | R*4 | Median power | in W |
| PC2SQ1PW | 4 | R*4 | 1st quartile of power | in W |
| PC2SQ3PW | 4 | R*4 | 3rd quartile of power | in W |
| PC2SPLEN | 4 | I*4 | Chopper plateau length in $2^{-7}$ s | effective time– –after discarding signals |
| PC2SNSIG | 4 | I*4 | No. of valid signals on the plateau | |
| PC2SFLAG | 4 | I*1 | Status flags | see section 12.3.12 |

### 12.3.5 Product PSSS

PHT-SS Standard Processed Data

**HEADER**
Product specific header entries:

| FIELD | T | Description | Comment |
|---|---|---|---|
| CALDATE | C | Date cal defaults generated | |
| PTOREXT | C | Point(P) or Extended(E) | |
| LAMBDAd | C | Central wavelength of pixel (m) | |
| LUNCd | C | Uncertainty (m) | |
| RESPPd | C | Point source srf (V/s)/Jy | if point source |
| RPUNCd | C | Uncertainty (V/s)/Jy) | if point source |
| RESPEd | C | Extended source srf (V/s)/(MJy/sr) | if extended source |
| REUNCd | C | Uncertainty (V/s)/(MJy/sr) | if extended source |

note:
d = 1,...,64
srf = spectral response function

**RECORD**
Record length: 1892

| FIELD | N | T | Description | Comment |
|---|---|---|---|---|
| GPSCTKEY | 1 | I*4 | Instrument time key | |
| GPSCRPID | 2 | I*1 | Raster point ID | points and lines |
| GPSCFILL | 1 | I*2 | Filler | |
| PSSSKYID | 1 | I*2 | Keyword identifier | |
| PSSSMNUM | 1 | I*2 | Measurement number | |
| PSSSSPAR | 3 | I*2 | Spare | |
| PSSSPOLZ | 1 | I*2 | CHW1 position | value: 1 - 14, see A.1 |
| PSSSNDRS | 1 | I*2 | Number of destructive readouts | |
| PSSSCSTP | 1 | I*2 | Chopper step number | |
| PSSSDWEL | 1 | I*4 | Chopper dwell time in $2^{-7}$ s | commanded |
| PSSSMEAS | 1 | I*4 | Measurement time (secs) | |
| PSSSCPOS | 1 | I*4 | Chopper position (arcsec) | |
| PSSSMNPW | 64 | R*4 | Mean or fitted signal | in V/s |
| PSSSMNPU | 64 | R*4 | Uncertainty | in V/s |
| PSSSMDPW | 64 | R*4 | Median signal | in V/s |
| PSSSQ1PW | 64 | R*4 | 1st quartile of signal | in V/s |
| PSSSQ3PW | 64 | R*4 | 3rd quartile of signal | in V/s |
| PSSSPLEN | 64 | I*4 | Chopper plateau length in $2^{-7}$ s | effective time–<br>–after discarding signals |
| PSSSNSIG | 64 | I*4 | No. of valid signals on the plateau | |
| PSSSFLAG | 64 | I*1 | Status flags | see section 12.3.12 |

### 12.3.6 Product PSLS

PHT-SL Standard Processed Data

**HEADER**
Product specific header entries are the same as for product PSSS

**RECORD**
Record length: 1892

| FIELD | N | T | Description | Comment |
|---|---|---|---|---|
| GPSCTKEY | 1 | I*4 | Instrument time key | |
| GPSCRPID | 2 | I*1 | Raster point ID | points and lines |
| GPSCFILL | 1 | I*2 | Filler | |
| PSLSKYID | 1 | I*2 | Keyword identifier | |
| PSLSMNUM | 1 | I*2 | Measurement number | |
| PSLSSPAR | 3 | I*2 | Spare | |
| PSLSPOLZ | 1 | I*2 | CHWI position | |
| PSLSNDRS | 1 | I*2 | Number of destructive readouts | |
| PSLSCSTP | 1 | I*2 | Chopper step number | |
| PSLSDWEL | 1 | I*4 | Chopper dwell time in $2^{-7}$ s | commanded |
| PSLSMEAS | 1 | I*4 | Measurement time (secs) | |
| PSLSCPOS | 1 | I*4 | Chopper position (arcsec) | |
| PSLSMNPW | 64 | R*4 | Mean or fitted signal | in V/s |
| PSLSMNPU | 64 | R*4 | Uncertainty in mean signal | in V/s |
| PSLSMDPW | 64 | R*4 | Median signal | in V/s |
| PSLSQ1PW | 64 | R*4 | 1st quartile of signal | in V/s |
| PSLSQ3PW | 64 | R*4 | 3rd quartile of signal | in V/s |
| PSLSPLEN | 64 | I*4 | Chopper plateau length in $2^{-7}$ s | effective time– –after discarding signals |
| PSLSNSIG | 64 | I*4 | No. of valid signals on the plateau | |
| PSLSFLAG | 64 | I*1 | Status flags | see section 12.3.12 |

### 12.3.7 Product PPxA

PPxA (where x=1,2,3) contains the SPD of the FCS measurements obtained with detector P1, P2 or P3. PPxA products are also referred to as Cal A files (see section 5.7.2). The product of a chopped measurement contains 1 record per chopper plateau. In case a cold FCS measurement is selected in the absolute photometry AOT PHT05, the first record contains the cold FCS measurement and the second record contains the results of the heated FCS measurement.

**RECORD**
Record length: 84

| FIELD | N | T | Description | Comment |
|---|---|---|---|---|
| GPSCTKEY | 1 | I*4 | Instrument time key | |
| GPSCRPID | 2 | I*1 | Raster point ID | points and lines |
| GPSCFILL | 1 | I*2 | Filler | |
| PPxAQFLG | 1 | I*2 | Quality flag | |
| PPxAKYID | 1 | I*2 | Keyword identifier | |
| PPxAMNUM | 1 | I*2 | Measurement number | |
| PPxASPAR | 1 | I*2 | Spare | |
| PPxAFILT | 1 | I*2 | CHW3 position | value: 1 - 14, see A.1 |
| PPxAAPER | 1 | I*2 | CHW2 position | idem |
| PPxAPOLZ | 1 | I*2 | CHW1 position | idem |
| PPxASTAT | 1 | I*2 | FPC state (0 = CFOV, 1 = FCS1, 2 = FCS2) | |
| PPxADWEL | 1 | I*4 | Commmanded chopper dwell time in $2^{-7}$ s | |
| PPxACPOS | 1 | R*4 | Chopper position (arcsec) | |
| PPxAFCS1 | 1 | R*4 | Measured FCS1 power (mW) | |
| PPxAFCS2 | 1 | R*4 | Measured FCS2 power (mW) | |
| PPxATEMP | 1 | R*4 | Detector temperature (K) | |
| PPxAFILR | 1 | R*4 | Filler | |
| PPxABIAS | 1 | R*4 | Measured bias voltage (V) | |
| PPxAMNSG | 1 | R*4 | Mean or fitted signal (V/s) | |
| PPxAMNSU | 1 | R*4 | Uncertainty(V/s) | |
| PPxAMDSG | 1 | R*4 | Median signal (V/s) | |

| | | | | |
|---|---|---|---|---|
| PPxAQ1SG | 1 | R*4 | 1st quartile of signal (V/s) | |
| PPxAQ3SG | 1 | R*4 | 3rd quartile of signal (V/s) | |
| PPxAPLEN | 1 | I*4 | Chopper plateau length in $2^{-7}$ s | effective time after discarding signals |
| PPxANSIG | 1 | I*4 | No. of valid signals on the plateau | |
| PPxAFLAG | 1 | I*1 | Status flag | |
| PPxAFILI | 3 | I*1 | Filler | |

Note: FPC state (PPxASTAT) cannot be zero for these measurements.

### 12.3.8 Product PCxA

PCxA (where x=1 or 2) is a Cal A product which contains the SPD of the FCS measurements obtained with the C100 or C200 detector arrays. In case a cold FCS measurement is selected in the absolute photometry AOT PHT25, the first record contains the cold FCS measurement and the second record contains the results of the heated FCS measurement.

**RECORD**
Record length: 316 for x=1, 180 for x=2

| **FIELD** | **N** | **T** | **Description** | **Comment** |
|---|---|---|---|---|
| GPSCTKEY | 1 | I*4 | Instrument time key | |
| GPSCRPID | 2 | I*1 | Raster point ID | points and lines |
| GPSCFILL | 1 | I*2 | Filler | |
| PCxAQFLG | 1 | I*2 | Quality flag | |
| PCxAKYID | 1 | I*2 | Keyword identifier | |
| PCxAMNUM | 1 | I*2 | Measurement number | |
| PCxASPAR | 1 | I*2 | Spare | |
| PCxAFILT | 1 | I*2 | CHW3 position | value: 1 - 14, see A.1 |
| PCxAAPER | 1 | I*2 | CHW2 position | idem |
| PCxAPOLZ | 1 | I*2 | CHW1 position | idem |
| PCxASTAT | 1 | I*2 | FPC state (0 = CFOV, 1 = FCS1, 2 = FCS2) | |
| PCxADWEL | 1 | I*4 | Commanded chopper dwell time in $2^{-7}$ s | |
| PCxACPOS | 1 | R*4 | Chopper position (arcsec) | |
| PCxAFCS1 | 1 | R*4 | Measured FCS1 power (mW) | |
| PCxAFCS2 | 1 | R*4 | Measured FCS2 power (mW) | |
| PCxATEMP | 1 | R*4 | Detector temperature (K) | |
| PCxAFILL | 1 | R*4 | Filler | |
| PCxABIAS | 1 | R*4 | Measured bias voltage (V) | |
| PCxAMNSG | j | R*4 | Mean or fitted signal (V/s) | |
| PCxAMNSU | j | R*4 | Uncertainty (V/s) | |
| PCxAMDSG | j | R*4 | Median signal (V/s) | |
| PCxAQ1SG | j | R*4 | 1st quartile of signal (V/s) | |
| PCxAQ3SG | j | R*4 | 3rd quartile of signal (V/s) | |
| PCxAPLEN | 1 | I*4 | Chopper plateau length in $2^{-7}$ s | effective time after discarding signals |
| PCxANSIG | 1 | I*4 | No. of valid signals on the plateau | |
| PCxAFLAG | j | I*1 | Status flags | |
| PCxAFILL | k | I*1 | Filler | |

For product PC1A the parameters $j$ and $k$ are 9 and 3, respectively; for product PC2A both $j$ and $k$ are 4.

Note: FPC state (PCxASTAT) is the cannot be zero for these measurements.
Also for the product PC2A replace PC1A with PC2A above.

### 12.3.9 Product PPxD

PPxD (where x=1,2,3) contains the SPD of the dark measurements obtained with detector P1, P2 or P3. These measurements are only obtained with AOT P05.

**RECORD**
Record length: 24

| FIELD | N | T | Description | Comment |
|---|---|---|---|---|
| GPSCTKEY | 1 | I*4 | Instrument time key | |
| GPSCRPID | 2 | I*1 | Raster point ID | points and lines |
| GPSCFILL | 1 | I*2 | Filler | |
| PPxDDARK | 1 | R*4 | Dark current (V/s) | |
| PPxDDUNC | 1 | R*4 | Uncertainty (V/s) | |
| PPxDFLAG | 1 | I*1 | Status Flag | |
| PPxDNSIG | 1 | I*4 | No. of valid signals on the plateau | |
| PPxDFILI | 3 | R*4 | Filler | |

### 12.3.10 Product PC1D

PC1D contains the SPD of the dark measurements obtained with detector C100. These measurements are only carried out for AOT P25.

**RECORD**
Record length: 128

| FIELD | N | T | Description | Comment |
|---|---|---|---|---|
| GPSCTKEY | 1 | I*4 | Instrument time key | |
| GPSCRPID | 2 | I*1 | Raster point ID | points and lines |
| GPSCFILL | 1 | I*2 | Filler | |
| PC1DDARK | 9 | R*4 | Dark current (V/s) | |
| PC1DDUNC | 9 | R*4 | Uncertainty (V/s) | |
| PC1DNSIG | 9 | I*4 | No. of valid signals on the plateau | |
| PC1DFLAG | 9 | I*1 | Status Flag | |
| PC1DFILI | 3 | I*1 | Filler | |

### 12.3.11 Product PC2D

PC2D contains the SPD of the dark measurements obtained with detector C200. These measurements are only carried out for AOT P25.

**RECORD**
Record length: 60

| FIELD | N | T | Description | Comment |
|---|---|---|---|---|
| GPSCTKEY | 1 | I*4 | Instrument time key | |
| GPSCRPID | 2 | I*1 | Raster point ID | points and lines |
| GPSCFILL | 1 | I*2 | Filler | |
| PC2DDARK | 4 | R*4 | Dark current (V/s) | |
| PC2DDUNC | 4 | R*4 | Uncertainty (V/s) | |
| PC2DNSIG | 4 | I*4 | No. of valid signals on the plateau | |
| PC2DFLAG | 4 | I*1 | Status Flag | |

### 12.3.12 Pixel status flag

The pixel status flag in the SPD products gives an indication of the data processing quality for each detector pixel. The status flag is one byte of information, the coding of the decimal value of the byte is given in Table 12.3. All success and warning codes are even; all failure (do not process further) codes are odd.

Table 12.3: Coding of the pixel status flag

| **Decimal Value** | **Description** |
|---|---|
| 0 | normal (pixel ok) |
| 1 | calibration measurement saturated |
| 2 | plateau partly affected by drift |
| 3 | all ramps on plateau rejected |
| 4 | plateau data affected by residual drift |
| 5 | zero standard deviation |
| 6 | not used |
| 7 | zero signal for plateau |

## 12.4 AA product types

### 12.4.1 Rationale behind product design

The AAR products represent fully processed data, therefore each AAR product reflects not only the PHT subinstrument used but also the mode of operation. The definition of products necessarily involves a compromise between a number of conflicting desires. The naming convention for PHT Auto-Analysis products is to use the product type **PdAt**, where:

- *d* represents the detector, i.e.:
  - C is for PHT-C.
  - P is for PHT-P.
  - S is for PHT-SS.
  - L is for PHT-SL.
  - G is for generic (not detector-specific)
- *t* is a letter to identify the type of product. These are
  - P is for point source photometry or spectroscopy in staring mode (single point or raster).
  - E is for extended source photometry.
  - I is for a photometric image.
  - U is for an uncertainty map.
  - T is for an exposure time map.
  - S is for raster photometry (including linear scans).

The following table summarises the products that are associated with each AOT:

| | |
|---|---|
| PHT03 | PPAP, PPAE, PPAS, PGAI, PGAU, PGAT |
| PHT04 | PPAP, PPAE |
| PHT05 | PPAP, PPAE |
| PHT17/18/19 | PPAP, PPAE |
| PHT22 | PCAP, PCAE, PCAS, PGAI, PGAU, PGAT |
| PHT25 | PCAP, PCAE |
| PHT32 | PCAS, PGAI, PGAU, PGAT |
| PHT37/38/39 | PCAP, PCAE |
| PHT40 | PSAP, PSAE, PLAP, PLAE, PPAS, PLAS |

### 12.4.2 Product PPAP

PPAP is the standard product for PHT-P photometry AOTs when observing a point source. It contains the flux densities for each of the filters and/or apertures used.

```
Origin:         PHT03, PHT04, PHT05, PHT17, PHT18, PHT19
Units:          Jy
Format:         FITS binary table file
Limitations:    No colour correction performed
                Photometry from chopped observations is not scientifically
                validated
```

**HEADER**
The following product specific header keywords are present:

| FIELD | T | Description | Comment |
|---|---|---|---|
| FILTERn | C | Filter | |
| LAMBDAn | C | Central wavelength | |
| EXFLUXn | R | Expected source flux (Jy) | AOT input parameter |
| UNCFLXn | R | Uncertainty (Jy) | AOT input parameter |
| MXBACKn | R | Expected Maximum background (MJy/sr) | AOT input parameter |
| APERn | C | Aperture | |
| SOURCEn | R | Flux density of source (Jy) | only if chopped mode used |
| SOURCUn | R | uncertainty (Jy) | only if chopped mode used |
| SBACKn | R | Flux density of source plus background (Jy) | |
| SBACKUn | R | Uncertainty (Jy) | |
| BACKn | R | Measured background intensity (MJy/sr) | value = 0 if staring measurement |

**RECORD**
Record length: 64

| FIELD | Off | N | T | Description | Comment |
|---|---|---|---|---|---|
| PPAPFILT | 0 | 1 | I*4 | Filter ID (CHW3 position) | |
| PPAPAPER | 4 | 1 | I*4 | Aperture ID (CHW2 position) | |
| PPAPNBCK | 8 | 1 | I*4 | Number of background reference positions | |
| PPAPSRCE | 12 | 1 | R*4 | Source flux (Jy) | |
| PPAPSRCU | 16 | 1 | R*4 | Uncertainty (Jy) | |
| PPAPBACK | 20 | 1 | R*4 | Background for given aperture (Jy) | |
| PPAPBCKU | 24 | 1 | R*4 | Uncertainty (Jy) | |
| PPAPSPB | 28 | 1 | R*4 | Source plus background (Jy) | |
| PPAPSPBU | 32 | 1 | R*4 | Uncertainty (Jy) | |
| PPAPBCK1 | 36 | 1 | R*4 | Background reference 1 (Jy) | |
| PPAPBK1U | 40 | 1 | R*4 | Uncertainty (Jy) | |
| PPAPBCK2 | 44 | 1 | R*4 | Background reference 2 (Jy) | |
| PPAPBK2U | 48 | 1 | R*4 | Uncertainty (Jy) | |
| PPAPBINT | 52 | 1 | R*4 | Mean background intensity (MJy/sr) | |
| PPAPBINU | 56 | 1 | R*4 | Uncertainty (MJy/sr) | |
| PPAPNCYC | 60 | 1 | I*4 | Number of accepted chopper cycles | |

### 12.4.3 Product PPAE

PPAE is the standard product for PHT-P photometry AOTs when observing an extended source. It contains the surface brightness for each of the filters and/or apertures used.

```
Origin:         PHT03, PHT04, PHT05, PHT17, PHT18, PHT19
Units:          MJy/sr
Format:         FITS binary table file
Limitations:    No colour correction performed
                Surface brightness for non-standard apertures is not
                scientifically validated
                Photometry from chopped observations is not scientifically
                validated
```

**HEADER**
The following product specific header keywords are present:

| FIELD | T | Description | Comment |
|---|---|---|---|
| FILTERn | C | Filter (n is the record number). | |

| | | | |
|---|---|---|---|
| LAMBDAn | C | Central wavelength (n is the record number) | |
| EXBRGTn | R | Expected source brightness (MJy/sr) | AOT input parameter |
| UNCFLXn | R | Uncertainty (MJy/sr) | AOT input parameter |
| MXBACKn | R | Expected Maximum background (MJy/sr) | AOT input parameter |
| APERn | C | Aperture | |
| SBRGTn | R | Brightness of source(MJy/sr) | only if chopped mode used |
| SBRGTUn | R | Uncertainty (MJy/sr) | only if chopped mode used |
| SBBRGTn | R | Brightness of source plus background (MJy/sr) | |
| SBBRGTUn | R | Uncertainty (MJy/sr) | |
| BACKn | R | Measured background intensity (MJy/sr) | value=0 if staring measurement |

**RECORD**
Record length: 56

| FIELD | Off | N | T | Description | Comment |
|---|---|---|---|---|---|
| PPAEFILT | 0 | 1 | I*4 | Filter ID (CHW3 position) | |
| PPAEAPER | 4 | 1 | I*4 | Aperture ID (CHW2 position) | |
| PPAENBCK | 8 | 1 | I*4 | Number of background reference positions | |
| PPAESRCE | 12 | 1 | R*4 | Source brightness (MJy/sr) | |
| PPAESRCU | 16 | 1 | R*4 | Uncertainty (MJy/sr) | |
| PPAEBACK | 20 | 1 | R*4 | Background for given aperture (MJy/sr) | |
| PPAEBCKU | 24 | 1 | R*4 | Uncertainty (MJy/sr) | |
| PPAESPB | 28 | 1 | R*4 | Source plus background (MJy/sr) | |
| PPAESPBU | 32 | 1 | R*4 | Uncertainty (MJy/sr) | |
| PPAEBCK1 | 36 | 1 | R*4 | Background reference 1 (MJy/sr) | |
| PPAEBK1U | 40 | 1 | R*4 | Uncertainty (MJy/sr) | |
| PPAEBCK2 | 44 | 1 | R*4 | Background reference 2 (MJy/sr) | |
| PPAEBK2U | 48 | 1 | R*4 | Uncertainty (MJy/sr) | |
| PPAENCYC | 52 | 1 | I*4 | Number of accepted chopper cycles | |

### 12.4.4 Product PCAP

PCAP is the standard product for PHT-C photometry AOTs when observing a point source. It contains the flux densities for each of the filters used.

```
Origin:         PHT22, PHT25, PHT37, PHT38, PHT39
Units:          Jy
Format:         FITS binary table file
Limitations:    No colour correction performed
                Photometry from chopped observations is not scientifically
                validated.
```

**HEADER**
The following product specific header keywords are present:

| FIELD | T | Description | Comment |
|---|---|---|---|
| FILTERn | C | Filter (n is the record number). | |
| LAMBDAn | C | Central wavelength | |
| EXFLUXn | R | Expected source flux (Jy) | AOT input parameter |
| UNCFLXn | R | Uncertainty (Jy) | AOT input parameter |
| MXBACKn | R | Expected Maximum background (MJy/ster) | AOT input parameter |
| SOURCEn | R | Flux density of source (Jy) | only if chopped mode used |
| SOURCUn | R | Uncertainty (Jy) | only if chopped mode used |

| | | | |
|---|---|---|---|
| SBACKn | R | Flux density of source plus background (Jy) | |
| SBACKUn | R | Uncertainty (Jy) | |
| SBACKn | R | Measured background (MJy/ster) | value=0<br>if staring measurement |

**RECORD**
Record length: 56

| FIELD | Off | N | T | Description | Comment |
|---|---|---|---|---|---|
| PCAPFILT | 0 | 1 | I*4 | Filter ID (CHW2 position) | |
| PCAPNBCK | 4 | 1 | I*4 | Number of background reference positions | |
| PCAPNPIX | 8 | 1 | I*4 | Number of pixels defined | |
| PCAPSRCE | 12 | 9 | R*4 | Source flux (Jy) | |
| PCAPSRCU | 48 | 9 | R*4 | Uncertainty (Jy) | |
| PCAPSPB | 84 | 9 | R*4 | Source plus background (Jy) | |
| PCAPSPBU | 120 | 9 | R*4 | Uncertainty (Jy) | |
| PCAPB1 | 156 | 9 | R*4 | Background at off position 1 (MJy/sr) | |
| PCAPB1U | 192 | 9 | R*4 | Uncertainty (MJy/sr) | |
| PCAPB2 | 228 | 9 | R*4 | Background at off position 2 (MJy/sr) | |
| PCAPB2U | 264 | 9 | R*4 | Uncertainty (MJy/sr) | |
| PCAPPEAK | 300 | 1 | R*4 | Fitted source peak (Jy) | from Gaussian fitting |
| PCAPPKU | 304 | 1 | R*4 | Uncertainty (Jy) | |
| PCAPBCKS | 308 | 1 | R*4 | Background at source position (Jy) | |
| PCAPBKSU | 312 | 1 | R*4 | Uncertainty (Jy) | |
| PCAPBCK1 | 316 | 1 | R*4 | Avg. Background at off position 1 (Jy) | |
| PCAPBK1U | 320 | 1 | R*4 | Uncertainty (Jy) | |
| PCAPBCK2 | 324 | 1 | R*4 | Avg. Background at off position 2 (Jy) | |
| PCAPBK2U | 328 | 1 | R*4 | Uncertainty (Jy) | |
| PCAPBINS | 332 | 1 | R*4 | On-source background intensity (MJy/sr) | |
| PCAPBISU | 336 | 1 | R*4 | Uncertainty (MJy/sr) | |
| PCAPBIN1 | 340 | 1 | R*4 | Off-source background intensity 1 (MJy/sr) | |
| PCAPBI1U | 344 | 1 | R*4 | Uncertainty (MJy/sr) | |
| PCAPBIN2 | 348 | 1 | R*4 | Off-source background intensity 2 (MJy/sr) | |
| PCAPBI2U | 352 | 1 | R*4 | Uncertainty (MJy/sr) | |
| PCAPOFF | 356 | 2 | R*4 | (x,y) offset of source peak (arcsec) | see section 8.4.8.2– |
| PCAPOFFU | 364 | 2 | R*4 | (x,y) uncertainty in offset (arcsec) | –for gaussian fit |
| PCAPFITU | 372 | 1 | R*4 | Uncertainty of Gaussian fit (Jy) | |
| PCAPSTAT | 376 | 1 | I*4 | Fit status | |
| PCAPNCYC | 380 | 9 | I*4 | Number of accepted chopper cycles | |

### 12.4.5 Product PCAE

PCAE is the standard product for PHT-C photometry AOTs when observing an extended source. It contains the surface brightness for each of the filters used.

```
Origin:         PHT22, PHT25, PHT37, PHT38, PHT39
Units:          MJy/sr
Format:         FITS binary table file
Limitations:    No colour correction performed
                Photometry from chopped observations is not scientifically
                validated
```

**HEADER**
The following product specific header keywords are present:

| FIELD | T | Description | Comment |
|---|---|---|---|
| FILTERn | C | Filter (n is the record number) | |
| LAMBDAn | C | Central wavelength (n is the record number) | |
| EXBRGTn | R | Expected source brightness (MJy/sr) | AOT input parameter |
| UNCFLXn | R | Uncertainty (MJy/sr) | AOT input parameter |
| MXBACKn | R | Expected Maximum background (MJy/sr) | AOT input parameter |
| SBRGTn | R | Brightness of source (MJy/sr) | only if chopped mode used |
| SBRGTUn | R | Uncertainty (MJy/sr) | only if chopped mode used |
| SBBRGTn | R | Brightness of source plus background (MJy/sr) | |
| SBBRGTUn | R | Uncertainty (MJy/sr) | |
| BACKn | R | Measured background intensity (MJy/sr) | |

**RECORD**
Record length: 360

| FIELD | Off | N | T | Description | Comment |
|---|---|---|---|---|---|
| PCAEFILT | 0 | 1 | I*4 | Filter ID (CHW2 position) | |
| PCAENBCK | 4 | 1 | I*4 | Number of background reference positions | |
| PCAENPIX | 8 | 1 | I*4 | Number of pixels defined | |
| PCAESRCE | 12 | 9 | R*4 | Source brightness (MJy/sr) | |
| PCAESRCU | 48 | 9 | R*4 | Uncertainty (MJy/sr) | |
| PCAESPB | 84 | 9 | R*4 | Source plus background (MJy/sr) | |
| PCAESPBU | 120 | 9 | R*4 | Uncertainty (MJy/sr) | |
| PCAEB1 | 156 | 9 | R*4 | Background reference 1 (MJy/sr) | |
| PCAEB1U | 192 | 9 | R*4 | Uncertainty (MJy/sr) | |
| PCAEB2 | 228 | 9 | R*4 | Background reference 2 (MJy/sr) | |
| PCAEB2U | 264 | 9 | R*4 | Uncertainty (MJy/sr) | |
| PCAEBACK | 300 | 1 | R*4 | Average background (MJy/sr) | |
| PCAEBCKU | 304 | 1 | R*4 | Uncertainty (MJy/sr) | |
| PCAEBCK1 | 308 | 1 | R*4 | Avg. background at off position 1 (MJy/sr) | |
| PCAEBK1U | 312 | 1 | R*4 | Uncertainty (MJy/sr) | |
| PCAEBCK2 | 316 | 1 | R*4 | Avg. background at off position 2 (MJy/sr) | |
| PCAEBK2U | 320 | 1 | R*4 | Uncertainty (MJy/sr) | |
| PCAENCYC | 324 | 9 | I*4 | Number of accepted chopper cycles | |

### 12.4.6 Product PGAI

PGAI is the standard product for a photometric image. It contains a map of surface brightness.

```
Origin:         PHT03, PHT22, PHT32
Units:          MJy/sr
Format:         FITS Image
Limitations:    Maps are not scientifically validated
```

**HEADER**
The following product specific header keywords are present:

| FIELD | T | Description | Comment |
|---|---|---|---|
| NAXIS | 3 | number of axes | |
| NAXIS1 | I | Number of pixels per row of image | |
| NAXIS2 | I | Number of pixels per column of image | |
| NAXIS3 | I | Number of measurements (wavelengths) | |
| BUNIT | C | MJy/sr | |
| CTYPE1 | C | Right Ascension | |

| | | | |
|---|---|---|---|
| CTYPE2 | C | Declination | |
| CTYPE3 | C | wavelength | |
| BLANK | I | Blank value | value used: -987654322 |
| CRPIX1 | R | Pixel origin of RA-axis | image centre |
| CRPIX2 | R | Pixel origin of DEC-axis | image centre |
| CRPIX2 | R | | n/a |
| CRVAL1 | R | Right Ascension of raster centre | |
| CRVAL2 | R | Declination of raster centre | |
| CRVAL3 | R | Wavelength index | |
| CDELT1 | R | Pixel size (deg) | |
| CDELT2 | R | Pixel size (deg) | |
| CDELT3 | R | Index | |
| CROTA1 | R | Position angle of first axis | (=0) |
| CROTA2 | R | Position angle of second axis | (=0) |
| CROTA3 | R | | n/a |
| APERTURE | C | Aperture | (if PHT-P) |
| FILTERn | C | Filter | n=number of filters |
| LAMBDAn | C | Central Wavelength of filter (m) | |
| EXPUNCn | R | Expected maximum brightness (MJy/sr) | AOT input parameter |
| DATAMINn | R | Minimum brightness (MJy/sr) | for first filter |
| DATAMAXn | R | Maximum brightness (MJy/sr) | for first filter |

**Caveat:** In case an observer has selected in a multi-filter raster map PHT-03 different aperture sizes, the OLP Version 7 software does not recognize this. It assumes that there was only one single aperture size used for all filters and computes the maps accordingly with the wrong scaling. The header keywords do not reflect the filter dependent aperture size either.

**IMAGE**

| AXIS no | LENGTH | Description | Comment |
|---|---|---|---|
| 1 | N1 | Points per raster line | |
| 2 | N2 | Number of lines | |
| 3 | N3 | Filters | detector |

### 12.4.7 Product PGAU

PGAU is an accompanying product for a photometric image. It contains a map of uncertainty in the surface brightness as found in product PGAI.

```
Origin:         PHT03, PHT22, PHT32
Units:          MJy/sr
Format:         primary FITS file containing a real array
Limitations:    Maps are not scientifically validated
```

The product specific header keywords and image axis are the same as for PGAI, except for:

| FIELD | T | Description | Comment |
|---|---|---|---|
| DATAMIN | R | Minimum uncertainty | for first filter |
| DATAMAX | R | Maximum uncertainty | for first filter |

### 12.4.8 Product PGAT

This is an accompanying product for a photometric image. It contains a map of the exposure time as measured in product PGAI.

```
Origin:         PHT03, PHT22, PHT32.
Units:          Seconds
Format:         primary FITS file containing a real array
Limitations:    Maps are not scientifically validated
```

**HEADER**
The product specific header keywords and image axis are the same as for PGAI, except for:

| FIELD | T | Description | Comment |
|---|---|---|---|
| DATAMIN | R | Minimum exposure | for first filter |
| DATAMAX | R | Maximum exposure | for first filter |
| DATAAVG | R | Average exposure | for first filter |

### 12.4.9 Product PPAS

This is the photometric table product for PHT-P raster maps. The data serve as input for alternative image reconstruction algorithms. Each record contains the surface brightness and sky coordinates for each sampled position. The records are ordered in time according to the raster scan, records of a next filter are appended to the ones of the previous.

```
Origin:         PHT03
Units:          MJy/sr
Format:         FITS binary table file
Limitations:    Uncertainties in coordinates are currently not available
                Maps are not scientifically validated
```

**HEADER**
The following product specific header keywords are present:

| FIELD | T | Description | Comment |
|---|---|---|---|
| FILTERn | C | Filter identifier | |
| LAMBDAn | C | Reference Wavelength of filter (m) | |
| EXFLUXn | R | Expected source brightness (MJy/sr) | AOT input parameter |
| UNCFLXn | R | Uncertainty (MJy/sr) | AOT input parameter |
| MXBACKn | R | Max.expected background (MJy/sr) | AOT input parameter |
| MXBRGTn | R | Measured maximum brightness (MJy/sr) | |
| UNBRGTn | R | Uncertainty (MJy/sr) | |

**RECORD**
Record length: 40 bytes

| FIELD | Off | N | T | Description | Comment |
|---|---|---|---|---|---|
| PPASFILT | 0 | 1 | I*4 | Filter ID (CHW3 position) | |
| PPASRA | 4 | 1 | R*4 | Right Ascension | |
| PPASRAU | 8 | 1 | R*4 | Uncertainty | |
| PPASDEC | 12 | 1 | R*4 | Declination | |
| PPASDECU | 16 | 1 | R*4 | Uncertainty | |
| PPASROLL | 20 | 1 | R*4 | Roll angle | |
| PPASROLU | 24 | 1 | R*4 | Uncertainty | |
| PPASBRGT | 28 | 1 | R*4 | Surface brightness (MJy/sr) | |
| PPASBRGU | 32 | 1 | R*4 | Uncertainty (MJy/sr) | |
| PPASSTAT | 36 | 1 | I*1 | Status flag (from SPD) | |
| PPASFILL | 37 | 3 | I*1 | Filler | |

### 12.4.10 Product PCAS

This is the photometric table product for PHT-C raster maps. The data serve as input for alternative image reconstruction algorithms. Each record contains the surface brightness and sky coordinates for each sampled position. The records are ordered in time according to the raster scan, records of a next filter are appended to the ones of the previous. For PHT32 observations each record contains data of a chopper plateau.

```
Origin:         PHT22, PHT32
Units:          MJy/sr
Format:         FITS binary table file
Limitations:    Uncertainties in coordinates are currently not available
                Maps are not scientifically validated
```

**HEADER**
The following product specific keywords are present:

| | | | |
|---|---|---|---|
| FPCMODE | C | Chopper mode | (ST= staring, RE= rectangular, SW= sawtooth, TR= triangular |
| FILTERn | C | Filter identifier | see A.1 |
| LAMBDAn | C | Reference Wavelength of filter (m) | |
| EXFLUXn | R | Expected source brightness (MJy/sr) | AOT input parameter |
| UNCFLXn | R | Uncertainty (MJy/sr) | AOT input parameter |
| MXBACKn | R | Max. expected background (MJy/sr) | AOT input parameter |
| MXBRGTn | R | Measured maximum brightness (MJy/sr) | |
| UNBRGTn | R | Uncertainty (MJy/sr) | |

**RECORD**
Record length: 120 bytes

| FIELD | Off | N | T | Description | Comment |
|---|---|---|---|---|---|
| PCASFILT | 0 | 1 | I*4 | Filter ID (CHW2 position) | |
| PCASRA | 4 | 1 | R*4 | Right Ascension | |
| PCASRAU | 8 | 1 | R*4 | Uncertainty | |
| PCASDEC | 12 | 1 | R*4 | Declination | |
| PCASDECU | 16 | 1 | R*4 | Uncertainty | |
| PCASROLL | 20 | 1 | R*4 | Roll angle | |
| PCASROLU | 24 | 1 | R*4 | Uncertainty | |
| PCASAVGB | 28 | 1 | R*4 | Average brightness over array (MJy/sr) | |
| PCASNPIX | 32 | 1 | I*4 | Number of pixels defined | |
| PCASBRGT | 36 | 9 | R*4 | Surface brightness (MJy/sr) | |
| PCASBRGU | 72 | 9 | R*4 | Uncertainty (MJy/sr) | |
| PCASSTAT | 108 | 9 | I*1 | Status flags | from SPD |
| PCASFILL | 117 | 3 | I*1 | Filler | |

### 12.4.11 Product PSAP

This is the photometric table product for PHT-SS single pointing of a point source.

```
Origin:         PHT40
Units:          W/m^2/micron
Format:         FITS binary table file
Limitations:    -
```

**HEADER**
The following product specific keywords are present:

| | | | |
|---|---|---|---|
| CALSEQ | I | Calibration Sequence | |
| CALDATE | C | Date Calibration defaults generated | |
| FPCMODE | C | Focal plane chopper mode | (ST, RE, SW or TR) |
| LAMBDAd | R | Central Wavelength of pixel (m) | d = 1,2,...,64 |

**RECORD**
Record length: 2568 bytes

| FIELD | Off | N | T | Description | Comment |
|---|---|---|---|---|---|
| PSAPDFLG | 0 | 1 | I*4 | Dark background flag | dark=1, otherwise=0 |
| PSAPNBCK | 4 | 1 | I*4 | Number of background reference positions | |
| PSAPSRCE | 8 | 64 | R*4 | Source Flux in $Wm^{-2}\mu m^{-1}$ | |
| PSAPSRCU | 264 | 64 | R*4 | Uncertainty in $Wm^{-2}\mu m^{-1}$ | |
| PSAPBCK | 520 | 64 | R*4 | Mean Background in $Wm^{-2}\mu m^{-1}$ | |
| PSAPBCKU | 776 | 64 | R*4 | Uncertainty in $Wm^{-2}\mu m^{-1}$ | |
| PSAPSPB | 1032 | 64 | R*4 | Source + Background in $Wm^{-2}\mu m^{-1}$ | |
| PSAPSPBU | 1288 | 64 | R*4 | Uncertainty in $Wm^{-2}\mu m^{-1}$ | |
| PSAPBCK1 | 1544 | 64 | R*4 | Background reference 1 in $Wm^{-2}\mu m^{-1}$ | |
| PSAPBK1U | 1800 | 64 | R*4 | Uncertainty in $Wm^{-2}\mu m^{-1}$ | |
| PSAPBCK2 | 2056 | 64 | R*4 | Background reference 2 in $Wm^{-2}\mu m^{-1}$ | |
| PSAPBK2U | 2312 | 64 | R*4 | Uncertainty in $Wm^{-2}\mu m^{-1}$ | |

### 12.4.12 Product PLAP

This is the photometric table product for PHT-SL single pointing of a point source.

```
Origin:         PHT40
Units:          W/m^2/micron
Format:         FITS binary table file
Limitations:    -
```

**HEADER**
Similar to product PSAP

**RECORD**
Similar to product PSAP, only all record keywords start with 'PLAP'

### 12.4.13 Product PSAE

This is the photometric table product for PHT-SS single pointing of an extended source.

```
Origin:         PHT40
Units:          of W/m^2/micron/sr
Format:         FITS binary table file
Limitations:    -
```

**HEADER**
Similar to product PSAP

**RECORD**
Similar to product PSAP, only all record keywords start with 'PSAE' and all surface brightness values are in units of $W/m^2/\mu m/sr$.

### 12.4.14 Product PLAE

This is the photometric table product for PHT-SL single pointing of an extended source.

```
Origin:         PHT40
Units:          W/m^2/micron/sr
Format:         FITS binary table file
Limitations:    -
```

**HEADER**
Similar to product PSAP

**RECORD**
Similar to product PSAP, only all record keywords start with 'PLAE' and all surface brightness values are in units of $W/m^2/\mu m/sr$.

### 12.4.15 Product PSAS

This is the photometric table product for PHT-SS raster pointing. Each record contains the surface brightness and sky coordinates for each sampled position. The records are ordered in time according to the raster scan.

```
Origin:         PHT40
Units:          W/m^2/micron/sr
Format:         FITS binary table file
Limitations:    -
```

**HEADER**
The following product specific keywords are present:

| | | | |
|---|---|---|---|
| CALSEQ | I | Calibration Sequence | |
| CALDATE | C | Date Calibration defaults generated | |
| LAMBDAd | R | Central Wavelength of pixel (m) | d=1,64 |

**RECORD**
Record length: 604 bytes

| FIELD | Off | N | T | Description | Comment |
|---|---|---|---|---|---|
| PSASDFLG | 0 | 1 | I*4 | Dark background flag | dark=1, otherwise=0 |
| PSASRA | 4 | 1 | R*4 | Right Ascension of raster point | |
| PSASRAU | 8 | 1 | R*4 | Uncertainty in Right Ascension | |
| PSASDEC | 12 | 1 | R*4 | Declination of raster point | |
| PSASDECU | 16 | 1 | R*4 | Uncertainty in Declination | |
| PSASROLL | 20 | 1 | R*4 | Roll angle | |
| PSASROLU | 24 | 1 | R*4 | Uncertainty in roll angle | |
| PSASSPB | 28 | 64 | R*4 | Source plus background in $Wm^{-2}\mu m^{-1}sr^{-1}$ | |
| PSASSPBU | 284 | 64 | R*4 | Uncertainty in $Wm^{-2}\mu m^{-1}sr^{-1}$ | |
| PSASSTAT | 540 | 64 | I*1 | Status flags | |

### 12.4.16 Product PLAS

This is the photometric table product for PHT-SL raster pointing.

```
Origin:         PHT40
Units:          W/m^2/micron/sr
Format:         FITS binary table file
Limitations:    No image product available
```

**HEADER**
Similar to product PSAS

**RECORD**
Similar to product PSAP, only all record keywords start with 'PLAS'

# Chapter 13

# Calibration G Products

## 13.1 Overview

General calibration files or "Cal G" files contain either correction factors or instrumental parameters necessary to

- steer the processing,
- to remove or to correct for instrumental effects in the data, and
- to carry out the flux calibration.

The contents of the Cal G files reflect the best or most recent instrument calibration parameters. The files can only be updated as part of an official upgrade of the OLP software. In this chapter detailed descriptions are given of the structure and contents of the Cal G files.

Note:
• See section 3.4.2 for definition of C-arrays pixel identifiers throughout this chapter.

## 13.2 Observation time dependent calibration

| | |
|---|---|
| `Description Parameter:` | `section 7.4.6` |
| `Processing Level:` | `SPD` |
| `Usage in processing:` | `section 7.4.6` |
| `File Type:` | `Binary FITS table` |
| `File names:` | `PTIMEDEP` |

During the mission two events took place that directly affected calibration parameters of the instrument:

- the change in the illumination properties of the TRS2 of FCS1 which took place in the activation window of revolution 94. The illumination power for the same electrical power applied to the FCS increased by approximately a factor two. The cause of the change is not clear. The change in FCS properties requires different calibration parameters for FCS related calibrations of P3, C100 and C200.
- the addition of an extra curing procedure for detectors P3, C100 and C200 during the otherwise idle telescope time in ground station handover between VILSPA and Goldstone sometime after the apogee passage of ISO. The extra curing was introduced on rev 150 and affects the orbit dependent responsivity of the three detectors.

Consequently, the OLP must use different sets of Cal G files depending on the date and time of the observation. This calibration file lists the names of the Cal G files that are affected together with the date and time when the change took place. Depending on the time of the observation the appropriate Cal G files are selected.

### 13.2.1 Product PTIMEDEP: PHT calibration time dependency

Binary FITS table with record length 80. The record fields are:

| Field | Offset | Number | Type | Description |
|---|---|---|---|---|
| CALGROOT | 0 | 1 | C*12 | Root name: referred to when file is opened |
| CALGFILE | 12 | 1 | C*12 | Corresponding filename |
| CALGTIME | 24 | 1 | C*11 | Time from which this file applies in yydddhhmmss |
| CALGCOMM | 35 | 1 | C*45 | Optional comment |

## 13.3 DIE power calibration tables

```
Description Parameter:          section 3.2.3
Processing Level:               SPD
Usage in processing:            section 7.2.5
File Type:                      Binary FITS table
Number of Records:              3
File Names:                     PDIE1TRANS, PDIE2TRANS
```

There are 2 sets of Detector Interface Electronics (DIE) in the external electronics unit (see section 3.2.3). The DIE subtracts a commandable offset from the cold readout electronics voltage and amplifies the difference with a commandable gain factor. There were 3 possible DIE settings available but in practice only one was used. To convert the digital numbers (DNs) to Voltages, a set of "gain" parameters were used depending on which of the 3 possible settings were commanded. See also section 7.2.5 for the conversion formula.

Table 13.1: DIE used for detector:

| DIE number | detector |
|---|---|
| 1 | P1, P2, SL, C200 |
| 2 | P3, SS, C100, C200 |

The possible settings of the 2 DIEs are stored in 2 Cal G products. Both DIEs were used during operations depending on which detector was active, the relation between detector and DIE is given in Table 13.1. Each record in the Cal G products refers to the settings for a given DIE gain that was commanded, see Table 13.2.

Table 13.2: Conversion from record in Cal G to gain value.

| Record number | Gain |
|---|---|
| 1 | 1 |
| 2 | 8 |
| 3 | 40 |

### 13.3.1 Product PDIE1TRANS: PHT DIE1 power calibration table

Binary FITS table with record length 16. The record fields are:

| Field | Offset | Number | Type | Description |
|---|---|---|---|---|
| PDIE1FIX | 0 | 1 | R*4 | Fixed offset |
| PDIE1UOF | 4 | 1 | R*4 | Offset dependent on signal gain in V |
| PDIE1GN1 | 8 | 1 | R*4 | Signal gain (=$GAIN_1$) |
| PDIE1GN1 | 12 | 1 | R*4 | Offset gain (=$GAIN_2$) |

### 13.3.2 Product PDIE2TRANS: PHT DIE2 power calibration table

Similar to PDIE1TRANS, but DIE1 should be substituted by DIE2.

## 13.4 Selection of read-outs

```
Description Parameter:          section 4.3.1
Processing Level:               SPD
Usage in processing:            section 7.2.2
File Type:                      Binary Fits Table
Number of Records:              8
File Names:                     PSELNDR
```

It has been observed that the first few readouts of each integration ramp do not increase in a linear way but can stay flat for a while or can even decrease. The disturbance is due to the preceding reset and is a switch-on effect of the integrator which is independent of the reset voltage level. This effect is not related to the voltage dependent non-linearity for which the corrections are stored in the Cal G linearisation files (section 13.5)). The best correction method so far is to discard these readouts. The number of readouts that should be removed is a function of the number of readouts per ramp. The optimum values have been determined in flight.

In total there are 8 records, each record gives the number of readouts to be discarded for a given NDR value. The record ordering is as follows:

Table 13.3: Relation between record number and NDR in PSELNDR.

| Record number | number of non-destructive readouts | Record number | number of non-destructive readouts |
|---|---|---|---|
| 1 | 0 | 5 | 15 |
| 2 | 1 | 6 | 31 |
| 3 | 3 | 7 | 63 |
| 4 | 7 | 8 | 127 |

### 13.4.1 Product PSELNDR: PHT non-destructive read-out selection

Binary FITS table with record length 32. The record fields are:

| Field | Offset | Number | Type | Description |
|---|---|---|---|---|
| PP1SNDR | 0 | 1 | I*4 | NDRs to discard for PHT-P1 |
| PP2SNDR | 4 | 1 | I*4 | NDRs to discard for PHT-P2 |
| PP3SNDR | 8 | 1 | I*4 | NDRs to discard for PHT-P3 |
| PFILSNDR | 12 | 1 | I*4 | Filler |
| PSSSNDR | 16 | 1 | I*4 | NDRs to discard for PHT-SS |
| PSLSNDR | 20 | 1 | I*4 | NDRs to discard for PHT-SL |

| | | | | |
|---|---|---|---|---|
| PC1SNDR | 24 | 1 | I*4 | NDRs to discard for PHT-C100 |
| PC2SNDR | 28 | 1 | I*4 | NDRs to discard for PHT-C200 |

## 13.5 CRE linearisation corrections

```
Description Parameter:          section 4.3.2
Processing Level:               SPD
Usage in processing:            section 7.2.7
File Type:                      FITS Image
Units:                          V
File Names:                     PPCRELIN, PC1CRELIN, PC2CRELIN
```

The linearisation of ramps is performed by adding a correction voltage to each readout voltage. The value of the correction depends on the the value of the readout voltage itself, the detector used, and the readout clock frequency. The correction tables are provided by FITS images for the P, C100, and C200 detectors, respectively.

The index is determined in axis 1 which corresponds to the CRE output voltage. For the given detector (or pixel) and readout clock frequency, the voltage correction and uncertainty are provided through axis 4.

All products have:
NAXIS = 4
TYPE = R*4

### 13.5.1 Product PPCRELIN: Linearisations for P1, P2, and P3

| AXIS | Length | Description |
|---|---|---|
| 1 | 121 | CRE Output Voltages. The voltages are binned in steps of 0.02 V in the voltage range -1.2 V to +1.2 V |
| 2 | 3 | PHT-P detectors: P1, P2, P3 |
| 3 | 3 | readout clock frequency 1, 4, 8 kHz |
| 4 | 2 | Correction voltage and uncertainty in V |

### 13.5.2 Product PC1CRELIN: Linearisations for C100

Same as PPCRELIN, but for AXIS 2:
Length = 9, Description = C100 pixels

### 13.5.3 Product PC2CRELIN: Linearisations for C200

Same as PPCRELIN, but for AXIS 2:
Length = 4, Description = C200 pixels.

## 13.6 Signal correction reset interval

```
Description Parameter:          section 4.3.3
Processing Level:               SPD
Usage in processing:            section 7.3.1
File Type:                      Binary FITS Table
File Names:                     PP1RESETI, PP2RESETI, PP3RESETI,
                                PC1RESETI, PC2RESETI
```

In Derive_SPD, each signal is transformed to the equivalent signal for a reference reset interval of 1/4 seconds. The Cal G files provide the correction parameters $A_0$ and $A_1$ as defined in section 7.3.1.

### 13.6.1 Product PP1RESETI: parameters for conversion to 1/4s reset interval for P1

Binary FITS table with record length 24. The record fields are:

| Field | Offset | Number | Type | Description |
|---|---|---|---|---|
| PP1RESRI | 0 | 1 | I*4 | Reset interval, n, with $t_{RI} = 2^{7-n}$ s |
| PP1RESDR | 4 | 1 | I*4 | Data reduction factor |
| PP1RESA0 | 4 | 1 | R*4 | Offset correction, $A_0$ (V/s) |
| PP1RESA1 | 4 | 1 | R*4 | Slope correction, $A_1$ |
| PP1RESE0 | 4 | 1 | R*4 | Error(standard deviation) in $A_0$ (V/s) |
| PP1RESE1 | 4 | 1 | R*4 | Error(standard deviation) in $A_1$ |

### 13.6.2 Product PP2RESETI: parameters for conversion to 1/4s reset interval for P2

Similar as PP1RESETI, all field keywords start with PP2.

### 13.6.3 Product PP3RESETI: parameters for conversion to 1/4s reset interval for P3

Similar as PP1RESETI, all field keywords start with PP3.

### 13.6.4 Product PC1RESETI: parameters for conversion to 1/4s reset interval for C100

Similar as PP1RESETI, all field keywords start with PC1.

### 13.6.5 Product PC2RESETI: parameters for conversion to 1/4s reset interval for C200

Similar as PP1RESETI, all field keywords start with PC2.

## 13.7 Detector dark signals

```
Description Parameter:          section 4.2.5
Processing Level:               SPD
Usage in processing:            section 7.3.2
File Type:                      FITS Image
Units:                          V/s
File Names:                     PSDARK, PPDARK, PC1DARK, PC2DARK
```

To derive the absolute power falling on the detector it is necessary to remove the detector dark signal. For chopped measurements where only the signal difference matters, the dark signal correction is in principle not required. In the Cal G file the unit for the detector dark currents is V/s.

The dark signal depends on the orbital phase of the satellite during the observation like the detector responsivity, but is not influenced by the curing in the handover window.

All products have:
NAXIS = 3
TYPE = R*4

### 13.7.1 Product PSDARK: PHT-S dark signals

| AXIS | Length | Description |
|---|---|---|
| 1 | 100 | Orbital phase: each element corresponds to a phase in the range from 0.01 to 1.0 in steps of 0.01 |
| 2 | 128 | Pixels - PHT-SS (1-64) and PHT-SL (65-128) |
| 3 | 2 | Dark signal and uncertainty |

### 13.7.2 Product PPDARK: dark signals for detectors P1, P2, and P3

| AXIS | Length | Description |
|---|---|---|
| 1 | 100 | Orbital phase: each element corresponds to a phase in the range from 0.01 to 1.0 in steps of 0.01 |
| 2 | 3 | PHT-P detectors, P1,P2,P3 |
| 3 | 2 | Dark signal and uncertainty |

### 13.7.3 Product PC1DARK: dark signals for detector C100

| AXIS | Length | Description |
|---|---|---|
| 1 | 100 | Orbital phase: each element corresponds to a phase in the range from 0.01 to 1.0 in steps of 0.01 |
| 2 | 9 | C100 pixels, in same order as SPD. |
| 3 | 2 | Dark signal and uncertainty |

### 13.7.4 Product PC2DARK: dark signals for detector C200

| AXIS | Length | Description |
|---|---|---|
| 1 | 100 | Orbital phase: each element corresponds to a phase in the range from 0.01 to 1.0 in steps of 0.01 |
| 2 | 4 | C200 pixels, in same order as SPD. |
| 3 | 2 | Dark signal and uncertainty |

## 13.8 Vignetting Corrections

```
Description Parameter:          section 4.5.1
Processing Level:               SPD
Usage in processing:            section 7.3.8
File Type:                      FITS Image
Units:                          dimensionless
File Names:                     PP1VIGN, PP2VIGN, PP3VIGN,
                                PC1VIGN, PC2VIGN
```

The light deflected by the chopper mirror can be vignetted and possible vignetting corrections should be applied. Since the chopper deflection can only take place along the spacecraft Y direction, the corrections are tabulated as a function of Y offset, detector, filter, and aperture, if any. The correction factors are multiplied with the mean and median signal per chopper plateau for a given chopper throw.

The vignetting Cal G files related to OLP Version 7 contain no corrections for detectors P1, P2, and P3, i.e. all correction factors are unity for these detectors.

All products have:
NAXIS = 3
TYPE = R*4

### 13.8.1 Product PP1VIGN: vignetting corrections for P1

| AXIS | Length | Description |
|---|---|---|
| 1 | 14 | Apertures: CHWII position, see section A.1) |
| 2 | 25 | Chopper position: from $-180''$ to $+180''$ in 15 arcsec steps |
| 3 | 10 | Filters: CHWIII position, see section A.1) |

### 13.8.2 Product PP2VIGN: vignetting corrections for P2

| AXIS | Length | Description |
|---|---|---|
| 1 | 14 | Apertures: CHWII position, see section A.1) |
| 2 | 25 | Chopper position: from $-180''$ to $+180''$ in 15 arcsec steps |
| 3 | 2 | Filters: 20, 25 $\mu$m |

### 13.8.3 Product PP3VIGN: vignetting corrections for P3

see Product PP2VIGN, with filters: 60 and 100 $\mu$m.

### 13.8.4 Product PC1VIGN: vignetting corrections for C100

| AXIS | Length | Description |
|---|---|---|
| 1 | 9 | C100 Pixels: index 1= pixel [1,1], 2= [1,2], etc |
| 2 | 25 | Chopper position: from $-180''$ to $+180''$ in 15 arcsec steps |
| 3 | 7 | Filters: [CHWII position $-$ 1], see section A.1 |

### 13.8.5 Product PC2VIGN: vignetting corrections for C200

| AXIS | Length | Description |
|---|---|---|
| 1 | 4 | C200 Pixels: pixel 1= [1,1], 2= [1,2], etc |
| 2 | 25 | Chopper position: from $-180''$ to $+180''$ in 15 arcsec steps |
| 3 | 5 | Filters: CHWII $-$ 8 position, see section A.1 |

## 13.9 Correction for signal losses in chopped mode

`Description Parameter:` `none`

```
Processing Level:              SPD, AAR
Usage in processing:           Section 7.3.9, 8.4.6
File Type:                     FITS Image
Units:                         Dimensionless
File Names:                    PPCHOPCOR, PC1CHOPCOR, PC2CHOPCOR
```

The signal difference between the on- and off-chopper plateaux is observed to be lower than the signal difference obtained from the same source-background position combination in staring or nodding mode. The effect is attributed to the detector transient responsivity behaviour of the detectors which underestimates the on-signal and overestimates the background signal. The calibration files contain for each detector the parameters necessary to correct the difference signal for the signal loss. The parameters are a function of the chopper plateau time. The correction is applied by dividing by a given parameter.

For all chopped signal corrections, the following FITS keywords are common:

NAXIS = 3
TYPE = REAL*4

### 13.9.1 Product PPCHOPCOR: chopper correction factors for PHT-P

| AXIS | Length | Description |
|---|---|---|
| 1 | 3 | PHT-P1,P2,P3 |
| 2 | 8 | Chopper plateau time given by n, $t = 2^{n-1}$ s, n=1,8 |
| 3 | 2 | Correction and uncertainty |

### 13.9.2 Product PC1CHOPCOR: chopper correction factors for C100

| AXIS | Length | Description |
|---|---|---|
| 1 | 9 | C100 pixels in the same order as in SPD |
| 2 | 8 | Chopper plateau time given by n, $t = 2^{n-1}$ s, n=1,8 |
| 3 | 2 | Correction and uncertainty |

### 13.9.3 Product PC2CHOPCOR: chopper correction factors for C200

| AXIS | Length | Description |
|---|---|---|
| 1 | 4 | C200 pixels in the same order as in SPD |
| 2 | 8 | Chopper plateau time given by n, $t = 2^{n-1}$ s, n=1,8 |
| 3 | 2 | Correction and uncertainty |

## 13.10 FCS power calibration tables

```
Description Parameter:         section 3.5, 5.2.2
Processing Level:              SPD
Usage in processing:           section 7.4
File Type:                     FITS Image
Units:                         mW
File names:                    PP1FCSPOW, PP2FCSPOW,
                               PP3FCSPOW_01, PP3FCSPOW_02,
```

PC1FCSPOW_01, PC1FCSPOW_02,
PC2FCSPOW_01, PC2FCSPOW_02

The FCS power calibration tables give the electrical power in mW applied to the FCS as a function of filter, TRS, FCS and the *index* in the table listing the in-band power on the detector in regular logarithmic intervals. For a given filter, TRS, and FCS combination the indices $i-1, i$ and $P_{FCS}(i-1)$, $P_{FCS}(i)$ are retrieved from the Cal G file. $P_{FCS}(i)$ is the first FCS power in the table higher than the actual FCS power $P_{FCS,meas}$ used in the FCS measurement. Once the indices have been determined Table 13.4 is used to convert these to in-band powers on the detector $P_{det}$.

Table 13.4: Conversion index of axis 1 to power in W for C100 and C200 or $Wmm^{-2}$ for P1, P2, and P3.

| index | $P_{det}$ | index | $P_{det}$ | index | $P_{det}$ |
|---|---|---|---|---|---|
| 1 | 1.78E-20 | 16 | 1.00E-16 | 31 | 5.62E-13 |
| 2 | 3.16E-20 | 17 | 1.78E-16 | 32 | 1.00E-12 |
| 3 | 5.62E-20 | 18 | 3.16E-16 | 33 | 1.78E-12 |
| 4 | 100.E-19 | 19 | 5.62E-16 | 34 | 3.16E-12 |
| 5 | 1.78E-19 | 20 | 1.00E-15 | 35 | 5.62E-12 |
| 6 | 3.16E-19 | 21 | 1.78E-15 | 36 | 1.00E-11 |
| 7 | 5.62E-19 | 22 | 3.16E-15 | 37 | 1.78E-11 |
| 8 | 1.00E-18 | 23 | 5.62E-15 | 38 | 3.16E-11 |
| 9 | 1.78E-18 | 24 | 1.00E-14 | 39 | 5.62E-11 |
| 10 | 3.16E-18 | 25 | 1.78E-14 | 40 | 1.00E-10 |
| 11 | 5.62E-18 | 26 | 3.16E-14 | 41 | 1.78E-10 |
| 12 | 1.00E-17 | 27 | 5.62E-14 | 42 | 3.16E-10 |
| 13 | 1.78E-17 | 28 | 1.00E-13 | 43 | 5.62E-10 |
| 14 | 3.16E-17 | 29 | 1.78E-13 | 44 | 1.00E-09 |
| 15 | 5.62E-17 | 30 | 3.16E-13 | 45 | 1.78E-09 |

The final in-band power obtained in OLP is derived from a linear interpolation in logarithmic space in between $log(P_{det}(i-1))$ and $log(P_{det}(i))$ based on $P_{FCS}(i-1)$, $P_{FCS}(i)$ and $P_{FCS,meas}$.

The properties (FCS1,TRS2) altered between rev 93 and 94 due to unknown reasons. This event changed the FCS calibration for those detectors for which the (FCS1,TRS2) combination is used namely: P3, C100, and C200. For these detectors two calibration files are available: one for FCS measurements obtained before rev 94 (suffix _01) and one for rev 94 and higher (suffix _02).

During the ISO mission only specific FCS/TRS combinations were used. Entries in the Cal G files that do not refer to these settings have been set to zero:

- FCS1/TRS1: P1, P2
- FCS1/TRS2: P3, C100, C200
- FCS2/TRS1: P1, P2 chopped mode
- FCS2/TRS2: P3, C100, C200 chopped mode

Example: for detector P2, settings FCS1/TRS2 and FCS2/TRS2 are not allowed and therefore set to zero in the corresponding table.

For all FCS power calibration tables, the following FITS keywords are common:
NAXIS = 4
TYPE = REAL*4

### 13.10.1 Product PP1FCSPOW: PHT-P1 FCS power calibration table

| AXIS | Length | Description |
|---|---|---|
| 1 | 45 | Index for in-band optical power on detector |
| 2 | 10 | Filters ordered according to (see section A.1): 3.3, 3.6, 4.8, 7.3, 7.7, 10, 11.3, 12.8, 15, 11.5 $\mu$m |
| 3 | 2 | Each TRS: TRS1, TRS2 |
| 4 | 2 | Each FCS: FCS1, FCS2 |

### 13.10.2 Product PP2FCSPOW: PHT-P2 FCS power calibration table

| AXIS | Length | Description |
|---|---|---|
| 1 | 45 | Index for in-band optical power on detector |
| 2 | 2 | Filters ordered according to: 20, 25 $\mu$m |
| 3 | 2 | Each TRS: TRS1, TRS2 |
| 4 | 2 | Each FCS: FCS1, FCS2 |

### 13.10.3 Product PP3FCSPOW_01/02: PHT-P3 FCS power calibration table

| AXIS | Length | Description |
|---|---|---|
| 1 | 45 | Index for in-band optical power on detector |
| 2 | 2 | Filters ordered according to: 60, 100 $\mu$m |
| 3 | 2 | Each TRS: TRS1, TRS2 |
| 4 | 2 | Each FCS: FCS1, FCS2 |

### 13.10.4 Product PC1FCSPOW_01/02: PHT-C100 FCS power calibration table

| AXIS | Length | Description |
|---|---|---|
| 1 | 45 | Index for in-band optical power on detector (see section A.1) |
| 2 | 7 | Filters ordered according to (see section A.1): 90(backup), 70, 60, 80, 90, 105, 90 $\mu$m |
| 3 | 2 | Each TRS: TRS1, TRS2 |
| 4 | 2 | Each FCS: FCS1, FCS2 |

### 13.10.5 Product PC2FCSPOW_01/02: PHT-C200 FCS power calibration table

| AXIS | Length | Description |
|---|---|---|
| 1 | 45 | Index for in-band optical power on detector |
| 2 | 5 | Filters ordered according to (see section A.1): 170, 200, 180, 150, 120 $\mu$m |
| 3 | 2 | Each TRS: TRS1, TRS2 |
| 4 | 2 | Each FCS: FCS1, FCS2 |

## 13.11 PHT-P and PHT-C default responsivities

```
Description Parameter:          Section 4.2.1
Processing Level:               SPD
Usage in processing:            section 7.4
File Type:                      FITS Image
Units:                          A/W
File names:                     PPRESP_01, PPRESP_02,
                                PC1RESP_01, PC1RESP_02,
                                PC2RESP_01, PC2RESP_02
```

Default responsivities are used in case:

- no FCS measurements were collected during an observation (except for P40, see section 13.16),
- chopped mode is used.

For staring mode observations with the PHT-P or PHT-C subsystems, default detector responsivities are not needed as long as at least one FCS measurement was obtained per detector. However, it can happen that no FCS measurements were collected (due to e.g. data dropouts from telemetry loss) or that the quality of the FCS measurement is insufficient (due to e.g. complete saturation). In those cases default responsivities will be applied in the conversion from signal in V/s to an in-band power on the detector in W.

Default detector responsivities are also applied in case of chopped mode observations. For chopped mode observations, the accompanying FCS measurement - which is also in chopped mode between FCS1 and FCS2 - is not used in OLP Version 7 due to the disturbing signal transients between the chopper plateaux.

The detector responsivity is a function of orbital phase. At the end of the science window the responsivities of all detectors are higher than at the beginning. For detectors P3, C100, and C200 two sets of orbital dependencies are provided: one set for observations before rev 150 (files have suffix _01), the other set for rev 150 and later (files have suffix _02). At rev 150 an additional detector curing procedure was introduced sometime after apogee passage which restores the responsivity to the same level as that at the beginning of the science window.

Since the responsivities are provided in A/W, the conversion from V/s to W can only be carried out if the integration capacities $C_{int}$ associated with a detector are known, see also section 4.2.1. The capacitances are listed in Table 13.5.

Table 13.5: Integration capacities associated with detectors

| Detector | Capacitance (As/V) |
|---|---|
| P1 | $9\times10^{-14}$ |
| P2 | $9\times10^{-14}$ |
| P3 | $9\times10^{-14}$ |
| C100 | $9\times10^{-14}$ |
| C200 | $14\times10^{-14}$ |
| SS | $5.26\times10^{-14}$ |
| SL | $6.3\times10^{-14}$ |

Notes

- 1 A/(V/s) = 1 Farad
- For the arrays, capacitances refer to individual pixels.

For all default responsivity tables, the following FITS keywords are common:
NAXIS = 3
TYPE = REAL*4

### 13.11.1 Product PRESP_01/02: PHT default responsivities for P1, P2 and P3 detectors

| AXIS | Length | Description |
|---|---|---|
| 1 | 100 | Orbital phase: each element corresponds to a phase in the range from 0.01 to 1.0 in steps of 0.01 |
| 2 | 3 | PHT-P detectors, P1,P2,P3 |
| 3 | 2 | Default responsivity and uncertainty |

### 13.11.2 Product PC1RESP_01/02: PHT default responsivities for the C100 detector

| AXIS | Length | Description |
|---|---|---|
| 1 | 100 | Orbital phase: each element corresponds to a phase in the range from 0.01 to 1.0 in steps of 0.01 |
| 2 | 9 | C100 pixels, in same order as in SPD |
| 3 | 2 | Default responsivity and uncertainty |

### 13.11.3 Product PC2RESP_01/02: PHT default responsivities for the C200 detector

| AXIS | Length | Description |
|---|---|---|
| 1 | 100 | Orbital phase: each element corresponds to a phase in the range from 0.01 to 1.0 in steps of 0.01 |
| 2 | 4 | C200 pixels, in same order as SPD |
| 3 | 2 | Default responsivity and uncertainty |

Note:
• see section 3.4.2 for definition of C-arrays pixel identifiers

## 13.12 Array Illumination by FCS

```
Description Parameter:        section 4.5.4
Processing Level:             SPD
Usage in processing:          section 7.4.3
File Type:                    Fits Image
Units:                        dimensionless
Number of Records:            1
File Names:                   PC1ILLUM_01, PC1ILLUM_02,
                              PC2ILLUM_01, PC2ILLUM_02,
```

The FCS illumination is not uniform. For the PHT-C arrays, the non-uniform illumination requires a pixel dependent correction to the FCS power calibration table which gives only the mean value over the pixel array. Note that the illumination correction products contain only 1 record.

The properties (FCS1,TRS2) altered between rev 93 and 94 due to unknown reasons. This event changed the FCS illumination pattern. Therefore two calibration files are available: one for before rev 94 (suffix _01) and one for rev 94 and higher (suffix _02).

All products have:
NAXIS = 4
TYPE = R*4

### 13.12.1 Product PC1ILLUM_01/02: FCS illumination for C100

| AXIS | Length | Description |
|---|---|---|
| 1 | 9 | C100 Pixels, in same order as SPD |
| 2 | 7 | [CHWII position − 1] (see section A.1) |
| 3 | 2 | each FCS |
| 4 | 2 | Correction and uncertainty |

### 13.12.2 Product PC2ILLUM_01/02: FCS illumination for C200

| AXIS | Length | Description |
|---|---|---|
| 1 | 4 | C200 Pixels, in same order as SPD |
| 2 | 5 | [CHWII position − 8] (see section A.1) |
| 3 | 2 | each FCS |
| 4 | 2 | Correction and uncertainty |

## 13.13 Inhomogeneous FCS illumination of PHT-P

```
Description Parameter:          section 4.5.4
Processing Level:               SPD
Usage in processing:            section 7.4.2
File Type:                      FITS Image
Units:                          dimensionless
File Names:                     PP1FCSAP, PP2FCSAP, PP3FCSAP,
```

As already implemented in the case of PHT-C (FCS illumination matrixes "PC1ILLUM" in section 13.12.1 and "PC2ILLUM" in section 13.12.2), also the inhomogenous FCS illumination for PHT-P must be corrected for in PHT OLP. This implies that the power on the detector from the FCS does not scale directly with the aperture area (which whould be the case for a perfectly homogeneous illumination) but that an additional correction factor is necessary.

For all aperture correction Cal G files the following FITS keywords are common:
NAXIS = 4
TYPE = REAL*4

### 13.13.1 Product PP1FCSAP: FCS aperture correction tables for P1

| AXIS | Length | Description |
|---|---|---|
| 1 | 14 | apertures: CHWII position (see section A.1) |
| 2 | 10 | filters: CHWIII position (see section A.1) |
| 3 | 2 | Each FCS |
| 4 | 2 | Correction and uncertainty |

### 13.13.2 Product PP2FCSAP: FCS aperture correction tables for P2

| AXIS | Length | Description |
|---|---|---|
| 1 | 14 | apertures: CHWII position (see section A.1) |
| 2 | 2 | filters: 20, 25 $\mu$m |
| 3 | 2 | Each FCS |
| 4 | 2 | Correction and uncertainty |

### 13.13.3 Product PP3FCSAP: FCS aperture correction tables for P3

| AXIS | Length | Description |
|---|---|---|
| 1 | 14 | Apertures: CHWII position (see section A.1) |
| 2 | 2 | Filters: 60, 100 $\mu$m |
| 3 | 2 | Each FCS |
| 4 | 2 | Correction and uncertainty |

## 13.14 Wavelength dependent detector flat fields

```
Description Parameter:      section 4.2.6
Processing Level:           SPD
Usage in processing:        section 7.4.3
File Type:                  FITS Image
Units:                      Dimensionless
File Names:                 PC1FLAT, PC2FLAT
```

The responsivity of the individual detector pixels in the C100 and the C200 arrays vary from one filter to the other. These variations are different for different pixels in the array. Consequently, the flatfield of the array differs from one filter to the other. The flatfield is in principle calibrated out by the FCS measurement, but for multi-filter measurements where only 1 FCS measurement is taken, the flatfield correction must be applied when determining the fluxes in the filters in which the FCS was not taken.

For both detector flat field calibration files the following FITS keywords are common:
NAXIS = 3
TYPE = REAL*4

### 13.14.1 Product PC1FLAT: PHT C100 filter-to-filter flatfield correction

| AXIS | Length | Description |
|---|---|---|
| 1 | 9 | C100 pixels, in same order as SPD. |
| 2 | 7 | filters: [CHWII position $-$ 1] (see section A.1) |
| 3 | 2 | Correction and uncertainty |

### 13.14.2 Product PC2FLAT: PHT C200 filter-to-filter flatfield correction

| AXIS | Length | Description |
|---|---|---|
| 1 | 4 | C200 pixels in the same order as in SPD |
| 2 | 5 | Filters: [CHWII position $-$ 8] (see section A.1) |
| 3 | 2 | Correction and uncertainty |

## 13.15 Point spread function corrections

```
Description Parameter:          section 4.5.2
Processing Level:               AAR
Usage in processing:            section 8.4.9, 8.4.10
File Type:                      FITS Image
Units:                          dimensionless
File Name:                      PPSF
```

This calibration product lists for each wavelength band of PHT-P the fraction of the point source power that passes a given aperture size. The correction factors are needed in the conversion from power on the detector in W to point source flux in Jy.

For the C100 and C200 arrays the fraction of point source power falling on the entire array is listed.

### 13.15.1 Product PPSF: point spread function corrections

NAXIS = 2
TYPE = R*4

| AXIS | Length | Description |
|---|---|---|
| 1 | 15 | Corrections: for 14 P-apertures and for PHT-C100/C200 |
| 2 | 14 | Filter wheel positions |

## 13.16 PHT-S Wavelength and Signal Calibration

```
Description Parameter:          section 4.6.2, 5.2.4
Processing Level:               AAR
Usage in processing:            sections 8.4.9 and 8.4.10
File Type:                      Binary Fits Table
Number of Records:              128
File Names:                     PSPECAL
```

For each pixel in the PHT-SS and PHT-SL array the corresponding central wavelengths and spectral response are listed. The spectral response is given in units of V/s/Jy for point sources and in V/s/(MJy/sr) for extended sources. These numbers provide a direct conversion from a pixel signal to a point source flux (in Jy) or a surface brightness (in MJy/sr) on the sky. The conversion assumes (1) a constant responsivity for the PHT-S arrays with time and orbital position and (2) no positional dependence of the source with respect to the centre of the aperture. The records are filled as follows: data of PHT-SS pixels 1-64 are stored in records 1-64, PHT-SL pixels 1-64 are stored in records 65-128.

### 13.16.1 Product PSPECAL: PHT-S wavelength and signal calibration

Binary FITS table with record length 16. The record fields are:

| Field | Offset | Number | Type | Description |
|---|---|---|---|---|
| PSPELAMB | 0 | 1 | R*4 | Wavelength (in m, increasing) |
| PSPELUNC | 4 | 1 | R*4 | Uncertainty in wavelength (m) |
| PSPESRFP | 8 | 1 | R*4 | Point source srf (V/s/Jy) |
| PSPESRUP | 12 | 1 | R*4 | Uncertainty point source srf (V/s/Jy) |
| PSPESRFE | 16 | 1 | R*4 | Extended source srf (V/s/(MJy/sr)) |

| | | | | |
|---|---|---|---|---|
| PSPESRUE | 20 | 1 | R*4 | Uncertainty extended source srf (V/s/(MJy/sr)) |

Note:
srf = spectral response function

## 13.17 Conversion from power on detector to flux density

```
Description Parameter:          sections 5.6 and 5.7
Processing Level:               AAR
Usage in processing:            section 8.4.9 and 8.4.10
File Type:                      FITS Header
File Names:                     PFLUXCONV
```

The transmission of the whole optical path for each filter is characterized by the parameter C1 in $m^2Hz$. The effective size of the primary mirror, reflections, filter transmission, spectral response of the detector, etc. are included. The C1 values for all filters are given in this calibration file.

### 13.17.1 Product PFLUXCONV: PHT-P/C power calibration

PFLUXCONV is a FITS header *without* accompanying data. All entries have unit: $m^2Hz$.

| Keyword | Type | Description |
|---|---|---|
| FCP3P29 | R | conversion for PHT-P1 3.3 $\mu$m filter |
| FCP3P6 | R | conversion for PHT-P1 3.6 $\mu$m filter |
| FCP4P85 | R | conversion for PHT-P1 4.8 $\mu$m filter |
| FCP7P3 | R | conversion for PHT-P1 7.3 $\mu$m filter |
| FCP7P7 | R | conversion for PHT-P1 7.7 $\mu$m filter |
| FCP10 | R | conversion for PHT-P1 10 $\mu$m filter |
| FCP11P3 | R | conversion for PHT-P1 11.3 $\mu$m filter |
| FCP11P5 | R | conversion for PHT-P1 12 $\mu$m filter |
| FCP12P8 | R | conversion for PHT-P1 12.8 $\mu$m filter |
| FCP16 | R | conversion for PHT-P1 15 $\mu$m filter |
| FCP20 | R | conversion for PHT-P2 20 $\mu$m filter |
| FCP25 | R | conversion for PHT-P2 25 $\mu$m filter |
| FCP60 | R | conversion for PHT-P3 60 $\mu$m filter |
| FCP100 | R | conversion for PHT-P3 100 $\mu$m filter |
| FCC50 | R | conversion for C100 70 $\mu$m filter |
| FCC60 | R | conversion for C100 60 $\mu$m filter |
| FCC70 | R | conversion for C100 80 $\mu$m filter |
| FCC90 | R | conversion for C100 90 $\mu$m filter |
| FCC100 | R | conversion for C100 100 $\mu$m filter |
| FCC105 | R | conversion for C100 105 $\mu$m filter |
| FCC120 | R | conversion for C200 120 $\mu$m filter |
| FCC135 | R | conversion for C200 150 $\mu$m filter |
| FCC160 | R | conversion for C200 170 $\mu$m filter |
| FCC180 | R | conversion for C200 180 $\mu$m filter |
| FCC200 | R | conversion for C200 200 $\mu$m filter |
| FCC105 | R | conversion for C200 105 $\mu$m filter |

## 13.18 Effective solid angles of apertures and pixels

```
Description Parameter:          sections 4.5.1 and 5.3
Processing Level:               AAR
Usage in processing:            section 8.4.10
File Type:                      Binary FITS Table
File Names:                     PPOMEGA, PC1OMEGA, PC2OMEGA
```

In the conversion from flux per pixel or per aperture (in Jy/beam) to surface brightness (in MJy/sr) the effective solid angles $\Omega_{eff}$ are required. In the present set of Cal G files, the effective solid angles were obtained from a model calculation which takes into account the ISO primary mirror, secondary mirror, tripod, and the linear sizes of the apertures and the detectors as measured pre-flight.

The Cal G files also contain the dimensions of the apertures (in case of P1, P2, and P3) or the offsets and dimensions of the detector pixels (in case of C100 and C200) as projected on the sky in arcseconds. Fields for the uncertainties of all parameters are included.

The Cal G files related to OLP Version 7 contain the following limitations:

- all uncertainties have been set to zero,
- the effective solid angles of the PHT-P apertures are the physical dimensions of the apertures in the focal plane projected on the sky.

### 13.18.1 Product PPOMEGA: aperture dimensions and solid angles for P1, P2, and P3

Binary FITS table with record length 32. The record fields are:

| Field | Offset | Number | Type | Description |
|---|---|---|---|---|
| PPOMFILT | 0 | 1 | I*4 | Filter (CHW position) |
| PPOMAPER | 4 | 1 | I*4 | Aperture (CHW position) |
| PPOMDASY | 8 | 1 | R*4 | Aperture diameter in Y in arcsec |
| PPOMDAYU | 12 | 1 | R*4 | Uncertainty in aperture diameter in Y in arcsec |
| PPOMDASZ | 16 | 1 | R*4 | Aperture diameter in Z in arcsec |
| PPOMDAZU | 20 | 1 | R*4 | Uncertainty in aperture diameter in Z in arcsec |
| PPOMDAEG | 24 | 1 | R*4 | Effective Omega (in $10^{-7}$sr) |
| PPOMDAUN | 28 | 1 | R*4 | Uncertainty in Omega (in $10^{-7}$sr) |

### 13.18.2 Product PC1OMEGA: dimensions and solid angles for C100 pixels

Binary FITS table with record length 48. The record fields are:

| Field | Offset | Number | Type | Description |
|---|---|---|---|---|
| PC1OMFIL | 0 | 1 | I*4 | Filter (CHW position) |
| PC1OMPIX | 4 | 1 | I*4 | Pixel in SPD order |
| PC1OMOFY | 8 | 1 | R*4 | Offset in y relative to centre of array in arcsec |
| PC1OMOYU | 12 | 1 | R*4 | Uncertainty in offset in y in arcsec |
| PC1OMOFZ | 16 | 1 | R*4 | Offset in z relative to centre of array in arcsec |
| PC1OMOZU | 20 | 1 | R*4 | Uncertainty in offset in Z in arcsec |
| PC1OMDAY | 24 | 1 | R*4 | Aperture dimension y in arcsec |
| PC1OMDYU | 28 | 1 | R*4 | Uncertainty in aperture dimension y in arcsec |
| PC1OMDAY | 32 | 1 | R*4 | Aperture dimension z in arcsec |
| PC1OMDYU | 36 | 1 | R*4 | Uncertainty in aperture dimension z in arcsec |

| | | | | |
|---|---|---|---|---|
| PC1OMOME | 40 | 1 | R*4 | Effective Omega (in $10^{-7}$sr) |
| PC1OMOMU | 44 | 1 | R*4 | Uncertainty in omega (in $10^{-7}$sr) |

### 13.18.3 Product PC2OMEGA: dimensions and solid angles for C200 pixels

Same file and record structure as PC1OMEGA (section 13.18.2), however all keywords start with "PC2" instead of PC1.

## 13.19 Colour corrections

```
Description Parameter:          Appendix C
Processing Level:               none
Usage in processing:            N/A
File Type:                      Binary FITS Table
File Names:                     PCCBB, PCCMBBONE, PCCMBBTWO, PCCPOWER
```

The colour correction tables are not used in OLP. Since the colour corrections depend on source specific assumptions, no efforts were made for implementation in OLP. The Cal G products give the observer the possibility to apply colour corrections. Colour corrections are provided for 4 different models of the infrared continuum: blackbody $B_\nu(T)$, modified blackbodies $\nu^\alpha \cdot B_\nu(T)$ with $\alpha = 1$ and 2, and power law continua $\nu^\alpha$. A description of the derivation of the colour corrections is given in Appendix C.

The flux density value in OLP which refers to a source spectrum $F_\nu \propto \nu^{-1}$ has to be *divided* by the colour correction factor associated to the assumed source spectrum.

### 13.19.1 Product PCCBB: black body $B_\nu(T)$ colour correction

Binary FITS table with record length 104. The record fields are:

| Field | Offset | Number | Type | Description |
|---|---|---|---|---|
| TEMP | 0 | 1 | R*4 | Temperature in K |
| P1_3.29 | 4 | 1 | R*4 | P1 3.3 $\mu$m correction |
| P1_3.60 | 8 | 1 | R*4 | P1 3.6 $\mu$m correction |
| P1_4.85 | 12 | 1 | R*4 | P1 4.8 $\mu$m correction |
| P1_7.30 | 16 | 1 | R*4 | P1 7.3 $\mu$m correction |
| P1_7.70 | 20 | 1 | R*4 | P1 7.7 $\mu$m correction |
| P1_10.0 | 24 | 1 | R*4 | P1 10 $\mu$m correction |
| P1_11.3 | 28 | 1 | R*4 | P1 11.3 $\mu$m correction |
| P1_11.5 | 32 | 1 | R*4 | P1 12 $\mu$m correction |
| P1_12.8 | 36 | 1 | R*4 | P1 12.8 $\mu$m correction |
| P1_16.0 | 40 | 1 | R*4 | P1 15 $\mu$m correction |
| P2_20 | 44 | 1 | R*4 | P2 20 $\mu$m correction |
| P2_25 | 48 | 1 | R*4 | P2 25 $\mu$m correction |
| P3_60 | 52 | 1 | R*4 | P3 60 $\mu$m correction |
| P3_100 | 56 | 1 | R*4 | P3 100 $\mu$m correction |
| C1_50 | 60 | 1 | R*4 | C100 70 $\mu$m correction |
| C1_60 | 64 | 1 | R*4 | C100 60 $\mu$m correction |
| C1_70 | 68 | 1 | R*4 | C100 80 $\mu$m correction |
| C1_90 | 72 | 1 | R*4 | C100 90 $\mu$m correction |
| C1_100 | 76 | 1 | R*4 | C100 100 $\mu$m correction |
| C1_105 | 80 | 1 | R*4 | C100 105 $\mu$m correction |
| C2_120 | 84 | 1 | R*4 | C200 120 $\mu$m correction |
| C2_135 | 86 | 1 | R*4 | C200 150 $\mu$m correction |

| | | | | |
|---|---|---|---|---|
| C2_160 | 92 | 1 | R*4 | C200 170 $\mu$m correction |
| C2_180 | 96 | 1 | R*4 | C200 180 $\mu$m correction |
| C2_200 | 100 | 1 | R*4 | C200 200 $\mu$m correction |

### 13.19.2 Product PCCMBBONE: modified black body $\nu^1 \cdot B_\nu(T)$ colour correction

Same file structure as in section 13.19.1

### 13.19.3 Product PCCMBBTWO: modified black body $\nu^2 \cdot B_\nu(T)$ colour correction

Same file structure as in section 13.19.1

### 13.19.4 Product PCCPOWER: Power law $\nu^\alpha$ colour correction

Same file structure as in section 13.19.1, but instead of temperature in field 1, the exponent $\alpha$ of the power law is given.

# Appendix A

# Instrument Tables

## A.1 Mean Filter/Aperture Specifications

### A.1.1 PHT-P Filters

The PHT-P filters are located on Change Wheel III (CHW3). Each wheel position is indicated by an integer. In the following table the filter specifications corresponding to a Change Wheel III position have been listed. The values for the spectral resolution ($\lambda_c/\Delta\lambda$) and airy diameter ($d_{Airy}$) have been measured in laboratory. The system responses ($R_{mean}$) have been derived from in-flight data. The reference central wavelength ($\lambda_{ref}$) is defined as a wavelength close to the isophotal centre of the filter, and where possible, matching values given for filters corresponding to other ISO and IRAS instruments (see [20]).

### A.1.2 PHT-P Apertures

The PHT-P apertures are located on the inner circle of Change Wheel II (CHW2). Each wheel position is indicated by an integer. In the following table the aperture specifications corresponding to a Change Wheel II position have been listed.

### A.1.3 PHT-C Filters

The PHT-C filters are located in the outer circle of Change Wheel II (CHW2). In the following table the filter specifications corresponding to a Change Wheel II position have been listed. The values for the spectral resolution ($\lambda_c/\Delta\lambda$) and point spread function factor ($f_{psf}$) have been measured in laboratory. The system responses ($R_{mean}$) have been derived from in-flight data. The reference wavelength ($\lambda_{ref}$) is defined as a wavelength close to the isophotal centre of the filter, and where possible, matching values are given for filters corresponding to other ISO and IRAS instruments (see [20]).

The point spread function factor represents the fraction of the power in the beam falling on the whole detector array if the beam is centered on the array (the values have been derived from in-flight data, see section 9 for an explanation). The geometrical solid angles of the pixels are slightly filter dependent, their averages are:

$\Omega_{C100} = 0.0688 \times 10^{-6}$ sr
$\Omega_{C200} = 0.281 \times 10^{-6}$ sr

### A.1.4 Other Filterwheel Components

Change Wheel I (CHW1) is either used to redirect the light to the next optical component such as PHT-S, the inner Change Wheel II and the outer Change Wheel II, or is used to put a polariser in the beam. In the following table the specifications corresponding to a Change Wheel I position have been listed.

Table A.1: Description of the PHT-P filters on CHWIII

| **Wheel position** | **Filter ID** | $\lambda_{ref}$ ($\mu m$) | $\lambda_c/\Delta\lambda$ | $R_{mean}$ | $d_{Airy}$ (") | **description** |
|---|---|---|---|---|---|---|
| 1 | P1_3p29_UM | 3.3 | 15.160 | 0.103 | 2.8 | PAH |
| 2 | P1_3p6_UM | 3.6 | 3.620 | 0.127 | 3.0 | Cosmological gap, cf ISOCAM |
| 3 | P1_4p85_UM | 4.8 | 3.140 | 0.152 | 4.1 | Continuum |
| 4 | P1_7p3_UM | 7.3 | 2.190 | 0.212 | 6.2 | Continuum |
| 5 | P1_7p7_UM | 7.7 | 9.320 | 0.194 | 6.4 | PAH |
| 6 | P1_10_UM | 10 | 5.551 | 0.177 | 8.4 | sillicate feature |
| 7 | P1_11p3_UM | 11.3 | 14.070 | 0.177 | 9.5 | PAH |
| 8 | P1_12p8_UM | 12.8 | 5.330 | 0.089 | 10.8 | Continuum |
| 9 | P1_16p0_UM | 15 | 1.820 | 0.130 | 13.8 | Continuum |
| 10 | P1_11p5_UM | 12 | 5.550 | 0.156 | 10.0 | IRAS 12 $\mu m$ cf. ISOCAM |
| 11 | P2_20_UM | 21.03 | 2.330 | 0.324 | 17.7 | Close to Q band |
| 12 | P2_25_UM | 25 | 2.610 | 0.370 | 20.0 | IRAS 25 $\mu m$ |
| 13 | P3_60_UM | 60 | 2.350 | 0.111 | 50.3 | IRAS 60 |
| 14 | P4_100_UM | 100 | 2.590 | 0.303 | 83.9 | IRAS 100 |

Table A.2: Description of the PHT-P apertures located on CHWII

| **Wheel position** | **Aperture ID** | **Diameter** (") | **Area** ($mm^2$) | **Solid Angle** ($10^{-8}$ **ster**) | **description** |
|---|---|---|---|---|---|
| 1 | 52_SEC | 52 | 4.1548 | 5.13 | circular 2.3 mm |
| 2 | 79_SEC | 79 | 9.0792 | 11.21 | circular 3.4 mm |
| 3 | 99_SEC | 99 | 14.522 | 17.93 | circular |
| 4 | 120_SEC | 120 | 21.237 | 26.22 | circular |
| 5 | 127×127_SEC | 127×127 | 30.250 | 37.3 | square |
| 6 | 180_SEC | 180 | 48.398 | 59.8 | circular |
| 7 | 180_SEC_XBLK | | | | not used |
| 8 | 5_SEC | 5 | 0.0314 | 0.039 | circular |
| 9 | 7p6_SEC | 7.6 | 0.1001 | 0.124 | circular |
| 10 | 10_SEC | 10 | 0.1735 | 0.214 | circular |
| 11 | 13p8_SEC | 13.8 | 0.2827 | 0.349 | circular |
| 12 | 18_SEC | 18 | 0.5218 | 0.625 | circular |
| 13 | 20×32_SEC | 20×32 | 1.1288 | 1.39 | rectangular |
| 14 | 23_SEC | 23 | 0.7854 | 0.97 | circular |

Table A.3: Description of the PHT-C filters on CHWII

| **Wheel position** | **Filter ID** | $\lambda_{ref}$ ($\mu m$) | $\lambda_c/\Delta\lambda$ | $R_{mean}$ | $f_{psf}$ (") | **description** |
|---|---|---|---|---|---|---|
| 1 | C100_OPEN | | | | | not used |
| 2 | C100_90_RED | 90 | 1.730 | 0.296 | 0.900 | wide band cont.(backup) |
| 3 | C100_50_UM | 65 | 1.130 | 0.045 | 0.912 | continuum |
| 4 | C100_60_UM | 60 | 2.510 | 0.130 | 0.918 | continuum IRAS 60 $\mu m$ |
| 5 | C100_70_UM | 80 | 1.670 | 0.121 | 0.902 | continuum |
| 6 | C100_100_UM | 100 | 2.180 | 0.270 | 0.892 | continuum IRAS 100 $\mu m$ |
| 7 | C100_105_UM | 105 | 2.790 | 0.236 | 0.884 | continuum |
| 8 | C100_90_UM | 90 | 1.690 | 0.296 | 0.900 | wide band continuum |
| 9 | C200_160_UM | 170 | 1.940 | 0.431 | 0.708 | wide band continuum |
| 10 | C200_200_UM | 200 | 3.550 | 0.215 | 1.054 | continuum |
| 11 | C200_180_UM | 180 | 2.630 | 0.327 | 0.972 | continuum |
| 12 | C200_135_UM | 150 | 1.910 | 0.260 | 0.668 | continuum |
| 13 | C200_120_UM | 120 | 2.400 | 0.131 | 0.574 | continuum |
| 14 | C200_RETICLE | 0.00 | 0.00 | 0.00 | 0.00 | not used |

Table A.4: Description of CHWI

| **Wheel position** | **Element ID** | **description** |
|---|---|---|
| 1 | PHT_P_POL000 | PHT P Polariser 0deg |
| 2 | PHT_P_POL120 | PHT P Polariser 120deg |
| 3 | PHT_P_POL240 | PHT P Polariser 240deg |
| 4 | PHT_P_NO_POL | PHT P Flat mirror |
| 5 | PHT_S | PHT S Flat mirror |
| 6 | PHT_C_RETICL | PHT C C-cut Quartz |
| 7 | PHT_C_FREE1 | PHT C Free aperture |
| 8 | PHT_C_FREE2 | PHT C Free aperture |
| 9 | PHT_C_FREE3 | PHT C Free aperture |
| 10 | PHT_S_REDUND | PHT S Flat mirror (redundant) |
| 11 | PHT_C_POL000 | PHT C Polariser 0deg |
| 12 | PHT_C_POL120 | PHT C Polariser 120deg |
| 13 | PHT_C_POL240 | PHT C Polariser 240deg |
| 14 | PHT_C_NO_POL | PHT C Free aperture |

## A.2 Filter Transmission Data

By the time of writing this version of the idum, no transmission data could be made available.

# Appendix B

# Conversion Algorithms for ERD

## B.1 Temperature Sensors

**Detector Temperature**

To convert ERD voltage to actual detector temperature one should apply the following relationship:

$$T = B\frac{1}{{}^{10}\log(R_s) + \frac{K}{{}^{10}\log(R_s)} - A} \qquad (K) \tag{B.1}$$

where:

A, B, K = constants, different for each detector
$R_s$ = sensor resistance in $\Omega$, according to

$$\frac{\mathrm{R_s}}{1000} = \frac{1}{\frac{1}{\mathrm{C_1 \times tmd - C_2}} - \frac{1}{\mathrm{R_p}}} - \mathrm{R_k} \qquad (\Omega) \tag{B.2}$$

Where:

tmd = telemetry data value
$C_1, C_2$ = constants
$R_k$ = harness resistance in k$\Omega$
$R_p$ = EEU shunt resistor in parallel to sensor in k$\Omega$

| Sensor | A | B | K |
|---|---|---|---|
| FCS1 | 6.54 | 2.90 | 10.67 |
| FCS2 | 6.54 | 2.90 | 10.67 |
| C100 | 5.44 | 3.05 | 7.34 |
| C200 | 4.51 | 3.12 | 4.92 |
| P1 | 6.02 | 3.61 | 8.77 |
| P2 | 7.59 | 3.13 | 14.40 |
| P3 | 5.11 | 3.49 | 6.29 |
| S1 | 6.54 | 2.94 | 10.66 |
| S2 | 6.54 | 2.90 | 10.67 |

| Sensor | $C_1(k\Omega$ | $C_2(k\Omega$ | $R_k(k\Omega$ | $R_p(k\Omega$ |
|---|---|---|---|---|
| FCS1 | 0.259 | 495.83 | 1.12 | 1000 |
| FCS2 | 0.256 | 495.83 | 1.12 | 1000 |
| C100 | 0.099 | 146.38 | 1.34 | infinite |
| C200 | 0.048 | -78.32 | 0.67 | infinite |
| P1 | 0.174 | 344.55 | 1.12 | 499 |
| P2 | 0.210 | 388.13 | 1.34 | 499 |
| P3 | 0.182 | 288.11 | 1.34 | infinite |
| S1 | 0.173 | 341.63 | 1.12 | 499 |
| S2 | 0.170 | 336.88 | 1.12 | 499 |

**EEU temperature**

$$T = \frac{B}{A + ln(R_s)} \qquad (K) \tag{B.3}$$

with

$$R_s = \frac{tmd - 2048}{4096 - tmd} \times 7500 \qquad (\Omega) \tag{B.4}$$

where

A = 3.9489
B = 3442 K
$R_s$ = sensor resistance in $\Omega$
T = EEU Temperature in K
tmd = telemetry data value

## B.2 Selected FCS Power

Conversion from telemetered FCS power data in PSTA to a real power in mW

$$P_{fcs} = \frac{P_{max} \times tmd}{tmd_{max}} \qquad (mW) \tag{B.5}$$

where

tmd = telemetry data value = PSTA1TS or PSTA2TS
$tmd_{max}$ = maximum value of telemetry word = 4095
$P_{max}$ = maximum commandable power = 50 mW

## B.3 Focal Plane Chopper Deflection

The telemetry contains the actual (measured) chopper position. The value represents a voltage which is non-linear to the chopper angle on the sky, and non-synchronous to IR readout data. The conversion is dependent upon the chopper mode and submode.

The initial step is the conversion of the data word to a voltage (V) according to :

```
in_volt = C * (RAW_FPC_POSN * Q/P - R)

C = 1.0          P = 4096
Q = 20.0V        R = 10.0V
```

This quantity is converted to mV

```
in_volt = 1000 * in_volt
```

At this stage the voltage is checked to see if it corresponds to an FCS for FPC_MODE_2 or FPC_MODE_32 else a crude first approximation to the chopper angle is calculated from a simple linear model

```
angle_line = - in_volt - b            (arcsec)
               -----------
                     a
```

In the case of FPC_MODE_1, FPC_MODE_31N/P, and FPC_MODE_4, the approximation is then corrected for deviations from the line approximation using the following :

```
Angle_approx = angle_line - DU_DC(<angle>)   (arcsec)
                            -------------
                                  a
```

Where DU_DC is a linear interpolation to a correction table. The value of $rm < angle >$ depends on the chopper mode.

Corrections must be made for hysteresis effects in the chopper position the case of FPC_MODE_1 and FPC_MODE_4.

For FPC_MODE_1, the correction is

```
(1) sky_angle = angle_approx - DU_ACI(+1)    |angle_approx|    (arcsec)
                               ---------  *  -------------
                                   a             150
for angle_approx > 0

(2) sky_angle = angle_approx - DU_ACD(-1)    |angle_approx|    (arcsec)
                               ---------  *  -------------
                                   a              150
for angle_approx < 0


For FPC_MODE_4, the correction is

(1) For saw-tooth profile SUBMODE(0)

sky_angle = angle_approx -  A   [DU_ACI(angle_approx/A)]    (arcsec)
                           ------
                            150*a

(2) for triangular-tooth profile SUBMODE(1)

sky_angle = angle_approx -  A   [DU_ACI(angle_approx/A)]    (arcsec)
                           ------
                            150*a
for increasing angle.

sky_angle = angle_approx -  A   [DU_ACD(angle_approx/A)]    (arcsec)
                           ------
                            150*a
for decreasing angle.
```

The converted angle is returned. If the FCSs are used then the FPC_STATE variable indicates which one is in use. If an invalid raw position is given, FPC_STATE is set to -1. Any other position gives a value of 0.

Values of the different parameters:

```
 PARAMETER (C=1.0)            ! initial conversion
 PARAMETER (P=4096)           ! a voltage
 PARAMETER (Q=20.0)
 PARAMETER (R=10.0)


 PARAMETER (A=9.862622)       ! the line approx
 PARAMETER (B=-20.0057)

 PARAMETER (U_ACF1=4238.0)    ! values for the voltage
 PARAMETER (U_DCF1=4238.0)    ! the beam from the FCSs
 PARAMETER (U_OF1=131.0)
 PARAMETER (U_OF2=239.0)
 PARAMETER (TOLERANCE=6.0)

DATA ANG_DEV  /-180.0,-162.0,-144.0,-126.0,-108.0, -90.0, -72.0,
#               -54.0, -36.0, -18.0,   0.0,  18.0,  36.0,  54.0,
#                72.0,  90.0, 108.0, 126.0, 144.0, 162.0, 180.0/
 DATA DU_DC     /-11.4, -10.4, -11.5, -12.5, -13.6, -15.1, -15.2,
#               -14.2, -11.5,  -8.1,  -2.9,  -1.0,  -2.9,  -2.4,
#                -1.6,  -0.8,   0.3,   1.7,   3.9,   6.1,   9.1/
 DATA NORM_ANG  / -1.0,  -0.9,  -0.8,  -0.7,  -0.6,  -0.5,  -0.4,
#                -0.3,  -0.2,  -0.1,   0.0,   0.1,   0.2,   0.3,
#                 0.4,   0.5,   0.6,   0.7,   0.8,   0.9,   1.0/
 DATA DU_ACD    /  0.0,  -2.8,  -5.7,  -8.7, -11.7, -13.6, -15.5,
#               -15.2, -14.8, -12.6, -10.3,  -7.8,  -5.4,  -3.1,
#                -0.9,   0.6,   2.1,   1.6,   1.0,  -1.3,  -3.6/
 DATA DU_ACI    /  0.0,  -7.4, -14.8, -21.5, -28.2, -32.8, -37.4,
#               -39.4, -41.4, -41.0, -40.5, -37.3, -34.1, -30.2,
#               -26.3, -22.6, -18.9, -15.5, -12.0,  -7.8,  -3.6/
```

## B.4 Description of the pixel status flag PIXF in ERD products

See Table B.1.

Table B.1: Description of 16 bits ERD bit flag variable PPERPIXF. LSB = 0, MSB = 15.

| **bit range** | **item** | **decimal value** | **meaning** |
|---|---|---|---|
| 0 | auto data reduction | 0 | not active; all telemetry (TM) blocks can be transferred |
| | | 1 | active; one or more TM blocks of the measurement could not be transmitted. science data shall not be used, they may be corrupted. |
| 1-2 | not used | – | none |
| 3-4 | selected TRS of FCS1 | 0 | both TRSs not connected |
| | | 1 | only TRS1 connected |
| | | 2 | only TRS2 connected |
| 5-6 | selected TRS of FCS2 | 0 | both TRSs not connected |
| | | 1 | only TRS1 connected |
| | | 2 | only TRS2 connected |
| 7 | SW override | 0 | not active |
| | | 1 | active; no operational but purely diagnostic set-up |
| 8-11 | TM data structure | 0 | P1 data structure |
| | | 1 | P2 data structure |
| | | 2 | P3 data structure |
| | | 3 | PHT-S data structure |
| | | 4,5 | not used |
| | | 6 | C100 data structure |
| | | 7 | C200 data structure |
| | | 8..12 | not used |
| | | 13 | diagnostic data structure |
| | | 14 | extended house-keeping (HK) data structure |
| | | 15 | not used |
| 12-15 | integration time | 0..15 | selected fundamental integration time (reset interval) exponent n in $2^{(7-n)}$ [s] $0 \leq n \leq 15$ |

# Appendix C

# Colour Corrections

## C.1 Application of Tabulated Colour Correction Factors

The flux densities quoted in the ISOPHOT AAR results have been derived from the detector in-band powers assuming an energy distribution of the source which is constant in the flux per logarithmic frequency interval; i.e., the flux density with frequency $\nu$ goes as $f_\nu \propto \nu^{-1}$. This is the same convention as used for IRAS data.

In order to derive the flux density for any other spectral energy distribution (SED) a "colour correction" must be applied to the background subtracted source flux density in the following way:

$$F_{\nu_{\rm ref}}(SED) = F_{\nu_{\rm ref}}(\nu^{-1}) \ / \ K_{\rm cc}(SED) \tag{C.1}$$

where:

$F_{\nu_{\rm ref}}(SED)$ = flux density for applied SED
$F_{\nu_{\rm ref}}(\nu^{-1})$ = quoted flux density in AAR
$K_{\rm cc}(SED)$ = tabulated colour correction factor for applied SED

Tabulated colour correction factors are available for

1) power laws $F(\nu^\alpha), -3 \ \leq \ \alpha \ \leq \ +3$
   → cal-G file PCCPOWER

2) black bodies $F(B(\nu,T))$
   → cal-G file PCCB

3) modified black bodies $F(\nu^{+1} \cdot B(\nu,T))$ and $F(\nu^{+2} \cdot B(\nu,T))$
   → cal-G files PCCMBBONE and PCCMBBTWO

## C.2 Computation of Colour Correction Factors

### C.2.1 Derivation of Flux Density Values from In-band Power Values

In order to derive flux density values (monochromatic fluxes) from measured in-band powers the following corrections and calibrations have to be done:

a) correction for effective telescope area;

b) correction for reflection losses on all optical elements in the beam from the primary mirror to the detector;

c) correction for the beam profile related to the selected aperture or array;

d) correction for the bandpass transmission, determined by the filter and field lens transmission and the relative detector response. The product of these factors is called the relative system response.

The latter correction contains the determination of the relative contribution of the flux density at the central wavelength of the band to the to the total flux in the band, depending on the assumed spectral shape of the source. Doing this calculation for a variety of source spectra and computing the ratios provides the colour correction factors between the various SEDs.

The flux conversion can be written in the following form:

$$IBP = T_{\mathrm{refl}} \cdot A \cdot \int f_{\mathrm{beam}}(\lambda) \cdot F(\lambda) \cdot R(\lambda)\, d\lambda \tag{C.2}$$

where:

| | |
|---|---|
| $IBP$ | = in-band power (unit: W) |
| $T_{\mathrm{refl}}$ | = reflection losses on optical elements |
| $A$ | = primary mirror area |
| $f_{\mathrm{beam}}(\lambda)$ | = wavelength dependent beam profile function |
| $F(\lambda)$ | = flux density of source at specific wavelength $\lambda$ |
| $R(\lambda)$ | = system response at specific wavelength $\lambda$ |

Currently the in-band power calculation contains some simplification, in particular related to the beam profiles.

For point source fluxes the following calculation is done:

$$IBP = T_{\mathrm{refl}} \cdot A \cdot f_{\mathrm{psf}}(\lambda_{\mathrm{ref}}) \cdot \int F(\lambda) \cdot R(\lambda)\, d\lambda \tag{C.3}$$

where:

| | |
|---|---|
| $f_{\mathrm{psf}}(\lambda_{\mathrm{ref}})$ | = fraction of the point spread function at the reference wavelength $\lambda_{\mathrm{ref}}$ inside the aperture or pixel $\rightarrow$ cal-G file PPSF |

For extended source fluxes the corresponding calculation is done:

$$IBP = T_{\mathrm{refl}} \cdot A \cdot (1 - \varepsilon^2) \cdot \Omega \cdot \int F(\lambda) \cdot R(\lambda)\, d\lambda \tag{C.4}$$

where:

| | |
|---|---|
| $\varepsilon$ | = central obscuration factor by the secondary mirror |
| $\Omega$ | = solid angle of selected aperture or pixel |

In order to derive the flux density for the central wavelength, or more general a reference wavelength, of the bandpass the spectral energy distribution function is normalised with respect to the flux density at this wavelength:

$$F(\lambda) = F(\lambda_{\mathrm{ref}}) \cdot \frac{SED(\lambda)}{SED(\lambda_{\mathrm{ref}})} \tag{C.5}$$

where:

$F(\lambda)$ = flux density at any wavelength $\lambda$
$F(\lambda_{\rm ref})$ = flux density at reference wavelength $\lambda_{\rm ref}$
$SED(\lambda)$ = functional dependence of spectral energy distribution of source with wavelength

Furthermore, for conversion between frequency range and wavelength range the following convention is used:

$$\lambda \cdot F(\lambda) = \nu \cdot F(\nu) \tag{C.6}$$

where:

$F(\lambda)$ = flux density in wavelength range (unit: $\mathrm{W\,m^{-2}\,\mu m^{-1}}$)
$F(\nu)$ = flux density in frequency range (unit: $\mathrm{W\,m^{-2}\,Hz^{-1}}$ or Jy)

Solving this equation for $F(\nu)$ yields:

$$F(\nu) = \frac{\lambda^2}{c_{\rm light}} \cdot F(\lambda) \tag{C.7}$$

where:

$c_{\rm light}$ = speed of light

Using the normalisation with respect to the flux density value at the reference wavelength and the convention for conversion of $F(\lambda)$ into $F(\nu)$ the above formula of the in-band power can be solved for $F(\nu)$ for a general source energy distribution $SED(\lambda)$:

$$F(\nu_{\rm ref}) = \frac{1}{b \cdot c_{\rm light}} \cdot \lambda_{\rm ref}^2 \cdot SED(\lambda_{\rm ref}) \cdot \frac{IBP}{\int SED(\lambda) \cdot R(\lambda)\, d\lambda} \tag{C.8}$$

where:

$b$ = $A \cdot T_{\rm refl} \cdot f_{\rm psf}(\lambda_{\rm ref})$

### C.2.2 Flux Density Conversion Factors for Different Spectral Energy Distributions

In the formula for the flux density $F(\nu)$ the term, which is dependent on the shape of the spectral energy distribution of the source, is called the flux density conversion factor $a(SED)$

$$a(SED) = \frac{\lambda_{\rm ref}^2 \cdot SED(\lambda_{\rm ref})}{c_{\rm light} \cdot \int SED(\lambda) \cdot R(\lambda)\, d\lambda} \tag{C.9}$$

In the following the conversion factors for specific SEDs are listed:

1) flux density $\propto \nu^\alpha, F(\nu) = constant \cdot \nu^\alpha$

$$a(\nu^\alpha) = \frac{1}{c_{\rm light} \cdot \lambda_{\rm ref}^\alpha \cdot \int \frac{R(\lambda)}{\lambda^{2+\alpha}}\, d\lambda} \tag{C.10}$$

2) flux density is a modified black body function with emissivity $\propto \nu^\beta, F(\nu) = \nu^\beta \cdot B(\nu, T)$ ($\beta = 0$: pure black body)

$$a(\nu^\beta \cdot B(\nu,T)) = \frac{B(\lambda_{\rm ref}, T)}{c_{\rm light} \cdot \lambda_{\rm ref}^\beta \cdot \int \frac{B(\lambda,T)}{\lambda^{2+\beta}} \cdot R(\lambda)\, d\lambda} \tag{C.11}$$

Note that:

$$B(\lambda, T) = \frac{2 \cdot h \cdot c_{\text{light}}^2}{\lambda^5} \cdot \frac{1}{e^{\frac{h \cdot c_{\text{light}}}{k \cdot \lambda \cdot T}} - 1} \tag{C.12}$$

where:

$h$ = Planck constant
$k$ = Boltzmann constant

### C.2.3 Derivation of Colour Correction Factors from Flux Density Conversion Factors

From the general formula of the colour correction in Appendix C.1 it follows that

$$K_{\text{cc}}(SED) = F_{\nu_{\text{ref}}}(\nu^{-1}) \;/\; F_{\nu_{\text{ref}}}(SED) \tag{C.13}$$

and with the formulae from Appendix C.2.1 for $F(\nu_{\text{ref}})$

$$K_{\text{cc}}(SED) = a(\nu^{-1}) \;/\; a(SED) \tag{C.14}$$

the colour correction factor is the ratio of the flux density conversion factors.

Inserting the formulae from Appendix C.2.2 for both flux density conversion factors this yields

$$K_{\text{cc}}(SED) = \frac{1}{\lambda_{\text{ref}} \cdot SED(\lambda_{\text{ref}})} \cdot \frac{\int SED(\lambda) \cdot R(\lambda)\, d\lambda}{\int \frac{R(\lambda)}{\lambda}\, d\lambda} \tag{C.15}$$

In order to calculate the colour correction factors this needs a numerical solution of the two integrals using the tabulated relative system response $R(\lambda_{\text{i}})$. The relative system responses for all PHT-P and PHT-C bandpasses will be soon provided in cal-G FITS files.

The published cal-G files with colour correction factors have been computed using a minimum threshold of the bandpass transmission of $10^{-4}$ in the numerical integrations. Tests using thresholds of $10^{-3}$ and $10^{-5}$, respectively, showed that the results were pretty stable.

# Appendix D

# Acronyms

| | |
|---|---|
| AAR | auto-analysis results |
| AD | analog to digital |
| ADD | architectural design document |
| AOCS | attitude and orbit control system |
| AOT | astronomical observation template |
| CFOV | centre field of view |
| CHW | change wheel |
| CRE | cold readout electronics |
| CSH | compact status history |
| DIE | detector interface electronics |
| DN | digitized numbers |
| DR | destructive read-out |
| DUM | data users manual |
| EEU | external electronic unit |
| EOH | executed observation history |
| ERD | edited raw data |
| FCS | fine calibration source |
| FITS | flexible image transfer system |
| FPC | focal plane chopper |
| FPG | focal plane geometry |
| HTML | hyper-text mark-up language |
| ID | identifier |
| IDPD | ISO data product document |
| IDUM | ISOPHOT data users manual |
| IRPH | instrument reference pointing history |
| ISDM | ISO satellite and data manual |
| ITK | instrument time key ($=2^{-14}$ sec) |
| NDR | non-destructive read-out |
| OLP | off-line processing |
| OPF | on-position flag |
| OTF | on-target flag |
| PHT | ISOPHOT |
| RI | reset interval |
| ROT | read-out timing |
| SPD | standard processed data |
| srf | spectral response function |
| TDF | telemetry data file |
| TDT | target dedicated time |
| TRS | thermal radiation source |

# Appendix E

# Glossary

| | |
|---|---|
| auto analysis results | *auto analysis results* (AAR) are the products from the auto-analysis processing |
| glitch | a *glitch* is a short duration anomaly in the datastream, usually caused by an ionizing particle. |
| in-band power | the power (in W) falling on the detector for a filter, aperture, and polariser combination |
| measurement | see definition section 3.3 |
| preformance verification | the *performance verification* (PV) phase comprises the first 80 days of the ISO mission and has been exclusively reserved for instruments check-out, calibrations, and AOT commissioning. |
| product | a *product* is a FITS file defined by the Science Operations Centre and contains the ISO data for official distribution. |
| observation | An *observation* refers to the acquisition of the scientifically useful data during one AOT by the prime instrument requested by the proposer. The term "observation" also loosely refers to the data products created from the acquired data. An observation has a one-to-one association with an ISO Observation Number (ION). |
| ramp | a *ramp* is formed by the read-outs collected during one and the same reset interval |
| responsivity | the detector *responsivity* (in A/W) is the ratio between electrical current through a detector and the illuminating power falling on the detector. |
| standard processed data | *standard processed data* (SPD) are the products from the standard processing, chapter 7 |
| target dedicated time | a *target dedicated time* (TDT) is the entire contiguous time period scheduled for performing the N observations of a concatenated group. (N = 1 if no concatenation). All overheads, including slewing, are included (TDT = observation time plus overheads time). The start of a TDT is defined as the time of the first AOCS command to point at the new target. The end of the TDT is defined as the time at which all instrument activities connected with the (N) observation(s) have been completed. Note that the above restrictions on concatenation imply that one TDT can belong to |

only one proposer.

# Bibliography


[1] Acosta-Pulido, J., Cabriel C., Catañeda, H: Transient effects in ISOPHOT data: status of modelling and correction procedures, in Proceedings of the ISO detector workshop, to be published in Experimental Astronomy (1999)

[2] Blackwell, D.E., Booth, A.J., Petford, A.D., Leggett, S.K., Mountain, C.M., Selby, M.J. 1986, MNRAS, 221, 427

[3] Cohen M., Witteborn F.C., Walker R.G., Bregman J.D., Wooden D.H. 1995, AJ 110, 275.

[4] Gabriel C., Acosta-Pulido J.: Deglitching methods by the ISOPHOT interactive analysis procedures, in Proceedings of the ISO detector workshop, to be published in Experimental Astronomy (1999)

[5] Guest S.: Deglitching of ISOPHOT Data, 13 July 1993, ISOPHOT internal report

[6] Guest S., Richards P.J., Williams S.R.: Architectural Design Document for PHT Auto Analysis, Version 1.1, 20 July 1994 (DRAL)

[7] Hammersley P.L., Jourdain de Muizon M., Kessler M.F., Bouchet P., Joseph R.D., Habing H.J., Salama A., Metcalfe L. 1998, A&AS 128, 207.

[8] Herbstmeier U., Ábrahám P., Lemke D., Laureijs R.J., Klaas U., Mattila K., Leinert C., Surace C., Kunkel M. 1998, A&A 332, 793

[9] Herbstmeier U., Kunkel K., Gabriel C.: PHT Interactive Users Manual, see ISO Explanatory Library on the WEB

[10] Klaas U., Krüger H., Heinrichsen I., Heske A., and Laureijs R. (Eds): Observer's Manual for the ISO Photo-Polarimeter ISOPHOT, Version 3.1, 7 April 1994.

[11] Klaas U., Laureijs R.J., Radovich M., Schulz B.: "ISOPHOT Calibration Accuracies", IDC Report SAI/98-092/Dc, Version 1.0 (September, 1998)

[12] Klaas U., M. Radovich M.: Report on the PHT Scientific Validation for OLP Version 7.0, IDC Report SAI/98-049/Rp, Version 2.0 (July 20, 1998)

[13] Klaas U., Lemke D., Krantz T. et al. 1998, Infrared straylight measurements of the ISO telescope, in "Infrared astronomical instrumentation conference", Proc. SPIE 3354-111.

[14] Laureijs R.J., Levine D. (Eds): "Taking ISO to the limits: exploring the faintest sources in the infrared" - Invited and Contributed papers, proceedings of a workshop held at the ISO Science Operations Centre VILSPA, Feb 3 and 4, 1997.

[15] Laureijs R.J., Klaas U.: "ISOPHOT Error Budgets", IDC Report SAI/98-091/Dc, Version 1.0, October 1998

[16] Lebofsky, L.A. & Spencer, J.R. 1989, in Asteroids II, eds. R.P. Binzel, T. Gehrels, M.S. Matthews, Univ. of Arizona Press, p. 128.

[17] Leech K., A.M.T. Pollock, J.M. Sternberg, ISO Satellite and Data Manual, SAI/98-094/Dc, Issue 1

[18] Lemke D., Klaas U., Abolins J. et al.: ISOPHOT - capabilities and performance AA 315, L64, 1996

[19] Metcalfe L.: Scientific Capabilities of the ISO Payload, ISO-SSD-8805 Issue 1.0, 29 November 1991.

[20] Moneti A., Metcalfe L., Schulz B. Reference wavelengths for ISO: CAM and PHOT filters, SAI/97-002/Dc, 17 Jan 1997.

[21] Müller, T.: Asteroïden als Kalibratoren für ISOPHOT, Dissertation (Ruprecht-Karls-Universität Heidelberg), 1996

[22] Müller T., Lagerros J. 1998, A&A in preparation.

[23] Jourdain de Muizon M., Habing H. 1992, Les Houches series Infrared Astronomy with ISO, Eds Th. Encrenaz & M.F. Kessler, p129

[24] ISOPHOT Instrument User Manual, ISO-SST-UM-0166-SIM, Issue 1 Revision 0, 8 March 1995 (ESOC)

[25] Saxton, R.D. (Ed.) ISO Data Product Document, ISO-SSD-9111A, draft 4, 18 January 1995 [IDPD].

[26] Polarimetry with ISOPHOT, Schlötelburg, M. 1992, ISOPHOT Internal Report, MPIA Heidelberg

[27] Schubert, J., Fouks, B.I., Lemke, D., Wolf, J. 1995 Transient Response of ISOPHOT Si:Ga Infrared Photodetectors: Experimental Results ans Application of the Theory of Non-stationary Processes, in "Infrared Spaceborne Remote Sensing III", Proc. SPIE 2553, 42.

[28] Schulz, B: Bodencalibration des Infrarotmeters im Satellitenexperiment ISOPHOT, Dissertation (Ruprecht-Karls-Universität Heidelberg), 16 June 1993

[29] B. Schulz & S. Huth, "Explanatory Supplement for FCS Monitoring Observations", Draft 2.0, 20-June-97 and related diagrams

[30] Schulz B., Huth S., Kinkel U., et al. 1999: A&AS in preparation.

[31] Spencer, J.R. 1990, ICARUS, 83, 27

[32] Sternberg J.: Architectural Design Document (for off-line analysis software), ISO-SSD-9105 Version 1.1, 6t October 1994.

[33] Sternberg J., Laureijs R.J. (Eds): Baseline Requirements Document for Off-line Scientific Data Processing, ISO-SSD-9010, issue 2.0, 1 February 1994.

[34] van der Bliek, N.S., Bouchet, P., Habing, H.J., Jourdain de Muizon, M., Blackwell, E.E., Gustafsson, B., Hammersley, P.L., Kessler, M.F., Lim, T.L., Manfroid, J., Metcalfe, L, Salama, A.: Standard Stars for the Infrared Space Observatory, ISO, The Messenger 70, 28, 1992

[35] van der Bliek, N.S., Bouchet, P. Manfroid, J.: Infrared aperture photometry at ESO (1983-1994) and its future use, A&AS, 119, 547, 1996

[36] Untersuchung von Detektordriften des C200-Detectors im Satellitenexperiment ISOPHOT und deren Kalibration, Diplomarbeit, K. Wilke (Ruprecht-Karls-Universität Heidelberg), 1995.

[37] Wolf J.: Photoconductors and arrays for the far-infrared, proceedings of "Photon Detectors for Space Instrumentation", ESA Special Publication SP-356.

[38] "Statistik" - Lehr und Handbuch der angewandten Statistik, J.Hartung 1991, R.Oldenburg Verlag